

Turkish Journal of

Analytical Chemistry

Volume 6

Issue 2

December 2024

<https://dergipark.org.tr/tr/pub/turkjac>

Turkish Journal of
**Analytical
Chemistry**
TurkJAC

Volume 6
Issue 2
December 2024

Publication Type: Peer-reviewed scientific journal

Publication Date: December 20, 2024

Publication Language: English

Published two times a year (June, December)

Owner

Prof. Miraç Ocak

Karadeniz Technical University, Faculty of Sciences, Department of Chemistry

Executive Editor

Prof. Ümmühan Ocak

Karadeniz Technical University, Faculty of Sciences, Department of Chemistry

Co-Editor

Ender Çekirge

Karadeniz Technical University, Institute of Forensic Sciences

Layout Editor

Ender Çekirge

Karadeniz Technical University, Institute of Forensic Sciences

Editorial Secretary

Ender Çekirge

Karadeniz Technical University, Institute of Forensic Sciences

Language Editors

Nurhayat Özbek

Karadeniz Technical University, Faculty of Sciences, Department of Chemistry

Prof. Miraç Ocak

Karadeniz Technical University, Faculty of Sciences, Department of Chemistry

Aslıhan Yılmaz Çamoğlu

Karadeniz Technical University, Faculty of Sciences, Department of Chemistry

Copyeditor

Nurhayat Özbek

Karadeniz Technical University, Faculty of Sciences, Department of Chemistry

Aslıhan Yılmaz Çamoğlu

Karadeniz Technical University, Faculty of Sciences, Department of Chemistry

Prof. Miraç Ocak

Karadeniz Technical University, Faculty of Sciences, Department of Chemistry

Proofreader

Nurhayat Özbek

Karadeniz Technical University, Faculty of Sciences, Department of Chemistry

Aslıhan Yılmaz Çamoğlu

Karadeniz Technical University, Faculty of Sciences, Department of Chemistry

Editors

Prof. Ümmühan Ocak

Karadeniz Technical University, Faculty of Sciences, Department of Chemistry

Prof. Miraç Ocak

Karadeniz Technical University, Faculty of Sciences, Department of Chemistry

Prof. Ali Gündoğdu

Karadeniz Technical University, Maçka Vocational School, Department of Pharmacy Services

Section Editors

Prof. Zekeriya Bıyıklıoğlu

Karadeniz Technical University, Faculty of Sciences, Department of Chemistry

Editor Board

Prof. Selehattin Yılmaz

Çanakkale Onsekiz Mart University, Faculty of Science and Literature, Department of Chemistry

Prof. Ali Gündoğdu

Karadeniz Technical University, Maçka Vocational School, Department of Pharmacy Services

Prof. Hakan Alp

Karadeniz Technical University, Faculty of Sciences, Department of Chemistry

Prof. Volkan Numan Bulut

Karadeniz Technical University, Maçka Vocational School, Department of Chemistry and Chemical Processing Technologies

Prof. Celal Duran

Karadeniz Technical University, Faculty of Sciences, Department of Chemistry

Asst. Prof. Aysel Başoğlu

Gümüşhane University, Faculty of Health Sciences, Department of Occupational Health and Safety

Prof. Ayşegül İyidoğan

Gaziantep University, Faculty of Science and Literature, Department of Chemistry

Prof. Sevgi Kolaylı

Karadeniz Technical University, Faculty of Sciences, Department of Chemistry

Prof. Hüseyin Serencam

Trabzon University, College of Applied Sciences, Department of Gastronomy and culinary arts

Assoc. Prof. Fatma Ağin

Karadeniz Technical University, Faculty of Pharmacy, Department of Basic Pharmaceutical Sciences

Prof. Duygu Özdeş

Gümüşhane University, Gümüşhane Vocational School, Department of Chemistry and Chemical Processing Technologies

Dr. Mustafa Z. Özel

University of York, Department of Chemistry

Prof. Małgorzata Wiśniewska

University of Maria Curie- Sklodowska, Faculty of Chemistry, Institute of Chemical Sciences, Department of Radiochemistry and Environmental Chemistry

Prof. Dilek Kul

Karadeniz Technical University, Faculty of Pharmacy, Department of Basic Pharmaceutical Sciences

Prof. Sławomira Skrzypek

University of Lodz, Faculty of Chemistry, Department of Inorganic and Analytical Chemistry

Prof. Fatih İslamoğlu

Recep Tayyip Erdoğan University, Faculty of Science and Literature, Department of Chemistry

Asst. Prof. Zekeriyya Bahadır	Giresun University, Faculty of Science and Literature, Department of Chemistry
Asst. Prof. Yasemin Çağlar	Giresun University, Faculty of Engineering, Department of Genetic and Bioengineering
Prof. Agnieszka Nosal-Wiercińska	University of Maria Curie- Sklodowska, Faculty of Chemistry, Institute of Chemical Sciences, Department of Analytical Chemistry
Assoc. Prof. Dr. Halit Arslan	Gazi University, Faculty of Science, Department of Chemistry
Assoc. Prof. Cemalettin Baltacı	Gümüşhane University, Faculty of Engineering and Natural Sciences, Department of Food Engineering
Asst. Prof. Zafer Ocak	Kafkas University, Education Faculty, Mathematics and Science Education
Prof. Mustafa İmamoğlu	Sakarya Univer.sity, Faculty of Science and Literature, Department of Chemistry
Assoc. Prof. Esra Bağda	Sivas Cumhuriyet University, Faculty of Pharmacy, Department of Basic Pharmaceutical Sciences, Analytical Chemistry Division
Assoc. Prof. Hüseyin Altundağ	Sakarya University, Faculty of Science and Literature, Department of Chemistry
Asst. Prof. Mehmet Başoğlu	Gümüşhane University, Faculty of Engineering and Natural Sciences, Department of Energy Systems Engineering

Publishing Board

Prof. Latif Elçi	Pamukkale University, Faculty of Science and Literature, Department of Chemistry
Prof. Münevver Sökmen	Konya Food and Agriculture University, Faculty of Engineering and Architecture, Department of Bioengineering
Prof. Atalay Sökmen	Konya Food and Agriculture University, Faculty of Engineering and Architecture, Department of Bioengineering
Prof. Kamil Kaygusuz	Karadeniz Technical University, Faculty of Sciences, Department of Chemistry
Prof. Yaşar Gök	Pamukkale University, Faculty of Science and Literature, Department of Chemistry
Prof. Ayşegül Gölcü	İstanbul Technical University, Faculty of Science and Literature, Department of Chemistry
Prof. Mustafa Tüzen	Gaziosmanpaşa University, Faculty of Science and Literature, Department of Chemistry
Prof. Mustafa Soylak	Erciyes University, Faculty of Sciences, Department of Chemistry
Prof. Fikret Karadeniz	Kafkas University, Faculty of Science and Literature, Department of Chemistry
Prof. Mehmet Yaman	Fırat University, Faculty of Sciences, Department of Chemistry

Prof. Halit Kantekin	Karadeniz Technical University, Faculty of Sciences, Department of Chemistry
Prof. Esin Canel	Ankara University, Faculty of Sciences, Department of Chemistry
Prof. Dilek Ak	Anadolu University, Faculty of Pharmacy, Department of Basic Pharmaceutical Sciences
Prof. Mustafa Küçükislamođlu	Sakarya University, Faculty of Science and Literature, Department of Chemistry
Prof. Salih Zeki Yıldız	Sakarya University, Faculty of Science and Literature, Department of Chemistry
Prof. Recai İnam	Gazi University, Faculty of Sciences, Department of Chemistry
Prof. Dr. Durişehvar Ünal	İstanbul University, Faculty of Pharmacy, Department of Basic Pharmaceutical Sciences
Prof. Mehmet Tüfekçi	Avrasya University, Faculty of Science and Literature, Department of Biochemistry
Prof. Hüseyin Kara	Selçuk University, Faculty of Sciences, Department of Chemistry
Prof. Sezgin Bakirdere	Yıldız Technical University, Faculty of Science and Literature, Department of Chemistry
Prof. Hasan Basri Şentürk	Karadeniz Technical University, Faculty of Sciences, Department of Chemistry
Prof. Yusuf Atalay	Sakarya University, Faculty of Science and Literature, Department of Physics
Prof. Salih Zeki Yıldız	Sakarya University, Faculty of Science and Literature, Department of Chemistry

Authorship, Originality, and Plagiarism: The authors accept that the work is completely original and that the works of others have been appropriately cited or quoted in the text with the necessary permissions. The authors should avoid plagiarism. It is recommended that they check the article using appropriate software such as Ithenticate and CrossCheck. The responsibility for this matter rests entirely with the authors. All authors will be notified when the manuscript is submitted. If a change of author is needed, the reason for the change should be indicated. Once the manuscript is accepted, no author changes can be made.

Aims and Scope

“Turkish Journal of Analytical Chemistry” publishes original full-text research articles and reviews covering a variety of topics in analytical chemistry. Original research articles may be improved versions of known analytical methods. However, studies involving new and innovative methods are preferred. Topics covered include:

- Analytical materials
- Atomic methods
- Biochemical methods
- Chromatographic methods
- Electrochemical methods
- Environmental analysis
- Food analysis
- Forensic analysis
- Optical methods
- Pharmaceutical analysis
- Plant analysis
- Theoretical calculations
- Nanostructures for analytical purposes
- Chemometric methods
- Energy

ETHICAL GUIDELINES

TurkJAC follows ethical tasks and responsibilities are defined by the Committee on Publication Ethics (COPE) in publication procedure. Based on this guide, the rules regarding publication ethics are presented in the following sections.

Ethical Approval

Ethics committee approval must be obtained for studies on clinical and experimental regarding human and animals that require an ethical committee decision, this approval must be stated in the article and documented in the submission. In such articles, the statement that research and publication ethics are complied with should include. Information about the approval such as committee name, date, and number should be included in the method section and also on the first/last page of the article.

Editors

1. In the preliminary evaluation of a submission, the editor of the journal evaluates the article's suitability for the purpose and scope of the journal, whether it is similar to other articles in the literature, and whether it meets the expectations regarding the language of writing. When it meets the mentioned criteria, the scientific evaluation process is started by assigning a section editor if necessary.
2. A peer-reviewed publication policy is employed in all original studies, taking into full account of possible problems due to related or conflicting interests.

3. Section editors work on the articles with a specific subject and their suggestion is effective in the journal editor's decision about acceptance or rejection of the article.
4. No section editor contacts anyone except the authors, reviewers, and the journal editor about articles in the continued evaluation process.
5. In the journal editor's decision to accept or reject an article, in the addition of section editor's suggestion in consequence of scientific reviewing, the importance of the article, clarity and originality are decisive. The final decision, in this case, belongs to the journal editor.

Authors

1. The authors should actively contribute to the design and execution of the work. Authorship should not be given to a person who does not have at least one specific task in the study.
2. Normally all authors are responsible for the content of the article. However, in interdisciplinary studies with many authors, the part that each author is responsible for should be explained in the cover letter.
3. Before the start of the study, it would be better to determine the authors, contributors, and who will be acknowledged in order to avoid conflict in academic credits.
4. The corresponding author is one of the authors of the article submitted to the journal for publication. All communications will be conducted with this person until the publication of the article. The copyright form will be signed by the corresponding author on all the authors' behalf.
5. It is unacceptable to submit an article that has already been published entirely or partly in other publication media. In such situation, the responsibility lies with all authors. It is also unacceptable that the same article has been sent to TurkJAC and another journal simultaneously for publication. Authors should pay attention to this situation in terms of publication ethics.
6. Plagiarism from others' publications or their own publications and slicing of the same study is not acceptable.
7. All authors agree that the data presented in the article are real and original. In case of an error in the data presented, the authors have to be involved in the withdraw and correction process.
8. All authors must contribute to the peer-reviewed procedure.

Reviewers

1. Peer reviewers worked voluntarily are external experts assigned by editors to improve the submitted article.
2. It is extremely important that the referee performs the review on time so that the process does not prolong. Therefore, when the invitation is agreed upon, the reviewer is expected to do this on time. Also, the reviewer agrees that there are no conflicts of interest regarding the research, the authors, and/or the research funders.
3. Reviewers are expected not to share the articles reviewed with other people. The review process should be done securely.
4. Reviewers are scored according to criteria such as responding to the invitations, whether their evaluations are comprehensive and acting in accordance with deadlines, and the article submissions that they can make to TurkJAC are handled with priority.

Contents

Research Articles

- The relationship between hydrothermal alteration and element accumulation in sessile oak (*Quercus petraea* L.): A case study from the Canca hydrothermal alteration zone (Gümüşhane, Türkiye)
Alaaddin Vural 61–70
- Determination of trace heavy metals content of various herbal drinks marketed in Ilorin Metropolis, Nigeria
S. W. Olokoba 71–77
- Catalytic oxidation of aromatic aldehydes to carboxylic acids in mild conditions with NaClO₂
*Gizem Boyoğlu, A. Berat Karabina, Ecem Bellikan, Salih Zeki Yıldız** 78–90
- Parentucellia viscosa* (growing in Türkiye): Essential oil, phenolic composition, antimicrobial and lipase inhibition
Büşra Korkmaz, Gözde Bozdağ, Büşra Şahin, Sila Özlem Sener, Elif Öztürk, Seda Fındaklı, Şengül Alpay Karaoğlu, Nurettin Yaylı* 91–96
- Metabolic stability of a hydrazone derivative: *N'*-[(4-chlorophenyl)methylidene]-4-[(4-methylphenyl)sulfonyloxy]benzohydrazide
Hasan Erdinç Sellitepe, Göknil Pelin Coşkun, Kaan Birgül, Mert Ülgen, İnci Selin Doğan* 97–101
- Isocratic liquid chromatography technique for the analysis of cyanocobalamin from beef liver and heart muscle extracts
Labaran Ibrahim 102–107
- Investigation of extracellular metabolites in cancer and healthy colon cells in a time-dependent manner
*Esra Bulut Atalay, Hülya Ayar Kayali** 108–114
- Evaluation of photocytotoxic activity of water-soluble Zn(II) phthalocyanine on cancer cells and molecular docking studies
*Ugur UZUNER, Selcen CELİK-UZUNER, Hakkı İsmail KAYA, Çağla AKKOL, Meryem YILMAZ, Ece Tuğba SAKA** 115–128
- Schiff Base Catalysts for the Oxidation of Benzyl Alcohol to Benzaldehyde
Çağla Akkol, Serdar Karaböcek, Ece Tuğba Saka, Bekir Sıtkı Çevrimli* 129–137



The relationship between hydrothermal alteration and element accumulation in sessile oak (*Quercus petraea* L.): A case study from the Canca hydrothermal alteration zone (Gümüşhane, Türkiye)

Alaaddin Vural 

Ankara University, Faculty of Engineering, Department of Geological Engineering, 06830, Ankara, Türkiye

Abstract

The aim of this study is to investigate the element accumulation capability of sessile oak trees, specifically focusing on their ability and characteristics to accumulate trace elements in the context of plants/trees in alteration zones. The Canca hydrothermal alteration zone (Gümüşhane, Türkiye) is located in Gümüşhane, one of Türkiye's significant mining provinces, which hosts numerous mineralizations. The area has been subjected to intense hydrothermal alteration, making it particularly notable for signs of precious and base metal mineralization. Sessile oak (*Quercus petraea* L.) leaves were collected from the Canca hydrothermal alteration zone, and their analyses were conducted using an ICP-MS device. The trace element concentrations in the oak leaves were evaluated geostatistically, and the element distributions in the Canca area were examined using element distribution maps created by spatial geostatistical methods. When the findings were collectively evaluated, it was determined that the trace element contents in the sessile oak leaves were generally higher than normal element contents, associated with the alteration in the area. Notably, a more significant enrichment of Mo (from 0.05 to 5.47 ppm, with a median value of 0.71 ppm), Cu (from 2.85 to 14.64 ppm, with a median value of 5.97 ppm) As (from 0.01 to 1.36 ppm, with a median value of 0.14 ppm), Zn (from 7.37 to 52.53 ppm, with a median value of 19.15 ppm) and Pb (from 0.29 to 2.23 ppm, with a median value of 0.83 ppm) elements was found to be related to the alteration. In addition, a slight enrichment by other elements (Cr, Mn, Co, Ni, Sb and Ba) has been detected. As a result, this study contributes to the related literature by elucidating the elemental accumulation pattern and alteration relationship of sessile oak leaves grown in the alteration zone associated with mineralization.

Keywords: Biogeochemistry, element accumulation, exploration geochemistry, hydrothermal alteration, trace elements

1. Introduction

The geochemical properties of elements and their mobility in different environments are among the many factors influencing element accumulation in plants [1–5]. Therefore, the use of plants for geochemical prospecting in mineral exploration began in the 1950s, yielding satisfactory results from these studies. Such biogeochemical studies have contributed to the discovery of many mineral deposits during that period. Today, exploration geochemistry continues to utilize the element accumulation capabilities of plants.

The geochemical properties of elements, along with various physicochemical factors such as pH and Eh, and their mobility in different environments, significantly influence element accumulation in plants [2,6,7]. Therefore, the use of plants for geochemical prospecting in mineral exploration began in the 1950s, and these

studies have yielded satisfactory results. Such biogeochemical studies contributed to the discovery of many mineral deposits during that period. Today, exploration geochemistry continues to benefit from the element accumulation capabilities of plants.

The Gümüşhane region has been the site of numerous mining activities since ancient times [8]. During the Republic period, exploration efforts in the region led to the discovery of many mineral deposits, which were subsequently developed for the national economy through the efforts of both the private sector and public institutions such as the General Directorate of Mineral Research and Exploration (MTA). The Canca (Gümüşhane, Türkiye) hydrothermal alteration zone, where the oak leaves were collected (Fig. 1), is part of the Eastern Black Sea Tectonic Belt, which forms a section of

Citation: A. Vural, The relationship between hydrothermal alteration and element accumulation in sessile oak (*Quercus petraea* L.): A case study from the Canca hydrothermal alteration zone (Gümüşhane, Türkiye), Turk J Anal Chem, 6(2), 2024, 61–70.

 <https://doi.org/10.51435/turkjac.1494920>

Author of correspondence: alaaddinvural@hotmail.com

Received: June 4, 2024

Tel: +90 (312) 203 3402

Accepted: June 27, 2024

Fax: +90 (312) 215 04 87

the 6000 km long metallogenic belt extending from the Balkans to the Himalayas [9,10].

The region, situated at the transition between the Black Sea Climate and Continental climate, boasts a rich diversity of flora. Considering the mining potential of the region and its diverse plant life, it is evident that phytogeochemical studies conducted in the area would significantly contribute to mineral exploration efforts. Such studies are also crucial for investigating the element accumulation capabilities of plants in hydrothermal alteration and mineralization areas. Therefore, the Canca hydrothermal alteration zone, characterized by intense hydrothermal alteration and a dense sessile oak (*Quercus petraea* L.) forest, was selected as the target area for this study. A biogeochemistry/phytogeochimical study was conducted in the area to examine the relationship

between the element accumulation capability of oak trees and hydrothermal alteration.

2. Materials and methods

2.1. Geological and Geographical Characteristics of the Region

The Canca hydrothermal alteration zone exhibits a rugged topography characterized by deep valleys and high peaks because of its geological and geotectonic history. The region experiences a transitional climate between a continental climate, characterized by hot and dry summers, and a Black Sea climate, characterized by cold and snowy winters.

The Canca area has been subjected to intense hydrothermal alteration due to the influence of Upper Cretaceous-Eocene magmatism. Considering the study

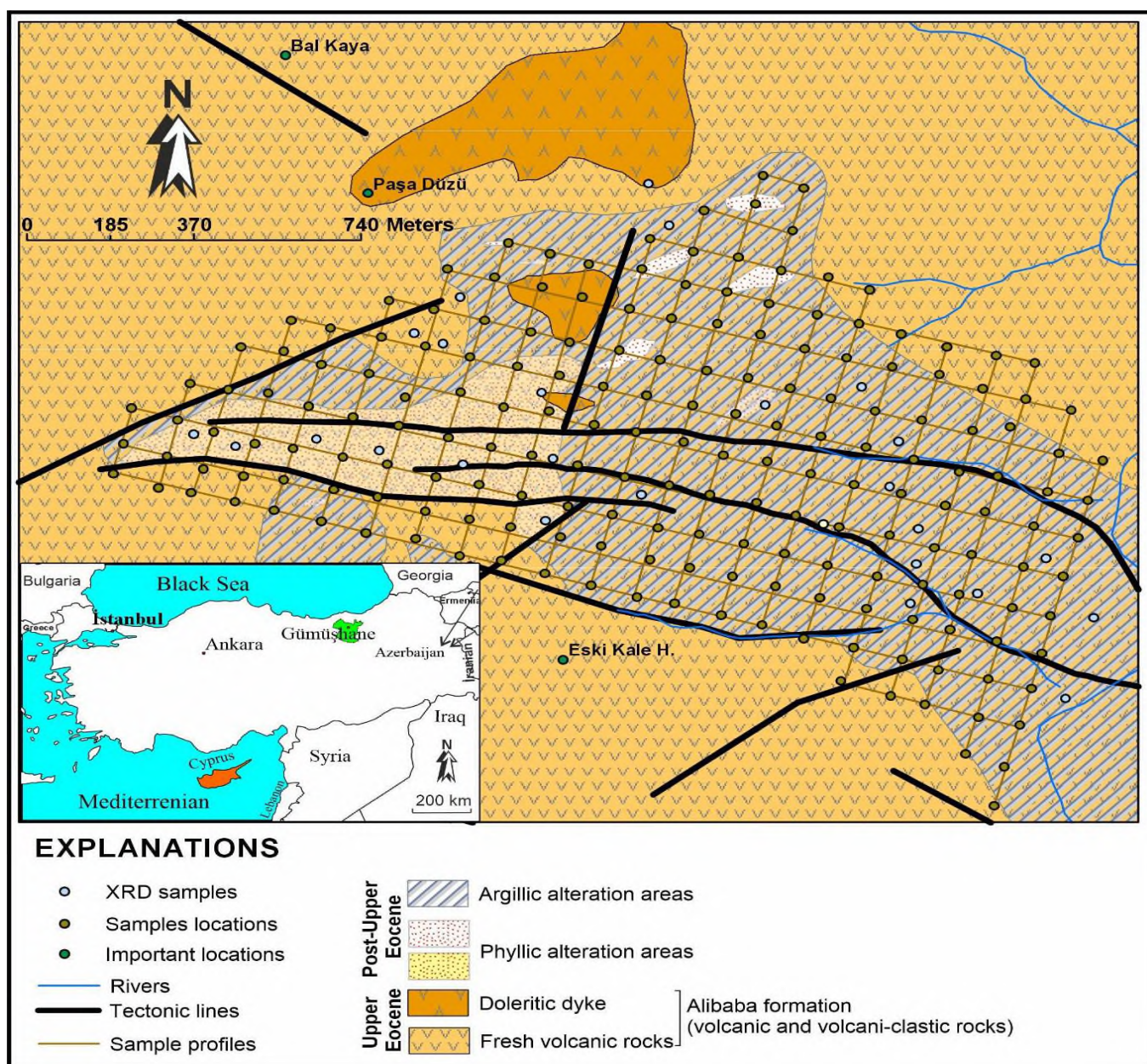


Figure 1. Geological and alteration map of the Canca (Gümüşhane, Türkiye) field [3]

area and its immediate surroundings, the primary rocks of the region consist of metamorphic rocks of the Eastern Black Sea Tectonic Belt and unmetamorphosed granitic plutons intruding them [11–13]. These primary rocks are unconformably cut by Early-Middle Jurassic volcanoclastic rocks (Zimonköy Formation) [14]. The Zimonköy Formation, in turn, is overlain by Late Jurassic-Early Cretaceous carbonate rocks (Berdiga Formation) [15]. The Berdiga Formation is covered by the Late Cretaceous Kermtudere Formation [16]. All of these units are intruded by Late Cretaceous intrusions on the northwest and southwest sides of Gümüşhane, near Torul [17,18]. In different locations northeast and southwest of Gümüşhane, Late Cretaceous volcanics overlay the formations. The Late Cretaceous sedimentary/volcanic/volcano-clastic units are overlain by Eocene volcanic and volcano-clastic units and intruded by coeval granitic rocks [9,19–22].

In the Canca area, the oldest unit is composed of Eocene volcano-clastic rocks (Fig. 1) [23]. These rocks have undergone intense hydrothermal alteration. The alteration in the area is predominantly characterized by argillic and phyllic alteration, and as a result of alteration, a well-developed soil cover of grayish, light brown podzolic type is commonly observed on the surface [4,24]. The youngest units in the region consist of recent travertine, alluvium, and slope debris [25].

2.2. Sample collection, analysis processes, and data evaluation

Sampling was conducted using sessile oak leaves due to the dense oak forest observed in the Canca hydrothermal alteration zone for biogeochemical purposes. A total of 226 plant samples were collected. Sample collection took place within the months of June and July in 2014, and the details of the sampling and analysis processes are provided in Vural [3].

The analyses of oak leaves were carried out at the Central Laboratory of Gümüşhane University using an ICP-MS device (Agilent 7700x ICP-MS, Santa Clara, California, USA). Many elements were measured in sessile oak leaves as part of a project, however, this study focused on Cr, Mn, Fe, Co, Ni, Cu, Zn, As, Sr, Mo, Cd, Sb, Ba, and Pb.

All the chemicals used were analytical reagent grade and were bought from Merck (Darmstadt, Germany). Standard solutions were prepared to construct calibration graphs in ICP-MS by diluting the stock solution with 1000 mg/L concentrations of each metal in appropriate proportions. Polypropylene bottles were used to store standard solutions. Before usage, the vials were immersed in 10% nitric acid overnight, washed with ultrapure water, and finally dried.

The sessile oak leaves were ground into powder. Approximately 0.5 g of the powder samples were weighed and placed in Teflon vessels in a high-pressure and closed-coated microwave oven (Sineo MDS-8, Shanghai, China). After 7 mL of HNO₃ and 3 mL of H₂O₂ were added to the beakers, the contents were digested for approximately 30 minutes. Completely solubilized limpid solutions were finally quantitatively made up to 50 mL with distilled/deionized water and analyzed for the metals they contained by ICP-MS (Inductively Plasma – Mass Spectrometer) and MP-AES (Microwave Plasma – Atomic Emission Spectrometer). Metal concentrations measured in mg/L units in the devices were then converted to mg/kg (ppm) units with Formula 1 [26,27].

$$\text{Concentration (mg/kg, ppm)} = \frac{C \times V \times S}{m} \quad (1)$$

Where, C is the mg/L concentration value measured in aqueous solution in the devices, V is the final volume (mL) completed after microwave solubilization, m is the weighed sample mass (g), and S is the dilution coefficient.

Accuracy/precision tests for the analyses were conducted according to relevant analysis procedures. To test the accuracy of the measurement method, standards of known concentrations were added to the samples at three consecutive levels. Concentrations of spiked samples were measured again by ICP-MS. Recovery percentages for added standard concentrations were calculated from the differences between the measurement results of the sample with spiked standard and the measurement results of the original sample without spiked standard. Spiked/recovery test results were between 92.8–108.0% satisfactory for all metals.

Another accuracy test was conducted by analyzing a certified reference material. The certified results and the measurements taken in this study with ICP-MS were found to be in very good agreement.

Relative standard deviations (RSD) were evaluated for the precision of metal measurements by ICP-MS. The standard deviation of each metal was divided by its average, and the result was multiplied by 100 to calculate the percent RSDs. From the results obtained, it was observed that RSD values varied between 0.7 and 2.8%.

Descriptive statistical parameters for element concentrations were calculated, and the distribution characteristics of the concentrations were attempted to be understood through statistical methods. Since the element contents of oak leaves did not follow a perfect normal distribution, average element concentrations were determined considering median values in an effort to reduce the influence of outliers. Threshold values for

Table 1. The instrumental conditions used for XRD analyses

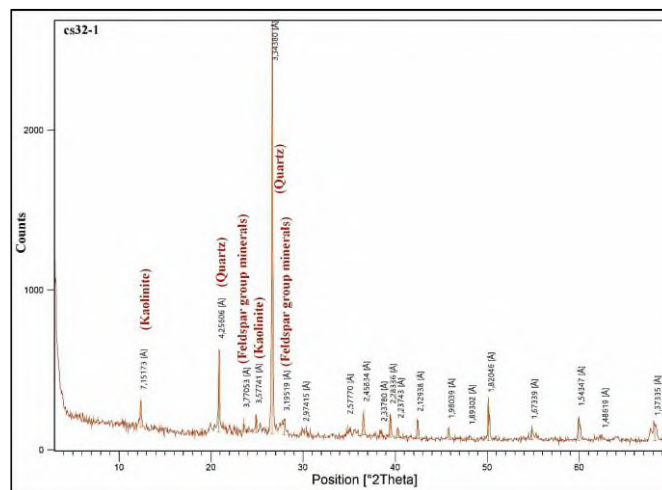
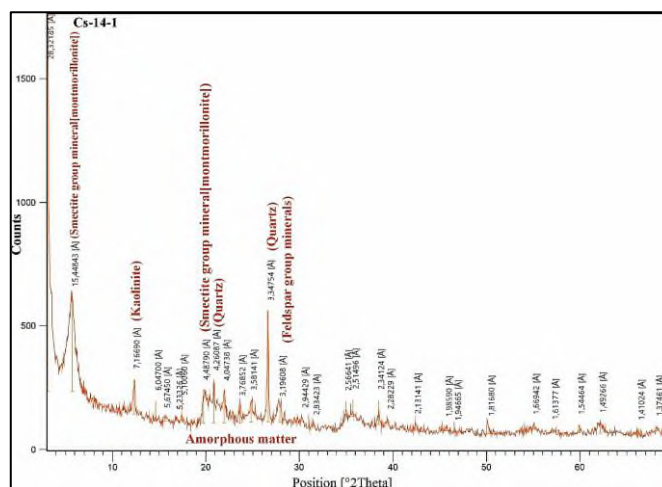
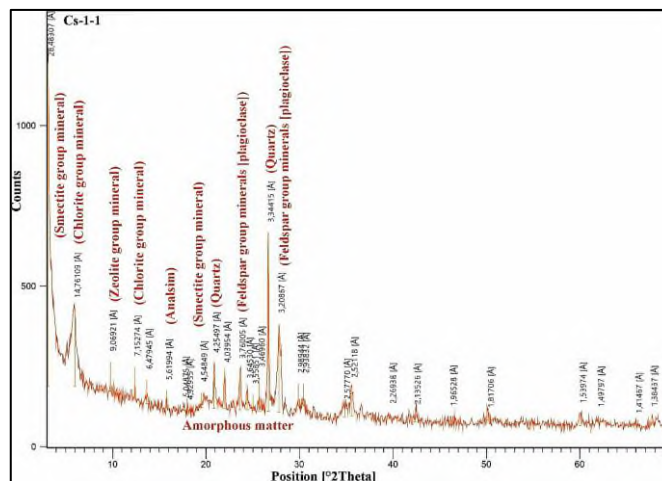
Anode	Cu (CuK α =1.541871 Å)
Filter	Ni
Voltage	35 kV
Goniometer Speed	2°/minute
Paper Speed	2 cm/min
Sensitivity	4.102
Time Constant	1 sn
Slits	1°-0.1mm-1°
Paper Interval	TK 2 θ = 2–70°, KF 2 θ = 2–40°

the elements were determined by adding 2 median absolute deviations (MAD) to the median values [4]. To examine the effect of alteration on oak element accumulation, XRD analyses were conducted considering the alteration patterns in the field, aiming to characterize mineral assemblages typical of alteration suites. XRD analyses were performed at the Mineralogy Petrography Service of the General Directorate of Mineral Analysis and Technology of the MTA. The instrumental conditions used for XRD examinations are summarized in Table 1. In XRD studies, predominantly soil samples, and a small amount of altered rock samples have been used.

3. Results

When evaluating the element concentrations in sessile oak leaves (Cd and Sb in ppb, others in ppm), it was found that Cr concentrations ranged from 0.21 to 8.4 ppm, with a median value of 1.86 ppm. Similarly, Mn ranged from 13.6 to 1374.2 ppm (median: 162.8 ppm), Fe from 50.19 to 990.05 ppm (median: 317.6), Co from 0.05 to 0.89 ppm (median: 0.15 ppm), Ni from 0.33 to 8.75 ppm (median: 2.77 ppm), Cu from 2.85 to 14.64 ppm (median: 5.97 ppm), Zn from 7.37 to 52.53 ppm (median: 19.15 ppm), As from 0.01 to 1.36 ppm (median: 0.14 ppm), Mo from 0.05 to 5.47 ppm (median: 0.71 ppm), Cd from 6.84 to 249.5 ppb (median: 30.21 ppb), Sb from 10.96 to 2364 ppb (median: 95.1 ppb), Ba from 11.5 to 387.34 ppm (median: 113.35 ppm), and Pb from 0.29 to 2.23 ppm (median: 0.83 ppm) [4]. Compared to the literature data from samples collected in areas unaffected by hydrothermal alteration, these concentrations indicate an enrichment in especially Cr, Mn, Co, Ni, Cu, Zn, As, Mo, Sb, Ba, and Pb [3,28].

Based on XRD data and field observations, three types of alteration have been identified in the area: silicification, characterized by pervasive sericitization and pyritization, accompanied by hematite and limonite formations (silicification - phyllic alteration) (Fig. 1 and Fig. 2); argillic alteration, which includes kaolinite, illite, smectite, and alunite (Fig. 1 and Fig. 3). The argillic alteration surrounds the silicified zones and is widespread throughout the field. Silicification is predominantly associated with tectonic lines and fractures, observed

**Figure 2.** XRD pattern of the silicification-phyllitic alteration zone**Figure 3.** XRD patterns of the zones with intense argillic alteration**Figure 4.** XRD patterns of the propylitic alteration areas

mainly in the western and eastern parts of the area in the phyllic zones (Fig. 1 and Fig. 4). These silicified zones are primarily developed due to hydrothermal effects and are influenced by plutonic processes, indicating that mineralizations are likely to develop in these alteration zones.

Argillic alteration areas are predominantly influenced by weathering, developing supergene and indicating lower temperature effects, transitioning to

Table 2. Correlation coefficients (Spearman's rho) between elements in sessile oak leaves

	Cr	Mn	Fe	Co	Ni	Cu	Zn	As	Sr	Mo	Cd	Sb	Ba	Pb
Cr	1.000													
Mn	0.380	1.000												
Fe	0.964	0.412	1.000											
Co	0.662	0.589	0.698	1.000										
Ni	0.518	0.659	0.475	0.544	1.000									
Cu	0.602	0.045	0.641	0.452	0.136	1.000								
Zn	0.250	-0.007	0.286	0.235	-0.047	0.677	1.000							
As	0.627	0.176	0.782	0.482	0.070	0.588	0.325	1.000						
Sr	0.384	-0.065	0.497	0.245	0.063	0.586	0.332	0.632	1.000					
Mo	0.735	0.208	0.816	0.484	0.187	0.639	0.312	0.846	0.707	1.000				
Cd	0.176	0.420	0.228	0.481	0.326	0.312	0.496	0.115	0.019	0.027	1.000			
Sb	0.751	0.464	0.741	0.671	0.394	0.476	0.281	0.456	0.347	0.557	0.307	1.000		
Ba	0.026	0.060	0.003	-0.183	0.212	0.032	-0.116	-0.080	0.303	0.083	-0.188	-0.101	1.000	
Pb	0.548	0.291	0.681	0.551	0.232	0.600	0.507	0.783	0.528	0.651	0.479	0.405	0.048	1.000

propylitic alteration with a lower degree of hydrothermal alteration (Fig. 1 and Fig 4). Propylitic alteration areas predominantly consist of chlorite minerals, smectite group clay minerals, and a small amount of zeolite group minerals. These areas are the least affected by hydrothermal alteration, with weathering also contributing to the alteration. These zones exhibit minimal ore formation and element enrichment.

The relationship between the element contents of sessile oak leaves was examined by calculating the Spearman's rho nonparametric correlation coefficient (Table 2). The Spearman correlation coefficients (Spearman's rho) between the elements in sessile oak leaves indicate the strength and direction of the monotonic relationships between pairs of elements. Positive values suggest a positive correlation, where higher concentrations of one element are associated with higher concentrations of another, while negative values suggest an inverse relationship. Values closer to 1 or -1 indicate stronger correlations.

According to the correlation coefficients, a significant correlation was observed between Cr and Fe, Co, Ni, Cu, As, Mo, Sb, and Pb. Additionally, a notable correlation can be noted between Mn and Co, Ni, suggesting that Mn, Co, and Ni exhibit similar geochemical behaviors, indicating the influence of environmental/parental rock factors in this relationship. Spearman correlation coefficients also reveal a significant correlation between Co and Sb and Pb. Furthermore, a substantial correlation relationship is evident between Cu and As, Sr, Mo, and Pb elements. Moreover, significant correlations are observed between Zn and Cd, Pb; As and Mo, Pb; Mo and Sb, Pb; and Cd and Pb.

3.1. The spatial distributions of plants

Spatial distribution maps of element concentrations in oak leaves were plotted to examine the behavior of elements in relation to the geological environment (Fig. 5). The kriging method was employed in the generation of distribution maps [29], and the spatial

weights of sample points were calculated using the variogram method [30]. The variogram function ($\gamma(h)$) expresses the variance of differences between two randomly separated variables as a function of distance. The semivariogram function is half of the variogram function and is computed by the following equation.

$$\gamma(h) = \frac{1}{2N(h)} \sum_{i=1}^{N(h)} [(x_i) - z(x_i + h)]^2 \quad (2)$$

Here, h denotes the lag distance, $\gamma(h)$ semivariogram, $N(h)$ corresponds to pairs of sample points associated with distance h (Krige, 1951; Matheron, 1963; Yaylılı-Abanuz et al., 2011). Lag distance and $\gamma(h)$ semivariogram are plotted on the semivariogram graph. The purpose is to draw the most appropriate theoretical semivariogram for the experimental semivariogram. The kriging technique facilitates the estimation of variations at unsampled points with close accuracy using the structural components obtained from semivariograms. The kriging value is calculated using the following formula:

$$Z^*(x_o) = \sum_{i=1}^n \lambda_i Z(x_i) \quad (3)$$

Here, $Z^*(x_o)$: represents the unknown and estimated value at point (x_o), $Z(x_i)$ is the data used in the estimation at point (x_o), and λ_i is the weight assigned to these data. The values of variables at points (x_i) = 1 are known, but the weights assigned to them need to be calculated. In the kriging method, these weights should be defined such that the average of the predicted errors is zero and the variance is minimized. The conditions for optimality are expressed as follows:

$$E[Z(x_o) - Z^*(x_o)] = 0 \quad (4)$$

To minimize the variance of the prediction error, the variance $E[Z(x_o) - Z^*(x_o)]$ must be minimized. For interpolation to be unbiased, the sum of weights $\sum_{i=1}^n \lambda_i = 1$, thereby deriving n unknowns and $n+1$ equations. If the multipliers are solved using the Lagrange method, the number of equations equals the number of unknowns.

$$\sum_{i=1}^n \lambda_i \gamma(x_i - x_j) - m = \gamma(x_o - x_j) \quad (5)$$

Where m is the Lagrange multiplier and γ is the variogram value for the distance between points x_i and x_j . The kriging variance is solved from the following equation:

$$\sigma^2 = \sum_{i=1}^n \lambda_i \gamma(x_i - x_j) - m = \gamma(x_o - x_j) \quad (6)$$

Due to its superiority in providing the best linear system of equations for interpolation compared to other techniques, the kriging method is preferred more often (It should also be noted that the inverse distance weighting (IDW) method does not differ significantly from the kriging method). Therefore, the kriging method was applied to the elements Cr, Mn, Fe, Co, Ni, Cu, Zn, As, Sr, Mo, Pb, Cd, Sb, Ba and Pb using data obtained from the semivariogram model (Fig. 5). For the preparation of anomaly maps, the ARCGIS 10.8 program, which is developed for such studies and efficiently applies the theory of semivariogram and kriging method, was utilized. During the drawings, the spherical model of the kriging method was found to be the most suitable, and it was preferred to smooth out the roughness in the maps created by the kriging method. The element distribution maps were also created using the IDW method for the same elements. In general, no significant difference was observed in the distribution maps.

When examining the element distribution maps of sessile oak leaves, it is observed that chromium (Cr) distributions are concentrated in the west, northeast, and east of the field center in the west-east direction. Elevated Cr values were detected in the leaves of trees growing in areas with argillic alteration zones and fresh volcanic rocks transition. Contrary to expectations, lower Cr concentrations were found in areas where dolerite rocks surfaced (Fig. 5).

Mn values are mostly found in the western part of the field within the argillic alteration zone and near the phyllitic zone. Additionally, high Mn values are observed in a small area in the east of the field within the

argillic alteration zone. These enrichments are also thought to be related to tectonism. This is because the higher Mn values along the tectonic line are striking (Fig. 5).

Fe concentrations are high towards the southeast in the center of the field, which is also consistent with the main tectonic line. The distribution of Fe concentrations in the field is not uniform, but it shows a similar pattern to the distribution of Mn. High Fe concentrations are also relatively concentrated within the argillic alteration zone (Fig. 1 and Fig 5).

High Co values are observed in the northeastern part of the field, especially in areas with fresh rocks. Considering the association of high Co concentrations with alteration, it can be said that areas with both argillic and phyllic alteration zones (for the region in question) exhibit high values. For the western and southern parts of the field, high values are more likely associated with argillic alteration (Fig. 5).

The Ni concentrations in oak leaves also show relatively parallel distributions with Mn. High Ni distributions were observed mainly in areas with fresh rocks and in areas subjected to argillic alteration (Fig. 5).

Cu concentration distributions are higher in the northern and eastern parts of the field, within the argillite zone, compared to other parts of the region. The association of Cu enrichments in the eastern section with tectonic faults is also striking. While Zn concentrations overlap with Cu in some points, there is an inverse relationship in some areas, as seen from the distribution maps (Fig. 5 and Fig. 6). Zn enrichments (in the eastern part of the field) are associated with tectonic faults and argillic alteration (Fig. 6).

As distributions are concentrated in a limited area in the field and intensify towards the northwest-southeast direction from the center of the field. The intensification is mainly observed within the argillic zone and tectonic lines.

A high Sr element distribution was also observed in the eastern part of the field where there is tectonic intensity and intense alteration (especially argillic alteration) (in the range of 200370 ppm). In the areas where fresh rocks are exposed, the Sr element exhibits a distribution pattern of small values (in the range of 12–31 ppm) (Fig. 6).

Concentrations of Mo are concentrated in a limited area of the field and in the northern part within the argillic-phyllitic transition zone (Fig. 6). It is also observed that Mo distributions relatively overlap with As distributions.

The Cd distributions in the field are mostly found in fresh rocks and relatively in the argillic alteration zones (up to in the range of 120–250 ppb).

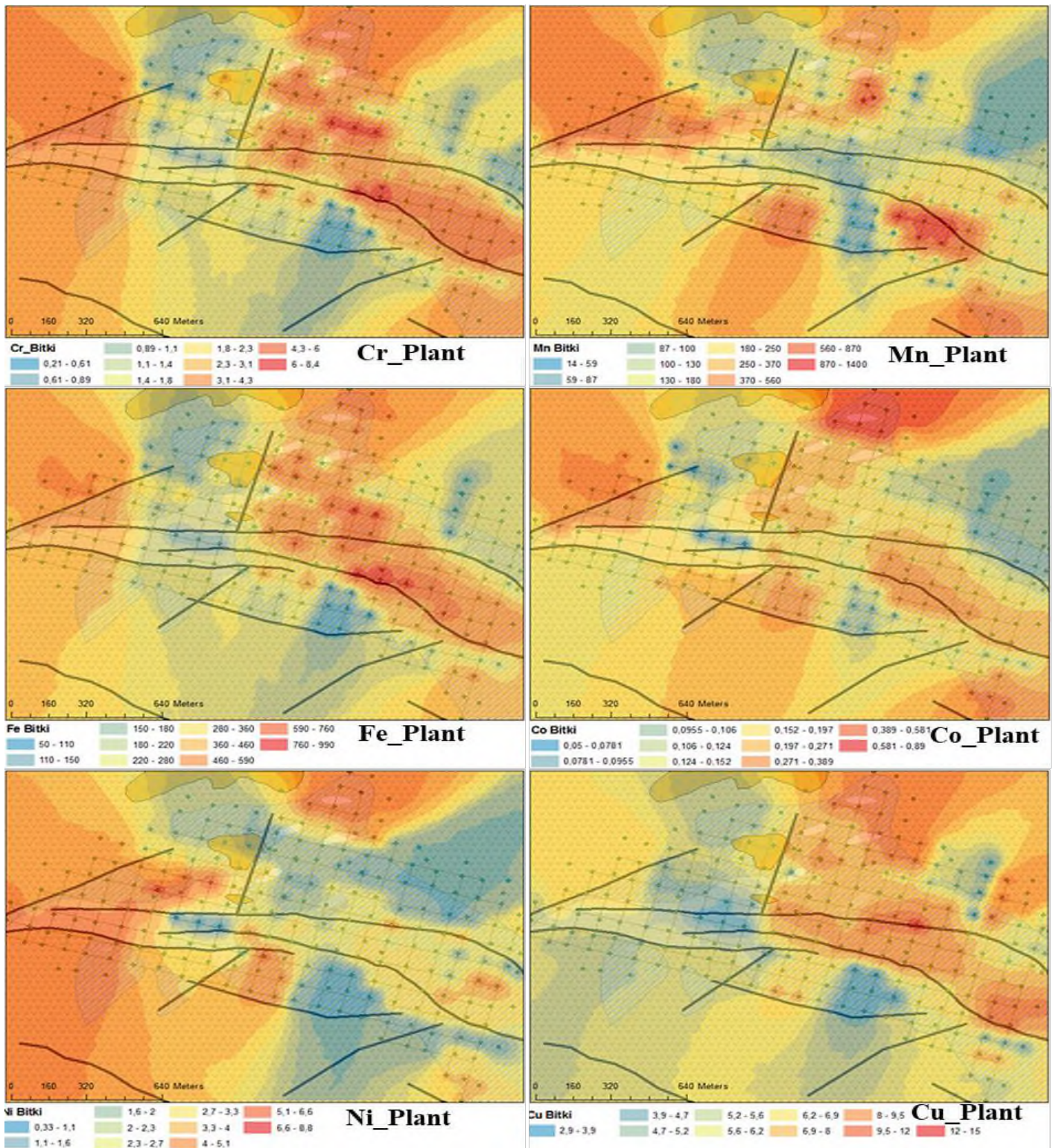


Figure 5. Spatial distribution maps of plant elements Cr, Mn, Fe, Co, Ni and Cu (Refer to Fig. 1 for geological alteration legend explanations)

The high Cd values observed near the Trabzon-Gümüşhane state highway are striking and suggest that traffic may also contribute to the high Cd values in sessile oak leaves (Fig. 6). The presence of high traffic-related Cd values in studies [e.g. 31] conducted in the region further supports this possibility.

Areas with high Sb element concentrations are observed in the southeastern and central parts of the field. High-value Sb (up to in the range of 630–1200 ppb

in the southeastern and up to in the range of 1200–2400 ppb in the central part) areas are particularly striking in areas with argillic alteration and tectonic faults (Fig. 6). The areas in question are also the areas that show high concentration patterns for almost all elements, especially the sampling point in the central part of the field. In addition, relatively high Sb values were also detected in the area where phyllic alteration is surrounded by argillic alteration in the northeast of the field.

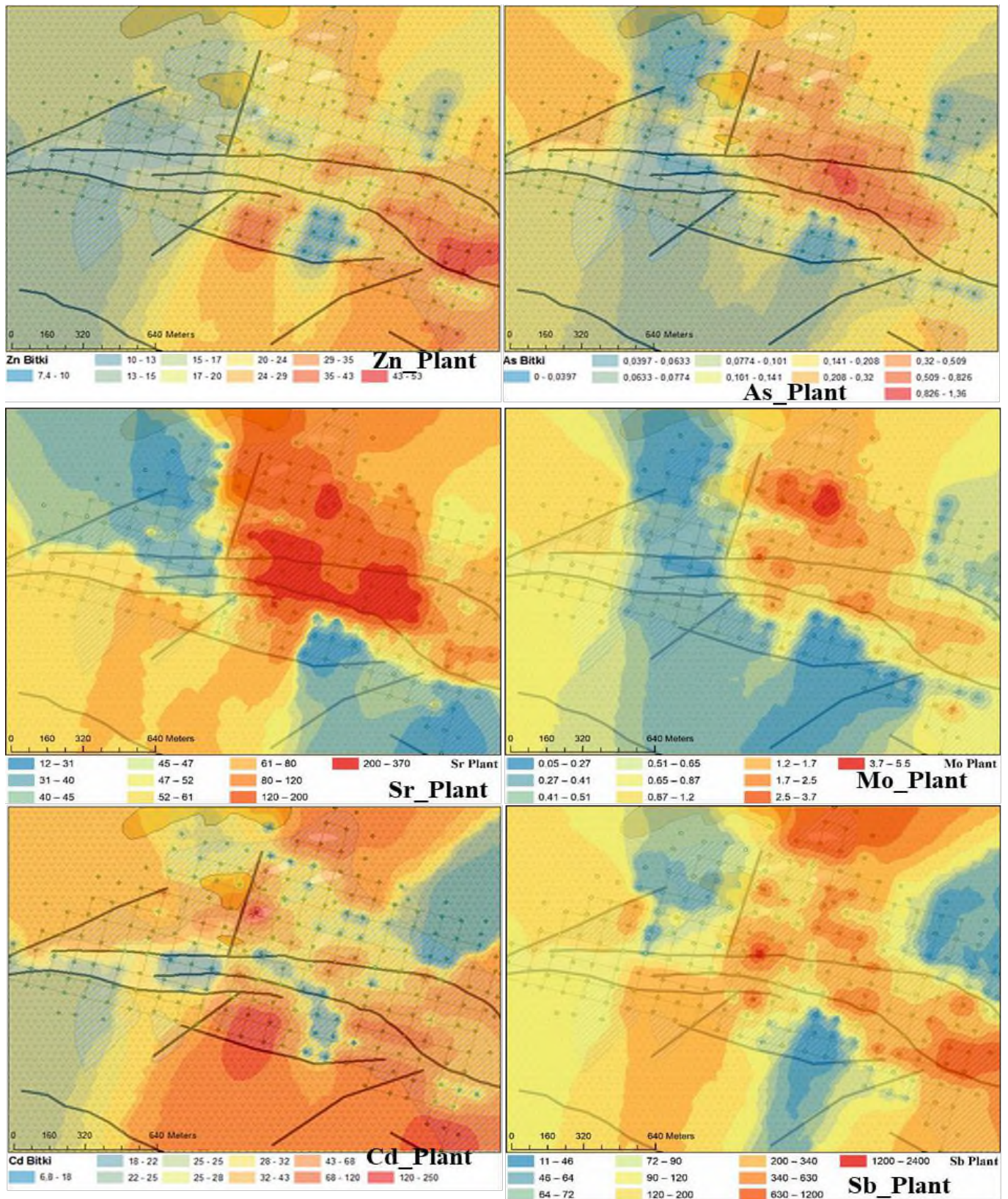


Figure 6. Spatial distribution maps of plant elements Zn, As, Sr, Mo, Cd and Sb (Refer to Fig. 1 for geological alteration legend explanations)

Barium (Ba) element concentrations exhibit high-value patterns in the east of the study area, and parallel to the tectonic fault in the middle of the study area, and again in the west of the study area in the argillic alteration and fresh rock zone associated with the tectonic fault. Ba values in the eastern part of the study area are relatively higher than other parts (Fig. 7).

Lead (Pb) concentrations in sessile oak leaves reach high values (up to 1.4-1.7 ppm) in the argillic alteration zone with intense tectonic faults in the east of the study area. Additionally, high Pb distribution areas associated with the tectonic fault have been identified in the transition zone of fresh rock-argillic alteration in the northwest of the study area (Fig. 7).

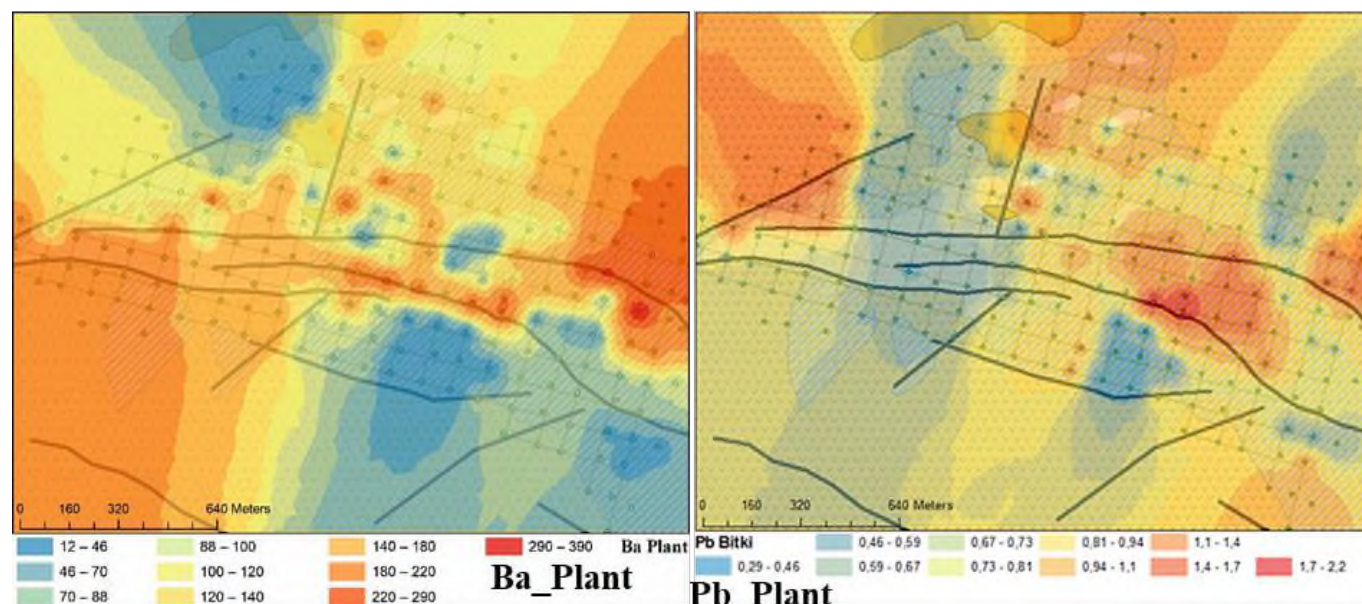


Figure 7. Spatial distribution maps of plant elements Ba and Pb (Refer to Fig. 1 for geological alteration legend explanations)

It has been observed that the concentrations of most elements in the leaves of sessile oak trees growing in the area reach high values associated with alteration and tectonic faults. When comparing the element contents of sessile oak leaves with previous studies [4,28,32,33], it has been observed that the concentrations of elements in altered sections differ from those in unaltered/fresh rock-dominant sections.

4. Conclusions

This study aimed to investigate the relationship between the concentrations of certain trace elements in sessile oak leaves and alteration zones. In this context, element analyses were performed on tree leaves collected from the Canca (Gümüşhane, Türkiye) hydrothermal alteration area. Descriptive statistical evaluations of the element concentrations in the leaves were performed. It was determined that the element concentrations in the leaves were within a wide range and above the values known for sessile oak leaves (and plants in general). Moreover, considering the median values, it was found that sessile oak leaves growing in the area were enriched with the studied trace elements. It was observed that the high element concentrations in the leaves were particularly high in the argillic zones, associated with alteration and tectonic faults (fracture zones) in the field, and that most elements reached higher concentrations compared to fresh rocks. As a result of the study, it was concluded that the element enrichments in the leaves were significantly by the elements Mo, Cu, As, Zn, and Pb, and that there was also a remarkable enrichment by the elements Cr, Mn, Co, Ni, Sb, and Ba.

Acknowledgments

This research was supported by Scientific Research Projects of TÜBİTAK under Grant Number: 113Y569. The author(s) dedicate(s) this study to the Department of Geological Engineering (Ankara Geology) on the occasion of its 90th anniversary in education (1934–2024).

References

- [1] A. Vural, Investigation of the relationship between rare earth elements, trace elements, and major oxides in soil geochemistry, *Environ Monit Assess*, 192 (2020) 124.
- [2] A. Vural, Gold and Silver Content of Plant *Helichrysum Arenarium*, Popularly Known as the Golden Flower, Growing in Gümüşhane, NE Turkey, *Acta Phys Pol A*, 132 (2017) 978–980.
- [3] A. Vural, Canca (Gümüşhane) Alterasyon Sahasında Toprak ve Bitki Jeokimyası Çalışmaları ile Altın Potansiyelinin Araştırılması, Ankara, Türkiye, 2014.
- [4] A. Vural, Assessment of Sessile Oak (*Quercus petraea* L.) Leaf as Bioindicator for Exploration Geochemistry, *Acta Phys Pol A*, 130 (2016) 191–193.
- [5] G. Kirat, N. Aydın, Pb-Zn Accumulation in Plants Grown in and Around a Pb-Zn Mine, *Polish J Environ Stud*, 24 (2015) 545–554.
- [6] G. Kirat, N. Aydın, Phytoremediation with plants for soils polluted by boron at Akdagmadeni Pb-Zn mining district and surroundings, *Yozgat, Turkey, Gazi Univ J Sci*, 29 (2016) 963–970.
- [7] G. Kirat, Investigation of the Biogeochemical Anomalies of *Euphorbia cyparissias* plant in Gümüşhacıköy-Amasya Pb-Zn-Ag Deposits, Turkey, *Indian J Forensic Med Pathol*, 13 (2020).
- [8] A. Vural, S. Kaya, N. Başaran, O.T. Songören, Anadolu Madencilğinde İlk Adımlar, Maden Tetkik ve Arama Genel Müdürlüğü, MTA Kültür Serisi-3, Ankara, Türkiye, 2009.
- [9] A. Vural, A. Kaygusuz, Geochronology, petrogenesis and tectonic importance of Eocene I-type magmatism in the Eastern Pontides, NE Turkey, *Arab J Geosci*, 14 (2021) 467.

- [10] A. Vural, A. Kaygusuz, Petrographic and geochemical characteristics of late Cretaceous volcanic rocks in the vicinity of Avliyana (Gümüşhane, NE Turkey), *J Eng Res Appl Sci*, 10 (2021) 1796–1810.
- [11] G. Topuz, R. Altherr, W. Siebel, W.H. Schwarz, T. Zack, A. Hasözbeke, M. Barth, M. Satir, C. Şen, Carboniferous high-potassium I-type granitoid magmatism in the Eastern Pontides: The Gümüşhane pluton (NE Turkey), *Lithos*, 116 (2010) 92–110.
- [12] A. Kaygusuz, Geochronological age relationships of Carboniferous Plutons in the Eastern Pontides (NE Turkey), *J Eng Res Appl Sci*, 9 (2020) 1299–1307.
- [13] G. Topuz, R. Altherr, W.H. Schwarz, A. Dokuz, H.P. Meyer, Variscan amphibolite-facies rocks from the Kurtoğlu metamorphic complex (Gümüşhane area, Eastern Pontides, Turkey), *Int J Earth Sci*, 96 (2007) 861–873.
- [14] M. Eren, Gümüşhane-Kale Arasının Jeolojisi ve Mikrofasiyesi incelemesi, Karadeniz Teknik Üniversitesi, 1983.
- [15] S. Pelin, Alucra (Giresun) Güneydoğu Yöresinin Petrol Olanakları Bakımından Jeolojik İncelenmesi, Karadeniz Teknik Üniversitesi, 1977.
- [16] S. Tokel, Stratigraphical and volcanic history of Gümüşhane region, 1972.
- [17] A. Kaygusuz, W. Siebel, C. Şen, M. Satir, Petrochemistry and petrology of I-type granitoids in an arc setting: the composite Torul pluton, Eastern Pontides, NE Turkey, *Int J Earth Sci*, 97 (2008) 739–764.
- [18] A. Kaygusuz, Torul ve çevresinde yüzeylenen kayaçların petrografik ve jeokimyasal incelenmesi, Doktora Tezi, Karadeniz Teknik Üniversitesi, Trabzon, 227s, 2000.
- [19] Ç. Saydam Eker, Petrography and geochemistry of Eocene sandstones from eastern Pontides (NE TURKEY): Implications for source area weathering, provenance and tectonic setting, *Geochemistry Int*, 50 (2012) 683–701.
- [20] A. Kaygusuz, M. Öztürk, Geochronology, geochemistry, and petrogenesis of the Eocene Bayburt intrusions, Eastern Pontide, NE Turkey: implications for lithospheric mantle and lower crustal sources in the high-K calc-alkaline magmatism, *J Asian Earth Sci*, 108 (2015) 97–116.
- [21] İ. Temizel, E. Abdioğlu Yazar, M. Arslan, A. Kaygusuz, Z. Aslan, Mineral chemistry, whole-rock geochemistry and petrology of Eocene I-type shoshonitic plutons in the Gököy area (Ordu, NE Turkey), *Bull Miner Res Explor*, 157 (2018) 121–152.
- [22] I. Temizel, M. Arslan, C. Yücel, E. Abdioğlu Yazar, A. Kaygusuz, Z. Aslan, Eocene tonalite–granodiorite from the Havza (Samsun) area, northern Turkey: adakite-like melts of lithospheric mantle and crust generated in a post-collisional setting, *Int Geol Rev*, 62 (2020) 1131–1158.
- [23] A. Kaygusuz, A. Arslan, W. Siebel, C. Şen, Geochemical and Sr-Nd Isotopic Characteristics of Post-Collisional Calc-Alkaline Volcanics in the Eastern Pontides (NE Turkey), *Turkish J Earth Sci*, 20 (2011) 137–159.
- [24] A. Vural, Hidrotermal Alterasyona Bağlı Element Kirliliği : Canca (Gümüşhane - Türkiye), *J Investig Eng Technol*, 5 (2022) 87–103.
- [25] A. Vural, G. Külekçi, Zenginleştirilmiş Jeoturizm Güzergahı:Gümüşhane-Bahçecik Köyü, *Euroasia J Math Eng Nat Med Sci*, 8 (2021) 1–23.
- [26] B. Karayigit, N. Colak, F. Ozogul, A. Gundogdu, H. Inceer, N. Bilgiçli, F.A. Ayaz, The biogenic amine and mineral contents of different milling fractions of bread and durum wheat (*Triticum L*) cultivars, *Food Biosci*, 37 (2020) 100676.
- [27] A. Kurt, N. Colak, A. Bengu, A. Gundogdu, E. Akpınar, S. Hayirlioglu-Ayaz, F.A. Ayaz, A nutritional evaluation of the berry of a new grape: "Karaerik" (*Vitis vinifera L*), *Int J Food Stud*, 7 (2018) 98–116.
- [28] J.Y. Park, S.H. Jeon, J.N. Kim, H.T. Chon, A biogeochemical orientation study in Mo skarn deposits, Jecheon district in Korea, *J Geochemical Explor*, 146 (2014) 9–16.
- [29] D.G. Krige, A statistical Approach to Some Basic Mine Valuation Problems on the Witwatersrand, *J Chem Metall Soc South Min Africa*, 52 (1951) 119–139.
- [30] G. Matheron, Principles of geostatistics, *Econ. Geol.*, 58 (1963) 1246–1266.
- [31] A. Vural, Assessment of Heavy Metal Accumulation in the Roadside Soil and Plants of *Robinia pseudoacacia*, in Gumushane, Northeastern Turkey, *Ekoloji*, 22 (2013) 1–10.
- [32] C. Anjos, C.M.F. Magalhaes, M.M. Abreu, Metal (Al, Mn, Pb and Zn) soils extractable reagents for available fraction assessment: Comparison using plants, and dry and moist soils from the Braçal abandoned lead mine area, Portugal, *J Geochemical Explor*, 113 (2012) 45–55.
- [33] H. Turan, Z. Özdemir, S. Zorlu, Çiftelhan (Ulukışla-Niğde) Bölgesinin Biyoeokimyasal Anomalilerinin Araştırılması, İstanbul Üniversitesi Mühendislik Fakültesi Yerbilim Derg, 19 (2006) 131–140.



Determination of trace heavy metals content of various herbal drinks marketed in Ilorin Metropolis, Nigeria

S. W. Olokoba 

Kwara State University, Department of Chemistry and Industrial Chemistry, Malete, PMB 1530, Ilorin, Kwara State, Nigeria

Abstract

The study encompasses an evaluation of the health risk and hazard profiles of heavy metals contents in various herbal drinks (AGBO) products marketed in Ilorin metropolis, Nigeria. Twenty herbal drinks samples from four (4) different study (saw-mil, Osere, Oja-oba and Oke-odo) areas were collected randomly, digested and analyzed. Zinc, Lead, Copper, Iron, Manganese, Cadmium, Chromium and Nickel were analyzed using Atomic Absorption Spectrometer. The results of this study indicated that most of the heavy metals (Zn, Pb, Cu and Mn) in the herbal drinks were below the WHO recommended permissible limits. Chromium (Cr) and Cadmium (Cd) are not detected in all of the herbal drinks analyzed. However, sample C2 and D2 among other analyzed herbal samples contained unsafe concentrations of iron (Fe) and nickel (Ni) that exceeded the WHO recommended permissible limits. From the health point of view, the EDIs value of all the herbal drinks are below the daily reference dose. The non-carcinous (HQ) and hazard index (HI) value of all the herbal samples are less than one (1). Based on the results obtained in this study, there would be a non-carcinogenic health risk and hazard effects to the people taking and consuming the herbal drinks marketed in all the study areas.

Keywords: Herbal product, heavy metals, estimated daily intakes EDIs, non-carcinous HQ, hazard index

1. Introduction

The use of Herbal remedies or consumptions is presently prevalent all over the world. They are widely used as an active part in the prevention, management as well as treatment of various ailments and illnesses such as fever, pain, headache, diabetes, hypertension, rheumatism, and many others [1]. According to World Health Organization (WHO), approximately 70–80% of the global population still primarily rely on traditional medications, from herbal based products to orthodox for basic health care. The utilization of many herbal medicines for improving well-being is gaining popularity around the world due to its low cost, availability, lesser side effects, affordability and enhanced effectiveness. Also, because of poverty and limited access to modern medicine among other reasons [2]. The safety and quality of herbal medicinal plants during germination and growth are determined by several factors which include climatic conditions, seed selection, fertilizers application, harvesting and storage. Factors such as industrialization, the use of fertilizers, ineffective pollution control and pesticide residues and inconsiderate extraction method and handling are some

of the factors which largely contribute to contamination of herbal products with pollutants such as heavy metals which can significantly affect and alter properties, efficacy and the quality of the herbal medicinal plants and their formulations [3,4]. The bio-accumulation of Heavy metals by the herbal plants from the soil can be highly toxic to human health and may cause serious health hazards such as decrease in immunological defenses, renal failure, gastrointestinal cancer, impaired psychological, cardiac dysfunction, fetal malformation and neurological behavior [5]. In many Africa countries such as Nigeria, most herbal traders sell their products along busy traffic urban centers [6]. These Herbal drinks are displayed outside their shops and stores exposing them to air-borne heavy metals contamination [7]. The precise knowledge of amount of Heavy metals concentration present in herbal product is important for the estimation of whether the ingested heavy metal concentration will be within the WHO PL values or not [8]. The WHO has formulated guidelines for quality assurance and control of herbal medicine, but most traditional practitioners lack this information. There are

Citation: S. W. Olokoba, Determination of trace heavy metals content of various herbal drinks marketed in Ilorin Metropolis, Nigeria, Turk J Anal Chem, 6(2), 2024, 71–77.

 <https://doi.org/10.51435/turkjac.1493128>

Author of correspondence: sulemanolokoba@gmail.com

Received: May 31, 2024

Tel: +234 (816) 508 61 81

Accepted: July 12, 2024

Fax: N/A

many research papers dealing with heavy metals content in herbal product to determine their safe daily intake, but few of them are reported [9]. Recently, a lot of cases of health risk from heavy metals such as manganese, lead, iron, cadmium and mercury remain underreported while some are not recorded due to poor bookkeeping in the developing countries [10].

The accurate determination of heavy metals using analytical method in herbal plants is vital as they have a narrow range of quality and safety between adequate levels and excessive intake of the herbal products. Among the various analytical methods used for heavy metals analysis in herbal plants, Atomic Absorption Spectrometry (AAS) is one of the most frequently used because of its simplicity, low detection limits, low volume requirements [11]. Therefore, there's a need for more studies in examining the safety and quality of the herbal products. Therefore, this research study focused on determination of Heavy metals contents in various herbal drinks products marketed within Ilorin metropolis, Nigeria. The objectives of the study were: (1) to determine the concentrations of Heavy metals in selected herbal drinks products in various locations in Ilorin, (2) to calculate the average estimated daily intake of heavy metals in herbal drinks samples and (3) to assess the non-cancerous risk and potential health hazard of the consumption of these herbal drinks products based on the World Health Organization (WHO) standard limit.

2. Materials and methods

2.1. Sample collection

The samples were collected in four different areas which includes; Saw mill, Osere, Oja-oba area and Oke-odo area and as label as sample areas A, B, C, D respectively. The herbal drinks that were gotten from this study areas are; malaria herb (Iba), All-purpose herb (gbogbo leshe), Deidra herb (jedi-jedi), Typhoid herb, Back pain herb (opa-eyin), Manhood power (Ale). The samples collected are used in the treatment of typhoid, fever, back pain, headache, body pain, malaria. The herbal drinks samples were collected into a clean bottles and labeled accordingly so as to avoid error or confusion among the samples. The experimental work for the determination of heavy metals in herbal drinks was conducted at the Chemistry Department Laboratory of the University of Ilorin, Ilorin, Nigeria. The samples collection areas, locations coordinates, sample code and their traditional use are presented in Table 1. The samples were then kept in a dry place of 10°C before being taken for analysis.

2.1.1. Sample preparation and digestion

All reagents and solvents, including nitric acid, hydrochloric acid and deionized water, were of the analytical reagent grade and was purchased from Sigma Aldrich. The digestion procedure employed for the elements (except Hg) was as described by [12] with little modification. The project was carried out using an Aqua-regia method in ratio (3:1) of HCl and HNO₃ respectively. 2.0 g of the herbal drinks (Agbo) was accurately measured into a conical flask, 15 mL concentrated nitric acid was added followed by 5 mL concentrated hydrochloric acid. The flask was closed and left for 15 minutes to ensure complete reaction. The mixture was heated for about 150°C until no browner fumes were produced. The samples solution was then cooled, and 50 mL of deionized water were added. The solution was filtered through whatmann filter paper No. 1 into a 100 mL volumetric flask and diluted to a volume with deionized water and pour into a sample bottles before taken for analysis.

2.1.2. Sample Analysis

Digest samples were analyzed for Zn, Pb, Cu, Fe, Cd, Mn, Cr and Ni using BUCK Scientific (ACCUSYS 211) atomic Absorption spectrophotometer (AAS). The 1000 ppm standard solutions of elements were diluted in five different concentrations to obtain calibration curve for quantitative analysis. All the measurements were run in triplicate for the sample and standard solutions.

2.2. Data analyses and evaluation methods

Statistical and data analysis was carried out on the results obtained in order to enhance data interpretation. The statistical data were analyzed using Microsoft Excel 2019. The concentration results of heavy metals were calculated as mean \pm standard deviation ($\mu\text{g/L}$) of triplicate analysis.

2.3. Health risk and hazard evaluation of heavy metals.

In order to fully assess the health risk and Hazard of heavy metals in the herbal products, various evaluation methods are employed such as Estimated Daily Intake (EDI) of metal, Hazard Quotient (HQ), and Hazard Index (HI) [13].

2.3.1. The estimated daily intake dose (EDI)

The EDI of Zn, Pb, Cu, Fe, Mn, and Ni were calculated to estimate the average daily intake or consumption of heavy metals to a specified bodyweight, according to the mean concentrations of each heavy metal in the herbal products and the consumption rate as described by [13–15], in the Equation 1:

$$EDI = \frac{C_{HM} \times AIR}{BW_{average}} \quad (1)$$

Table 1. Study locations coordinates, samples code and traditional use

Collection area	Latitude	Longitude	Sample Code	Traditional use
Saw-mill (Ilorin west) area	8.4707° N	4.52620° E	A1	Malaria (Iba)
			A2	All-Purpose Herbs (Gbogbo Leshe)
			A3	Pile (Jedi-jedi)
			A4	Typhoid
			A5	Back Pain Herbs (Opa-eyin)
			A6	Manhood Power (Ale)
Osere (Ilorin West) area	8.09142° N	4.63767° E	B1	Malaria (Iba)
			B2	All-Purpose Herbs (Gbogbo Leshe)
			B3	Pile (Jedi-jedi)
			B4	Typhoid
			B5	Back Pain Herbs (Opa-eyin)
			B6	Manhood Power (Ale)
Oja-oba (Ilorin West) area	8.4760° N	4.4560° E	C1	Malaria (Iba)
			C2	Pile (Jedi-jedi)
			C3	Typhoid
			C4	Back Pain Herbs (Opa-eyin)
			C5	Manhood Power (Ale)
Oke-odo (Ilorin south) area	8.4799° N	4.5418° E	D1	Malaria (Iba)
			D2	Pile (Jedi-jedi)
			D3	Typhoid

Where: C_{HM} = the concentration of heavy metals in the herbal products in mg/L. A_{IR} = the average ingestion rate or daily intake of herbal products in kg, An average daily consumption or ingestion rate of 0.01 kg of herbal products was assumed in this study. $BW_{average}$ = average body weight in kg per person. The average body weight of an adult was considered to be 60 kg. This method was used because herbal products are widely consumed as a major part of the diet.

2.3.2. Hazard quotient (HQ)

Hazard Quotient was used to evaluate the non-carcinogenic risks to humans from long-term consumption of heavy metals from herbal products, according to [16]. The HQ is the ratio of the calculated dose to the oral reference dose as described by [16], in the Equation 2:

$$HQ = \frac{EDI}{Rf_{Do}} \quad (2)$$

where EDI = average estimated daily intake or consumption of herbal products in (mg/L day⁻¹) and

Table 2. LOD, Reference dose used in this study & WHO recommended PL [18–20]

Heavy metal	LOD (µg/L)	LOQ (µg/L)	RfDo (µg/L)	WHO PL (µg/L)
Zn	0.008	0.079	300.00	5000.00
Pb	0.060	0.57	40.00	10.00
Cu	0.02	0.15	700.00	2000.00
Fe	0.045	0.45	140.00	100.00
Mn	0.03	0.28	20.00	40.00
Cd	—	—	3.50	30.00
Cr	—	—	5.00	50.00
Ni	0.006	0.058	3.00	20.00

Rf_{Do} = reference dose of each heavy metal in (mg/kg day⁻¹), which is an average daily tolerable consumption or intake to which a person is expected to have without any significant health risk effects for a long period of time. The following reference doses of heavy metals used and WHO recommended permissible limits in this study are presented in (Table 2). HQs of heavy metals in herbal products were evaluated according to the procedure described by the Environmental Protection Agency (EPA) [17]. If HQ is < 1 indicate no potential health risks effects due to herbal product consumption, while HQ is > 1 indicate that there are potential health risks and hazard due to consumption or intake of herbal product.

2.3.3. Hazard index (HI)

Hazard Index (HI) was used to calculate the total value of non-carcinogenic risks to human health causing by all heavy metal in herbal product. It is also the summation of the hazardous quotient (HQ) of each heavy metal detected in the herbal product as described in the Equation 3: [16, 21].

$$HI = \sum_{n=1}^{m=8} THQ_i \quad (3)$$

HQ < 1, indicate there is no possibility of adverse health risk effects on human [22,23].

2.4. Quality control

The % recovery evaluation was carried out using the Equation 4.

$$\% \text{ recovery} = \frac{\text{spiked} - \text{unspiked}}{\text{spiked}} \times 100 \quad (4)$$

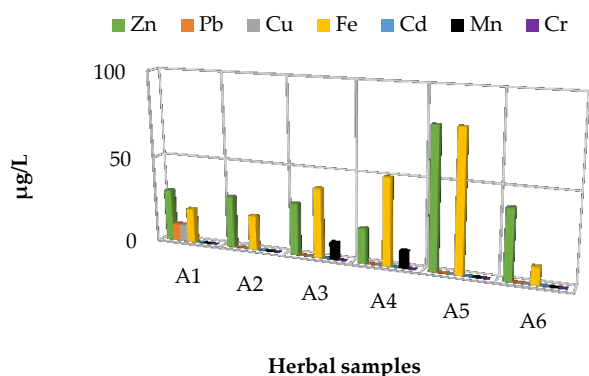


Figure 1. concentration of heavy metals in Saw-mill (A) study area

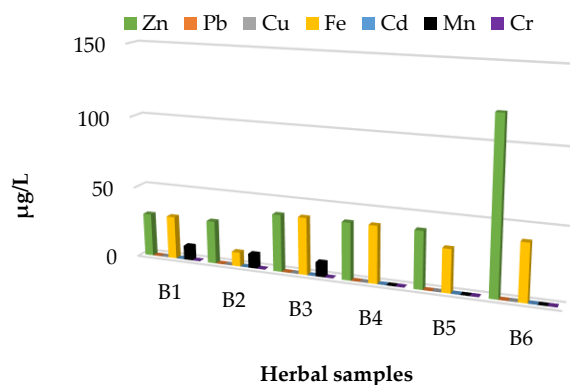


Figure 2. concentration of heavy metals in Osere (B) study area

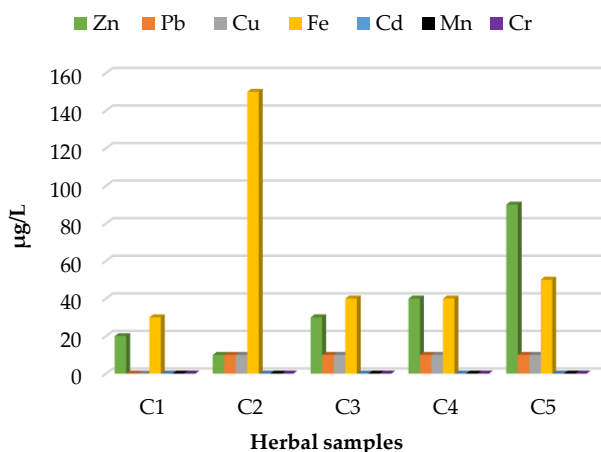


Figure 3. Concentration of heavy metals in Oja-oba (C) study area

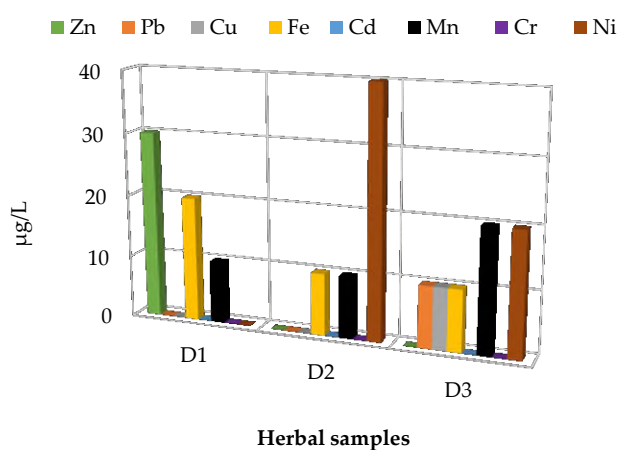


Figure 4. concentration of heavy metals in Oke-odo (D) study area

This was performed by calculating the concentration levels of the heavy metals in herbal drink of spiked and un-spiked samples, and the mean % recovery of the heavy metals ranging from 87 to 103 % were obtained.

2.4.1. Limits of detection (LOD) and quantification (LOQ)

The limit of detection was evaluated by using Perkin Elmer method. A sample solution of 10 µg/L of all the study heavy metals were aspirated and the intensities for these metals and blank are calculated and their LOD were recorded (Table 2). The limit of quantification was considered as an acceptable level of accuracy. In order to calculate the LOQ, the standard sample solution of 0.1 µg/L of all the study metals were prepared and aspirated in the AAS system. LOQ is considered to be approximately ten times the minimum of LOD.

3. Result and discussions

3.1. Determination of heavy metals in various herbal samples

The results of the heavy metals (Zn, Cu, Pb, Fe, Cd, Mn, Cr and Ni) concentration in the six (6) common herbal products in various locations in Ilorin metropolis are presented in the (Table 3 and Fig.1–Fig.4). The minimum and maximum mean concentration of heavy metals in the herbal product samples are; Zn (10.00 – 120.00 µg/L), Pb (0.00 - 10.00 µg/L), Cu (0.00 - 10.00 µg/L), Fe (10.00 –

150.00 µg/L), Mn (10.00 – 20.00 µg/L) and Ni (20.00 – 40.00 µg/L). The results showed that the concentration of all metals detected in the herbal samples are below the WHO recommended permissible limits, except iron (Fe) and nickel (Ni) in C2 and D2 herbal samples respectively. However, the concentration levels of all the study heavy metals were slightly comparable to the data reported by [24], which revealed the heavy metal concentration levels of commonly consumed herbal bitters in Ilorin, Nigeria. His research showed that majority of the herbal samples contained heavy metals concentrations significantly lower than the permissible limits. The concentration of nickel (Ni) was 20.00 µg/L and it's WHO permissible limits was (20.00 µg/L). Iron metal (Fe) has the highest concentration value in C2 sample product its average value was of 150.00 µg/L, this shows an indication that the herbal product was a little bit contaminated with iron (Fe) above WHO permissible limits of (10.00 µg/L). Zinc (Zn) has the highest concentration in B2 herbal sample, its mean concentration value was 120.00 µg/L. Both zinc (Zn) and iron (Fe) have the highest concentrations in A5 herbal sample, their mean concentrations were 80.00 µg/L in A5 herbal sample. The results of this study however show lower concentrations of zinc (Zn) and iron (Fe) when compared with the work of [25], after they assessed the heavy metals (Fe, Zn, Pb, Cd, Cr, Cu, Mn, and As) hazard from Nigerian spices and the concentrations of zinc and

Table 3. Concentration of heavy metals in herbal samples in different study area

Sample Code	Zn (µg/L)	Pb (µg/L)	Cu (µg/L)	Fe (µg/L)	Cd (µg/L)	Mn (µg/L)	Cr (µg/L)	Ni (µg/L)
A1	30.00 ± 0.002	10.00 ± 0.02	10.00 ± 0.002	20.00 ± 0.06	ND	ND	ND	ND
A2	30.00 ± 0.001	0.00 ± 0.00	ND	20.00 ± 0.06	ND	ND	ND	ND
A3	30.00 ± 0.001	ND	ND	40.00 ± 0.08	ND	10.00 ± 0.02	ND	ND
A4	20.00 ± 0.001	ND	0.00 ± 0.00	50.00 ± 0.10	ND	10.00 ± 0.01	ND	ND
A5	80.00 ± 0.004	ND	ND	80.00 ± 0.10	ND	ND	ND	ND
A6	40.00 ± 0.008	ND	ND	10.00 ± 0.05	ND	ND	ND	ND
B1	30.00 ± 0.002	ND	ND	30.00 ± 0.02	ND	10.00 ± 0.02	ND	ND
B2	30.00 ± 0.001	ND	ND	10.00 ± 0.03	ND	10.00 ± 0.01	ND	ND
B3	40.00 ± 0.002	ND	ND	40.00 ± 0.08	ND	10.00 ± 0.01	ND	ND
B4	40.00 ± 0.01	ND	ND	40.00 ± 0.02	ND	ND	ND	ND
B5	40.00 ± 0.01	ND	ND	30.00 ± 0.06	ND	ND	ND	ND
B6	120.00 ± 0.08	ND	ND	40.00 ± 0.04	ND	ND	ND	ND
C1	20.00 ± 0.02	ND	ND	30.00 ± 0.09	ND	ND	ND	ND
C2	10.00 ± 0.01	10.00 ± 0.06	10.00 ± 0.01	150.00 ± 0.012	ND	ND	ND	ND
C3	30.00 ± 0.01	10.00 ± 0.01	10.00 ± 0.04	40.00 ± 0.004	ND	ND	ND	ND
C4	40.00 ± 0.01	10.00 ± 0.01	10.00 ± 0.02	40.00 ± 0.008	ND	ND	ND	ND
C5	90.00 ± 0.15	10.00 ± 0.03	10.00 ± 0.01	50.00 ± 0.006	ND	ND	ND	ND
D1	30.00 ± 0.02	ND	ND	20.00 ± 0.001	ND	10.00 ± 0.01	ND	ND
D2	ND	ND	ND	10.00 ± 0.001	ND	10.00 ± 0.01	ND	40.00 ± 0.002
D3	ND	10.00 ± 0.01	10.00 ± 0.002	10.00 ± 0.004	ND	20.00 ± 0.002	ND	20.00 ± 0.001

ND = not detected; Values: means ± S.E.M (n=3)

iron in all the spices samples was relatively high when compared with other heavy metals present in different samples. Lead (Pb), copper (Cu) and Manganese (Mn) have the lowest concentrations in the samples, their average mean concentrations were within 10.00–20.00 µg/L. Hence, all the herbal samples characterized were below WHO recommended permissible limit which was comparable to the results of [26] research report of different samples of herbal products marketed in Saudi Arabia, with the concentration levels of study heavy metals within the WHO recommended permissible limit [25]. Except for iron (Fe) and nickel (Ni), they may be contaminated due to anthropogenic activities during drying or preparation processes, which are considered a

health risk if they are consumed and may cause damage to lung and blood circulation. Recent studies have revealed that when people take above the permissible safe limit of nickel and iron, either from orthodox or traditional herbal products, untoward reactions may occur [24]. Lead (Pb) and copper (Cu) are not detected in all Osere (B1, B2, B3, B4, B5, B6) herbal samples, manganese (Mn) is not detected in all Oja-oba (C1, C2, C3, C4, C5) herbal samples and nickel is only detected in Oke-odo (D2 & D3) herbal samples. Meanwhile, cadmium (Cd) and chromium (Cr) were not detected in all the herbal product samples in the study areas.

Table 4. The estimated daily intake (EDI) for heavy metals in herbal samples

Sample Code	Estimate Daily Intake (EDI)					
	Zn	Pb	Cu	Fe	Mn	Ni
A1	0.000005	1.66667 × 10 ⁻⁰⁶	1.67 × 10 ⁻⁰⁶	6.67 × 10 ⁻⁰⁶	0	0
A2	0.000005	0	0	3.33 × 10 ⁻⁰⁶	0	0
A3	0.000005	0	0	6.67 × 10 ⁻⁰⁶	1.67 × 10 ⁻⁰⁶	0
A4	3.33 × 10 ⁻⁰⁶	0	0	8.33 × 10 ⁻⁰⁶	1.67 × 10 ⁻⁰⁶	0
A5	1.33 × 10 ⁻⁰⁵	0	0	1.33 × 10 ⁻⁰⁵	0	0
A6	6.67 × 10 ⁻⁰⁶	0	0	1.67 × 10 ⁻⁰⁶	0	0
B1	0.000005	0	0	0.000005	1.66667 × 10 ⁻⁰⁶	0
B2	0.000005	0	0	1.66667 × 10 ⁻⁰⁶	1.66667 × 10 ⁻⁰⁶	0
B3	6.67 × 10 ⁻⁰⁶	0	0	6.66667 × 10 ⁻⁰⁶	1.66667 × 10 ⁻⁰⁶	0
B4	6.67 × 10 ⁻⁰⁶	0	0	6.66667 × 10 ⁻⁰⁶	0	0
B5	6.67 × 10 ⁻⁰⁶	0	0	0.000005	0	0
B6	0.000002	0	0	6.66667 × 10 ⁻⁰⁶	0	0
C1	3.33 × 10 ⁻⁰⁶	0	0	0.000005	0	0
C2	1.67 × 10 ⁻⁰⁶	1.66667 × 10 ⁻⁰⁶	1.67 × 10 ⁻⁰⁶	0.000025	0	0
C3	0.000005	1.66667 × 10 ⁻⁰⁶	1.67 × 10 ⁻⁰⁶	6.66667 × 10 ⁻⁰⁶	0	0
C4	6.67 × 10 ⁻⁰⁶	1.66667 × 10 ⁻⁰⁶	1.67 × 10 ⁻⁰⁶	6.66667 × 10 ⁻⁰⁶	0	0
C5	0.000015	1.66667 × 10 ⁻⁰⁶	1.67 × 10 ⁻⁰⁶	8.3333 × 10 ⁻⁰⁶	0	0
D1	0.000005	0	0	3.3333 × 10 ⁻⁰⁶	1.66667 × 10 ⁻⁰⁶	0
D2	0	0	0	1.66667 × 10 ⁻⁰⁶	1.66667 × 10 ⁻⁰⁶	6.66667 × 10 ⁻⁰⁶
D3	0	1.66667 × 10 ⁻⁰⁶	1.67 × 10 ⁻⁰⁶	1.66667 × 10 ⁻⁰⁶	3.33333 × 10 ⁻⁰⁶	3.33333 × 10 ⁻⁰⁶

Table 5. The non-carcinogenic hazard quotient (HQ) and hazard index (HI) of heavy metals in the herbal samples.

Sample Code	Target Hazard Quotient (THQ)						Hazard Index (HI)
	Zn	Pb	Cu	Fe	Mn	Ni	
A1	1.67×10^{-05}	0.00047619	4.17×10^{-05}	9.5238×10^{-06}	0	0	0.000544048
A2	1.67×10^{-05}	0	0	4.7619×10^{-06}	0	0	2.14286×10^{-05}
A3	1.67×10^{-05}	0	0	9.5238×10^{-06}	1.19048×10^{-05}	0	3.80952×10^{-05}
A4	1.11×10^{-05}	0	0	1.1905×10^{-05}	1.19048×10^{-05}	0	3.49206×10^{-05}
A5	4.44×10^{-05}	0	0	1.9048×10^{-05}	0	0	6.34921×10^{-05}
A6	2.22×10^{-05}	0	0	2.381×10^{-06}	0	0	2.46032×10^{-05}
B1	1.67×10^{-05}	0	0	7.1429×10^{-06}	1.19048×10^{-05}	0	3.57143×10^{-05}
B2	1.67×10^{-05}	0	0	2.381×10^{-06}	1.19048×10^{-05}	0	3.09524×10^{-05}
B3	2.22×10^{-05}	0	0	9.5238×10^{-06}	1.19048×10^{-05}	0	4.36508×10^{-05}
B4	2.22×10^{-05}	0	0	9.5238×10^{-06}	0	0	3.1746×10^{-05}
B5	2.22×10^{-05}	0	0	7.1429×10^{-06}	0	0	2.93651×10^{-05}
B6	6.67×10^{-05}	0	0	9.5238×10^{-06}	0	0	7.61905×10^{-05}
C1	1.11×10^{-05}	0	0	7.1429×10^{-06}	0	0	1.8254×10^{-05}
C2	5.56×10^{-06}	0.00047619	4.17×10^{-05}	3.5714×10^{-05}	0	0	0.000559127
C3	1.67×10^{-05}	0.00047619	4.17×10^{-05}	9.5238×10^{-06}	0	0	0.000544048
C4	2.22×10^{-05}	0.00047619	4.17×10^{-05}	9.5238×10^{-06}	0	0	0.000549603
C5	0.00005	0.00047619	4.17×10^{-05}	1.1905×10^{-05}	0	0	0.000579762
D1	1.67×10^{-05}	0	0	4.7619×10^{-06}	1.19048×10^{-05}	0	3.33333×10^{-05}
D2	0	0	0	2.381×10^{-06}	1.19048×10^{-05}	0.000333333	0.000347619
D3	0	0.00047619	4.17×10^{-05}	2.381×10^{-06}	2.38095×10^{-05}	0.000166667	0.000710714

3.2. Estimated daily intakes of heavy metals.

The daily intakes of Zn, Cu, Pb, Fe, Mn and Ni, from herbal samples were estimated according to the concentrations of each specific heavy metal in the herbal samples and the daily ingestion rate for adults with 60 kg average body weight.

The findings show that all the herbal samples had lower values of EDIs as presented in (Table 4). The EDI values of all the heavy metals in the herbals samples were below the tolerable daily intake reference dose (RfD) of individual heavy metals. These levels were below the WHO allowable daily dose of 0.01 kg/day for adults weighing 60 kg [18]. The EDIs increasing according to this trend: Pb < Cu < Ni < Zn < Fe. The iron (Fe) and zinc (Zn) contributions are the highest among the daily intake of heavy metals from the herbal products in the study locations.

3.3. Evaluation of non-carcinogenic hazard quotient (HQ) and hazard index (HI)

In order to evaluate the health risk effect of exposure to heavy metals through the daily intake of herbal product, the non-carcinogenic hazard quotient (HQ) and hazard index (HI) are calculated, and the obtained results are presented in (Table 5). As shown in (Table 5), the non-carcinogenic (HQ) values of all the study heavy metals (Zn, Cu, Pb, Fe, Mn and Ni) through the daily intake of herbal products were all below 1 (HQ < 1). The estimated values show an indication that the daily intake of heavy metals via the ingestion of herbal products would be unlikely to have adverse health risk effects on consumer, which is in agreement with [24]. The results of the health hazard index (HI) for all herbal samples in different locations in Ilorin metropolis were below 1 (HI < 1),

(Table 5). The findings of this study reveal that there are no health risks for consumption and ingestion of herbal products from all the four (4) study locations. According to the hazard index (HI) results, daily intake or consumption of the herbal products do not pose any health risk effects to humans. The results of the study are similar compared to [5] who reported the non-carcinogenic hazard quotient (HQ) and hazard index (HI) of study heavy metals investigated in 14 different herbal plants obtained from the three regions in Central Serbia, Zlatar, Sokobanja, and Kopaonik were below 1. The hazard index findings suggest that more attention should be paid to determining the amount of daily intakes of Heavy Metals from herbal products consumption and their potentially negative effects according to [27].

4. Conclusion

The research study aimed to determine the level of trace heavy metals (Zn, Pb, Cu, Fe, Mn, Cd, Cr, and Ni) contents of various herbal drinks (AGBO) marketed in Ilorin metropolis, Nigeria. The results of this study indicated that most of the heavy metals in the herbal drinks (Zn, Pb, Cu and Mn) were below the WHO recommended permissible limits. Chromium and Cadmium are not detected in all of the herbal drinks analyzed. However, sample C2 and D2 of all of the analyzed herbal samples contained unsafe concentrations of iron (Fe) and nickel (Ni) that exceeded the WHO recommended permissible limits. From the health point of view, the EDIs value of all the herbal drinks are below the daily reference dose. The non-cancerous (HQ) and hazard index (HI) value of all the herbal samples are less than 1, suggesting no potential

health risk effects. Based on the results obtained in this study, there would be non-carcinogenic health risk effects to the people taking the herbal drinks marketed in all the study areas.

Acknowledgements

The author wishes to acknowledge the technical support of University of Ilorin, Chemistry Central Laboratory for the sample's analysis and individuals from samples collections locations.

Funding:

No funding was provided.

References

- [1] R. Dghaim, S. Khatib, H. Rasool, M. Khan, Determination of heavy metals concentration in traditional herbs commonly consumed in the United Arab Emirates, *J Environ Health Sci Eng*, 2015, 236-257.
- [2] C.T. Onwordi, N. Agbo, I.A. Ogunwande, Levels of potentially toxic metals in selected herbal medicines in Lagos, Nigeria, *J Environ Health Sci Eng*, 2015, 3186, 148-157.
- [3] T. Quds, M. Ahmed, S. Shakeel, N. Jalbani, I. Azhar, Determination of the heavy metal contents of frequently used herbal products in Pakistan, *Trop J Pharm Res*, 2021, 377-382.
- [4] D. Eskinazi, M. Blumenthal, N. Farnsworth, C. Riggins, *Botanical Medicine: Efficacy, Quality, Assurance, and Regulation*, 1999, New York: Mary Ann Liebert.
- [5] I. Kandić, M. Kragović, J. Petrović, P. Janačković, M. Gavrilović, M. Momčilović, M. Stojmenović, Heavy metals content in selected medicinal plants produced and consumed in Serbia and their daily intake in herbal infusions, *Toxics*, 2023, 11, 198.
- [6] M. Idu, O. Oghale, A. Jimoh, Heavy metals contamination of some polyherbal products from Lagos state, Nigeria, *J Ayurveda Holist Med*, 2015, 1(2), 45-50.
- [7] C.O. Nwoko, L. Mgbeahuruike, Heavy metal contamination of ready-to-use herbal remedies in South Eastern Nigeria, *Pak J Nutr*, 2011, 10, 959-964.
- [8] N.S. Mokgalaka, R.I. McCrindle, B.M. Botha, Multielement analysis of tea leaves by inductively coupled plasma optical emission spectrometry using slurry nebulisation, *J Anal At Spectrom*, 2004, 19, 1375-1378.
- [9] World Health Organization, *Guideline for Good Manufacturing Practices for Herbal Medicine*, Geneva, 2007.
- [10] S.I. Korfali, T. Hawi, M. Mroueh, Evaluation of heavy metals content in dietary supplements in Lebanon, *Chem Cent J*, 2013, 7, 10.
- [11] A.M. Bobaker, I. Alakili, S.B. Sarmani, N. Al-ansari, Determination and assessment of the toxic heavy metal elements abstracted from the traditional plant cosmetics and medical remedies, *Int J Environ Res Public Health*, 2019, 16, 1957.
- [12] A.A. Adu, O.J. Aderinola, V. Kusemiju, Heavy metals concentration in garden lettuce grown along Badagry Expressway, Lagos, Nigeria, *Transnatl J Sci Technol*, 2012, 2, 115-130.
- [13] L. Zheng, Q. Zhang, Z. Li, R. Sun, S. Zhong, Exposure risk assessment of nine metal elements in Chongqing hotpot seasoning, *RSC Adv*, 2020, 10(4), 1971-1980.
- [14] F. Adusei-Mensah, D. Essumang, R. Agjei, J. Kauhanen, C. Tikkanen-Kaukanen, M. Ekor, Heavy metal content and health risk assessment of commonly patronized herbal medicinal preparations from the Kumasi metropolis of Ghana, *J Environ Health Sci Eng*, 2019, 17(2), 609-618.
- [15] M. Aschale, Y. Sileshi, M. Kelly-Quinn, Health risk assessment of potentially toxic elements via consumption of vegetables irrigated with polluted river water in Addis Ababa, Ethiopia, *Environ Syst Res*, 2019, 8(1), 29.
- [16] T. Adefa, M. Tefera, Heavy metal accumulation and health risk assessment in *Moringa oleifera* from Awi zone, Ethiopia, *Chem Afr*, 2020, 3, 1073-1079.
- [17] United States Environmental Protection Agency, *MidAtlantic Risk Assessment: Human Health Risk Assessment*, 2014.
- [18] H.R. Gebeyehu, L.D. Bayissa, Levels of heavy metals in soil and vegetables and associated health risks in Mojo area, Ethiopia, *PLoS One*, 2020, 15(1), e0227883.
- [19] WHO, *Guidelines for Drinking-water Quality*, 3rd ed., Chapter 8, DRAFT, Geneva, 2023.
- [20] World Health Organization. *Guideline for Good Manufacturing Practices for Herbal Medicine*, Geneva. 2007.
- [21] M. Aschale, Y. Sileshi, M. Kelly-Quinn, Health risk assessment of potentially toxic elements via consumption of vegetables irrigated with polluted river water in Addis Ababa, Ethiopia, *Environ Syst Res*, 2019, 8(1), 29.
- [22] USEPA, *Guidelines for the health risk assessment of chemical mixtures*, Fed Regist, 1986, 51, 34014-34025.
- [23] C. Meng, P. Wang, Z. Hao, Z. Gao, Q. Li, H. Gao, F. Feng, Ecological and health risk assessment of heavy metals in soil and Chinese herbal medicines, *Environ Geochem Health*, 2022, 44(3), 817-828.
- [24] R.O. Ayanniyi, S.O. Folami, H.A. Olumoh-Abdul, S.A. Atunwa, I.A. Oreagba, Heavy metal content of commonly consumed herbal bitters in Ilorin, *West Afr J Pharm*, 2017, 28(1), 147.
- [25] R.N. Asomugha, N.A. Udowelle, S.J. Offor, C.J. Njoku, I.V. Ofoma, C.C. Chukwuogo, O.E. Orisakwe, Heavy metals hazards from Nigerian spices, *Rocz Panstw Zakl Hig*, 2016, 67(3), 309-314.
- [26] I.A. Maghrabi, Determination of some mineral and heavy metals in Saudi Arabia popular herbal drugs using modern techniques, *Afr J Pharm Pharmacol*, 2014, 8(36), 893-898.
- [27] J. Zhang, R. Yang, R. Chen, Y. Peng, X. Wen, L. Gao, Accumulation of heavy metals in tea leaves and potential health risk assessment: A case study from Puan County, Guizhou Province, China, *Int J Environ Res Public Health*, 2018, 15, 133.



Catalytic oxidation of aromatic aldehydes to carboxylic acids in mild conditions with NaClO₂

Gizem Boyoğlu , A. Berat Karabina , Ecem Bellikan , Salih Zeki Yıldız* 

Sakarya University, Science Faculty, Department of Chemistry, 54050, Sakarya, Türkiye

Abstract

This study aimed to improve the conditions for the oxidation of benzaldehyde to benzoic acid using chlorine dioxide generated from sodium chlorite, across various pH ranges and different catalysts. The powerful oxidation capability of chlorine dioxide played a crucial role in enhancing the kinetic efficiency of the reactions. In our research, we examined various reaction conditions, including sodium dihydrogen phosphate, sodium dihydrogen phosphate together with sodium chlorite, sodium dihydrogen phosphate combined with sodium chlorite and potassium permanganate, and sodium dihydrogen phosphate with sodium chlorite and V₂O₅. Additionally, different oxidation combinations having the promoters with sodium chlorite such as sodium tripolyphosphate (STPP), 1-hydroxyethylidene-1,1-diphosphonic acid (HEDP), and formic acid were also tested. The stabilized chlorine dioxide solution was also used directly as the oxidation reagent. The role of chlorine dioxide in these combinations significantly impacted the selectivity and yield in terms of product.

Furthermore, some Mn(III) complexes (Cat.1 and Cat.2) were used as the catalysts in this study, and the findings revealed with chlorine dioxide are to be an effective oxidant for the selective oxidation of aromatic aldehydes to aromatic acids. For the catalytic applications in buffer solutions, a leveling effect was observed. When Mn(III) complexes were used, it showed a similar leveling effect in buffer solutions for pH >1, which was resulting in slow ClO₂ formation. With these findings it was found that the use of Mn(III) complexes in NaH₂PO₄+NaClO₂ combination provided the highest yield in the oxidation of aromatic aldehydes to acids. These results underscore the importance of chlorine dioxide as a powerful oxidant in the chemical transformation processes.

Keywords: Chlorine dioxide, catalysts, oxidation agent, aromatic aldehydes, aromatic acids

1. Introduction

Oxidation is a crucial process in organic synthesis, with various methods developed for the targeted purposes such as oxidation of alcohols to organic acids via aldehydes [1,2]. One significant yet less common transformation is the oxidation of aromatic aldehydes to aromatic acids, which holds industrial importance. Although only a limited number of methods are effective across different aldehydes [3], several reagents have been employed for this reaction in the literature [4]. Among these, sodium chlorite stands out as a selective and mild reagent for oxidizing aromatic aldehydes to acids [5,6]. Other oxidizing agents like hydrogen peroxide, sodium hypochlorite, and KMnO₄ can also be used, but they often produce undesirable by-products, reducing their appeal [7–9].

Chlorine dioxide (ClO₂) stands out as an effective alternative for oxidation reactions, particularly within the pH range of 3–5 with high yields. Known for its high efficiency and lack of by-products, chlorine dioxide

quickly gained attention upon its discovery, and it has a broad range of applications [10–13]. However, due to its high reactivity, it cannot be stabilized in pure form but can be maintained at low concentrations in various chemicals. This stabilization allows for safer and more controlled use, especially in specific applications, minimizing unwanted side effects and explosion risks. In practice, chlorine dioxide as an oxidant is generated from sodium chlorite in the reaction media by adjusting the pH with acids and catalysts, ensuring safe handling and optimal reaction conditions.

Chlorine dioxide is an eco-friendly oxidant that does not bioaccumulate or persist in the environment. Its use in catalytic methods is expected to grow, given its non-polluting nature. These qualities make ClO₂ highly valuable for both environmental and industrial applications. Its strong oxidizing properties are particularly effective in removing colored compounds, odors, and metal ions like iron and manganese [14].

Citation: G. Boyoğlu, A.B. Karabina, E. Bellikan, S.Z. Yıldız, Catalytic oxidation of aromatic aldehydes to carboxylic acids in mild conditions with NaClO₂, Turk J Anal Chem, 6(2), 2024, 78–90.

Author of correspondence: szy@sakarya.edu.tr

Received: June 24, 2024

Tel: +90 (264) 295 61 36

Accepted: August 22, 2024

Fax: +90 (264) 295 59 50

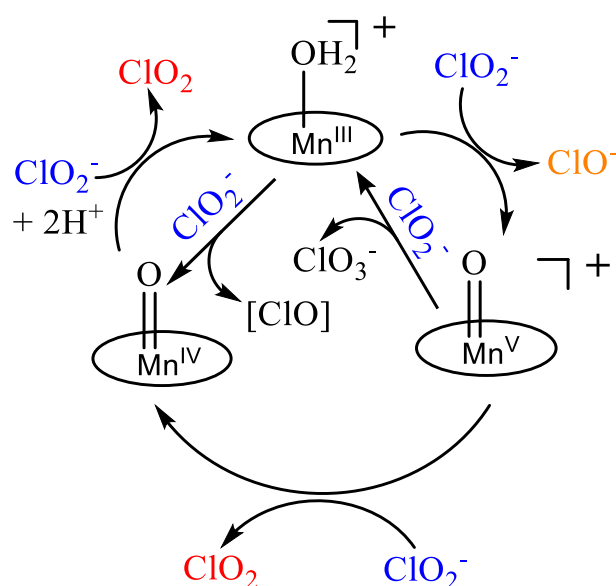


Figure 1. General mechanism for the conversion of chlorine dioxide in the presence of Mn(III) catalyst [19]

The conversion of aldehydes to aromatic acids is crucial due to its industrial applications. Various reagents have been explored for this purpose [15], but only a few are suitable for aldehydes [16]. Sodium chlorite is uniquely effective under mild conditions for converting aldehydes to carboxylic acids [17]. It acts as a chemoselective reagent that tolerates diverse functional groups and produces environmentally friendly by-products compared to metal-based oxidants [18].

In 2014, Scott D. Hicks and colleagues investigated the reactions of chlorine dioxide using manganese catalysts in water under mild conditions. They observed that chlorine dioxide forms catalytically at a pH of around 5 and ambient temperature, some oxy-chlorine species formed were presented in Fig. 1 [19].

In 2016, Kei Ohkubo and colleagues reported in their article that chlorite, combined with a strong Lewis acid like scandium triflate, accelerates the disproportionation of ClO₂ into ClO⁻ and ClO₃⁻ [20].

Oxidation in water purification uses oxidizing agents to convert contaminants into safer compounds. Meng-Yuan Xu and colleagues review the challenges of using ClO₂, focusing on controlling disinfection by-products (DBPs) in drinking water and highlighting the efficiency of the UV/ClO₂ process in both disinfection and reusing ClO₂⁻ [21]. Valentin Rougé and colleagues studied in 2022 and found that chlorite oxidation by chlorine which produces chlorate (60–70%) and ClO₂ (30–40%) can be modeled as the disinfecting and purifying agent for the domestic and waste waters. The study underscores that predicting chlorite and chlorate levels can optimize ClO₂ peroxidation, and increasing ClO₂ dosage can improve the mitigation of disinfection by-products [22].

In a 2023 study, A.V. Kutchin and colleagues explored the oxidation of various alkylphenols using

chlorine dioxide in water and dichloromethane. They discovered specific features of alkylphenol oxidation under different reaction conditions resulted in the formation of quinones and chlorinated products. The yields of quinones depended on the position of substituents on the aromatic ring of the starting phenols [23].

The chemoselective catalytic oxidation of 1,2-diols to α -hydroxy acids, a challenging process, has been successfully achieved. Various 1,2-diols were oxidized into their corresponding α -hydroxy acids, including optically active forms. A key finding was the CT complex formation during oxidation, significant for advancing nitroxyl-radical-catalyzed reactions, making this method a valuable tool in organic synthesis [24].

Based on this information, experiments in this study modified catalytic conditions for oxidizing aromatic aldehydes to acids using sodium chlorite. These adjustments resulted in high conversions with minimal by-products under mild conditions.

2. Experimental

2.1. Materials and methods

Sodium dihydrogen phosphate, potassium permanganate, sodium chlorite, benzaldehyde, stabilized chlorine dioxide, sodium tripolyphosphate (STPP), formic acid, HEDP (1-hydroxy ethylidene-1,1-diphosphonic acid), vanadium pentoxide, tetrahydrofuran (THF), ethyl acetate, dichloromethane, acetonitrile, glacial acetic acid, urotropine, 2,4-ditertbutylphenol, cis/trans 1,2-diaminocyclohexane, potassium hydroxide, Mn(CH₃COO)₂·4H₂O, LiCl, CoCl₂·6H₂O, diethylenetriamine and water were used as the reagents in Aldrich quality.

Experiments were conducted using various glassware and glass storage containers. In addition to these common laboratory equipment and tools were also used. Melting points were determined using a Barnstead-Electrothermal 9200 and a Stuart SMP 10 melting point determination device. For pH measurements, pH papers and a pH meter (PHM 210 STANDARD pH METER, analytical KCl.Ag meterLab) were used, while magnetic and mechanical stirrers were preferred for mixing solutions. Infrared spectra were recorded on a Perkin Elmer UATR-TWO FT-IR spectrophotometer equipped with a diamond ATR. UV-visible spectra were recorded using a Hitachi U-2900 UV-visible PC spectrophotometer. ¹H and ¹³C NMR spectra were recorded on a Varian Mercury Plus 300 MHz spectrometer. Finally, TLC plates (Silica Gel 60 ADAMANT on TLC Plates) and a rotary evaporator (BÜCHI Water bath B-480) were used.

2.2. Synthesis

2.2.1. $[Mn(III)(acacen)Cl]$ (Cat.1)

The synthesis of Mn(III) complex of bis-acetylacetonethylenediamine (acacen) $[Mn(III)(acacen)Cl]$ (Cat.1) (Fig. 2) was done according to the literature procedures [25].

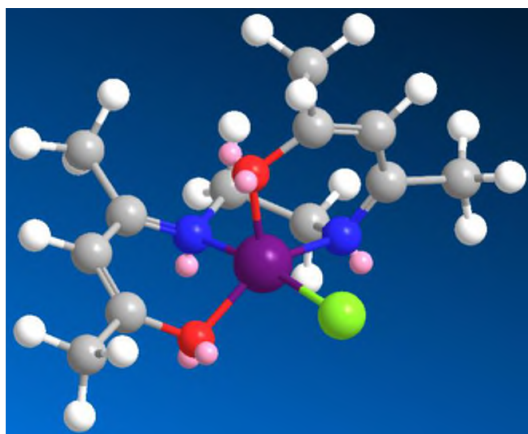
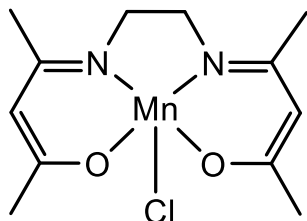


Figure 2. $[Mn(III)(acacen)Cl]$ (Cat.1) and its calculated molecule structure using chem 3D Pro

2.2.2. 6,6'-((1E,1'E)-(cyclohexane-1,2-diybis(azaneylylidene))bis(methaneylylidene))bis(2,4-di-tert-butylphenolate) $Mn(III)Cl$, $[Mn(III)(SchL)Cl]$ (Cat.2)

A Schiff base compound, 6,6'-((1E,1'E)-(cyclohexane-1,2-diybis(azaneylylidene))bis(methaneylylidene))bis(2,4-di-tert-butylphenol) (SchLH₂) was synthesized through the literature procedure [26]. The complexation process for the Mn(III) ion was carried out as follows, as well;

SchLH₂ (0.2 g, 0.37 mmol), KOH (42 mg, 0.75 mmol), and Mn(OAc)₂·4H₂O (90 mg, 0.37 mmol) were mixed and heated to boiling for 4 hours in an ethanol (20 mL) solution using a 250 mL round-bottom flask equipped with a condenser. After the completion of the reaction, the mixture was cooled down to room temperature, and LiCl (42 mg, 0.75 mmol) was added. The reaction was then continued for an additional 3 hours while passing air through the mixture. The progress of the reaction was monitored by TLC (60F₂₅₄-SiO₂, fixed phase / THF:Hexane (3:4), mobile phase) for both steps. After the reaction was complete, the mixture was cooled to room temperature, appeared precipitate filtered, and thoroughly washed with distilled water and methanol respectively. Finally, the product (Cat.2) was dried for spectroscopic measurements and analysis in a vacuum oven at 50 °C.

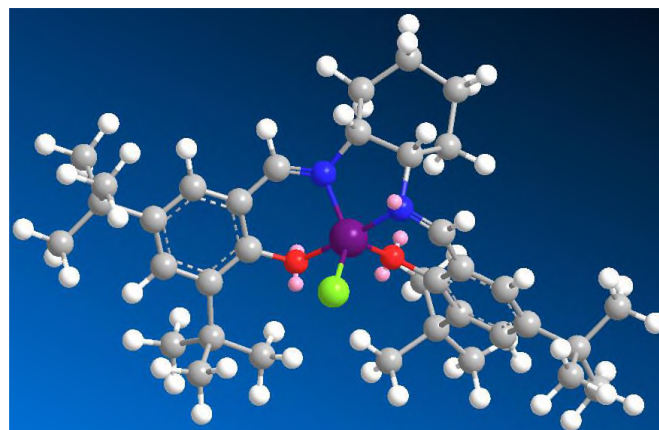
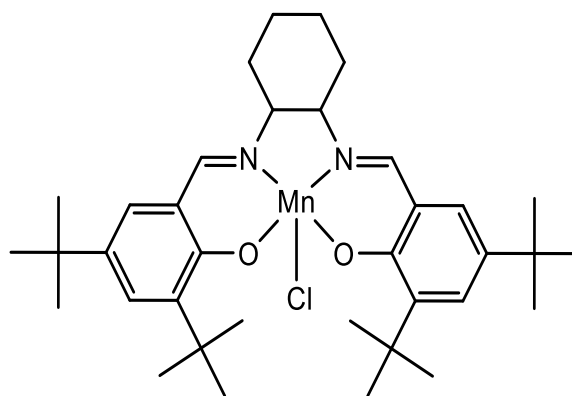


Figure 3. $[Mn(III)(SchL)Cl]$ (Cat.2) and its calculated molecule structure using chem 3D Pro

Yield: 0.192 g, 82%; **m.p.:** 240–250 °C (decomposition).

FT-IR (PIKE Miracle TM ATR) V_{max}/cm^{-1} : 3055 (Ar, C-H), 2951-2866 (Aliph., C-H), 1608 (C=N), 1535 (Ar, C=C), 1458-1388 (Aliph., C-C), 1249, 1172.

UV-Vis. (CHCl₃-1x10⁻⁵ M) λ_{max} (nm) (log ϵ): 258 (4.02), 294 (4.23), 329 (4.01), 444 (3.54).

Theoretical compound, (C₃₆H₅₂ClMnN₂O₂) (%): C, 68.07; H, 8.25; N, 4.41; O, 5.04; Cl, 5.58; Mn, 8.65; **Found (%):** C, 68.40; H, 8.77; N, 5.16; Mn, 8.12 (ICP-OES).

2.3. Thin Layer (TLC) Chromatography System

TLC analyses were performed to examine the conversion of aromatic aldehydes to aromatic acids. All experiments progressed in various reaction conditions using different catalysts were performed and monitored using thin layer chromatography. Pre-coated silica gel plates fixed on glass were used as the stationary phase. The pre-coated plates, originally sized 20x20 cm, were cut to 2x5 cm dimensions using a diamond cutter. Application points were marked on the prepared plates with a pencil. For the mobile phase, a 1/5-THF/hexane mixture was prepared as a 25 mL stock solution and stored in a sealed bottle. 25 mL tall beakers were used as chromatography tanks. The separation power of the mobile phase was tested using benzaldehyde as the starting material and benzoic acid as the main product.

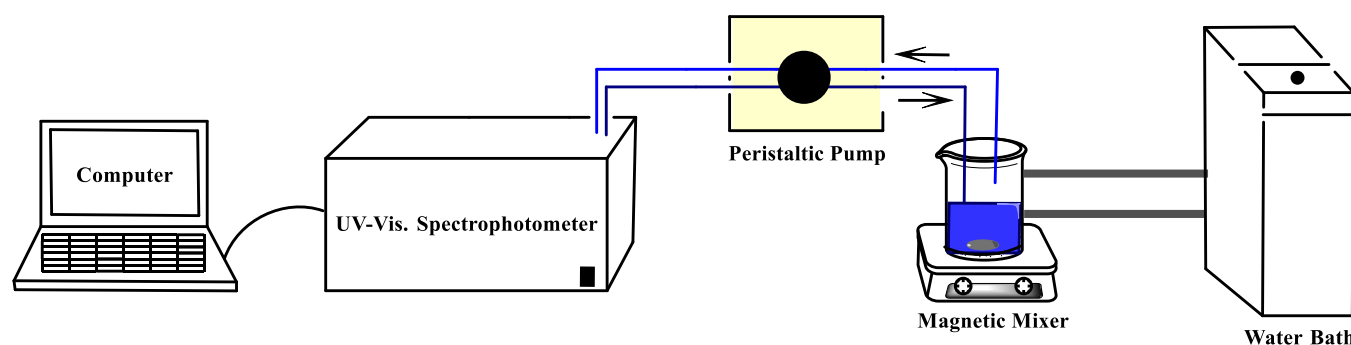


Figure 4. System for catalytic kinetic oxidation measurement of H_2O_2 [29]

2.4. Solution preparation

2.4.1. Preparation of Stabilized Chlorine Dioxide Solution

31% sodium chlorite (13.7 g) was taken and mixed with 2 g of light soda. The mixture was dissolved in 100 mL of distilled water and then diluted to a total volume of 900 ml. Separately, a solution containing 5.33 g of sodium persulfate and 2 g of sodium bisulfate dissolved in 100 ml of water was prepared and added to the mixture. The resulting solution was left to stand in a dark place for 3 days to ensure the stability [27]. The ClO_2 amount was measured as 3000 ppm by using ClO_2 strips (Bart-ration ClO_2 measurement strips 0–500 ppm range, made in USA).

2.4.2. Preparation of Buffer Solution

Buffer solutions with different pH values to be used to take catalytic measurements were created using literature sources [28].

Preparing buffers involves a series of precise steps to ensure they are suitable for their intended use. First, we calculated the required components concentrations and amounts based on the specific application and target volume. Next, we carefully weigh the components and dissolve them in an appropriate solvent. After dissolving, for adjusting the pH of the solution to the desired level we used pH meters and appropriate reagents. Once the pH was adjusted, we diluted the solution to the final desired volume. Finally, we labeled the buffer clearly to indicate its contents and any important details. And use some of it directly for experiments and stored some for future use.

2.5. Kinetic studies

The system used for catalytic kinetic oxidation measurement of H_2O_2 in the literature was modified to allow for ClO_2 measurements [29]. To prevent the evaporation and light interaction of ClO_2 , the reaction vessel was specifically modified into a sealed, amber-colored reaction vessel. The schematic demonstration of the modified system is shown in Fig. 4.

The synthesized Mn(III)SchLCl complex (Cat.2) is shown in Fig. 3. Dimethyl sulfoxide (DMSO) solutions of Cat.2 were prepared. Buffers at different pH levels (pH= 1, 2, 4, 6) and their respective preparation materials are listed in Table 1. The experimental conditions were set up with 10^{-2} M sodium chlorite, 10^{-5} M metal complex, and 0.1 M buffer in a total volume of 100 ml vessel. The production of ClO_2 was monitored automatically using a UV-VIS Spectrophotometer at 360 nm for 90 minutes in a kinetic cuvette. Changes in the absorbance at 360 nm for the recorded spectra were attributed to variations in ClO_2 concentration.

2.6. The oxidation of benzaldehyde to benzoic acid studies

In the studies of the oxidation of benzaldehyde to benzoic acid, experiments were conducted using different reaction conditions and catalysts while considering the parameters such as pH, reaction time, and yield. The results related to the studies are provided in Table 2 as isolated benzoic acid yield percentage.

Table 2 Reaction conditions of preparation of aromatic acids from aromatic aldehydes.

Table 1. The reaction conditions of ClO_2 generation kinetic studies and results

No	Starting Material	Formation product	Complexes (10^{-5} M)	Buffer Conditions	Molarity of Buffer	Buffer pH	Time (min.)	% Formation
1	0.01 M NaClO_2	ClO_2	—	HCl-KCl	0.1 M	1.05	1.5 h	16.41
2	0.01 M NaClO_2	ClO_2	—	Citric Acid NaH_2PO_4	0.1 M	2.10	1.5 h	1.45
3	0.01 M NaClO_2	ClO_2	—	Citric Acid NaH_2PO_4	0.1 M	4.07	1.5 h	0.442
4	0.01 M NaClO_2	ClO_2	—	Citric Acid NaH_2PO_4	0.1 M	6.02	1.5 h	0.013
5	0.01 M NaClO_2	ClO_2	Complex Cat.2	HCl-KCl	0.1 M	1.05	1.5 h	9.29
6	0.01 M NaClO_2	ClO_2	Complex Cat.2	Citric Acid NaH_2PO_4	0.1 M	2.10	1.5 h	10.32
7	0.01 M NaClO_2	ClO_2	Complex Cat.2	Citric Acid NaH_2PO_4	0.1 M	4.07	1.5 h	5.59
8	0.01 M NaClO_2	ClO_2	Complex Cat.2	Citric Acid NaH_2PO_4	0.1 M	6.02	1.5 h	2.56

3. Result and discussion

In the present study, the oxidation of benzaldehyde to benzoic acid experiments were conducted considering pH, reaction time, and yield values applying different reaction conditions and catalysts. For this purpose, the study examined under mild conditions, using sodium chlorite as the oxidant and varying catalytic combinations to achieve high conversions with minimal side products (Fig. 5). As stated in the literature, the experiments were carried out in an acetonitrile-water medium [30].

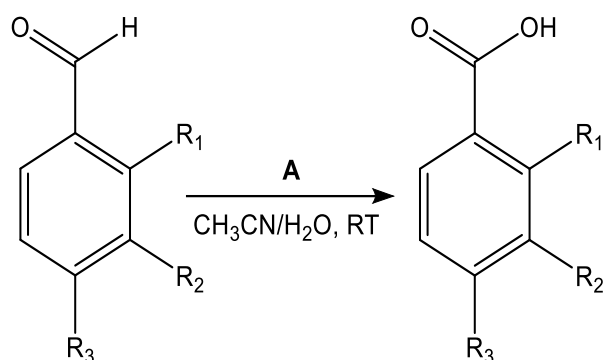


Figure 5. Reaction: preparation of aromatic acids from aromatic aldehydes, A: Catalysts and reaction conditions given in Table 2

The progress of the reactions was monitored by Thin Layer Chromatography (TLC). The resulting chromatogram is shown below in Fig. 6. The observed R_f values were: 2/3 for benzaldehyde and 1/3 for benzoic acid.

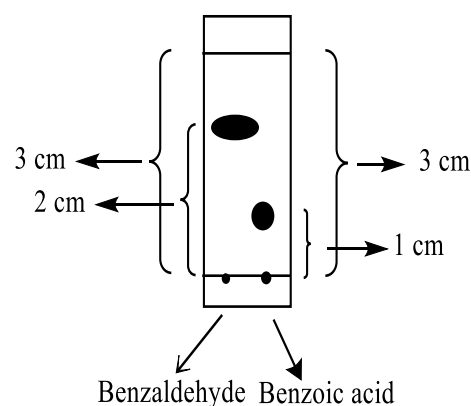


Figure 6. The TLC chromatography of benzaldehyde and benzoic acid

In the initial experiment, oxidation studies were performed using only sodium dihydrogen phosphate (NaH_2PO_4) as the basic reagent to make sure if there was any conversion without sodium chlorite. At 4.90 pH after 72 hours, benzoic acid was not obtained.

Table 2. Reaction conditions of preparation of aromatic acids from aromatic aldehydes

No	Starting Material	R_1, R_2, R_3	A	pH	Time	Yield, %
1	Benzaldehyde	$R_1, R_2, R_3 = \text{H}$	Stabilized ClO_2 solution	—	60 h	73.00
2	<i>m</i> -Tolyl Aldehyde	$R_1, R_3 = \text{H}, R_2 = \text{CH}_3$	Stabilized ClO_2 solution	—	96 h	13.20
3	<i>p</i> -Tolyl Aldehyde	$R_1, R_2 = \text{H}, R_3 = \text{CH}_3$	Stabilized ClO_2 solution	—	96 h	16.37
4	4-methyl Benzaldehyde	$R_1, R_2 = \text{H}, R_3 = \text{OCH}_3$	Stabilized ClO_2 solution	—	96 h	3.81
5	Salicylaldehyde	$R_2, R_3 = \text{H}, R_1 = \text{OH}$	Stabilized ClO_2 solution	—	96 h	—
6	4-Hydroxy Benzaldehyde	$R_1, R_2 = \text{H}, R_3 = \text{OH}$	Stabilized ClO_2 solution	—	96 h	—
7	Benzaldehyde	$R_1, R_2, R_3 = \text{H}$	NaH_2PO_4	4.90	72 h	—
8	Benzaldehyde	$R_1, R_2, R_3 = \text{H}$	$\text{NaH}_2\text{PO}_4 + \text{NaClO}_2$	6.98	48 h	33.10
9	Benzaldehyde	$R_1, R_2, R_3 = \text{H}$	$\text{NaH}_2\text{PO}_4 + \text{NaClO}_2$	6.05	48 h	38.50
10	Benzaldehyde	$R_1, R_2, R_3 = \text{H}$	$\text{NaH}_2\text{PO}_4 + \text{NaClO}_2$	5.65	48 h	43.10
11	Benzaldehyde	$R_1, R_2, R_3 = \text{H}$	$\text{NaH}_2\text{PO}_4 + \text{NaClO}_2$	5.45	48 h	64.60
12	Benzaldehyde	$R_1, R_2, R_3 = \text{H}$	$\text{NaH}_2\text{PO}_4 + \text{NaClO}_2$	5.30	48 h	78.10
13	Benzaldehyde	$R_1, R_2, R_3 = \text{H}$	$\text{NaClO}_2 + \text{HEDP}$	4.90	60 h	58.50
14	Benzaldehyde	$R_1, R_2, R_3 = \text{H}$	$\text{NaClO}_2 + \text{HEDP}$	3.50	60 h	75.00
15	Benzaldehyde	$R_1, R_2, R_3 = \text{H}$	$\text{NaClO}_2 + \text{STPP} + \text{Formic Acid}$	3.50	60 h	52.00
16	Benzaldehyde	$R_1, R_2, R_3 = \text{H}$	$\text{NaClO}_2 + \text{KMnO}_4$	11.90	48 h	—
17	Benzaldehyde	$R_1, R_2, R_3 = \text{H}$	$\text{NaH}_2\text{PO}_4 + \text{NaClO}_2 + \text{KMnO}_4$	6.10	48 h	16.10
18	Benzaldehyde	$R_1, R_2, R_3 = \text{H}$	$\text{NaH}_2\text{PO}_4 + \text{NaClO}_2 + \text{KMnO}_4$	5.85	48 h	28.00
19	Benzaldehyde	$R_1, R_2, R_3 = \text{H}$	$\text{NaH}_2\text{PO}_4 + \text{NaClO}_2 + \text{KMnO}_4$	5.40	48 h	64.80
20	Benzaldehyde	$R_1, R_2, R_3 = \text{H}$	$\text{NaClO}_2 + \text{V}_2\text{O}_5$	12.00	72 h	—
21	Benzaldehyde	$R_1, R_2, R_3 = \text{H}$	$\text{NaH}_2\text{PO}_4 + \text{NaClO}_2 + \text{V}_2\text{O}_5$	6.40	60 h	12.70
22	Benzaldehyde	$R_1, R_2, R_3 = \text{H}$	$\text{NaH}_2\text{PO}_4 + \text{NaClO}_2 + \text{V}_2\text{O}_5$	5.65	60 h	48.50
23	Benzaldehyde	$R_1, R_2, R_3 = \text{H}$	$\text{NaH}_2\text{PO}_4 + \text{NaClO}_2 + \text{V}_2\text{O}_5$	5.40	60 h	67.60
24	Benzaldehyde	$R_1, R_2, R_3 = \text{H}$	$\text{NaH}_2\text{PO}_4 + \text{NaClO}_2 + \text{Cat.1}$	11.88	60 h	2.78
25	Benzaldehyde	$R_1, R_2, R_3 = \text{H}$	$\text{NaH}_2\text{PO}_4 + \text{NaClO}_2 + \text{Cat.1}$	6.72	60 h	77.7
26	Benzaldehyde	$R_1, R_2, R_3 = \text{H}$	$\text{NaClO}_2 + \text{Cat.2}$	11.8	48 h	—
27	Benzaldehyde	$R_1, R_2, R_3 = \text{H}$	$\text{NaH}_2\text{PO}_4 + \text{NaClO}_2 + \text{Cat.2}$	7.12	48 h	34.32
28	Benzaldehyde	$R_1, R_2, R_3 = \text{H}$	$\text{NaH}_2\text{PO}_4 + \text{NaClO}_2 + \text{Cat.2}$	6.32	48 h	60.72
29	Benzaldehyde	$R_1, R_2, R_3 = \text{H}$	$\text{NaH}_2\text{PO}_4 + \text{NaClO}_2 + \text{Cat.2}$	5.77	48 h	74.64
30	Benzaldehyde	$R_1, R_2, R_3 = \text{H}$	$\text{NaH}_2\text{PO}_4 + \text{NaClO}_2 + \text{Cat.2}$	5.44	48 h	87.97
31	Benzaldehyde	$R_1, R_2, R_3 = \text{H}$	$\text{NaH}_2\text{PO}_4 + \text{NaClO}_2 + \text{Cat.2}$	5.40	48 h	90.08

In the subsequent studies, the combination of NaH_2PO_4 and sodium chlorite under the same conditions used to balance the oxidative strength of sodium chlorite, thereby increasing the selectivity of the reaction. To observe the catalytic difference when sodium chlorite is added, measurements were taken for 48 hours at different pH values. This allowed for a thorough analysis of how sodium chlorite affects the catalytic activity under various conditions. For this, the reaction was carried out firstly by adding NaH_2PO_4 to adjust the pH to 6.98 and using 7 mmol of NaClO_2 for 5 mmol of aldehyde. After the reaction for 48 hours, it was observed that pH decreased from high (basic) to low (acidic) values, the yield increased to 33.1% (Table 2). The results demonstrated that the yield of the reaction depends strictly on the pH. Specifically, at pH 6.05, the yield was 38.5%. When the pH was adjusted to 5.65, the yield increased to 43.1%. Further lowering the pH to 5.45 resulted in a yield of 64.6%, and at pH 5.30, the yield reached 78.1%. These findings indicate that a decrease in pH leads to a significant increase in reaction yield, suggesting that the catalytic activity of the system is enhanced under more acidic conditions. These results of different pH values are presented in Table 2.

However, increasing the benzoic acid yield at neutral pH is an important task in terms of industrial applications due to reducing the corrosion risks and making the facilities easier. To enhance the oxidation capacity for the catalytic purposes, the use of chlorine dioxide (ClO_2) in combination with potassium permanganate (KMnO_4) as a catalyst was attempted. Under the existing conditions, it was expected that it would cause NaClO_2 to decompose and release ClO_2 at high pH (11.9), but this did not happen, and no product was formed. Consequently, a system involving KMnO_4 and NaClO_2 was tested. By adding 5 mmol of KMnO_4 to the sodium chlorite and NaH_2PO_4 system and allowing the reaction to proceed for 48 hours, the pH decreased from 11.9 to 6.10. This process resulted in the formation of benzoic acid with a yield of 16.1%. Additionally, to observe the effects of lower pH values over the same period, further experiments were conducted. At pH: 5.85, the yield increased to 28%, and at pH: 5.40, the yield significantly rose to 64.8%. These results demonstrate that lowering the pH further enhances the yield at the same level with $\text{NaH}_2\text{PO}_4 + \text{NaClO}_2$ system, and there is no catalytic impact for KMnO_4 , as well.

In parallel, Vanadium Pentoxide (V_2O_5) as another oxidation catalyst like KMnO_4 was used additionally. The catalytic effect of V_2O_5 was studied under the same conditions to measure its influence on the oxidation process. When it was used solely with NaClO_2 at 12.0 pH, benzoic acid was not obtained after 72 hours. At pH: 6.40, benzoic acid with a yield of 12.7% was obtained by

adding 0.5 mmol of V_2O_5 to sodium dihydrogen phosphate and sodium chlorite combination after 60 hours of reaction. Also, at pH: 5.65 the yield increased to 48.5%, and at pH: 5.40 increased to 67.6% over the same period. All the experiments assessed the effect of pH but no catalytic effect for V_2O_5 on the reaction yield (Table 2).

Some other oxidation combinations were tested for the oxidation of benzaldehyde to benzoic acid, as well. Sodium chlorite was used in conjunction with Sodium Tripolyphosphate (STPP) and formic acid. The pH in the STPP/formic acid system was buffered to 3.5. At the end of a 60-hour reaction, benzoic acid was obtained with a yield of 52.0%. In another system, 1-Hydroxyethylidene-1,1-Diphosphonic Acid (HEDP) was used alongside sodium chlorite. Similarly, by adjusting the pH to 3.5 in the studies with HEDP, benzoic acid was obtained with a yield of 75.0% at the end of a 60-hour reaction. This was also tested in pH: 4.90 to see the difference of yield with this yield descend to 58.5%.

Additionally, measurements were taken by using stabilized chlorine dioxide solution directly as an oxidation reagent. In this study, 0.6 g of stabilized chlorine dioxide was added for 5 mmol of benzaldehyde. After 60 hours of reaction, benzoic acid was obtained with a yield of 73.0%.

Mn complexes are organic compounds containing transition metals and are effective catalysts in oxidative processes. We also investigated Mn complexes as catalysts, alongside using a stabilized chlorine dioxide solution as a direct oxidation reagent in various catalytic systems. In the final stage of our catalytic studies was focused on examining the catalytic effect of manganese-containing complexes in the presence of ClO_2 . To this end, manganese-containing complexes were synthesized, and their catalytic effects were studied under identical conditions. The Mn(III)(acen)Cl complex (Cat.1), known for its catalytic activity, was prepared following the procedure described in the literature and used as the catalyst [25]. However, no product was obtained at the end of this Cat.1 and NaClO_2 combination experiment at 11.8 pH after 48 hours. Therefore, the catalytic effect of 5 mmol Cat.1 in the presence of NaClO_2 and NaH_2PO_4 was investigated at different pHs for the same period. As a result, benzoic acid was obtained with a yield of 34.32% at 7.12 pH, 60.72% at 6.32 pH, 74.64% at 5.77 pH, 87.97% at 5.44 pH, and 90.08% at 5.40 pH, after adding the additives to the system under the same conditions. The significant catalytic effect was observed at the same pH levels for Cat.1 when it compared with the $\text{NaH}_2\text{PO}_4 + \text{NaClO}_2$ combination applications.

Specifically, we synthesized Mn(III)SchLCl complex (Cat.2) with a fine-tuned synthesis procedure starting from 3,5-di-tert-butyl-2-hydroxybenzaldehyde as the

specific Mn(III) catalyst known as “Jacobsen’s Catalysts” in the literature [26]. Initially, the Schiff base was formed by reacting the aldehyde with *cis/trans*-1,2-diaminocyclohexane in ethanol. This was followed by the addition of a metal salt in a basic media to complete the complex formation. The progress of this reaction was monitored by Thin Layer Chromatography (TLC). The formation of the Mn(III)SchLCl complex (Cat.2), obtained from the reaction of the Schiff base ligand with $\text{Mn}(\text{OAc})_2 \cdot 4\text{H}_2\text{O}$, is indicated by the spectroscopic analysis and elemental analysis. In the FTIR spectrum of Cat.2 the C=N band appeared at 1608 cm^{-1} , demonstrating the involvement of the imine group in the complex formation, shifted to lower wave-number when it compared with the related ligand [26]. The other signals recorded, were supported to the complex formation, as well. The elemental and ICP-OS analysis results of the prepared complex are consistent with the values theoretically calculated and given in the literature [26,31].

The catalytic effect of Cat.2 (Mn(III)SchLCl complex), in the presence of NaClO_2 and NaH_2PO_4 was investigated at different pHs for the same period of time. Catalytic measurements were recorded after 90 min. than adding Cat.2. UV-Vis graphs of these measurements and their comparison to buffers can be seen at Fig. 7. The recorded UV-Vis. spectra were examined, and ClO_2 generation was observed with the increase of the absorption at 360 nm by pH adjusting and catalysis which is accorded with the literature [19, 32]. In Fig. 7a, it is observed that ClO_2 formation proceeds with the effect of pH (pH:1 buffer) and therefore the catalytic effect cannot be predicted clearly. However, in the studies carried out in pH:2 buffer in Fig. 7b, it was determined that the Cat.2 catalyst added to the buffer increased the formation of ClO_2 . Although increasing the pH reduces this effect, it is seen in Fig. 7c that the catalytic effect continues in the pH:4 buffer. But, when Fig. 7d is examined, it is observed that the formation of ClO_2 in the pH:6 buffer in the aqueous environment decreases to an almost non-existent level by the pH effect or the catalytic effect.

The time-dependent absorptions of generated ClO_2 at different pHs were represented at Graph 1, while the catalytic activities and the yields were presented in Table 1. To be able to clarify the catalytic mechanism, we examined the ClO_2^- to ClO_2 conversion kinetics and compared with the literature results [32]. Under HCl and KCl buffer conditions at pH 1.05, conversion was 16.41% in 90 min. In this environment, a very rapid linear conversion occurs and the formation of ClO_2 are clearly visible.

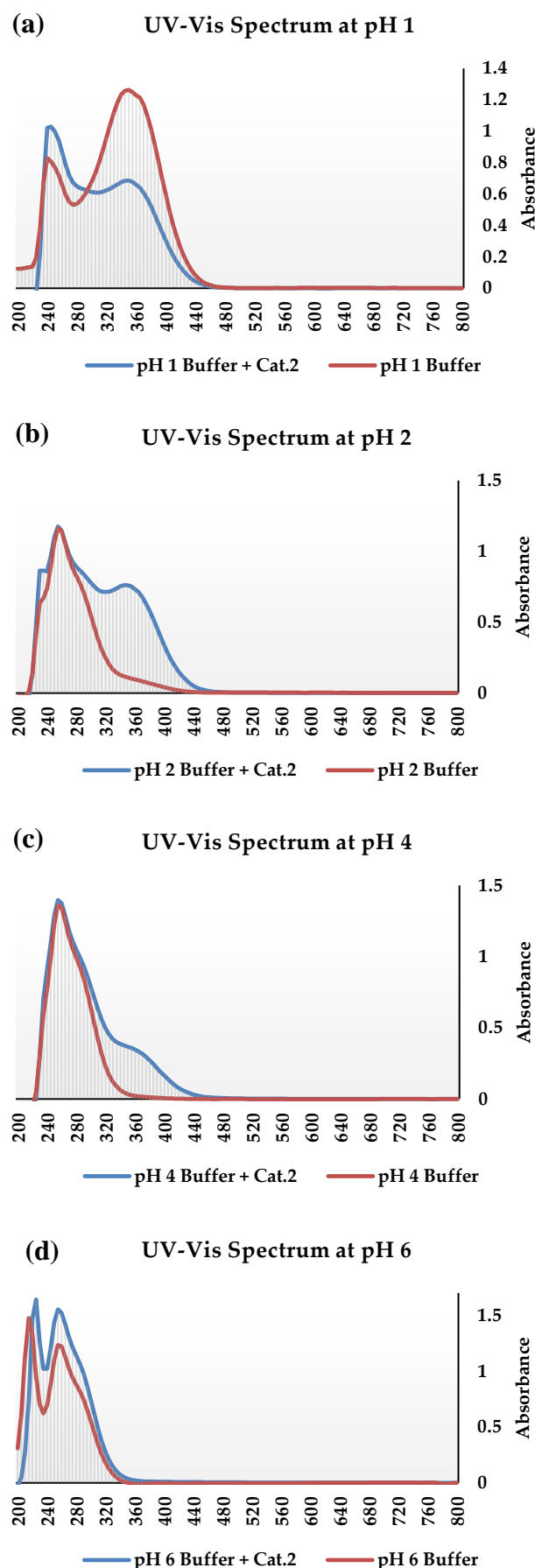
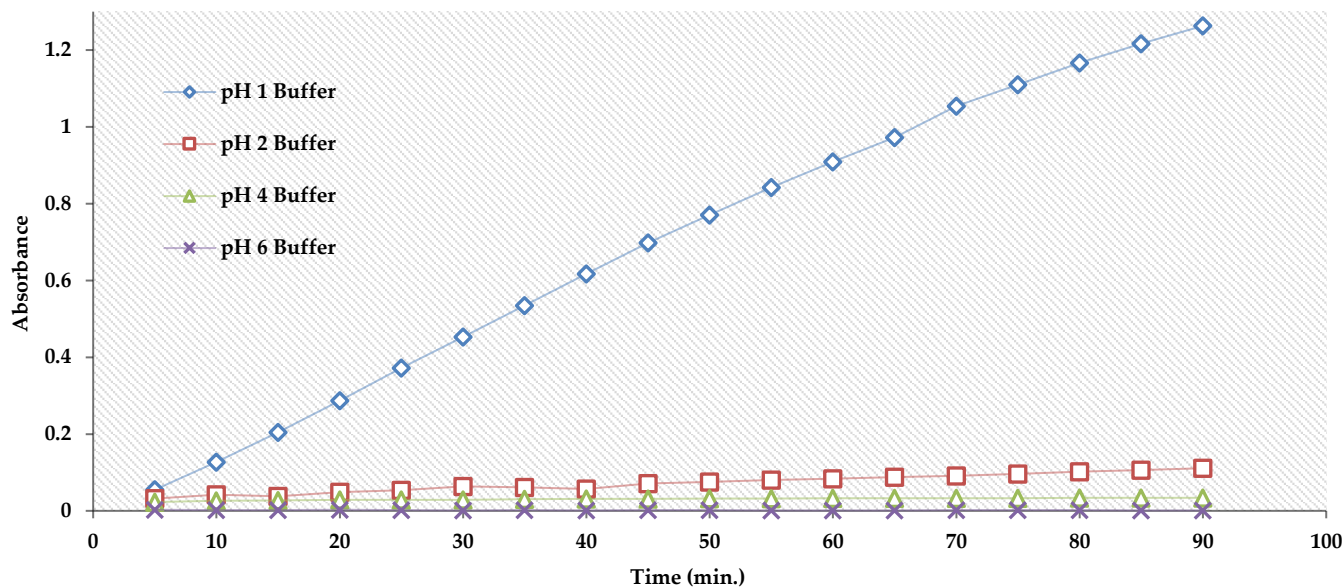


Figure 7. UV-Vis spectra of Cat.2 in buffer at: a) 1.05 pH after 90 minutes, b) 2.10 pH after 90 min., c) 4.07 pH after 90 min., d) 6.02 pH after 90 min.

Absorbance change of Chlorine Dioxide at 360 nm.



Graph 1. Absorbance change graph of Chlorine Dioxide in the specified buffers at 360 nm

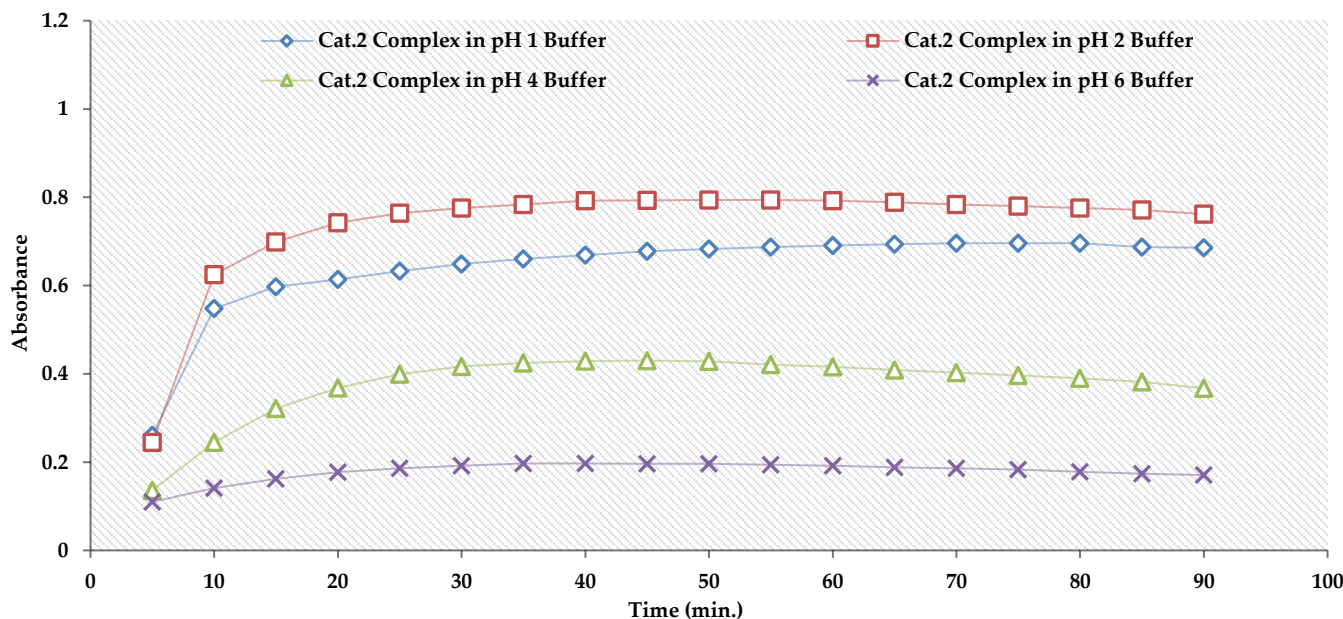
To see the conversion results of citric acid and NaH_2PO_4 combination at different pH, we tested them for 90 min. at similar conditions, as well. At pH:2.10, formation was 1.45%, at pH:4.07 formation was 0.442%, and at pH:6.02 formation was measured as 0.013%, respectively. In other pH experiments, conversion results in citric acid and NaH_2PO_4 buffer showed us that there was a leveling effect here and ClO_2 formation occurred slowly. When the buffer was changed, there were large differences in ClO_2 formation between the two measurements (Graph 1). The reason why the reaction is carried out in the presence of NaH_2PO_4 is that it acts as a buffer for the ClO_2 formed during the reaction. This buffering effect helps stabilize the ClO_2

concentration, allowing for more controlled and effective catalytic reactions [19,32,33].

The time-dependent absorption of ClO_2 with Cat.2., as well as citric acid and NaH_2PO_4 with Cat.2 were presented in Table 1. Also, activities at different pHs were presented in Graph 2 respectively.

Cat.2 in HCl and KCl buffer (pH: 1.05), ClO_2 formation was 9.29% in 90 minutes. under the same conditions. Although a leveling effect is observed here, the amount of ClO_2 in the environment is higher due to the catalyst effect. Since Cat.2 also buffers, a similar leveling effect can be seen even in buffer solutions where pH is close to 1. This shows us that measurements made

Absorbance change of Chlorine Dioxide with addition of Cat.2 at 360 nm.



Graph 2. Absorbance change graph of Chlorine Dioxide in the specified buffers with addition of Cat.2 (360 nm)

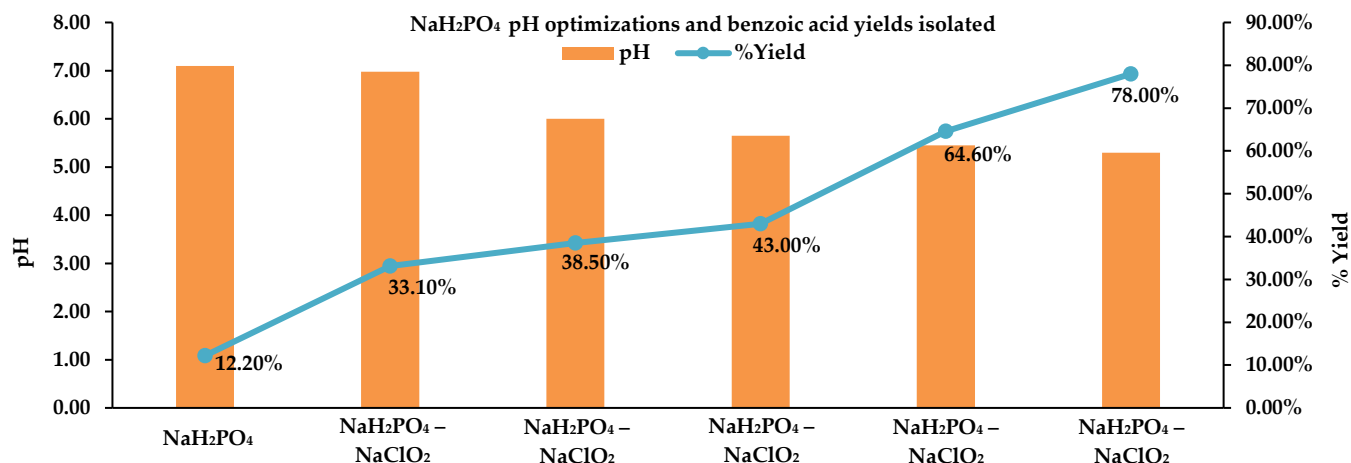


Figure 8. pH buffering with NaH₂PO₄ and benzoic acid yields isolated

with the metal complex in NaH₂PO₄ environment will give the highest conversion rate. As expected, the results of Cat.2 and NaH₂PO₄ formation in citric acid at different pH values were 10.32% at pH 2.10, 5.59% at pH 4.07 and 2.56% at pH 6.02 for 90 minutes.

The leveling effect seen here and increased by Cat.2 can be expected to make a positive contribution to the oxidative conversion of benzaldehyde to benzoic acid. When the yields of benzoic acid given in Table 2 are compared with the efficiencies obtained both in buffer solutions and when using catalyst together with buffer are quite high compared with the ClO₂ conversion efficiency. It can be interpreted that the effect of the mentioned leveling effect of ClO₂ which is increased by the ClO₂ complexes formed with the catalysts used, and in this case, high percentages of benzoic acid conversions are obtained even at pH close to neutral [34,35]. As a result, benzoic acid was obtained with the isolated yield of 2.78% at 11.82 pH, and 77.7% at 6.72 pH after 60 hours reaction.

In line with the studies, attempts were made to catalytically oxidize aromatic aldehydes including 4-methyl benzaldehyde, *m*-Tolyl Aldehyde, *p*-Tolyl

Aldehyde, Salicylaldehyde, and 4-Hydroxy benzaldehyde using stabilized chlorine dioxide. The results of the conducted studies are presented in Table 2.

Table 2 shows that 31 different experiments were carried out. As a first step of the experiments, different aldehyde derivatives (benzaldehyde, *m*-tolyl aldehyde, *p*-tolyl aldehyde, 4-methoxy benzaldehyde, 2-hydroxy benzaldehyde and 4-hydroxy benzaldehyde) were reacted with stabilized ClO₂ solution. At the end of the reaction, it was observed that there was no transformation in the aldehyde derivatives containing the free -OH group. It was interpreted that the antioxidant property of the phenolic structure in these molecules prevents the radical oxidation.

In the second stage of the experiments, the oxidation conditions and yields of benzaldehyde to benzoic acid in different pH buffers and catalysts in the presence of NaClO₂ were investigated. In the experiment performed with only NaH₂PO₄ without NaClO₂ at pH 4.90, no benzoic acid could be isolated after 72 hours. However, in the combination of NaH₂PO₄ + NaClO₂, benzoic acid was obtained at increasing rates from 33.1% to 78.1% at decreasing pH values from pH: 6.90 to pH: 5.30, respectively (Fig. 8).

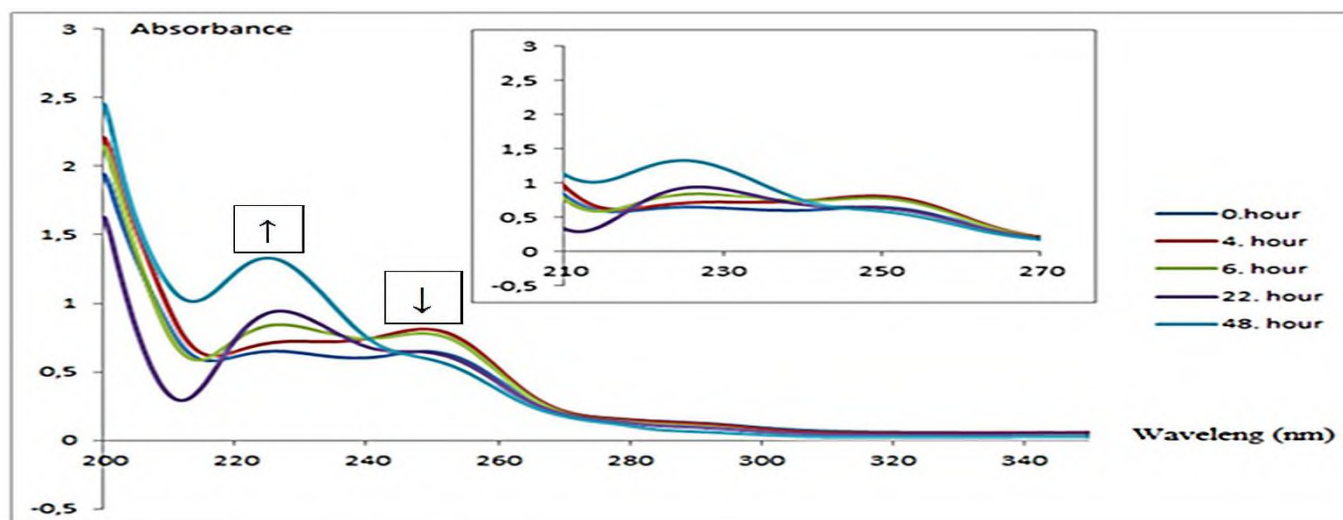


Figure 9. Absorption spectra of the conversion of benzaldehyde to product (benzoic acid)

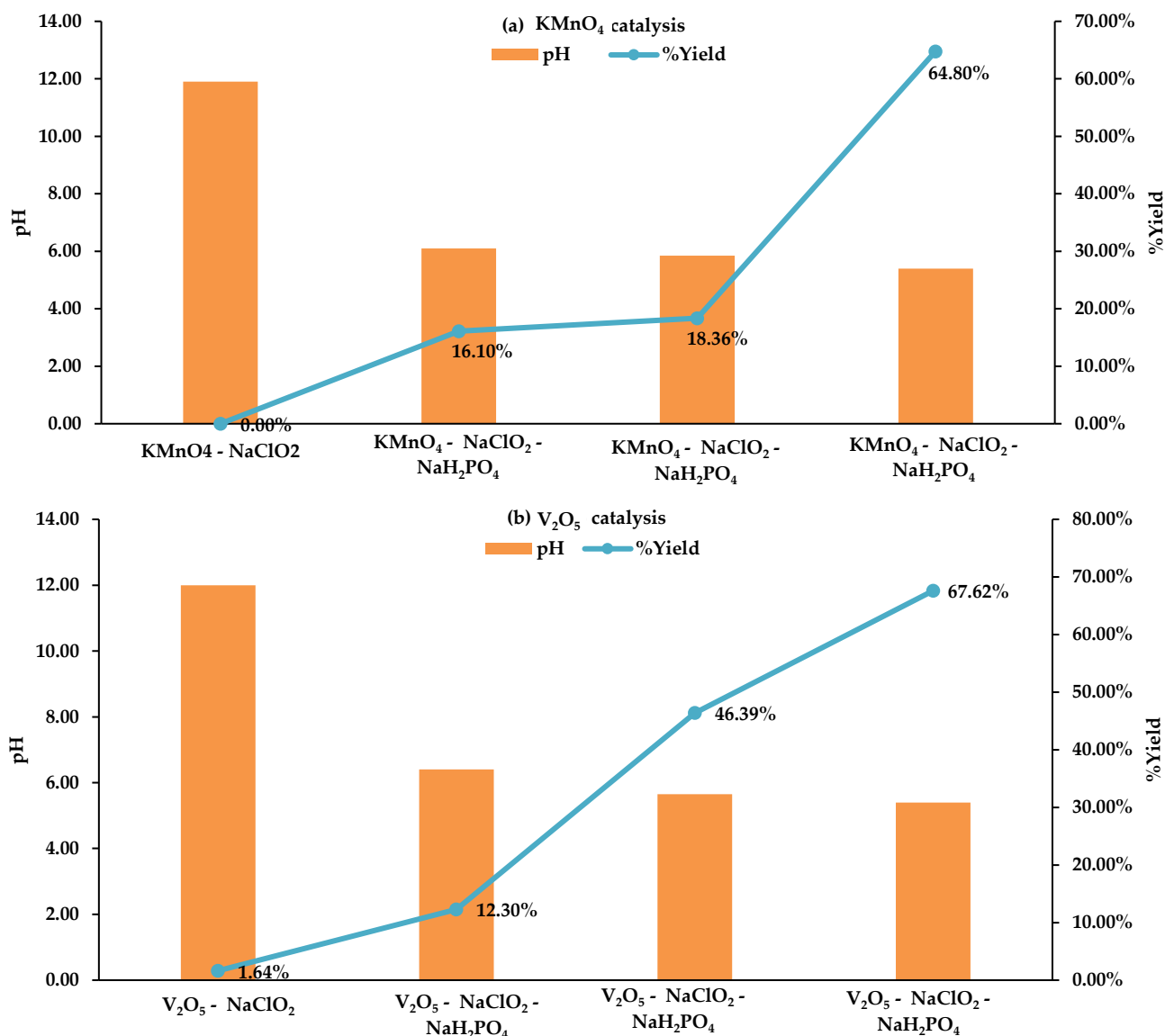


Figure 10. a) KMnO_4 catalysis with $\text{NaH}_2\text{PO}_4 + \text{NaClO}_2$ system, b) V_2O_5 catalysis with $\text{NaH}_2\text{PO}_4 + \text{NaClO}_2$ system

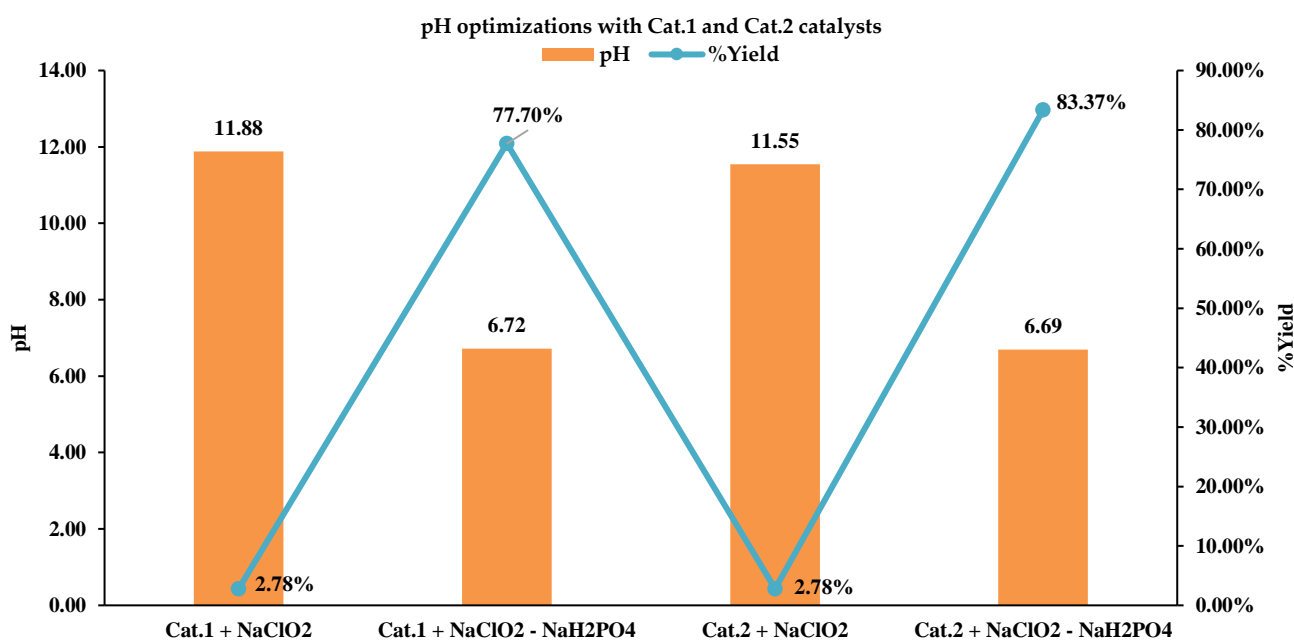


Figure 11. Catalytic conversion yields of benzoic acid at different pHs with Cat.1 and Cat.2

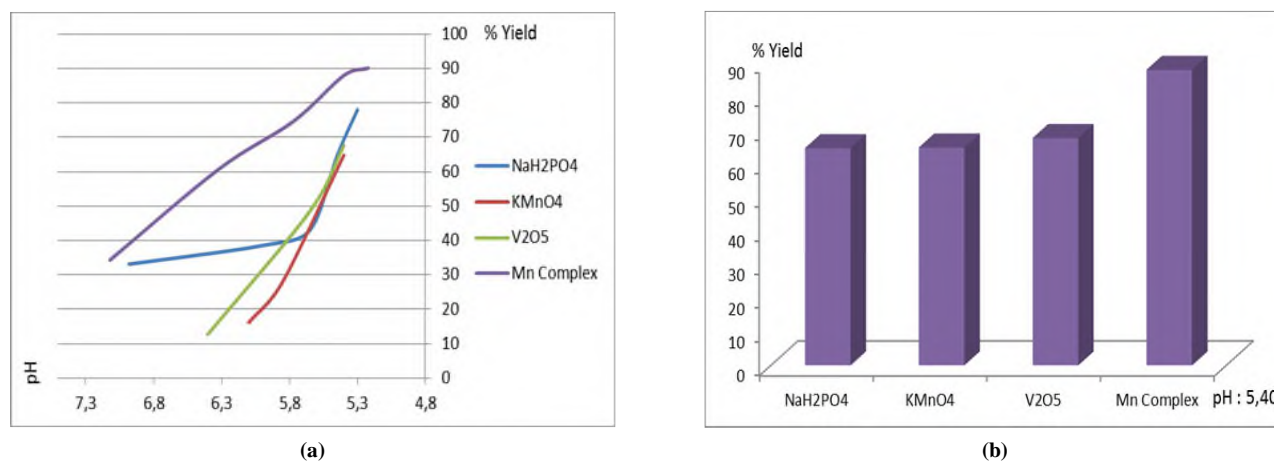


Figure 12. a) The pH-yield variation of catalysts, b) The yield comparison of catalysts at pH 5.40

Although benzoic acid conversion was monitored by UV-Vis spectroscopy (Fig. 9), the isolated benzoic acid yields were presented to justify the results.

Other organic acids such as HEDP and citric acid which have been known of their application with NaClO₂ were also used as buffering agents [36,37].

In these applications, benzoic acid yields gradually increasing with the pH structure were obtained.

The catalytic studies were continued with KMnO₄ and V₂O₅ which were used with the NaH₂PO₄+NaClO₂ combination. While no product was obtained with KMnO₄ at high pH (pH: 12), in the study conducted with the V₂O₅ catalyst, 1.6% benzoic acid yield was obtained at pH: 12. However, it was observed that the other yields obtained by pH change were lower compared to the yields obtained with the combination of NaH₂PO₄+NaClO₂, which was assigned that the catalysts were not sufficient to stabilize the formed ClO₂ (Fig. 10a and b).

In the last step of the study, the prepared complexes ([Mn(III)(acac)₃Cl] and [Mn(III)(SchL)Cl]) were used as catalysts (Cat.1 and Cat.2). For both complexes, benzoic acid formation was observed at pH values above 11.5. However, benzoic acid was obtained in very high yields of 77.7% and 83.4% at pH values close to neutral (pH: 6.72 and pH: 6.69), respectively by using Cat.1 and Cat.2 (Fig. 11).

Benzoic acid yields of the catalysts depending on pH are shown in the graph in Fig. 12a. It is seen that the benzoic acid yield in NaH₂PO₄ buffer depends entirely on the pH value and increases rapidly after pH: 5.8. For KMnO₄ and V₂O₅ catalysts, lower yields were obtained due to the reaction of the catalysts with ClO₂ formed at pH < 5.5, while the same effect was observed with buffer at pH > 5.5. When the graph of Cat.2, one of the prepared catalysts, was examined, the catalytic effect was clearly seen, and it was understood that the reaction was catalyzed at every pH value. The highest efficiency for Cat.2 was determined as 90% at pH: 5.40. The

comparative yields of other catalysts at the same pH value are given in Fig. 12b.

4. Conclusion

Firstly, measurements were taken by using stabilized chlorine dioxide solution directly as an oxidation reagent to make sure if the substituent bearing on the benzene ring effected the reaction kinetic. Free -OH group bearing benzaldehyde derivative did not give any conversion. NaH₂PO₄ was used as a buffering agent for adjusting the reaction pH to the desired value. The lower the pH, the greater the yield of benzoic acid obtained. Other oxidation combinations tested included Sodium Chlorite with Sodium Tripolyphosphate (STPP), 1-Hydroxyethylidene-1,1-Diphosphonic Acid (HEDP), and formic acid. STPP was used to modulate the oxidative capacity of sodium chlorite, phosphonic acid to enhance the effect of sodium chlorite, and formic acid to strengthen the oxidation process.

The combination of the catalyst with sodium chlorite was utilized to enhance the yield of the reaction by balancing the oxidative powers of sodium chlorite in the corresponding pH. Subsequently, the addition of KMnO₄ aimed to increase the oxidation capacity. Additionally, during the oxidation process, measurements were taken by adding V₂O₅ to the combination of Sodium Dihydrogen Phosphate and Sodium Chlorite as an extra catalyst. But not much improvement was observed for these applications.

Furthermore, Mn (III) complexes were also examined as catalysts (Cat.1 and Cat.2) which are organic compounds containing transition metals and are effective catalysts in oxidative processes. It was found that the use of Mn (III) complexes (Cat.1 and Cat.2) in NaH₂PO₄+NaClO₂ combination provided the highest yield in the oxidation of aromatic aldehydes to acids. For the catalytic application in buffer solutions, a leveling effect was observed which was resulting in slow ClO₂

formation. Mn complexes (Cat.1 and Cat.2) exhibited a similar leveling effect in buffer solutions with a pH >1. These findings proved that utilizing Mn complexes in a NaH₂PO₄ environment yields the highest conversion rates.

Acknowledgement

I would like to express my gratitude to the Scientific Research Projects Commission (BAP) of Sakarya University (Project No: 2014-02-04-007 and LÜTEP Project No: 2022-7-24-169) for their support in conducting and financially backing this study.

References

- [1] BÄCKVALL, Jan-Erling (ed.), *Modern oxidation methods* (2nd edition), 2011, USA, John Wiley & Sons.
- [2] B.O. Lindgren, T. Nilsson, *Preparation of carboxylic acids from aldehydes (including hydroxylated benzaldehydes) by oxidation with chlorite*, *Prep Org Chem*, 4, 1973, 35.
- [3] G. Tojo, M. Fernández, *Oxidation of primary alcohols to carboxylic acids: A guide to current common practice (Basic Reactions in Organic Synthesis)*, (2007th edition), 2006, USA, Springer.
- [4] A. Raach, O. Reiser, *Sodium chlorite-hydrogen peroxide—A mild and selective reagent for the oxidation of aldehydes to carboxylic acids*, *J Prakt Chem*, 342:6, 2000, 605-608.
- [5] J.M. Grill, J.W. Ogle, S.A. Miller, *An efficient and practical system for the catalytic oxidation of alcohols, aldehydes, and α , β -unsaturated carboxylic acids*, *J Org Chem*, 71:25, 2006, 9291-9296.
- [6] G. Pass, *Practical Inorganic Chemistry: Preparations, Reactions and Instrumental Methods* (2nd edition), 2013, USA, Springer Science & Business Media.
- [7] G. Lunn, E.B. Sansone, *Destruction of Hazardous Chemicals in the Laboratory* (4th edition), 2023, USA, John Wiley & Sons.
- [8] A. Asghar, A.A.A. Raman, W.M.A.W. Daud, *Advanced oxidation processes for in-situ production of hydrogen peroxide/hydroxyl radical for textile wastewater treatment: A review*, *J Clean Prod*, 87, 2015, 826–838.
- [9] H.B. Ji, *β -Cyclodextrin promoted oxidation of aldehydes to carboxylic acids in water*, *Chin Chem Lett*, 20, 2009, 139–142.
- [10] T. Beddoes, Davy, In *A History of Chemistry* (Latest edition), 1964, Palgrave, London.
- [11] N. Riegels, M.J. Richards, *Humphry Davy: His life, works, and contribution to anesthesiology*, *J Am Soc Anesthesiol*, 114, 2011, 1282–1288.
- [12] M. Zhao, *Oxidation of primary alcohols to carboxylic acids with sodium chlorite catalyzed by TEMPO and bleach*, *J Org Chem*, 64(7), 1999, 2564–2566.
- [13] S.B. Jonnalagadda, S. Nadupalli, *Chlorine dioxide for bleaching, industrial applications and water treatment*, *Indian Chem Eng*, 56(2), 2014, 123–136.
- [14] W. Gan, Y. Ge, Y. Zhong, X. Yang, *The reactions of chlorine dioxide with inorganic and organic compounds in water treatment: Kinetics and mechanisms*, *Environ Sci Water Res Technol*, 6(9), 2020, 2287–2312.
- [15] A.R. Mohite, R.G. Bhat, *A practical and convenient protocol for the synthesis of (E)- α , β -unsaturated acids*, *Org Lett*, 15(17), 2013, 4564–4567.
- [16] A.P. Krapcho, *Uses of sodium chlorite and sodium bromate in organic synthesis: A review*, *Org Prep Proced Int*, 38(2), 2009, 177–216.
- [17] S. Erdemir, *Schiff bazı ve polimerlerinin geçiş metal komplekslerinin sentezi karakterizasyonu ve oksidasyon katalizörü olarak etkilerinin incelenmesi*, Doktora Tezi, Çukurova Üniversitesi, Fen Bilimleri Enstitüsü, 2007.
- [18] S. Abramovici, R. Neumann, Y. Sasson, *Sodium hypochlorite as oxidant in phase transfer catalytic systems: Part I. Oxidation of aromatic aldehydes*, *J Mol Catal*, 29(3), 1985, 291–297.
- [19] S.D. Hicks, *Non-heme manganese catalysts for on-demand production of chlorine dioxide in water and under mild conditions*, *J Am Chem Soc*, 136, 2014, 3680–3686.
- [20] K. Ohkubo, *Dihydroxylation of styrene by sodium chlorite with scandium triflate*, *J Phys Org Chem*, 30(e3619), 2016, 5.
- [21] M.Y. Xu, Y.L. Lin, T.Y. Zhang, C.Y. Hu, Y.L. Tang, J. Deng, B. Xu, *Chlorine dioxide-based oxidation processes for water purification: A review*, *J Hazard Mater*, 436, 2022, 129195.
- [22] V. Rougé, Y. Lee, U. von Gunten, S. Allard, *Kinetic and mechanistic understanding of chlorite oxidation during chlorination: Optimization of ClO₂ pre-oxidation for disinfection byproduct control*, *Water Res*, 220, 2022, 118515.
- [23] K. Furukawa, M. Shibuya, Y. Yamamoto, *Chemoselective catalytic oxidation of 1,2-diols to α -hydroxy acids controlled by TEMPO–ClO₂ charge-transfer complex*, *Org Lett*, 17(9), 2015, 2282–2285.
- [24] J. Cubillos, S. Vásquez, C.M. de Correa, *Salen manganese (III) complexes as catalysts for R-(+)-limonene oxidation*, *Appl Catal A Gen*, 373(1-2), 2010, 57–65.
- [25] A.V. Kutchin, I.V. Fedorova, I.V. Loginova, I.Y. Chukicheva, *Features of the use of ClO₂ in the oxidation of some alkylphenols*, *Russ Chem Bull*, 72(1), 2023, 202–212.
- [26] A. Westphal, A. Klinkebiel, H.M. Berends, H. Broda, P. Kurz, F. Tuczek, *Electronic structure and spectroscopic properties of mononuclear manganese (III) Schiff base complexes: A systematic study on [Mn(acen)X] complexes by EPR, UV/vis, and MCD spectroscopy (X= Hal, N CS)*, *Inorg Chem*, 52(5), 2013, 2372–2387.
- [27] R. Habib, *Method for the production of chlorine dioxide*, 1993, US5380518A.
- [28] S.S. Nielsen, C. Tyl, B. P. Ismail, *Preparation of reagents and buffers*, *Food Analysis Laboratory Manual* (5th edition), 2017, 21–32.
- [29] P. Sen, D. Kara Simsek, S.Z. Yildiz, *Functional zinc (II) phthalocyanines bearing Schiff base complexes as oxidation catalysts for bleaching systems*, *Appl Organomet Chem*, 29(8), 2015, 509–516.
- [30] G. Kaya, *Oksidasyon katalizörü olarak çeşitli koordinasyon bileşiklerinin hazırlanması, karakterizasyonu ve etkinliklerinin ölçülmesi*, Doctoral Thesis, Sakarya University, Fen Bilimleri Enstitüsü, 2018.
- [31] E.N. Jacobsen, W. Zhang, A.R. Muci, J.R. Ecker, L. Deng, *Highly enantioselective epoxidation catalysts derived from 1,2-diaminocyclohexane*, *J Am Chem Soc*, 113(18), 1991, 7063–7064.
- [32] S.D. Hicks, S. Xiong, C. J. Bougher, G. A. Medvedev, J. Caruthers, M.M. Abu-Omar, *Mechanistic study of a manganese porphyrin catalyst for on-demand production of chlorine dioxide in water*, *J Porphyrins Phthalocyanines*, 19(01n03), 2015, 492–499.
- [33] P. Barman, A. S. Faponle, A. K. Vardhaman, D. Angelone, A. M. Lohr, W.R. Browne, S.P. de Visser, *Influence of ligand architecture in tuning reaction bifurcation pathways for chlorite oxidation by non-heme iron complexes*, *Inorg Chem*, 55(20), 2016, 10170–10181.
- [34] Z. Hu, H. Du, W.L. Man, C.F. Leung, H. Liang, T.C. Lau, *Catalytic reactions of chlorite with a polypyridylruthenium (II) complex: Disproportionation, chlorine dioxide formation and alcohol oxidation*, *Chem Commun*, 48(8), 2012, 1102–1104.
- [35] I. Fábíán, *The reactions of transition metal ions with chlorine (III)*, *Coord Chem Rev*, 216, 2001, 449–472.

- [36] S. Z. Yıldız, S. Dursun, The investigation of the effect of sodium chlorite and phosphonic acid catalysts on cotton bleaching process conditions, *Turk J Anal Chem*, 5(1), 2023, 61–69.
- [37] S. Dursun, S.Z. Yıldız, Eco-friendly bleaching of cotton fabrics without heating using direct process water in the presence of sodium chlorite and phosphonate, *J Nat Fibers*, 20(1), 2023, 2146248.



Parentucellia viscosa (growing in Türkiye): Essential Oil, Phenolic Composition, Antimicrobial and Lipase Inhibition

Büşra Korkmaz^{1,2*} , Gözde Bozdal¹ , Büşra Şahin¹ , Sıla Özlem Sener³ , Elif Öztürk⁴ , Seda Fandakli⁵ , Şengül Alpay Karaoğlu⁶ , Nurettin Yaylı¹ 

¹ Karadeniz Technical University, Faculty of Pharmacy, Department of Pharmacognosy, 61080, Trabzon, Türkiye.

² Karadeniz Technical University, Graduate School of Health Sciences, 61080, Trabzon, Türkiye.

³ Health Sciences University, Faculty of Gülhane Pharmacy, Department of Pharmacognosy, 06010, Ankara, Türkiye.

⁴ Karadeniz Technical University, Faculty of Health Sciences, Department of Nutrition and Dietetics, 61080, Trabzon, Türkiye.

⁵ Artvin Çoruh University, Vocational School of Health Services, Medical Laboratory Techniques Program, 08000, Artvin, Türkiye.

⁶ Recep Tayyip Erdoğan University, Faculty of Science, Department of Biology, 53100, Rize, Türkiye.

Abstract

The essential oil (EO) and phenolic constituents of *Parentucellia viscosa* L. were analyzed by GC-FID-MS and HPLC, respectively. A total of 20 volatile compounds were identified accounting for 99.97% in hydrodistillation. Monoterpenes (50.57%, 5 compounds) were the primary chemical class in the essential oil of *P. viscosa*. Limonene (44.02%) and 1-octen-3-ol (25.23%) were the major components in the essential oil of *P. viscosa*. The phenolic constituent analysis for the methanol extract of *P. viscosa* gave benzoic acid (0.97 mg/g) as the major compound. The antimicrobial activities of the EO and crude solvent (*n*-hexane, acetonitrile, methanol, and water) extracts of *P. viscosa* were screened *in vitro* against ten microorganisms. *n*-Hexane and the acetonitrile extracts of *P. viscosa* resulted in the best activity against *Mycobacterium smegmatis* with IC₅₀ values of 19.2 µg/mL and 53.8 µg/mL, respectively. The highest lipase enzyme inhibition activity was detected in the *n*-hexane extract with 44.22±1.1628 µg/mL IC₅₀ value.

Keywords: *Parentucellia viscosa*, essential oil, phenolic, antimicrobial, lipase

1. Introduction

Parentucellia viscosa (L.) Caruel is a genus of Orobanchaceae which mainly includes herbaceous parasitic plants and is the most significant parasitic angiosperm family [1]. Four species are distributed in central and southwestern Asia, western Europe, and the Mediterranean, such as *P. viscosa* (L.) Caruel [syn. *Bartsia viscosa* L., *Bellardia viscosa* (L.) Fisch. & C. A. Mey., *Eufragia viscosa* (L.) Benth., *Euphrasia viscosa* (L.) Benth., *Lasiopera viscosa* (L.) Hoffmanns. & Link, *Trixago viscosa* (L.) Rchb.], *Parentucellia latifolia* (L.) Caruel, *Parentucellia latifolia* subsp. *flaviflora* (Boiss.) Hand.-Mazz. and *Parentucellia floribunda* Viv. [2]. The plant is also known as Yellow Glandweed, characterized by the presence of glandular trichomes [3]. *P. viscosa* is endemic to Western Europe and often occurs in roadside vegetation, undeveloped pastures, and other weed species and introduced annual grass [4]. Many chronic metabolic diseases have resulted from obesity, a long-term man-kind problem that causes psychological and

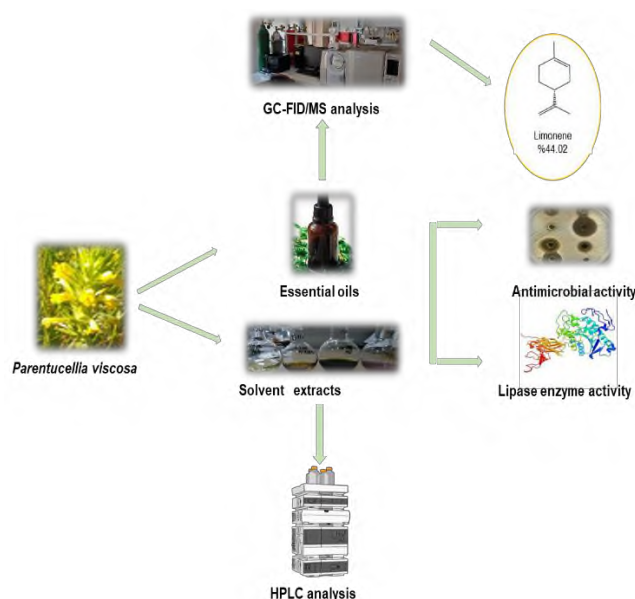


Figure 1. Graphical Illustration

Citation: B. Korkmaz, G. Bozdal, B. Şahin, S.Ö. Sener, E. Öztürk, S. Fandakli, Ş.A. Karaoğlu, N. Yaylı, *Parentucellia viscosa* (growing in Türkiye): Essential Oil, Phenolic Composition, Antimicrobial and Lipase Inhibition, Turk J Anal Chem, 6(2), 2024, 91–96.

doi <https://doi.org/10.51435/turkjac.1513093>

Author of correspondence: busra.yayli@ktu.edu.tr

Received: July 09, 2024

Tel: +90 (462) 325 6762

Accepted: September 09, 2024

Fax: +90 (462) 325 6717

physiological health problems. It is known that pancreatic lipase (PL) inhibitors are used to treat obesity. Research on this relationship has been increasing in recent years. Additionally, many studies have shown that natural products have strong to moderate PL inhibitory activity. These products are interesting for research due to their low toxicity. This low toxicity allows the development of new products in the pharmaceutical industry by utilizing natural resources. [5]. Previous phytochemical investigations of these species have led to the identification of several natural compounds such as iridoid glucosides, melampyroside, 8-epiloganin, gardoside methyl ester, shanzhiside methyl ester, aucubin, mannitol, benzoic acid, gallic acid, and diterpenes [3,6–10] have been reported. These compounds resulted in antibacterial activities [11]. The literature search revealed no research on the chemical composition of EO and phenolic compounds (HPLC). Therefore, in this study, we aimed to investigate the antimicrobial activities and lipase enzyme inhibition of EO and crude solvent (*n*-hexane, acetonitrile, methanol and water) extracts prepared from *P. viscosa*.

2. Material and Methods

2.1. Plant materials

The aerial part of *P. viscosa* (175 g, fresh) was harvested from the Karadeniz Technical University Campus at an altitude of 95 meters in May 2023. The plant was authenticated by Prof. Kamil Coşkunçelebi [1]. The voucher specimen (Coşkunçelebi 1250) has been deposited in the Herbarium of the Faculty of Biology, Karadeniz Technical University, Türkiye.

2.2. Chemicals and reagents

All solvents (*n*-hexane, acetonitrile, and methanol) and other chemicals (Tris-HCl and *p*-nitrophenyl butyrate) used were purchased from Sigma-Aldrich in analytical grade.

2.3. Isolation of essential oils

The aerial part of *P. viscosa* (115 g, fresh) was grounded with a plant mill into small pieces and then hydrodistilled (HD) with a modified Clevenger-type apparatus with a cooling bath (-10 °C, 3h), yield (*w/w*): 0.098%. After the HD, EO was extracted with HPLC grade *n*-hexane (0.5 mL) dried over anhydrous Na₂SO₄ and stored in a dark glass bottle in the refrigerator at -16 °C before the GC-FID-MS analysis [12–15].

2.4. Solvent extractions (*n*-hexane, acetonitrile, methanol, and water)

The aerial parts of the plant (55 g, dry) were blended into small pieces. Blended material (~12 g, each) was extracted (25 mL × 3; 12 h each) using the maceration method at room temperature with analytical grade

n-hexane, acetonitrile, methanol, and water solvents in flasks (50 mL) separately. After the suction filtration, the same extracts were combined and solvents were evaporated or lyophilized to yield crude *n*-hexane (0.0906 g), acetonitrile (0.0675 g), methanol (0.7820 g), and water extracts (0.0755 g) [15–16].

2.5. Gas chromatography-mass spectrometry (GC-FID-MS)

GC-FID-MS analysis of the EO was carried out by a Shimadzu QP2010 ultra, having Shimadzu 2010 plus FID, PAL AOC-5000 plus autosampler, and Shimadzu Class-5000 Chromatography Workstation software. Restek Rxi-5MS capillary column (30 mm × 0.25 mm × 0.25 µm) (USA) was used for the analysis. Sample (1 µL, in HPLC grade *n*-hexane) injection was performed in split mode (1:30) at 230°C. The initial column temperature was 60 °C for 2 min, then increased to 240 °C with a 3°C/min heating ramp. The final temperature for the oven was held at 250°C for 4 minutes. Helium (99.999 %) was the carrier gas with a 1 mL/min flow rate. MS detection was implemented in electronic impact mode (EI, 70 eV, and scan mode 40–450 *m/z*). The sample was analyzed, and the mean was reported [12–20].

2.6. HPLC analyses

HPLC chromatographic analysis of phenolic compounds of *P. viscosa* carried out at Shimadzu Prominence series HPLC instrument using Zorbax Eclipse Plus-C18 (150 mm × 4.6 mm, 5 µm) analytical column. The mobile phase was formed from methanol (A), 2% acetic acid solution (A, pH: 2.65), and ultra-pure water (B). The gradient applied is as follows: 0 min, 80% B; 4 min, 70% B; 7 min, 60% B; 10 min, 55% B; 12 min, 50% B; 14 min, 40% B; 16 min, 20% B. The sample injection volume is 20 µL, and the flow rate is 1.5 mL/min. The column furnace temperature is set at 25 °C. The photodiode array was detected at a wavelength of 270 nm [21].

2.7. Antimicrobial activities

All test microorganisms: *E. coli* ATCC35218, *Y. pseudotuberculosis* ATCC911, *P. aeruginosa* ATCC43288, *E. faecalis* ATCC29212, *S. aureus* ATCC25923, *B. cereus* 709 Roma, *L. monositogeneus* ATCC43251, *M. smegmatis* ATCC607, *C. albicans* ATCC60193, and *S. cerevisiae* RSKK 251 were obtained from the Hıfzısıhha Institute of Refik Saydam (Ankara, Türkiye). The adapted antimicrobial screening test (agar-well diffusion method) was used earlier [22,23,25]. Each tested microorganism was suspended in Brain Heart Infusion (BHI) and diluted approximately 10⁶ colony-forming units (per mL), which were “flood-inoculated” onto the surface of BHI agar and Sabouraud Dextrose Agar (SDA) and then dried. SDA was used for *C. albicans*. Wells (5 mm diameter) were cut from the agar, and the extracts (100 µL, each) were delivered into the wells. The plates were incubated (35 °C, 18h), and antimicrobial activity was evaluated by measuring the

inhibition zone against the test organism. The EO dissolved in n-hexane, and other solvent extracts (acetonitrile, methanol, and water solvents) were dissolved in dimethyl sulfoxide to prepare stock solutions (12,300–108,900 µg/mL). n-Hexane and dimethyl sulfoxide were used as solvent control with a dilution of 1:2. Ampicillin, streptomycin, and fluconazole were used as positive controls at 10 µg/mL, 10 µg/mL, and 5 µg/mL concentrations, respectively (Table 3). After the antimicrobial properties of the EO, n-hexane, acetonitrile, methanol, and water extracts of *P. viscosa* were investigated quantitatively, the minimal inhibition concentration (MIC) values (µg/mL) were calculated [23,25].

2.8. Lipase Assay

Lipase inhibitory assay for the EO and solvent extracts (*n*-hexane, acetonitrile, methanol, and water) of *P. viscosa* were studied by the modified method using *p*-nitrophenyl butyrate (*p*-NPB) as substrate [26]. All extracts (25, 100, 200 and 400 µg/mL concentrations) were dissolved in buffer solution (0.1 M Tris-HCl, pH = 8.0) and 0.1% DMSO. Orlistat was used as positive control and prepared 6.25, 12.5, 25, 50, and 100 µg/mL concentration solutions. The experimental method was designed with A, B, C and D wells; A: 90 enzyme solution [(Crude porcine PL type II)-(200 units/mL)], 5 µL substrate solution (10 mM *p*-NPB in acetonitrile); 5 µL buffer solution (0.1 M Tris-HCl buffer, pH = 8.0); B: 90 µL enzyme solution, 10 µL buffer solution; C: 90 µL enzyme, 5 µL sample solution, 5 µL substrate solution; and D: 90 µL enzyme solution], 5 µL sample solution, 5 µL buffer solution. The plates were incubated at 37 °C (15 min) then substrate solution (10 mM *p*-NPB in acetonitrile) was added to each related well which was incubated again at 37 °C (15 min). The absorbance of the solutions was observed at 405 nm in a 96-well microplate using a SpectrostarNano-BMG LABTECH spectrophotometer. Experiments were carried out in triplicate. Results were stated (Table 4) as mean ± standard deviation (SD). The statistical significance level was considered as $p < 0.05$. The percentage of PPL inhibition was calculated by the following equation: PPL inhibition (%) = $[(A-B)-(C-D)]/(A-B) \times 100$. Finally, IC₅₀ values for the PPL were calculated graphically [26].

3. Results and Discussion

GC-MS analysis was performed on volatile components found in the *P. viscosa* EO using the Rxi-5MS capillary column. By comparing RI and MS data with libraries from NIST, Wiley7NL, FFNSC1.2, and W9N11, the

Table 1. GC-FID-MS analysis of the EO obtained from *P. viscosa*

Compounds	RI*	RI ^a	(%) ^b
2-Ethylfuran	728	731	2.72
1,3,5-Cycloheptatriene	765	767	2.34
Capronaldehyde	803	801	3.96
2-(<i>E</i>)-hexenal	855	858	4.05
Hexanol	863	864	1.58
Benzaldehyde	960	965	2.61
1-Octen-3-ol	978	978	25.23
3-Octanone	979	982	2.19
Myrcene	988	987	0.91
α -Terpinene	1014	1015	0.46
<i>o</i> -Cymene	1022	1023	1.67
Limonene	1031	1030	44.02
Phenyl acetaldehyde	1044	1043	1.31
γ -Terpinene	1054	1058	3.51
Pelargonaldehyde	1100	1101	0.38
Terpinen-4-ol	1174	1179	1.10
β -Cyclocitral	1224	1224	0.47
Theaspirane	1298	1301	0.38
β -Damascenone	1386	1386	0.61
Valencene	1496	1495	0.47
Chemical classes	NC ^c	% ^b	
Monoterpenes	5	50.57	
Oxygenated monoterpene	1	0.48	
Sesquiterpene	1	0.47	
Terpene related	2	0.99	
Aldehydes	5	12.31	
Alcohols	3	27.91	
Aliphatic hydrocarbon	1	2.34	
Aromatic hydrocarbon	1	2.72	
Ketone	1	2.19	
Total	20	99.97	

*Literature RI values.

^aRetention Index calculated from retention times relative to that of the *n*-alkane series (C₆–C₃₀).

^b%. Percentages obtained by FID peak-area normalization.

^cNC: Number of compounds.

chemical components in the EO were determined [12–20,24]. Table 1 shows the chemical compound structure, % concentration, and computed retention indices for the constituents of *P. viscosa*. GC-FID/MS analyses for the fresh aerial part of *P. viscosa* revealed 20 natural compounds within the ratio of 99.97%. Limonene (44.02%), 1-octen-3-ol (25.23%), (2*E*)-hexenal (4.05%), capronaldehyde (3.96%), and γ -terpinene (3.51%) were found to be major compounds in the EO of the *P. viscosa* (Table 1). The results revealed that the high terpene chemicals were monoterpenes, which are the primary components of EO derived from *P. viscosa*'s aerial parts. Alcohol (27.91%) and aldehyde (12.31%) were found to be the second main components in the EO of *P. viscosa*. In comparison to the previously published data, the EO of *Parentucellia latifolia* has been reported and 5 components were characterized, representing 99.5% of the oil.

Table 2. Phenolic constituent of the methanol extract obtained from *P. viscosa*

Extract	<i>p</i> -OH benzoic acid	Vanillic acid	Syringaldehyde	Coumaric acid	Sinapic acid	Benzoic acid	Quercetin
mg/g							
Methanol	—	0.51	—	—	0.79	0.97	0.39

Table 3. Antimicrobial activity of the EO and solvent extracts obtained from *P. viscosa*.

Sample extracts	Const. (µg/mL)	Microorganisms, inhibition zone (mm), and MIC (µg/mL)										
		Zone	Gram (-)				Gram (+)			No Gr.		Fungi
			<i>Ec.</i>	<i>Yp.</i>	<i>Pa.</i>	<i>Ef.</i>	<i>Sa.</i>	<i>Bc.</i>	<i>Li.</i>	<i>Ms.</i>	<i>Ca.</i>	<i>Sc.</i>
EO	86000	Zone	—	—	—	—	7	—	—	9	—	—
		MIC	—	—	—	—	4300	—	—	2150	—	—
<i>n</i> -Hexane	12300	Zone	—	—	—	—	—	8	—	15	—	—
		MIC	—	—	—	—	—	307.5	—	19.2	—	—
Acetonitrile	34400	Zone	—	—	—	—	—	—	6	16	—	—
		MIC	—	—	—	—	—	—	1720	53.8	—	—
Methanol	137000	Zone	—	—	—	—	—	7	—	10	—	—
		MIC	—	—	—	—	—	3424	—	1712	—	—
Water	108900	Zone	—	—	—	—	—	—	—	—	—	—
		MIC	—	—	—	—	—	—	—	—	—	—
Amp.	10	Zone	10	10	18	10	10	15	—	—	—	—
		MIC	10	18	128	35	10	15	—	—	—	—
Strep.	10	Zone	—	—	—	—	—	—	35	—	—	—
		MIC	—	—	—	—	—	—	4	—	—	—
Flu.	5	Zone	—	—	—	—	—	—	—	25	25	25
		MIC	—	—	—	—	—	—	—	<8	<8	<8

Ec.: *Escherichia coli*, *Yp.*: *Yersinia pseudotuberculosis*, *Pa.*: *Pseudomonas aeruginosa*, *Sa.*: *Staphylococcus aureus*, *Ef.*: *Enterococcus faecalis*, *Bc.*: *Bacillus cereus* 702 Roma, *Li.*: *Listeria monositogenez*, *Ms.*: *Mycobacterium smegmatis*, *Ca.*: *Candida albicans*, *Sc.*: *Saccharomyces cerevisiae*, Amp.: Ampicillin, Strep.: Streptomycin, Flu.: Fluconazole, (-): no activity of test concentrations

Germacrene D and germacrene B were the main compounds as sesquiterpene hydrocarbons accounting for 59.2% and 24.3% of the oil, respectively [2]. However, in this work, limonene and 1-octen-3-ol were the major constituents in the EO of the *P. viscosa* which could be used as a taxonomical marker. Volatile constituent variations in the EO of *P. viscosa* with another genus could be the environmental and analysis conditions.

HPLC was used to examine the phenolic profile of methanol extract from *P. viscosa*, using standards including *p*-hydroxybenzoic acid, benzoic acid, quercetin, vanillic acid, sinapic acid, syringaldehyde, and *p*-coumaric acid. Results indicated that benzoic acid (0.97 mg/g), sinapic acid (0.79 mg/g), and vanillic acid (0.51 mg/g) were major constituents of *P. viscosa*. Quercetin was also found in the amount of 0.39 mg/g in the methanol extract (Table 2).

The antimicrobial activities of *P. viscosa* EO and solvent extracts were tested against *Escherichia coli*, *Yersinia pseudotuberculosis*, *Pseudomonas aeruginosa*, *Staphylococcus aureus*, *Enterococcus faecalis*, *Bacillus cereus*, *Listeria monositogenez*, *M. smegmatis*, *Candida albicans*, and *Saccharomyces cerevisiae* using an in vitro agar diffusion method (Table 3). Inhibition zones were measured in mm and then MIC (µg/mL) values were calculated

Table 4. Lipase inhibition of the EO and solvent extracts obtained from *P. viscosa*

Extracts	IC ₅₀ (µg/mL)*
Essential oil	49.50 ± 2.12
<i>n</i> -Hexane	44.22 ± 1.16
Acetonitrile	199.42 ± 4.88
Methanol	78.89 ± 3.42
Water	52.60 ± 1.88
Orlistat	13.52 ± 1.42

*Results were stated as mean ± standard deviation (SD). The statistical significance level was considered as $p < 0.05$

[22–23]. The crude *n*-hexane extract of *P. viscosa* had the highest activity against *M. smegmatis* with a 15 mm inhibition zone diameter (MIC, 19.2 µg/mL) and *B. cereus* with an 8 mm inhibition zone (MIC, 307.5 µg/mL). The EO was only active against *S. aureus* and *M. smegmatis* which was effective in anti-tuberculosis activity against *M. smegmatis* within 2150 µg/ml MIC values. The most active extract of *P. viscosa* against *M. smegmatis* (16 mm, 53.8 µg/mL) was found in acetonitrile. It was discovered that the EO and solvent extracts (without water) were more efficient in eliminating no-gram bacteria (*M. smegmatis*). No activity against gram-negative or fungi was detected in essential oils and extracts. Antimicrobial activity results indicate the presence of active compounds in *n*-hexane, acetonitrile, and EO extracts. The previous antimicrobial assessment of crude dichloromethane and methanol extracts obtained from *P. viscosa* showed the greatest inhibition zone diameter against *P. aeruginosa*, *Proteus vulgaris*, *Klebsiella pneumoniae*, *Enterobacter*, *E. coli*, and *S. aureus*, respectively [11]. In our case, extracts (except water extract) were more active to *M. smegmatis*, which could be the fact of the location and time collection of the plant.

Research has shown that terpenoids, polyphenols, flavonoids, and other naturally occurring chemicals can suppress the activity of lipase [5]. Terpenoids are often the main components of *n*-hexane extract and essential oil [13,14]. As a result, we evaluated the lipase activity of *P. viscosa* essential oil and solvent extracts. Lipase enzyme inhibition activities of solvent extracts and essential oil of *P. viscosa* were investigated against orlistat as a positive control (IC₅₀: 13.52±1.42 µg/mL) (Table 4). The *n*-hexane extract showed the highest

activity, with an IC₅₀ of 44.22±1.16 µg/mL. Afterward, the best activity was found in essential oil (IC₅₀: 49.50±2.1220 µg/mL). Lipase inhibition activities of acetonitrile, methanol, and water extracts of *P. viscosa* were found with IC₅₀ values of 199.42±4.88 µg/mL, 78.89±3.42 µg/mL, and 52.60±1.88 µg/mL, respectively. The lowest activity was observed at the highest polarity. A positive correlation was observed between polarity reduction and lipase activity.

4. Conclusions

The EO and phenolic composition for the aerial part of the *P. viscosa* were characterized by GC-FID-MS and HPLC, respectively. Monoterpenes (50.57%) were identified as the main chemical class in the EO of *P. viscosa*. The major components in the EO of *P. viscosa* were limonene and 1-octen-3-ol. The antimicrobial activities for the EO and crude solvent extracts of *P. viscosa* showed that *n*-hexane and acetonitrile extracts showed the best activity against *M. smegmatis* with IC₅₀ values of 19.2 and 53.8 µg/mL, respectively. Resulted antimicrobial activities suggest the availability of active compounds in *n*-hexane, acetonitrile extracts, and the oil. The highest lipase enzyme inhibition activity was detected in the *n*-hexane extract with an IC₅₀ value of 44.22 ± 1.16 µg/mL. A positive correlation was observed between polarity reduction and lipase activity. Thus, the reported lipase enzyme and antimicrobial assay results collectively imply that *P. viscosa* EO, *n*-hexane, and acetonitrile extracts may hold promise for use in medicinal applications. In a future investigation, bio-guided activity isolation and purification of *P. viscosa*, particularly the *n*-hexane extract, could be performed to improve bioavailability.

Acknowledgments

We are thankful to Karadeniz Technical University for the financial support and to Prof. Dr. Kamil Coşkunçelebi for identifying the plant.

References

- [1] A. Güner, S. Aslan, T. Ekim, M. Vural, M. T. Babaç, Türkiye Plants List; Vascular Plants, Nezahat Gökyiğit Botanical Garden and Flora Research Association Publication, 2012, 657.
- [2] N. Badalamenti, M. Bruno, C. Formisano, and D. Rigano, Effect of Germacrene-Rich Essential Oil of *Parentucellia latifolia* (L.) Caruel Collected in Central Sicily on the Growth of Microorganisms Inhabiting Historical Textiles, *Nat Prod Comm*, 17(4), 2022, 1934578X221096963.
- [3] A. Venditti, M. Ballero, M. Serafini, A. Bianco, Polar compounds from *Parentucellia viscosa* (L.) Caruel from Sardinia, *Nat Prod Res*, 29(7), 2015, 602-606.
- [4] J. Pate, T. Bell, Host associations of the introduced annual hemiparasite *Parentucellia viscosa* in agricultural and bushland settings in Western Australia, *Ann Bot*, 85(2), 2000, 203-213.
- [5] T.T. Liu, X.T. Liu, Q.X. Chen, Y. Shi, Lipase inhibitors for obesity: A review, *Biomed Pharmacother*, 128, 2020, 110314.
- [6] A. Bianco, P. Passacantilli, G. Righi, M. Nicoletti, Iridoid glucosides from *Parentucellia viscosa*, *Phytochemistry*, 24(8), 1985, 1843-1845.
- [7] M. Grande, A. Fernández-Mateos, J.J. Blanco, M.M. Herrador, J.F.Q. del Moral, P. Arteaga, J.F. Arteaga, A.F. Barrero, Diversity on Diterpene Composition in Two Populations of *Parentucellia viscosa*: Labdane and Clerodane Chemotypes, *Nat Prod Commun*, 2(6), 2007, 621-624.
- [8] E.J. Llorent-Martínez, M.L. Fernández-de Córdoba, G. Zengin, M.B. Bahadori, M.Z. Aumeeruddy, K.R. Rengasamy, M.F. Mahomoodally, *Parentucellia latifolia* subsp. *latifolia*: A potential source for loganin iridoids by HPLC-ESI-MSn technique, *J Pharm Biomed*, 165, 2019, 374-380.
- [9] J. Urones, I. Marcos, I. Cubillo, N.M. Garrido, P. Basabe, Terpenoid compounds from *Parentucellia latifolia*, *Phytochemistry*, 29(7), 1990, 2223-2228.
- [10] J. Urones, I. Marcos, L. Cubillo, V. Monje, J. Hernández, P. Basabe, Derivatives of malonic acid in *Parentucellia latifolia*, *Phytochemistry*, 28(2), 1989, 651-653.
- [11] Z. Amar, S.N. Labib, G. Nouredine, R. Salah, Phytochemical screening of five Algerian plants and the assessment of the antibacterial activity of two *Euphorbia guyoniana* extracts, *Pharmacia Lettre*, 4(5), 2012, 1438-1444.
- [12] R.P. Adams, Identification of essential oil components by gas chromatography/mass spectrometry: Allured publishing corporation Carol Stream, IL, 2007.
- [13] G. Kılıç, B. Korkmaz, İ. Erik, S. Fandaklı, S.S. Yaylı, Ö. Faiz, Ş. Alpay Karaoğlu, N. Yaylı, Antimicrobial, antioxidant, tyrosinase activities and volatile compounds of the essential oil and solvent extract of *Epilobium hirsutum* L. growing in Turkey, *Turk J Chem*, 2(2), 2020, 87-94.
- [14] İ. Erik, G. Kılıç, E. Öztürk, Ş.A. Karaoğlu, N. Yaylı, Chemical composition, antimicrobial, and lipase enzyme activity of essential oil and solvent extracts from *Serapias orientalis* subsp. *orientalis*, *Turk J Chem*, 44(6), 2020, 1655-1662.
- [15] N. Yaylı, A. Yaşar, C. Güleç, A. Usta, S. Kolaylı, K. Coşkunçelebi, S.A. Karaoğlu, Composition and antimicrobial activity of essential oils from *Centaurea sessilis* and *Centaurea armena*, *Phytochemistry*, 66(14), 2005, 1741-1745.
- [16] N. Yaylı, E. Oksuz, B. Korkmaz, İ. Erik, S. Fandaklı, Ö. Faiz Ö. K. Coşkunçelebi, Volatile and Phenolic Contents, Antimicrobial and Tyrosinase activities of Two Endemic Species *Scorzonera pisidica* and *Scorzonera sandrasica* L. Grown in Turkey, *Rec Nat Prod*, 16(1), 2022, 46-57.
- [17] İ. Erik, G. Kılıç, B. Korkmaz, S. Fandaklı, Ş.A. Karaoğlu, N. Yaylı, Volatile constituents and antimicrobial activity of *Vinca major* L. subsp. *hirsuta* (Boiss) stearn grown in Turkey, *J Res Pharm*, 25(5), 2021, 581-588.
- [18] N. Yaylı, C. Güleç, O. Üçüncü, A. Yaşar, S. Ülker, K. Coşkunçelebi, S. Terzioğlu, Composition and antimicrobial activities of volatile components of *Minuartia meyeri*, *Turk J Chem*, 30(1), 2006, 71-76.
- [19] T.B. Cansu, B. Yaylı, T. Özdemir, N. Batan, Ş.A. Karaoğlu, N. Yaylı, Antimicrobial activity and chemical composition of the essential oils of mosses (*Hylocomium splendens* (Hedw.) Schimp. and *Leucodon sciuroides* (Hedw.) Schwägr.) growing in Turkey, *Turk J Chem*, 37(2), 2013, 213-219.
- [20] O.D. Sparkman, Identification of essential oil components by gas chromatography/quadrupole mass spectroscopy, *J Am Soc Mass Spectrom*, 16(11), 2005, 1902.
- [21] N. Korkmaz, S.O. Sener, N. Balturk, S. Kanbolat, M. Badem, R. Aliyazicioglu, U. Ozgen, A. Kandemir, S. Alpay Karaoğlu, Determination of Phenolic Contents by HPLC, and Antioxidant,

- Antimicrobial, Antityrosinase, and Anticholinesterase Activities of *Psephellus huber-morathii*, *J Pharm Res Int*, 26(1), 2019, 1-10.
- [22] A.L. Barry, Methods for determining bactericidal activity of antimicrobial agents: approved guideline, National Committee for Clinical Laboratory Standards: National Committee for Clinical Laboratory Standards Wayne, PA, 1999.
- [23] G.L. Woods, Susceptibility testing of mycobacteria, nocardiae, and other aerobic actinomycetes, *Approved Standard M24-A2*, 31(5), 2011.
- [24] N. Andriamaharavo, Retention Data NIST Mass Spectrometry Data Center, NIST Mass Spectrometry Data Center, 2014.
- [25] G.L. Woods, B.A. Brown-Elliott, E.P. Desmond, G.S. Hall, L. Heifets, G.E. Pfyffer, Susceptibility testing of mycobacteria, nocardiae, and other aerobic actinomycetes. approved standard, NCCLS document M24-A, 23(18), 2003.
- [26] S.O. Sener, U. Ozgen, S. Kanbolat, N. Korkmaz, M. Badem, H. Hanci, T. Dirmenci, T. Arabaci, R. Aliyazicioglu, E. Yenilmez, G. Saltan Işcan, Investigation of therapeutic potential of three endemic *Cirsium* species for global health problem obesity, *S Afr J Bot*, 141, 2021, 243-254.



Metabolic stability of a hydrazone derivative: *N'*-[(4-chlorophenyl)methylidene)]-4-[(4-methylphenyl)sulfonyloxy]benzohydrazide

Hasan Erdiñç Sellitepe^{1*} , Göknil Pelin Coşkun² , Kaan Birgöl³ , Mert Ülgen² , İnci Selin Doğan¹ 

¹ Karadeniz Technical University, Faculty of Pharmacy, Department of Pharmaceutical Chemistry, 61080, Trabzon, Türkiye

² Acibadem Mehmet Ali Aydınlar University, Faculty of Pharmacy, Department of Pharmaceutical Chemistry, 34684, İstanbul, Türkiye

³ Bahçeşehir University, Faculty of Pharmacy, Department of Pharmaceutical Chemistry, 34353, İstanbul, Türkiye

Abstract

Metabolic stability, a key parameter in drug development, refers to a drug substance's resistance to metabolism. The failure rate can be significantly reduced by conducting metabolism studies for the drug candidate compound from the early stages. These studies are primarily carried out on *in vitro* microsomal enzymes, which play a crucial role in the process. Various analytical methods, predominantly liquid chromatography, can be used for analysis. In this context, we conducted metabolic stability studies of a hydrazone-sulfonate derivative compound previously synthesized and investigated in terms of biological activity. Metabolic stability was determined by LC-MS/MS on rat microsomes *in vitro*. Analyses were performed at 0, 5, 10, 15, 30, and 60. minutes during incubation. The analysis revealed that the stability of the compound was highly cofactor-dependent, maintaining its stability without cofactor and in a buffer medium.

Keywords: Metabolic stability, LC-MS/MS, hydrazone, sulfonate

1. Introduction

Determination of metabolic profiles of drug candidates is one of the most critical steps in drug discovery [1].

Previously, metabolism studies were rarely conducted until they reached early clinical stages. Inadequate metabolism and pharmacokinetic parameters were the primary reasons for failure in the process [2,3]. Nowadays, metabolic studies are conducted at all stages of drug development [4].

Drug candidates' favorable metabolic stability profiles are characterized by enhanced bioavailability and prolonged half-life [4].

The liver widely excretes most oral medications, mainly through hepatic cytochrome P (CYP)-mediated metabolism. Therefore, precise estimation of hepatic metabolism and first-pass clearance is essential for early drug development and discovery [5].

Metabolic stability is generally first determined *in vitro* in liver microsomes because these microsomes are rich in CYP450 enzymes [6]. Hepatocytes provide a clearer picture but have some disadvantages [7].

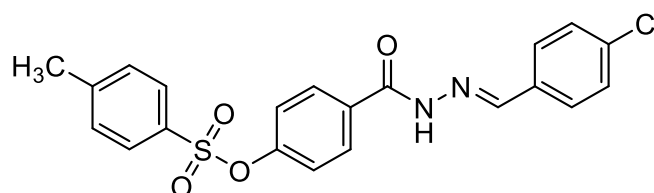


Figure 1. Structure of the tested compound

The National Center for Advancing Translational Sciences uses rat liver microsomes for *in vitro* experiments. This is because rats are involved after *in vitro* pharmacokinetics, efficacy, and toxicology studies *in vivo*. Furthermore, the data obtained can also correlate with human pharmacokinetic results [8].

Developing analytical methods can help achieve higher sensitivity, a higher detection limit, better resolution, precise and accurate quantification in metabolic stability studies [1,9].

This research investigates the metabolic stability of a tosyl-hydrazone derivative coded 3o. The structure of 3o

Citation: H.E. Sellitepe, G.P. Coşkun, K. Birgöl, M. Ülgen, İ.S. Doğan, Metabolic stability of a hydrazone derivative: *N'*-[(4-chlorophenyl)methylidene]-4-[(4-methylphenyl)sulfonyloxy]benzohydrazide, Turk J Anal Chem, 6(2), 2024, 97–101.

 <https://doi.org/10.51435/turkjac.1514896>

Author of correspondence: esellitepe@ktu.edu.tr

Received: July 22, 2024

Tel: +90 (462) 377 88 27

Accepted: September 24, 2024

Fax: +90 (462) 325 6717

(Fig. 1) molecule is *N'*-[(4-chlorophenyl)methylidene]-4-[(4-methylphenyl)sulfonyloxy]benzohydrazide which our research group previously developed. It was synthesized from the starting material, ethylparaben. It was reacted with hydrazine hydrate to obtain the hydrazide compound. Then, the reaction with 4-chlorobenzaldehyde and tosyl chloride, respectively, resulted in the final compound. The inhibitory activity against some metabolic enzymes was also investigated [10].

2. Material and methods

2.1. Chemicals and materials

All the chemicals were purchased from Merck (Darmstadt, Germany) and Sigma-Aldrich (St. Louis, MO). For the metabolic stability assay, β -Nicotinamide dinucleotide phosphate (disodium salt, NADP) and glucose-6-phosphate (disodium salt, G-6-P) were purchased from Sigma. Glucose-6-phosphate dehydrogenase suspension (Reinheit grade II, 10 mg per 2 mL; G-6-PD) was obtained from Sigma Aldrich. Dichloromethane was obtained from Merck. An Agilent 1260 Infinity II LC-MS/MS spectra equipped with G7115A 1260 DAD WR detector, G7104C 1260 Flexible Pump system, G7116A 1260 MCT Column Oven, G7129C 1260 Vialsampler autosample injection unit and G6465B LC/TQ MS/MS detector were used for both HPLC and mass analysis.

Retention times were recorded with an ACE C18 column (particle size: 3 μ m, pore size: 100 Å). The column temperature was adjusted to 25°C in the column compartment. The mobile phase consisted of an acetonitrile-water (90:10, v/v) mixture delivered at a 0.4 mL/min flow rate. The injection volume was 20 μ L. The UV detector was operated at 254 nm.

2.2. Preparation of rat liver microsomes and incubation and extraction procedures

Wistar albino rat liver was used in this study. The animals were deprived of food overnight before sacrifice but were allowed water *ad libitum*. They were previously fed on a balanced diet. Hepatic-washed pig microsomes were prepared as described by Coskun et al. [11]. Incubations were carried out in a shaking water bath at 37°C using a standard cofactor solution consisting of NADP (2 μ mole), G-6-P (10 μ mole), G-6-PD suspension (1 unit), and aqueous MgCl₂ (50% w/w) (20 μ mole) in phosphate buffer (0.2M, pH 7.4, 2 mL) at pH 7.4. Cofactors were pre-incubated for 5 min to generate NADPH before the addition of microsomes (1 mL equivalent to 0.5 g original liver) and substrate (5 μ mole) in methanol (50 μ L). Briefly, six test tubes for the substrate (**3o**) were prepared (2 for the test, 4 for the controls), and cofactors (2 mL in each tube), the

microsomal fraction (1 mL for each tube), and substrate (50 μ L for each tube) was added respectively (Table 1 and Table 2). The incubation was continued for 60 min, and samples were collected from each tube in 0, 5, 10, 15, 30, and 60. min. At the end of 60. min, the reaction terminated, and media was extracted with dichloromethane (3 \times 5 mL). The organic extracts were evaporated to dryness under a stream of nitrogen. The residues were reconstituted in methanol (200 μ L) for LC-MS/MS. The reconstituted extracts were analyzed using the reverse-phase LC-MS/MS system described in the text.

Table 1. Contents of the cofactor solution for each tube

NADP disodium	1.57 mg	2 μ mol
G6P disodium	3.04 mg	10 μ mol
G6P dehydrogenase	1.40 μ L	1 unit
MgCl ₂ (50% w/w)	8.00 μ L	20 μ mol

The materials above were prepared right before incubation by dissolving in 2 mL of phosphate buffer for one incubation tube. The G-6-P dehydrogenase enzyme was added to the cofactor solution right before pre-incubation. All cofactors were “pre-incubated” at a 37°C water bath for 5 minutes to create NADPH. The amount of microsomal preparation added to each incubation tube was 1 mL, and the cofactor solution was 2 mL. Control tubes were also prepared.

Table 2. Incubation protocol

Test Tube	No	Substrate ¹	Microsome ²	Cofactor ³
Test	1	Present	Present	Present
Test	2	Present	Present	Present
Control - Denatured microsomes	3	Present	Denatured	Present
Control - Denatured microsomes	4	Present	Denatured	Present
Control - No cofactor	5	Present	Present	Buffer
Control - No cofactor	6	Present	Present	Buffer

¹50 μ L in each tube

²1 mL in each tube

³2 mL in each tube

For control experiments, microsomes were denatured using boiling water. The necessary amount of freshly defrosted microsomes was taken in a test tube and placed in boiling water for 5 minutes. After the heat denaturation, the denatured microsomes were used for control experiments.

2.3. Autooxidation studies

The substrate (2 μ M) was dissolved in methanol (50 μ L). Then, phosphate buffer (0.2 M, pH 7.4) (3 mL) was added in the same incubation conditions as the test experiments. The test was performed according to the protocol as mentioned earlier. The reconstituted extracts were analyzed using the reverse-phase LC-MS/MS system described in the text.

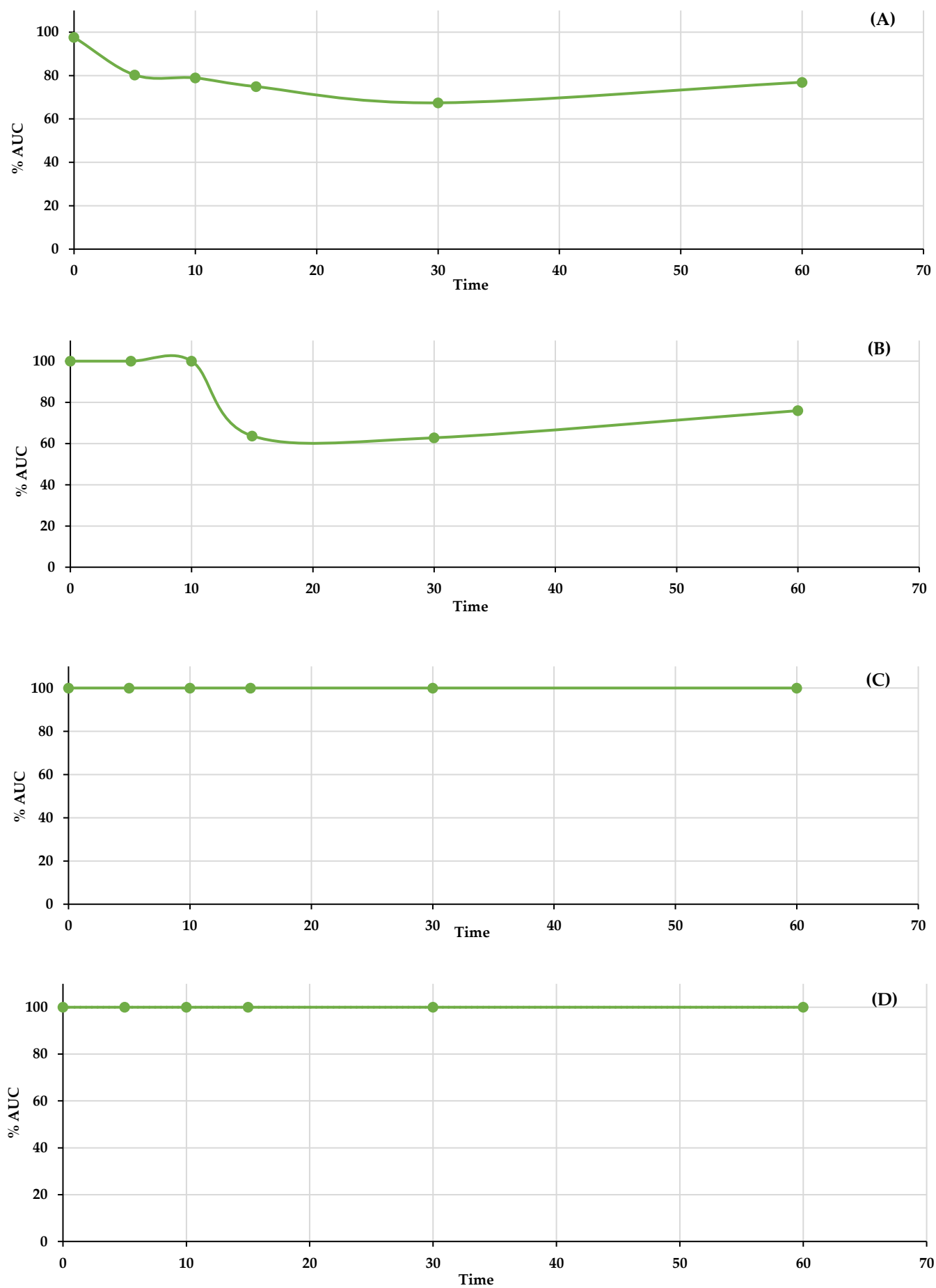


Figure 2. Metabolic stability results on 3o ($t_{1/2} > 60$ mins) (A) The test conditions. (B) The control conditions (denatured microsomes). (C) The control conditions (cofactor-free). (D) The control conditions (autooxidation).

2.4. Extraction of substrates and metabolites from the biological system

At the end of the incubation period, the tubes with the unchanged substrate and metabolites were placed immediately in an ice bath. The enzymatic process was stopped by adding dichloromethane, extracted, and evaporated under nitrogen. The extracts were analyzed by LC-MS/MS.

2.5. LC-MS/MS analysis

An acetonitrile/water (gradient elution) mobile phase mixture was used. The substrates and metabolic standards were separated according to their mass/charge ratio, and their molecular ion peaks were determined in the mass spectroscopy section. The retention times of the substrates and metabolic standards were recorded. A DAD detector was also used to compare the UV spectra of standard and metabolic products.

2.6. *In silico* prediction of metabolic pathways

For *in silico* prediction, a virtual preliminary metabolic evaluation software, SMARTCyp 3.0, was used [12].

3. Results and discussion

Metabolic stability is one of the most important pharmacokinetic parameters affecting the *in vivo* efficacy of drug candidates. Metabolism studies are common to many stages of the development of active pharmaceutical ingredients.

In this study, we performed metabolic stability studies of a compound (**3o**) whose biological activity was previously screened.

Sulfonyl group-bearing compounds such as sulfone, sulfonate, sulfonamide, and sulfamate are essential in medicinal chemistry [13]. Such compounds are most commonly hydrolyzed from the sulfonyl group in phase 1, resulting in more polar metabolites [14,15].

Hydrazones are also of interest to medicinal chemists. If the metabolism based on this functional group is scrutinized, it is indicated that possible metabolic pathways exist, such as hydrolysis of the *N*-acylhydrazone group and aromatic hydroxylation [16–19]. Studies have shown that aroyl hydrazones are stable in phosphate buffer saline at 37 °C but undergo rapid degradation in plasma [20–22].

Compound **3o** (Fig. 1) was tested for its metabolic stability. The compound was found to be stable in the microsomal environment, and half-life is over 60 mins in a 60 mins assay experiment. Control experiments were performed to understand whether the stability depends on microsomes, cofactors, or buffers. Metabolic stability was affected in both microsomes and cofactors; however,

a similar decrease was observed in denatured microsomes in LC-MS/MS experiments. It can be concluded that metabolic stability depends highly on cofactors. The compound was stable in cofactor-free and buffer environments (Fig. 2).

Metabolic stability is one of the most difficult parameters to estimate *in silico* due to the extreme complexity of the processes involved in xenobiotic transformations [23]. Nonetheless, researchers have made many online free predicting tools available to users [24,25]. The compound's metabolic stability was also calculated by SMARTCyp 3.0 software [12].

SMARTCyp predicted that the methyl group in the tosyl moiety would be most reactive for all three metabolic enzymes, Cyp 3A4, Cyp 2D6, and Cyp 2C9 (scores = 55.8, 63.9, 63.8, respectively). Table 3 shows the possible metabolic sites with energies less than 999, with similarities between 0.7 and 1.

Table 3. Metabolic site prediction scores

No	SMARTCyp Score*					
	3A4		2D6		2C9	
1	C.1	: 55.8	C.1	: 63.8	C.1	: 63.8
2	C.11	: 71.5	C.21	: 96.3	C.21	: 94.7
3	C.20	: 72.9	C.3	: 98.6	C.20	: 97.0
4	C.12	: 75.6	C.20	: 99.8	C.20	: 97.4
5	C.21	: 75.8	C.11	: 103.0	C.11	: 99.8
6	C.3	: 78.0	C.4	: 105.5	C.4	: 103.1
7	C.4	: 78.7	C.12	: 106.7	C.12	: 103.5

*Lower scores indicate a higher probability of being metabolized result

4. Conclusion

Herein, the metabolic stability of a hydrazone-sulfonate derivative compound was evaluated using rat liver microsomes *in vitro*. The metabolic stability of the compound depends on its certain functional groups. Hydrazones are expected to be more stable than hydrazines as the terminal nitrogen, which is a metabolic soft spot, is protected by an imine group. This study gave a good perspective on the stability of hydrazone group. On the other hand, sulfonates are a type of ester known to be metabolically unstable. However, the overall results showed that two functional groups enhanced the stability of the entire compound. Control experiments to detect metabolic soft spots in the compounds were also performed in this study. Co-factor and microsomes-free environments showed that the compound requires both microsomes and co-factors to be metabolized. On the other hand, autooxidation was also tested in a buffer environment, which proves that the compound does not provide any metabolites in an enzyme and co-factor-free environment. Overall results clearly show that the compound was stable in both the buffer and the cofactor-free environment, which shows that metabolic stability is highly dependent on cofactors. *In silico* calculations

indicated that the methyl group may be a possible site for metabolism and be considered a metabolic soft spot in the upcoming studies.

Ethics approval and consent to participate

The rat livers were donated by Acibadem University, Animal Laboratory Centre from the Project by Dr. Mehmet Emin Aksoy; laparoscopic and robotic surgery, with the 2021-01 ethical approval number. The liver tissue was obtained from the euthanized rats at the end of the course.

Human and animal rights

No humans were used in this study. All animal research procedures were followed in accordance with “Principles of Laboratory Animal Care” (NIH publication no. 85-23, revised 1985) and/or the declaration of Helsinki promulgated in 1964 as amended in 1996.

References

- [1] S.N.R. Gajula, N. Nadimpalli, R. Sonti, Drug metabolic stability in early drug discovery to develop potential lead compounds, *Drug Metab Rev*, 53(3), 2021, 459-477.
- [2] P. Baranczewski, A. Stanczak, K. Sundberg, R. Svensson, A. Wallin, J. Jansson, et al., Introduction to *in vitro* estimation of metabolic stability and drug interactions of new chemical entities in drug discovery and development, *Pharmacol Rep*, 58(4), 2006, 453.
- [3] R. Xu, M. Manuel, J. Cramlett, D.B. Kassel, A high throughput metabolic stability screening workflow with automated assessment of data quality in pharmaceutical industry, *J Chromatogr A*, 1217(10), 2010, 1616-1625.
- [4] K. Słoczyńska, A. Gunia-Krzyżak, P. Koczurkiewicz, K. Wójcik-Pszczola, D. Żelazczyk, J. Popiół, E. Pękała, Metabolic stability and its role in the discovery of new chemical entities, *Acta Pharm*, 69(3), 2019, 345-361.
- [5] Y. Li, Q. Meng, M. Yang, D. Liu, X. Hou, L. Tang, et al., Current trends in drug metabolism and pharmacokinetics, *Acta Pharm Sin B*, 9(6), 2019, 1113-1144.
- [6] G. Gross, Chapter 27 - Strategies for Enhancing Oral Bioavailability and Brain Penetration, *The Practice of Medicinal Chemistry (Fourth Edition)*, C.G. Wermuth, D. Aldous, P. Raboisson, D. Rognan, 2015, Academic Press, Elsevier.
- [7] Z. Wang, E.Y.Q. Leow, H.Y. Moy, E.C.Y. Chan, Advances in urinary biomarker research of synthetic cannabinoids, *Adv Clin Chem*, 115, 2023, 1-32.
- [8] V.B. Siramshetty, P. Shah, E. Kerns, K. Nguyen, K.R. Yu, M. Kabir, et al., Retrospective assessment of rat liver microsomal stability at NCATS: data and QSAR models, *Sci Rep*, 10(1), 2020, 20713.
- [9] S. Ulenberg, T. Bączek, Metabolic stability studies of lead compounds supported by separation techniques and chemometrics analysis, *J Sep Sci*, 44(1), 2021, 373-386.
- [10] H.E. Sellitepe, J.M. Oh, İ.S. Doğan, S. Yıldırım, A.B. Aksel, G.S. Jeong, et al., Synthesis of *N'*-(4-*o*-non-substitutedbenzylidene)-4-[(4-methylphenyl)sulfonyloxy]benzohydrazides and evaluation of their inhibitory activities against monoamine oxidases and β -secretase, *Appl Sci*, 11(13), 2021, 5830.
- [11] G.P. Coskun, H.E. Sellitepe, B. Kahveci, M. Ülgen, İ.S. Doğan, Formation of an *N*-oxide metabolite following metabolism of 1-(3-chlorobenzyl)[1,2,4]triazolo[4,3-*a*]quinoxaline by *in vitro* rat liver microsomal preparations, *Acta Pharm Sci*, 60(4), 2022, 437-449.
- [12] L. Olsen, M. Montefiori, K.P. Tran, F.S. Jørgensen, SMARTCyp 3.0: enhanced cytochrome P450 site-of-metabolism prediction server, *Bioinformatics*, 35(17), 2019, 3174-3175.
- [13] W. Yu, X. He, K. Vanommeslaeghe, A.D. MacKerell Jr, Extension of the CHARMM general force field to sulfonyl-containing compounds and its utility in biomolecular simulations, *J Comput Chem*, 33(31), 2012, 2451-2468.
- [14] M. Lee, G. Celenza, B. Boggess, J. Blase, Q. Shi, M. Toth, et al., A potent gelatinase inhibitor with anti-tumor-invasive activity and its metabolic disposition, *Chem Biol Drug Des*, 73(2), 2009, 189-202.
- [15] Y. Jiao, X. Li, Y. Tang, Y. Peng, G. Chen, X. Wang, et al., Distribution and metabolism of daidzein and its benzene sulfonates *in vivo* (in mice) based on MALDI-TOF MSI, *Front Pharmacol*, 13, 2022, 918087.
- [16] G.P. Coşkun, E.G. Algin, J.C. Karakoç, B.T. Erbul, M. Ülgen, Formation of *N*-Oxide metabolites from isoniazid hydrazones of substituted benzaldehydes by hepatic washed pig microsomal preparations, *J Res Pharm*, 27(1), 2023, 241-250.
- [17] A. Mateeva, L. Peikova, M. Kondeva-Burdina, M. Georgieva, Development of new HPLC method for identification of metabolic degradation of *N*-pyrrolylhydrazide hydrazones with determined MAO-B activity in cellular cultures, *Pharmacia*, 69(1), 2022, 15–20.
- [18] A. Mateeva, M. Kondeva-Burdina, P. Nedialkov, L. Peikova, M. Georgieva, Development of hyphenated techniques and network identification approaches for biotransformational evaluation of promising antitubercular *N*-pyrrolyl hydrazide-hydrazone in isolated rat hepatocytes, *Chromatographia*, 86(6), 2023, 497-505.
- [19] A. Mateeva, M. Kondeva-Burdina, E. Mateev, P. Nedialkov, K. Lyubomirova, L. Peikova, et al., *In silico* and chromatographic methods for analysis of biotransformation of prospective neuroprotective pyrrole-based hydrazone in isolated rat hepatocytes, *Molecules*, 29(7), 2024, 1474.
- [20] J. Kalia, R.T. Raines, Hydrolytic stability of hydrazones and oximes, *Angew Chem Int Ed*, 47(39), 2008, 7523-7526.
- [21] P. Kovafiková, Z. Mrkvičková, J. Klimeš, Investigation of the stability of aromatic hydrazones in plasma and related biological material, *J Pharm Biomed Anal*, 47(2), 2008, 360-370.
- [22] D.K. Kolmel, E.T. Kool, Oximes and hydrazones in bioconjugation: mechanism and catalysis, *Chem Rev*, 117(15), 2017, 10358-10376.
- [23] A. Wojtuch, R. Jankowski, S. Podlewska, S. How can SHAP values help to shape metabolic stability of chemical compounds?, *J Cheminf*, 13, 2021, 1-20.
- [24] S.Q. Pantaleão, P.O. Fernandes, J.E. Gonçalves, V.G. Maltarollo, K.M. Honorio, Recent advances in the prediction of pharmacokinetics properties in drug design studies: a review, *ChemMedChem*, 17(1), 2022, e202100542.
- [25] J. Zhai, V.H. Man, B. Ji, L. Cai, J. Wang, Comparison and summary of *in silico* prediction tools for CYP450-mediated drug metabolism, *Drug Discov Today*, 2023, 103728.



Isocratic liquid chromatography technique for the analysis of cyanocobalamin from beef liver and heart muscle extracts

Labaran Ibrahim 

¹ Federal University Dutse, Faculty of Life Sciences, Department of Biochemistry, P.M.B. 7156, Dutse, Jigawa State, Nigeria

Abstract

Reverse-phase high-performance liquid chromatography (RP-HPLC) is among the most widely recommended techniques for analyzing water-soluble vitamins, such as vitamins C and B-complexes. The research study was conducted to detect and quantify cyanocobalamin (vitamin B₁₂) from the beef liver and heart muscle extracts using a validated isocratic RP-HPLC procedure. The analytical column was Luna® Phenomenex 5 µm C₁₈ (2) 100 A LC-column (150 × 4.6 mm). The mobile phase consisted of water/ethanol in a ratio of 60:40 (v/v). An enzymatic digestion with 1% potassium cyanide was used for samples (beef liver and heart muscle) extraction. The validated method showed to be linear, R = 0.9977; fast, with a retention time of less than 6.00 min; precise, %RSD_r of 1.66 to 1.74%; and sensitive, with LOD and LOQ of 0.004 and 0.012 µg/mL, respectively. The detected values of cyanocobalamin from the beef liver (BLV) and heart muscle (HRM) extracts were 52.04 ± 0.13 and 42.04 ± 0.29 µg/mL, respectively. BLV extract indicated a higher level of cyanocobalamin. Hence, the validated isocratic RP-HPLC technique can be recommended to analyze cyanocobalamin and related compounds in research laboratories such as diagnostics, foods, and pharmaceuticals.

Keywords: Cyanocobalamin, ethanol, isocratic, mobile phase, beef liver extract

1. Introduction

Organic compounds required in a minute amount for body growth, proper immune function, and repair are called vitamins [1]. They can provide most nutrients for good health and well-being [2]. Vitamin deficiency-related physiological abnormalities are related to improper amounts in the diet [3]. Cyanocobalamin (Vitamin B₁₂) is a cobalt-centered and water-soluble vitamin [4]. It is predominantly synthesized by microorganisms [5], but it can also occur naturally in animal-based foods and synthetic dietary supplements [6,7]. Some foods containing or rich in cyanocobalamin include milk (dairy), meat, fish (shell), and eggs [8]. The amount of this vitamin reported from the above food substances was 385 µg (milk), 300 µg (meat), 85 µg (fish), and 46 µg (eggs) [9]. Usually, cyanocobalamin is not commonly accessible from plant-based food sources [5].

Cyanocobalamin is crucial in homocysteine balance, an arteriosclerosis risk factor [10]. In addition, it is a vital coenzyme in one-carbon metabolism for many enzymes involved in human growth and development [11]. Furthermore, it is essential for normal brain function, nervous system, and red blood cell synthesis [4]. The suggested daily intake of cyanocobalamin is 1.0 µg;

however, because of its low absorption rate in the small intestine, a 3.0 µg level is recommended [11]. In a normal population, cyanocobalamin deficiency rarely manifests. However, individuals with low-rate absorption disorder, infants, and pregnant women can be subjected to its deficiency as a result of their physiological and/or prescribed dietary needs [12]. Cyanocobalamin deficiency resulted in pernicious anemia, myelin damage, and spongy vacuolation of peripheral and central nervous systems [13]. A dietary supplement can be sufficient for persons at risk of this vitamin deficiency [14].

Cyanocobalamin can exist either in a free form or attached to biomolecules such as a protein. If attached to a biomolecule, it can be unbound by heating at 98 °C for 30 min with potassium cyanide (KCN) solution [15]. Autoclaving at 121 °C in a mixture of KCN and phosphate buffer is another method to unbound cyanocobalamin [16]. Sample digestion with α-amylase and/or pepsin with excess KCN solution is an additional suitable extraction procedure [17]. KCN is usually added to convert all forms of cobalamin into cyanocobalamin [18]. However, to avoid the use of this highly toxic

Citation: L. Ibrahim, Isocratic liquid chromatography technique for the analysis of cyanocobalamin from beef liver and heart muscle extracts, Turk J Anal Chem, 6(2), 2024, 102–107.

Author of correspondence: labaranibrahim80@gmail.com
labaran.ibrahim@fud.edu.ng

Received: July 9, 2024

Tel: +234 706 348 45 83

Accepted: October 22, 2024

Fax: N/A

compound, sodium metabisulphate and/or sodium nitrite can be considered as suitable alternative compounds [19].

One of the microbiological assays for vitamin B₁₂ analysis is the application of *Lactobacillus leishmania* [20]. Some disadvantages of the microbial method are time consumption and low specificity [21,22]. A liquid chromatography technique with a UV-visible detector is the recommended and suitable analytical procedure [22]. Other alternative protocols for cyanocobalamin analysis are polar-graphic and spectrophotometric [23].

Analysis of water-soluble vitamins with liquid chromatography technique in infant milk [24], okra fruit [25], dietary supplements and ingredients [26], and blood serum [27] have been cited in the existing literature. Recently, cyanocobalamin evaluation was cited using fish species [18], meat brand varieties [5], and plant-based sources such as edible mushroom and laver [28]. However, cyanocobalamin evaluation from the beef liver and heart muscle extracts is lacking. Hence, this research intends to separate, detect, and quantify the amount of cyanocobalamin from the beef liver and heart muscle extracts using a validated isocratic RP-HPLC technique.

2. Experimental

2.1. Chemical reagents and apparatus

The chemical reagents consist of cyanocobalamin (Catalog No. 9868-19-15, Sigma-Aldrich, USA), pepsin (Catalog No. 501784856, Sigma-Aldrich, USA), α -amylase (CAS No. 9000-90-2, Sigma-Aldrich, USA), and HPLC-grade ethanol (Catalog No. AC611050040, Sigma-Aldrich, USA). Other chemical reagents are potassium hydroxide (Catalog No. 109112000, Merck Millipore, Germany), potassium cyanide (Catalog No. 104965, Merck Millipore, Germany), and potassium hydrogen phosphate (Catalog No. 104873, Merck Millipore, Germany). The EMD-Millipore machine (Model No. 13681, Switzerland) was the source of the Milli-Q water. Apparatus includes; Filter papers (Whatman grade 1, 125 mm, Maidstone, England, United Kingdom, Code No. WHAT1001125), 0.22 μ m Syringe Filters (Minisart) (Bornstein, Germany, LOT No. 00807103), analytical weighing balance (RADWAG, 220 g \times 0.1 mg, Model No. AS/220/C/2, Poland), vortex machine (Model No. S10100A, BioRAD, USA), micropipettes, Eppendorf tubes, and falcon tubes. All chemical reagents used in this research study were of analytical grade.

2.2. Cyanocobalamin extraction from the beef liver and heart muscle

On the 24th of September 2021, fresh beef liver and heart muscle were purchased from Iyama-rama butchery, Grahamstown (Makhanda), Eastern Cape of South Africa. Each sample was washed separately with Milli-Q

and stored at -20 °C before analysis. The extraction of cyanocobalamin from each sample was carried out using an enzymatic method, a rarely reported procedure. Each sample was cut up into pieces and homogenized with a warring blender. To each 3.0 g of the homogenate, pepsin (40 mg) and α -amylase (60 mg) were added, followed by the addition of 10 mL of 1% potassium cyanide (KCN) solution. Pepsin and α -amylase enzymes unbound the cyanocobalamin attached to proteins and carbohydrates, respectively [4]. The 1% KCN converts all forms of vitamin B₁₂ to cyanocobalamin [4]. Each mixture was vortexed for 10 min, allowed to stand at 37 °C for 24 h, and filtered through Whatman No. 1 filter paper. Each filtrate (extract) was then diluted with a phosphate buffer, pH 5.8 (diluting solution), in a ratio of 5:10 (v/v). Lastly, each diluted extract was further filtered with a 0.22 μ m micro-pore filter syringe into their respective HPLC vials.

2.3. Preparation of standard stock and working solutions

The preparation of cyanocobalamin standard stock solution was as reported by [29], with modifications in the working concentration levels. 2 mg of the cyanocobalamin was dissolved in 5 mL of the diluting solution (phosphate buffer, pH 5.8) to produce a stock solution. The preparation of 200 μ g/mL working solution was from the stock to generate varying concentration levels of 0.01, 0.1, 0.25, 0.5, 1, 2.5, 15, 20, 30, 50, and 120 μ g/mL.

2.4. Instrumentation and chromatographic condition

The HPLC system (Shimadzu Corporation, Kyoto, Japan.) consists of a connector (LC-20AD), 20 MPa pump (LC-2AB), auto-sampler (SIL-2A), and diode array detector (SPDA-M20A). The PDA detector wavelength ranges from 190 to 800 nm. The control of the system, data acquisition, and evaluation were carried out by "LC Lab Solution" software. The chromatographic separation was done with a 5 μ m C18 (2) 100A Luna® column (150 \times 4.6 mm (Phenomenex, USA), maintained at room temperature (25 \pm 5 °C). The mobile phase delivery was isocratic, made up of water/ethanol in a 60:40 (v/v) ratio. The flow rate was 0.5 mL/min with an injection volume of 20 μ L for a 10 minute run. The detected UV-visible absorbance was at 270 nm wavelength [30]. The analysis of each working standard solution and sample extract was conducted in duplicate.

3. Results and discussion

3.1. Linearity

The linearity was carried out with a regression curve under 11 points. The regression curve was detected as linear, which indicates a high correlation between the varying working standard concentration levels and mean peak areas. The obtained regression curve value

Table 1. Characteristics of the validated isocratic RP-HPLC procedure

Characteristic variables	Cyanocobalamin (Vitamin B ₁₂)
Calibration range, µg/mL	0.01 to 120
Correlation coefficient, R	0.9977
Linear regression equation	$y = 18949x - 1411.4$
LOD ¹ , µg/mL	0.004
LOQ ² , µg/mL	0.012
Detection wavelength, nm	270

¹LOD, limit of detection; ²LOQ, limit of quantification

'R' was 0.9977 (Table 1). Fig. 1 shows the cyanocobalamin standard curve, generated over concentration levels of 0.01 to 120 µg/mL.

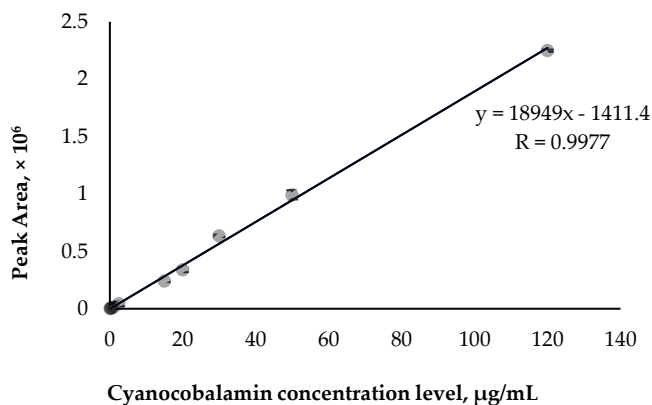


Figure 1. Cyanocobalamin standard curve. The standard curve was generated over concentration levels between 0.01 to 120 µg/mL with pure cyanocobalamin (HPLC grade) prepared in phosphate buffer, pH 5.8. The analysis was carried out in duplicate on the same day.

3.2. Sensitivity

The limit of detection (LOD) was calculated based on the 3.3-fold differences of the analyte signal and baseline noise. LOD implies a compound concentration that produces a signal-to-noise ratio of above 3.0. Whereas the limit of quantification (LOQ) was determined based on 10-fold variations. LOQ means a compound concentration equal to 10 times the value of the signal-to-noise ratio.

$$LOD = 3.3 \times \frac{(Sy)}{m} \quad (1)$$

$$LOQ = 10 \times \frac{(Sy)}{m} \quad (2)$$

Table 2. Precision and recovery accuracy of the validated isocratic RP-HPLC procedure

Content, µg/mL	Intra-day		Inter-day	
	Precision (RSD _r), % (n = 5)	Recovery accuracy, % (n = 5)	Precision (RSD _r), % (n = 5)	Recovery accuracy, % (n = 5)
7.5	1.74	97.05 ± 0.64	1.72	99.87 ± 0.32
15	1.66	91.10 ± 0.17	1.68	89.42 ± 0.63

¹RSD_r, relative standard deviation of repeatability; n = number of repeat in duplicate

The 'SY' denotes the standard deviation of the y-intercept and 'm' implies the slope of the linear regression curve. Both LOD and LOQ were determined as per the International Conference of Harmonization (ICH) guidelines. As depicted in Table 1, the LOD and LOQ values were obtained as 0.004 and 0.012 µg/mL respectively. Hence, these values indicated the high sensitivity of the validated analytical procedure.

3.3. Precision and recovery accuracy

The method precision was determined with two (2) varying standard concentration values of 7.5 and 15 µg/mL. These concentration values were not part of the regression curve points, analyzed in duplicate. Finally, the intra-day and inter-day precision was represented as a percentage relative standard deviation of repeatability (%RSD_r).

$$\%RSD = \frac{\text{Mean recovered standard deviation}}{\text{Mean recovered concentration level}} \times 100 \quad (3)$$

The intra-day and inter-day precision of repeatability were analyzed within the first day and between two (2) days, respectively. The analysis was conducted in one laboratory, by a single analyst. The intra-day and inter-day precision values are presented in Table 2. In addition, the accuracy recovery (intra-day and inter-day) was calculated using similar standard concentration values used for the intra-day and inter-day precision of repeatability evaluation. (Table 2). Hence, the low %RSD_r values of ≤ 2.5% as suggested by AOAC [31] and sufficient recovery values indicated the high precision and accuracy of the validated isocratic RP-HPLC technique. Notwithstanding, a higher %RSD_r values, ≤ 8% was recently adopted by AOAC, which as well indicated a high precision and accuracy of a liquid chromatography analytical procedure [32].

3.4. Accuracy spike

The accuracy-spike recovery was determined by spiking each extract of the beef liver and heart muscle with a known standard (reference standard) concentration value of 35 µg/mL in a 50:50 (v/v) ratio. The accuracy spike was calculated using the relation below.

$$\%MR = \frac{(P - Q)}{R} \times 100 \quad (4)$$

P, Q, R, and % MR represent peak areas of spiked sample extract, un-spiked (unspike) sample extract, reference standard, and percentage mean recovery (accuracy spike), respectively.

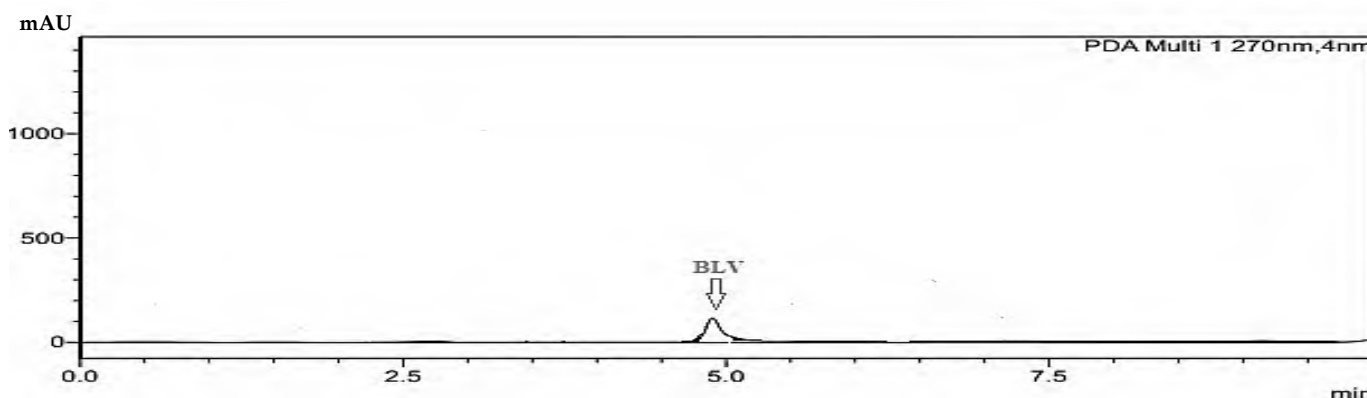


Figure 2. A chromatogram for the beef liver (BLV) extract, determined with a UV-visible detector using an isocratic gradient of 60% water/40% ethanol. The flow rate, injection volume, and detection wavelength were 0.5 mL/min, 20 μ L, and 270 nm, respectively.

Table 3 shows each sample extract accuracy spike and amounts of cyanocobalamin obtained. Fig. 2 and Fig. 3 reveal chromatograms of the beef liver (BLV) un-spike (unspike) and heart muscle (HRM) un-spike (unspike) extracts, respectively. Additionally, chromatograms of the beef liver spiked (BLVS) extract, heart muscle spiked (HRMS) extract, and reference standard (RSTD) for the accuracy spike were provided as supplementary materials.

Table 3. Each sample accuracy-spike and cyanocobalamin detected value

Sample extract	Accuracy-spike, % n = 2	Cyanocobalamin value, μ g/mL n = 2
Beef liver	109.29 \pm 0.11	52.04 \pm 0.13
Heart muscle	100.89 \pm 0.19	42.04 \pm 0.29

n = number of repeat in duplicate.

A naturally occurring vitamin B₁₂ exists in varying conformational structures. Thus, this vitamin requires transformation into a single form such as cyanocobalamin. The potassium cyanide (KCN) solution was used during each sample extraction to convert all forms of vitamin B₁₂ to cyanocobalamin [4]. Notwithstanding, the addition of KCN solution may produce a problem of this compound toxicity. During the method optimization, each sample extract with and without the addition of KCN solution was analyzed. An extract with the addition of KCN solution yielded an

adequate amount of cyanocobalamin. The mobile phase for the analytical procedure was selected after several evaluations with ethanol, methanol, acetonitrile, orthophosphoric acid, water, and buffer solution. Better separation and sensitivity were achieved with this mobile phase consisting of water/ethanol in a 60:40 (v/v) ratio. The examined flow rates were 0.5, 1.0, and 2 mL/min. A 0.5 mL/min flow rate produced an optimal signal-to-noise with minimum separation time. Both 270 nm and 360 nm wavelengths were tested. A 270 nm wavelength yielded a better resolution of peaks. However, a 360 nm wavelength was recommended by the AOAC official method [33]. The linearity, limit of detection (LOD), limit of quantification (LOQ), recovery accuracy, precision, and sensitivity analysis were detected within the valid ranges. The validation of this analytical procedure complied with the International Conference of Harmonization (ICH) [34].

The detected amounts of cyanocobalamin in the sample extracts of this study were similar to the reported values from multivitamin tablets [7]. However, the obtained levels were greater than the cited values from meat products [5], dietary ingredients/supplements [26], infant formula [33], and poly-vitaminated premixes [35]. The United States National Academy of Science (US-NAS) recommended an intake level of vitamin B₁₂ between 0.40–2.80 μ g/day for all ages.

Notwithstanding, a higher amount may be required by older persons [36] and individuals with low absorption rate disorders [12].

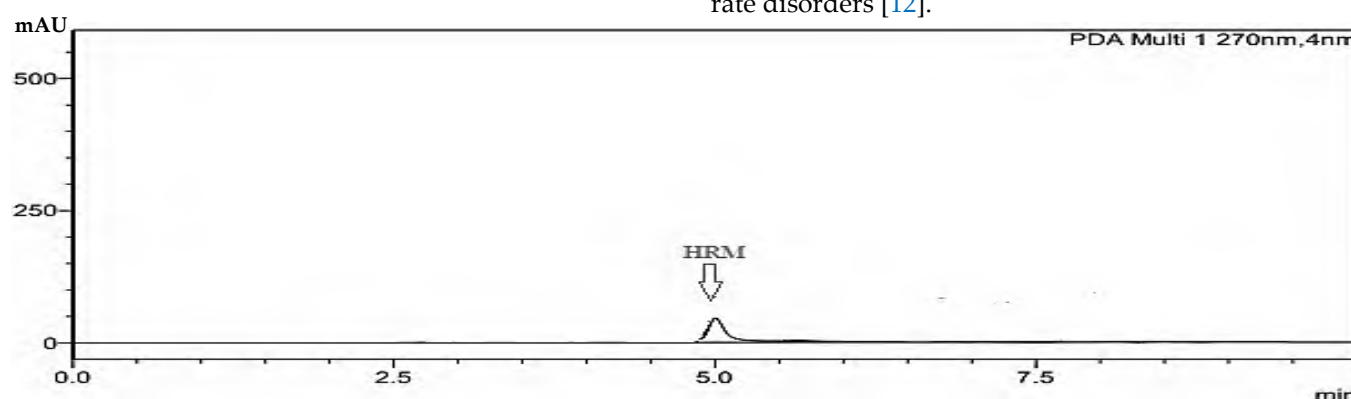


Figure 3. A chromatogram for the heart muscle (HRM) extract, determined with a UV-visible detector using an isocratic gradient of 60% water/40% ethanol. The flow rate, injection volume, and detection wavelength were 0.5 mL/min, 20 μ L, and 270 nm, respectively.

Table 4. Current isocratic RP-HPLC analytical procedure in comparison with previously reported methods

Parameters	Values obtained
1. Regression value, R	0.9977
Detection limit, µg/mL	0.00033
Quantification limit, µg/mL	0.00100
Precision, %	0.16 – 0.74
Recovery accuracy, %	89.42 – 99.87
Retention time, min	4.88 – 5.04
Detection wavelength, nm	270
Level detected, µg/mL	52.04 ± 0.13; 42.04 ± 0.29
Sample extracts	Beef liver and heart muscle
Reference	[*]
2. Regression value, R	0.9910
Detection limit, µg/mL	0.0625
Quantification limit, µg/mL	0.1250
Precision, %	0.40 – 4.10
Recovery accuracy, %	80.40 – 108.50
Retention time, min	8.53
Detection wavelength, nm	350
Concentration reported, µg/mL	45.86
Test sample	Multivitamin tablets
Reference	[7]
3. Regression value, R	0.9930
Detection limit, µg/mL	0.1600
Quantification limit, µg/mL	0.5200
Precision, %	1.41 – 4.64
Percentage recovery, %	96.00 – 101.10
Retention time, min	8.70
UV-visible wavelength, nm	328
Reported amount, µg/mL	1.80 – 2.69
Test sample	Dietary ingredients/supplements
Reference	[26]
4. Regression value R	Nr
Detection limit, µg/mL	Nr
Quantification limit, µg/mL	Nr
Precision, %	Nr
Percentage recovery, %	Nr
Retention time, min	12.35 – 12.50
UV-visible wavelength, nm	361
Reported amount, µg/mL	0.24 – 0.39
Test sample	Infant formula
Reference	[33]
5. Regression value, R	0.9950
Detection limit, µg/mL	0.2000
Quantification limit, µg/mL	0.3800
Precision, %	Nr
Percentage recovery, %	Nr
Retention time, min	16.00
UV-visible wavelength, nm	210
Reported concentration, µg/mL	Nr (less than LOD)
Test sample	Poly-vitaminated premixes
Reference	[35]
6. Regression value, R ²	0.9940
Detection limit, µg/mL	Nr
Quantification limit, µg/mL	0.007
Precision, %	1.50 – 7.26
Percentage recovery, %	79.61 – 88.80
Retention time, min	7.17
UV-visible wavelength, nm	361
Reported Level, µg/mL	3.85 – 8.78
Test sample	Meat product
Reference	[5]

[*], the current validated isocratic liquid chromatography technique; Nr, not reported

Table 5. Various analytes retention times of the validated isocratic liquid chromatography procedure

Analytes	Retention time, min
RSTD	4.90 ± 0.39
BLV	4.91 ± 0.05
BLVS	4.91 ± 0.09
HRM	5.01 ± 0.01
HRMS	4.91 ± 0.09

RSTD, reference standard; BLV, beef liver un-spike extract; BLVS, beef liver spiked extract, HRM, heart muscle un-spike; HRMS, heart muscle spiked.

From the result of this study, the beef liver and heart muscles can be considered as good dietary sources of cyanocobalamin.

Table 5 represents the retention times of the reference standard (RSTD) for the accuracy spike, beef liver (BLV) un spike, beef liver spiked (BLVS), heart muscle (HRM) unspike, and heart muscle spiked (HRMS) extracts. The consistency of the current validated analytical procedure in comparison to the previously reported methods is presented in Table 4. The validated isocratic liquid chromatography technique of this research is indicated to be more rapid (retention time), precise (%RSD), and sensitive (LOD and LOQ).

4. Conclusions

The validated isocratic RP-HPLC method was linear, rapid, precise, and sensitive. Also, the separation, detection, and quantification of cyanocobalamin from each sample extract were satisfactory. Hence, this analytical method can be significantly valuable in research laboratories for quality control purposes. In addition, the data obtained can be useful for nutritional labeling, education, and food-based dietary guidelines.

Acknowledgment

My appreciation to the Department of Biochemistry and Microbiology, Rhodes University, Grahamstown (Makhanda), Eastern Cape, South Africa. The Department provided resources (equipment, apparatus, and reagents) for the research work.

References

- [1] C. Anyakora, I. Afolami, T. Ehianeta, F. Onwumere, HPLC analysis of nicotinamide, pyridoxine, riboflavin, and thiamin in some selected food products in Nigeria, *Afri J Pharm Pharmacol*, 2, 2008, 29–36.
- [2] I. Ortigues-Marty, D. Micol, S. Prache, D. Dozias, C.L. Girard, Nutritional value of meat: the influence of nutrition and physical activity on vitamin B₁₂ concentrations in ruminant tissues, *Reprod Nutr Dev*, 45, 2005, 453–467.
- [3] W. Elfalleh, N. Nasri, N. Marzougui, Physico-chemical properties and DPPH-ABTS scavenging activity of some local pomegranate (*Punica granatum*) ecotypes, *Int J Food Sci Nutr*, 60(2), 2009, 197–210.

- [4] P. Laurence, Vitamin B₁₂—A review of analytical methods for use in food, Government Chemist Program Report, National Measurement System, United Kingdom, Report No., LGC/R/2014/378, 2015, 1–378.
- [5] D. Guggisberg, M.C. Risse, R. Hadorn, Determination of vitamin B₁₂ in meat products by RP-HPLC after enrichment and purification on an immunoaffinity column, *Meat Sci*, 90, 2012, 279–283.
- [6] R. van Breemen, J.M. Betz, L. Evans, A. Hall, M. Jennens, AOAC SMPR® 2016.017, Standard Method Performance Requirements (SMPRs) for quantitative measurement of vitamin B₁₂ in dietary supplements and ingredients, *J AOAC Int*, 100(1), 2017, 294–296.
- [7] P. Chen, W.R. Wolf, I. Castanheira, A.A. Sanches-Silva, LC/UV/Vis method for determination of cyanocobalamin (B₁₂) in multivitamin dietary supplements with online sample clean-up, *Anal Methods*, 2(8), 2010, 1171–1175.
- [8] F. Watanabe, Vitamin B₁₂ sources and bioavailability, *Exp Biol Med*, 222, 2007, 1266–1274.
- [9] R. Obeid, S.G. Heil, M.M.A. Verhoeven, E.G.H.M. van den Huevel, L.C.P.G.M. de Groot, S.J.P.M. Eussen, Vitamin B₁₂ intake from animal foods, biomarkers, and health aspects, *Front. Nutr.* 6(9), 2019, 1–18.
- [10] S.P. Stabler, Vitamin B₁₂, Editors: B.A. Bowman, R.M. Russell, Present knowledge in nutrition, 2006, Washington DC, USA, ILSI Press.
- [11] J. Selhub, Folate, vitamin B₁₂ and vitamin B₆ and one-carbon metabolism, *J Nutr Health Aging*, 6(1), 2002, 39–42.
- [12] R. Pawlak, S.J. Parrott, S. Raj, D. Cullum-Dugan, D. Lucas, How prevalent is vitamin B₁₂ deficiency among vegetarians, *Nutr Rev*, 71(2), 2013, 110–117.
- [13] A.J. Shubhangini, Nutrition and dietetics. (3 edition), 2010, McGraw Publishers, New Delhi, India.
- [14] US-DHHS (United States Department of Health and Human Service). Dietary Guidelines for Americans (8. edition), 2013, Washington DC.
- [15] E.P. Frenkel, R. Proughand, R.L. Kitchens, Measurement of tissue vitamin B₁₂ by radio-isotopic competitive inhibition assay and quantitation of tissue cobalamin fractions, *Methods Enzymol*, 7, 1980, 31–40.
- [16] H.E. Indyk, B.S. Persson, M.C.B. Caselunghe, A. Moberg, E.L. Filouzi, Determination of vitamin B₁₂ in milk products and selected foods by optical biosensor protein-binding assay: method comparison, *J AOAC Int*, 85, 2002, 72–82.
- [17] O. Heudi, T. Kilinc, P. Fontannaz, E. Marley, Determination of vitamin B₁₂ in food products and in premixes by reversed-phase high-performance liquid chromatography and immuno-affinity extraction, *J Chromatogr A*, 1101, 2006, 63–68.
- [18] L. Ibrahim, A. Usman, A simple and rapid RP-HPLC method for the assessment of cobalamin (vitamin B₁₂) in tilapia and snook fishes; *Turk J Chem*, 46, 2022, 320-329.
- [19] K. Muhammad, D. Briggs, The appropriateness of using cyanocobalamin as calibration standard in *Lactobacillus leishmannii* A. T.C.C. 7830 assay of vitamin B₁₂, *Food Chem*, 48(4), 1993, 427-429.
- [20] AOAC. Cobalamin in milk-based infant formula. *AOAC Int*, 2006, 1–986.
- [21] S.S. Kumar R.S. Chouhan, M.S. Thakur, Trends in analysis of vitamin B₁₂, *Anal Biochem*, 398(2), 2010, 139–149.
- [22] US-FDA (United States Department of Food and Drugs Administration), Analytical procedures and methods validation for drugs and biologics, 2015, New Hampshire Avenue, Hillandale Bldg., Silver Spring.
- [23] W. Lee, Y.B. Lee, M.H. Hub, J.K. Choi, Determination of the chemical stability of cyanocobalamin in medical foods by a validated immuno-affinity column-linked HPLC method, *J Food Qual*, 2022(1), 1–8.
- [24] S. Albala-Hurtado, M.T. Veciana-Nogues, M. Izquierdo-Pulido, A. Marine-Font, Determination of water-soluble vitamins in infant milk by high-performance liquid chromatography, *J Chromatogr A*, 778(1–2), 1997, 247–253.
- [25] R. Sami, Y. Li, B. Qi, S. Wang, Q. Zhang, HPLC analysis of water-soluble vitamins (B₁₂, B₃, B₆, B₁₂, and C) and fat-soluble vitamins (E, K, D, A, and β -Carotene) of Okra (*Abelmoschus esculentus*), *J Chem*, 2014(2), 2014, 1–6.
- [26] X. Qiu, H. Zhanga, Y. Yina, H. Brandesb, H. Marsalab, Determination of active vitamin B₁₂ (cobalamin) in dietary supplement and ingredients by reverse-phase liquid chromatography: Single-laboratory validation, *Food Chem*, 298, 2019, 1–6.
- [27] H.A. Schwertner, S. Valtier, V.S. Bebartha, Liquid chromatographic mass-spectrometric (LC/MS/MS) determination of plasma hydroxyl cobalamin and cyanocobalamin concentrations after hydroxyl cobalamin antidote treatment for cyanide poisoning, *J Chromatogr B*, 905, 2012, 10–16.
- [28] F. Watanabe, Y. Yabuta, T. Bitto, F. Teng, Vitamin B₁₂ containing plants foods sources for vegetarians, *Nutrients*, 6(5), 1861–1873.
- [29] F. Monajjemzadeh F. Ebrahimi, P. Zakeri-Milani, H. Valizadeh, Effects of formulation variables and storage conditions on light-protected vitamin B₁₂ mixed parenteral formulations, *Adv Pharm Bull*, 4(4), 2014, 329–338.
- [30] N. Marzougui, F. Guasmi, M. Mkaddem, Assessment of Tunisian *Trigonella foenum graecum* diversity using seed vitamin B₆, B₁, B₉, and C contents, *J Food Agric Environ*, 7(1), 2009, 56–61.
- [31] AOAC. Official methods of analysis (5th edition), 2010, USA, Arlington.
- [32] AOAC. Official methods of analysis, SMPR Guideline, 2016
- [33] E.C. Gimenez, F. Martin, Vitamin B₁₂ (cyanocobalamin) in infant formula adult/pediatric nutritional formula by liquid chromatography with Ultraviolet detection: collaborative study, *J AOAC Int*, 101, 2018, 1112–1118.
- [34] ICH Q2(R1), Expert working group ICH harmonized tripartite guidelines validation of analytical procedures, Text methodology, Step 4, 2005, 1–18.
- [35] O. Heudi, T. Kilinc, P. Fontannaz, Separation of water-soluble vitamins by reversed-phase high-performance liquid chromatography with ultra-violet detection: application to poly-vitaminated premixes, *J Chromatogr A*, 1070(1-2), 2005, 49–56.
- [36] US-NAS (United States National Academy of Sciences). Dietary reference intakes for thiamin, riboflavin, niacin, vitamin B₆, folate, and vitamin B₁₂, pantothenic acid, biotin, and choline, 1998, Washington DC, USA, National Academy Press.



Investigation of extracellular metabolites in cancer and healthy colon cells in a time-dependent manner

Esra Bulut Atalay^{1,2} , Hulya Ayar Kayali^{1,2,3*} 

¹ İzmir Biomedicine and Genome Center, İzmir, 35340, Türkiye

² Dokuz Eylül University, İzmir International Biomedicine and Genome Institute, 35340 İzmir, Türkiye

³ Dokuz Eylül University, Faculty of Science, Department of Chemistry, Division of Biochemistry, 35160, İzmir, Türkiye

Abstract

Metabolite analysis is critical in the cancer field because of provides information about the metabolic status of cells. The profiling of extracellular metabolites presents technical advantages over intracellular metabolites, such as easier access to extracellular metabolites without a quenching method and the growth medium containing high biomass. This study aimed to investigate the extracellular level of metabolites in colon cancer cells in a time-dependent manner. 1×10^6 cells were seeded in 4 Petri dishes and glucose, pyruvate, citric acid (TCA) cycle metabolites, and D2-Hydroxyglutarate (D2-HG) in the conditioned medium were determined by 3,5-Dinitro Salicylic Acid (DNS) and Ultra Performance Liquid Chromatography (UPLC) method and pyruvate assay for 24-96th hours. The results showed that glucose is consumed, and pyruvate and TCA cycle intermediates are released in decreasing amounts in all cell lines. It was also observed that glucose was more consumed, and TCA cycle metabolites were less released in metastatic colon cancer cells (SW620) than in primary colon adenocarcinoma cells (Caco-2). Most importantly, D2-HG oncometabolite was released more into the growth medium of colon cancer cells than normal colon cells for four days. In conclusion, the D2-HG is highly produced and released to the growth medium of colon cancer cell lines in a cancer-type-specific manner.

Keywords: Colon cancer, exametabolome analysis, metabolite, UPLC

1. Introduction

During carcinogenesis, cells undergo metabolic and behavioral changes in a multistage process due to mutations. Metabolic changes include reprogramming of intracellular metabolism that controls inappropriate cell proliferation and adapts to the tumor microenvironment [1]. Cancer has become the most common disease after significant developments in treating heart diseases [2]. There are more than 200 types of cancer; the third most common type in men and women is colon cancer. Because of its mortality and high incidence, approximately 2×10^6 new colon cancer cases were observed in 2020 in stages III and IV [3,4]. The results highlighted that we need new therapeutic methods to increase the 5-year survival rate for late-stage patients. Recently, metabolic reprogramming has become a field of increasing interest [5,6].

Metabolism consists of many vital reactions in which small molecules known as metabolites are produced [7,8]. Cells are like factories that produce a wide variety of chemicals including metabolites. The analysis of

metabolite levels is critical as it will provide information about the metabolic status of the cells and determines the risk and frequency of diseases [9–12]. Metabolites produced and accumulated inside the cell are secreted to the extracellular medium by specific metabolic overflow [13]. Analysis of the correct level of intracellular metabolites is essential because the reactions occur inside the cell. However, it is challenging due to finding a reliable quenching method that does not damage the cell membrane and there is a low biomass ratio in the intracellular medium. On the other hand, extracellular metabolites can be accessed more easily without a quenching method. In addition, profiling the extracellular metabolite provides information about the environmental conditions and the metabolic status of cells [14]. In recent years, the comprehensive profiling of extracellular metabolites known as exametabolome analysis to assess or compare the metabolic status of cancer cells has gained importance. In recent years, as a result of the valuable developments in the metabolomics

Citation: E.B Atalay, H.A. Kayali, Investigation of Extracellular Metabolites in Cancer and Healthy Colon Cells in a Time-Dependent Manner, Turk J Anal Chem, 6(2), 2024, 108–114.

Author of correspondence: hulya.kayali@deu.edu.tr

Received: June 11, 2024

Tel: +90 (232) 301 8690

Accepted: October 22, 2024

Fax: +90 (232) 453 4188

 <https://doi.org/10.51435/turkjac.1499235>

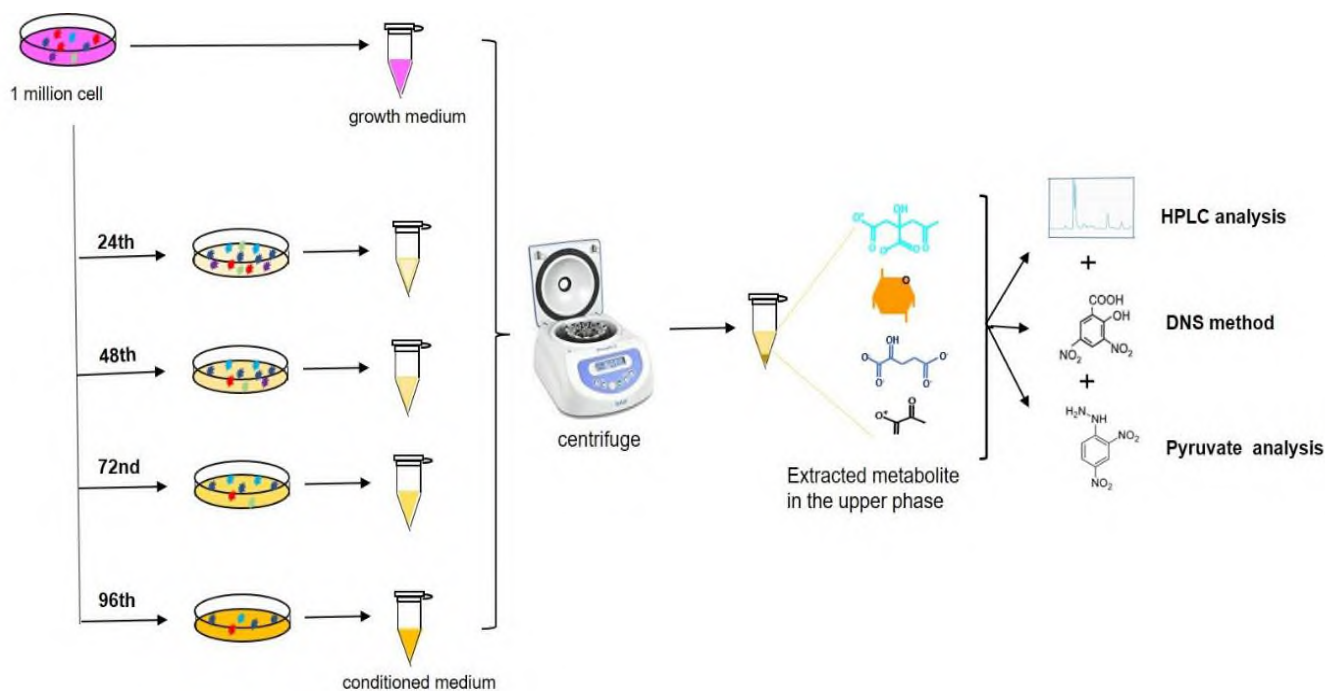


Figure 1. The extracellular metabolite extraction procedure. 1×10^6 cells were seeded in 4 Petri dishes. Approximately 300 μ l conditioned medium was obtained from the Petri dishes and the cell number was determined using Thoma lame after 24, 48, 72, and 96 hours. The conditioned media were centrifuged at 17,000 g and +4 °C for 15 minutes and the supernatants were used for further analysis. Glucose, pyruvate, TCA cycle metabolites, and D2-HG in the conditioned medium were determined by DNS and HPLC method and pyruvate assay for 24-96th hours

field, metabolite analysis has become the more affordable, reliable, and reproducible postgenomic method [15].

Metabolic reprogramming is one of the hallmarks of cancer cells, and some central metabolic pathways such as Glycolysis, TCA cycle, and pentose phosphate are aberrantly regulated during cancer progression [16]. The TCA cycle has been known as a signalling hub in cell metabolism because it connects many metabolic pathways. The TCA cycle plays a role in energy production and the biosynthesis of building blocks in the cell [17]. Recently it has been observed that the abnormal level of TCA cycle metabolites is related to different diseases such as obesity, diabetes, heart failure, and cancer [9,10,18,19]. Succinate, fumarate, and 2-hydroxyglutarate are the TCA cycle-related metabolites and they affect processes of cancer development and progression [20–22]. Until now, the level of TCA cycle-related metabolites has been investigated during colon cancer progression [23–25]. However, it is not known how the extracellular metabolite levels change while colon cancer cells gain metastatic properties.

The present study used primary and metastatic colon cancer cell lines, and the extracellular metabolite level changes were investigated when cells gained metastatic properties. The levels of extracellular metabolite in the TCA cycle and glycolysis were determined by the pyruvate assay and DNS and HPLC methods in healthy and cancer cell lines for four days, and colon cancer-specific metabolite was investigated.

2. Materials and Methods

2.1. Cell Lines

Normal colon (CCD-18Co), colon adenocarcinoma (Caco-2), and metastatic colon cancer (SW620) cell lines were grown in DMEM, MEM, and RPMI, respectively. The content of all growth media and incubation conditions of cells have been described in a previous study [26].

2.2. Metabolite Extraction From the Extracellular Medium

All cell lines were calculated as containing 1×10^6 cells and seeded into four Petri dishes. Approximately 300 μ l conditioned medium was obtained from the Petri dishes, and the cell number was determined using Thoma lame after 24, 48, 72, and 96 hours. The conditioned media were stored at -80 °C until the experiment. The mediums were centrifuged at 17,000 g and +4 °C for 15 minutes, and the supernatants were used for further analysis (HPLC method, glucose, and pyruvate determinations [27]).

The released and consumed metabolite concentration levels were calculated for 1×10^6 cells following previously published protocols [28]. The calibration curve's equation and R^2 value, as well as the concentrations of the standard glucose solutions, are given in Table 1.

2.3. 3,5-Dinitro Salicylic Acid (DNS) Method

The DNS method [29] is used to determine glucose content in the growth mediums. The sample (50 μ l) and

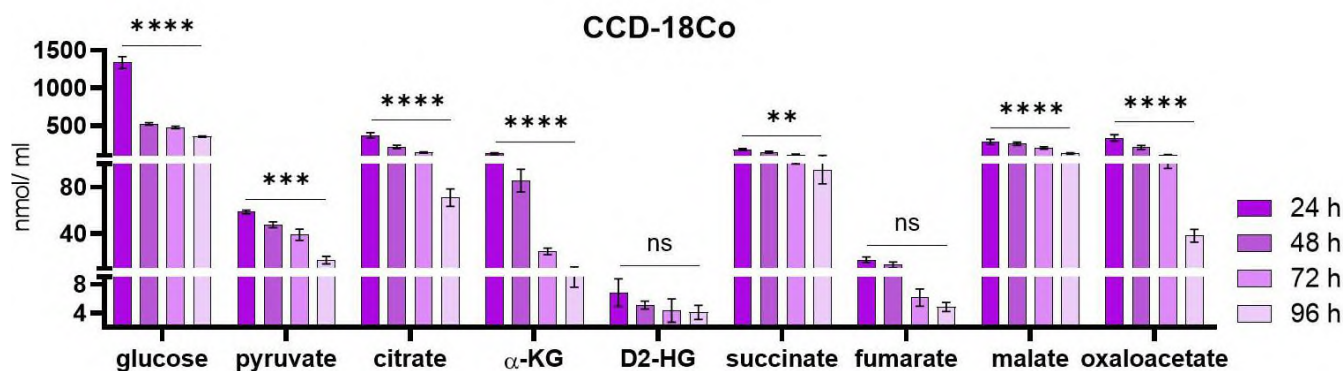


Figure 2. Time-dependent extracellular metabolite levels in CCD-18Co at 24–96 h. Metabolites were extracted from extracellular matrix of CCD-18Co cells in a time-dependent manner. Glucose and pyruvate levels were calculated by DNS method and pyruvate assay. The level of citrate, α -KG, D2-HG, succinate, fumarate, malate and oxaloacetate was determined by HPLC method. Abbreviations: ns, not significant. * $p < 0.05$, ** $p < 0.01$, *** $p < 0.001$, **** $p < 0.0001$

DNS reagent (1:1) were stirred at 140 rpm at 100 °C. After 10 minutes, it was incubated on ice for 1 minute. The standards and samples were measured at 540 nm [24] in a microplate reader (Multiskan™ GO, Thermo Scientific). The calibration curve's equality and R2 and the concentrations of the standard glucose solutions are given in Table 1.

2.4. Pyruvate Assay

The pyruvate assay determines the pyruvate content in the growth mediums [30] (Fig. 1). First, five mg of DNPH was dissolved in five ml of 2N HCl (37%), and then 10 μ l was added to each well. Then, 30 μ l of the samples were transferred to these wells and incubated for 5 minutes at room temperature. Finally, 60 μ l of 2N NaOH was added and incubated at room temperature for 10 minutes. The results were obtained at 520 nm absorbance in a microplate reader (Multiskan™ GO, Thermo Scientific). The calibration curve's equality and R2 and the concentrations of the standard pyruvate solutions are given in Table 1.

2.5. UPLC System

A UPLC (Agilent) device with an Alltech OA-1000 column which runs at 42 °C was used. All HPLC-grade

standards (Sigma Aldrich) are detected in a UV detector (210 nm). The flow rate was 0.4 mL/min, and the mobile phase was 9.0 mM H₂SO₄ [31]. Table 1 gives the calibration curve's equality, R2 value, and the concentrations of the standards for citrate, α -KG, oxaloacetate, malate, D2-HG, succinate, and fumarate.

2.6. Statistical Analysis

The experiments were carried out in three independent repeats. GraphPad Prism 8.0 (GraphPad Software, CA, USA) was used for statistical analysis. The statistical analysis (Two-way ANOVA and then Tukey's multiple comparisons test) was performed. To denote statistical significance between the control and the sample groups, the asterisk(s) is shown on the graph.

3. Results

3.1. Glucose is Consumed More in The Colon Cancer Cell Lines During 96 Hours

In the present study, changes in the extracellular metabolite levels were investigated in the primary and metastatic colon cancer cell lines in a time-dependent manner. The previous study determined only the extracellular metabolite levels at the 24th hour [24].

Reducing glucose to pyruvate is the first part of energy generation [32]. The consumed glucose levels were 1337.7–353.1 nmol/ml in the healthy cell line, while they were 1426.5–616.2 and 1609.8–638.8 nmol/ml in the Caco-2 and SW620, respectively. At the 96 h, glucose was 1.7 and 1.8-fold ($p < 0.05$) more consumed in the Caco-2 and SW620 than CCD-18Co, respectively (Fig. 2–Fig. 4).

3.2. The Pyruvate and TCA Cycle Metabolites Less Released from Colon Cancer Cell Lines During 96 Hours

Pyruvate, the end product of the glycolysis pathway, is converted to Acetyl CoA [32]. The released pyruvate levels were 58.6–17.2 nmol/ml in the healthy cell line,

Table 1. The calibration curve's equality and R2 and the concentrations of the standard solutions for glucose, pyruvate, citrate, α -KG, oxaloacetate, malate, D2-HG, succinate and fumarate.

	Calibration curve's equation	R ²	Concentrations of the standard (ppm)
glucose	$y=0,0005x+0,0078$	0,9998	500–1000–2000
	$y=0,0005x+0,0074$	0,9992	300–500–1000
	$y=0,0004x+0,0388$	0,9999	1250–2500–5000
pyruvate	$y=0,0235x+0,073$	0,9981	3.125–6.25–12.5–25
citrate	$y=3,9292x+1,55$	0,9975	12–24–48
α -KG	$y=17,787x+6,9123$	0,9998	2.5–5–10–25
oxaloacetate	$y=2,1623x-9,1$	1	25–50–100
malate	$y=2,7077x-17,45$	0,9995	25–50–100
D2-HG	$y=3,5866x-24,45$	0,9979	25–50–100
succinate	$y=1,9914x-1,9$	0,9998	5–10–20
fumarate	$y=124,57x-16,3$	0,9996	0.5–1–2

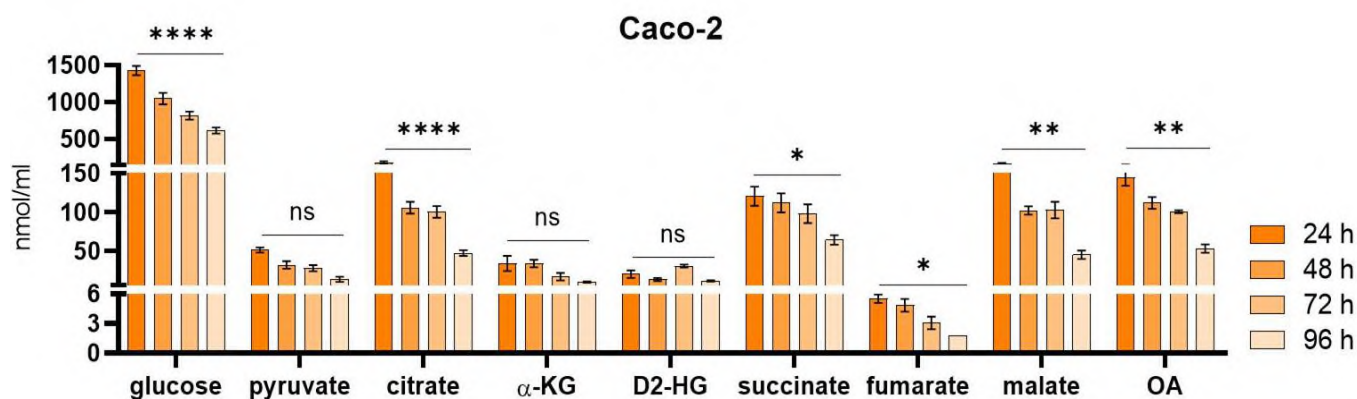


Figure 3. Time-dependent extracellular metabolite levels in Caco-2 at 24–96 h. Metabolites were extracted from extracellular matrix of Caco-2 cells in a time-dependent manner. Glucose and pyruvate levels were calculated by DNS method and pyruvate assay. The level of citrate, α -KG, D2-HG, succinate, fumarate, malate and oxaloacetate was determined by HPLC method. Abbreviations: ns, not significant. * $p < 0.05$, ** $p < 0.01$, *** $p < 0.001$, **** $p < 0.0001$

while they were 51.7–13.8 and 43.7–9.2 nmol/ml in the Caco-2 and SW620, respectively. At the 96 h, pyruvate was 1.9-fold ($p < 0.05$) less released into the environment of SW620 than CCD-18Co (Fig. 2–Fig. 4).

The released citrate levels were determined as 370.2–70.9 nmol/ml in the CCD-18Co (Fig. 2), while they were 180.1–47.6 and 121.6–52.9 nmol/ml in the Caco-2 and SW620, respectively (Fig. 3–Fig. 4). In the next step, isocitrate is oxidized to α -KG and thus the first oxidative decarboxylation reaction occurs [32].

The released extracellular α -KG levels were 126.0–9.6 nmol/ml in the CCD-18Co (Fig. 2), while they were 34.3–10.3 and 12.7–4.1 nmol/ml in the Caco-2 and SW620, respectively (Fig. 3–Fig. 4). The extracellular α -KG levels were highly decreased in the SW620 cell line according to CCD-18Co because intracellular D2-HG was highly elevated in these cells [24]. At the 96 h, the α -KG was 2.3-fold ($p < 0.05$) less released into the environment of metastatic colon cancer cells than normal cells (Fig. 2 and Fig. 4). The level of released extracellular succinate was 180.9–94.8 nmol/ml in the CCD-18Co (Fig. 2), while they were 120.6–64.6 and 94.8–6.8 nmol/ml in

the Caco-2 and SW620, respectively (Fig. 3–Fig. 4). At the 96 h, the extracellular succinate level was highly decreased in the SW620 because we found that most intracellular α -KG is reduced to D2-HG [24]. The released extracellular fumarate levels were determined as 17.6–4.9 nmol/ml in the CCD-18Co (Fig. 2), while they were 5.5–1.8 and 12.7–3.3 nmol/ml in the Caco-2 and SW620, respectively (Fig. 3–Fig. 4). In the next step of the TCA cycle, malate was synthesized from fumarate [32]. The released extracellular malate levels were 287.7–128.7 nmol/ml in the CCD-18Co (Fig. 2), while they were 166.6–45.4 and 134.7–41.7 nmol/ml in the Caco-2 and SW620, respectively (Fig. 3–Fig. 4). At the 96 h, malate was 2.8 and 3.1-fold ($p < 0.05$) less released into the Caco-2 and SW620 environment than CCD-18Co, respectively. In the last step of the TCA cycle, the oxaloacetate is synthesized from malate by the third oxidative decarboxylation reaction [32]. The released extracellular oxaloacetate levels were 335.7–38.2 nmol/ml in the CCD-18Co (Fig. 2), while they were 145–53.4 and 106.9–15.3 nmol/ml in the Caco-2 and SW620 cell lines, respectively (Fig. 3–Fig. 4). At the 96th h, oxaloacetate was 2.5–fold

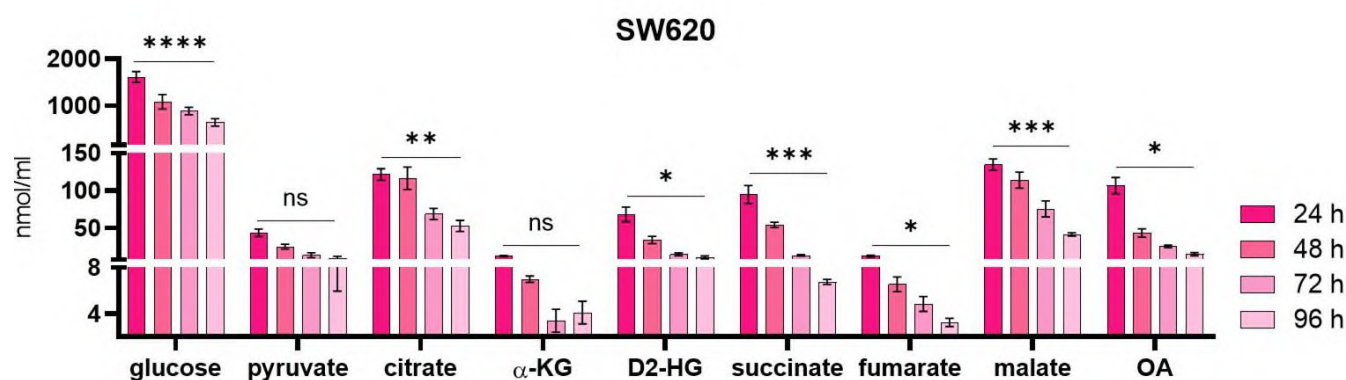


Figure 4. Time-dependent extracellular metabolite levels in SW620 at 24–96 h. Metabolites were extracted from extracellular matrix of SW620 cells in a time-dependent manner. Glucose and pyruvate levels were calculated by DNS method and pyruvate assay. The level of citrate, α -KG, D2-HG, succinate, fumarate, malate and oxaloacetate was determined by HPLC method. Abbreviations: ns, not significant. * $p < 0.05$, ** $p < 0.01$, *** $p < 0.001$, **** $p < 0.0001$

($p < 0.05$) less released into the SW620 environment than CCD-18Co.

3.3. D2-HG Oncometabolite Released More From Colon Cancer Cell Lines

D2-HG is converted from α -KG by the wild-type or mutant isocitrate dehydrogenase (IDH) 1/2 enzymes and involves in the cancer progression [20]. In our study, significant results were obtained in the time-dependent extracellular D2-HG oncometabolite. The released levels of D2-HG by cancer cell lines were increased for 96 hours. The released extracellular D2-HG levels were 6.9–4.1 nmol/ml in the CCD-18Co (Fig. 2), while they were 20.6–11.7 and 68.5–12.3 nmol/ml in the Caco-2 and SW620 cell lines, respectively (Fig. 3–Fig. 4). At the 96 h, D2-HG was 2.8 and 3.0-fold ($p < 0.01$) more released into the environment of Caco-2 and SW620 than the healthy cell.

4. Discussion

Cancer cells tend to Glycolysis, known as the Warburg effect, because they need more energy and intermediate. However, it has been found that cancer progression is not universal, and cancer cells exhibit metabolic diversity [33–35]. This allows cancer cells to adapt to changing metabolic pathways to survive and proliferate. Thus, metabolites produced in different forms due to mutations or changing their concentrations are significant therapeutic advantages for scientists [36]. Our study showed that the extracellular metabolite levels were significantly different between normal and cancer cells (Fig. 2–Fig. 4).

In the previous study, we investigated the level of intracellular metabolites produced in the TCA cycle and glycolysis in the cell lines (CCD-18Co, Caco-2, and SW620) and xenograft models generated with these cell lines. Unlike other metabolites, the elevated D2-HG level was found in the SW620 (152.6 $\mu\text{mol}/10^6$ cells), whereas it was not detected in the colon epithelial cells (CCD-18Co). In the xenograft models, the D2-HG level was 7.4 and 19.9-fold higher in Caco-2 and SW620 tumor tissues than in healthy tissue, respectively [24]. However, the time-dependent extracellular metabolite levels have not been detected until now. The present study, D2-HG-related metabolite levels were detected in the growth medium of CCD-18Co, Caco-2, and SW620 for 96 h. It was found that the D2-HG was 2.8 and 3.0-fold ($p < 0.01$) more released into the environment of Caco-2 and SW620 than the healthy cell (Fig. 2–Fig. 4). In relation to that, the α -KG was 2.3-fold ($p < 0.05$) less released into the environment of metastatic colon cancer cells than normal cells (Fig. 2–Fig. 4).

The TCA cycle is at the center of the mitochondrial metabolic pathway because coordinates energy generation, carbon metabolism, and biosynthetic pathways [37]. It has been observed that the abnormal level of TCA cycle metabolites is related to different diseases such as obesity, atrial fibrillation, heart failure, and cancer [9,10,18,38]. In the field of cancer, especially in colon cancer, the study of the amount of TCA cycle metabolites has recently increased [6]. As a result of our experiments, the levels of extracellular metabolites in cancer cells with a high metabolic rate differed significantly from healthy cells. In our study, Caco-2 and SW620 consumed 1.7 and 1.8-fold ($p < 0.05$) more glucose than CCD-18Co respectively. Pyruvate was 1.9-fold ($p < 0.05$) less released into the environment of SW620 than CCD-18Co (Fig. 2–Fig. 4). In addition, cancer cells released less TCA cycle intermediate than the healthy cells for 96 hours (Fig. 2–Fig. 4), consistent with the previous studies [39,40]. We showed that colon cancer cells exhibit the Warburg effect because of highly consumed glucose. On the other side, the TCA cycle intermediates is less released. All the results showed that metabolism does not proceed through Glycolysis, and the TCA cycle is active.

Based on the metabolic overflow concept, specific metabolites produced and accumulated inside the cell are secreted to the extracellular medium by specific metabolic overflow according to the needs of cell. Thus, information about the intracellular levels of these metabolites can be obtained by investigating the level of extracellular metabolites in the conditioned medium. When being studied experimentally, intracellular and extracellular metabolite levels must be determined simultaneously [14]. In the present study, unlike TCA cycle-related metabolites, the D2-HG oncometabolite, which is highly produced inside the cancer cells, was released more in the environment of Caco-2 and SW620 compared to normal cells for 24–96 hours (Fig. 2–Fig. 4). These results are consistent with the intracellular metabolite levels we obtained in the previous study [24].

During cancer development and progression, reversible reactions of metabolic pathways are optimized according to the conditions of the cell. Thus, the ATP and precursor molecules required for biosynthesis are highly synthesized in cancer cells [41]. As a result of the reorganization of energy metabolism, abnormal intracellular and extracellular levels of TCA cycle-related metabolites have been produced when cancer cells gain metastatic properties. In the previous studies, it has been observed that glucose consumption was decreased, and TCA cycle-related metabolites were more produced in the cancer cells according to a healthy cell. We know that D2-HG was highly produced in colon, breast, head and neck squamous metastatic cancer

cells [24,42,43]. In our study, the level of released D2-HG (in the conditioned medium) was increased when colon cancer cells gained metastatic potential, consistent with the earlier studies.

Our findings provide insight into the changes in time-dependent extracellular metabolite levels produced in glycolysis and the TCA cycle in both colon epithelial and colon cancer cell lines. We demonstrated that glucose is used to synthesize the TCA cycle intermediates which are then gradually released into the conditioned medium. Unlike TCA cycle-related metabolites, the D2-HG oncometabolite was released more in colon cancer than in normal cells. It is predicted that in the future, determining the levels of cancer-type-specific oncometabolite can be used for cancer diagnosis.

Funding

This work was supported by The Scientific and Technological Research Council of Turkey (TUBITAK) [grant number 218Z047].

References

- [1] D. Hanahan, R.A. Weinberg, The hallmarks of cancer. *Cell*, 100, 2000, 57–70.
- [2] R. Twombly, Cancer surpasses heart disease as leading cause of death for all but the very elderly. *J Natl Cancer Inst*, 2005, 97, 330–331.
- [3] H. Sung, J. Ferlay, R.L. Siegel, M. Laversanne, I. Soerjomataram, A. Jemal, F. Bray, Global cancer statistics 2020: GLOBOCAN estimates of incidence and mortality worldwide for 36 cancers in 185 countries, *CA-Cancer J Clin*, 71, 2021, 209–249.
- [4] C. Joachim, J. Macni, M. Drame, A. Pomier, P. Escarmant, J. Veronique-Baudin, V. Vinh-Hung, Overall survival of colorectal cancer by stage at diagnosis: Data from the Martinique Cancer Registry, *Medicine*, 98, 2019.
- [5] R.L. Siegel, K.D. Miller, A. Jemal, Cancer statistics, 2019, *CA-Cancer J Clin*, 69, 2019, 7–34.
- [6] C. Neitzel, P. Demuth, S. Wittmann, J. Fahrner, Targeting altered energy metabolism in colorectal cancer: oncogenic reprogramming, the central role of the TCA cycle and therapeutic opportunities, *Cancers*, 12, 2020, 1731.
- [7] A. Judge, M.S. Dodd, *Metabolism, Essays Biochem*, 64, 2020, 607–647.
- [8] E. Holmes, I.D. Wilson, J.K. Nicholson, Metabolic phenotyping in health and disease, *Cell*, 134, 2008, 714–717.
- [9] Y.J. Park, S.M. Han, J.Y. Huh, J.B. Kim, Emerging roles of epigenetic regulation in obesity and metabolic disease, *J Biol Chem*, 297, 2021.
- [10] M. Bulló, C. Papandreou, J. García-Gavilán, M. Ruiz-Canela, J. Li, M. Guasch-Ferré, E. Toledo, C. Clish, D. Corella, R. Estruch, E. Ros, M. Fitó, C.H. Lee, K. Pierce, C. Razquin, F. Arós, L. Serra-Majem, L. Liang, M.A. Martínez-González, F.B. Hu, J. Salas-Salvadó, Tricarboxylic acid cycle related-metabolites and risk of atrial fibrillation and heart failure, *Metabolism*, 125, 2021.
- [11] D.R. Schmidt, R. Patel, D.G. Kirsch, C. Lewis, M.V. Vander Heiden, J. Locasale, *Metabolomics in cancer research and emerging applications in clinical oncology, CA: Cancer J Clin*, 71, 2021, 333–358.
- [12] A. Galal, M. Talal, A. Moustafa, Applications of machine learning in metabolomics: Disease modeling and classification, *Front Genet*, 13, 2022.
- [13] N. Paczia, A. Nilgen, T. Lehmann, J. Gätgens, W. Wiechert, S. Noack, Extensive exometabolome analysis reveals extended overflow metabolism in various microorganisms, *Microb Cell Factories*, 11, 2012, 1–14.
- [14] N. Granucci, F.R. Pinu, T.L. Han, S.G. Villas-Boas, Can we predict the intracellular metabolic state of a cell based on extracellular metabolite data?, *Mol Biosyst*, 11, 2015, 3297–3304.
- [15] D. Hunerdosse, D.K. Nomura, Activity-based proteomic and metabolomic approaches for understanding metabolism, *Curr Opin Biotechnol*, 28, 2014, 116–126.
- [16] D. Hanahan, R.A. Weinberg, Hallmarks of cancer: the next generation, *Cell*, 144, 2011, 646–674.
- [17] I. Martínez-Reyes, N.S. Chandel, Mitochondrial TCA cycle metabolites control physiology and disease, *Nat Commun*, 11, 2020, 1–11.
- [18] X.W. Hou, Y. Wang, C.W. Pan, Metabolomics in diabetic retinopathy: A systematic review, *Investig Ophthalmol Vis Sci*, 62, 2021, 4–4.
- [19] M. Sciacovelli, E. Gonçalves, T.I. Johnson, V.R. Zecchini, A.S. Henriques da Costa, E. Gaude, A.V. Drubbel, S.J. Theobald, S.R. Abbo, M.G.B. Tran, V. Rajeeve, S. Cardaci, S. Foster, H. Yun, P. Cutillas, A. Warren, V. Gnanapragasam, E. Gottlieb, K. Franze, B. Huntly, E.R. Maher, P.H. Maxwell, J. Saez-Rodriguez, C. Frezza, Fumarate is an epigenetic modifier that elicits epithelial-to-mesenchymal transition, *Nature*, 537, 2016, 544–547.
- [20] L. Dang, D.W. White, S. Gross, B.D. Bennett, M.A. Bittinger, E.M. Driggers, V.R. Fantin, H.G. Jang, S. Jin, M.C. Keenan, K.M. Marks, R.M. Prins, P.S. Ward, K.E. Yen, L.M. Liao, J.D. Rabinowitz, L.C. Cantley, C.B. Thompson, M.G. Vander Heiden, S.M. Su, Cancer-associated IDH1 mutations produce 2-hydroxyglutarate, *Nature*, 462, 2009, 739–744.
- [21] I.P. Tomlinson, N.A. Alam, A.J. Rowan, E. Barclay, E.E.M. Jaeger, D. Kelsell, I. Leigh, P. Gorman, H. Lamlum, S. Rahman, R.R. Roylance, S. Olpin, Germline mutations in FH predispose to dominantly inherited uterine fibroids, skin leiomyomata and papillary renal cell cancer, *Nat Genet*, 30, 2002, 406.
- [22] H.X. Hao, O. Khalimonchuk, M. Schraders, N. Dephoure, J.P. Bayley, H. Kunst, P. Devilee, C.W.R.J. Cremers, J.D. Schiffman, B.G. Bentz, S.P. Gygi, D.R. Winge, H. Kremer, J. Rutter, SDH5, a gene required for flavination of succinate dehydrogenase, is mutated in paraganglioma, *Science*, 325, 2009, 1139–1142.
- [23] H. Colvin, N. Nishida, M. Konno, N. Haraguchi, H. Takahashi, J. Nishimura, T. Hata, K. Kawamoto, A. Asai, K. Tsunekuni, J. Koseki, T. Mizushima, T. Satoh, Y. Doki, M. Mori, H. Ishii, Oncometabolite D-2-hydroxyglutarate directly induces epithelial-mesenchymal transition and is associated with distant metastasis in colorectal cancer, *Sci Rep*, 6, 2016, 36289.
- [24] E.B. Atalay, H.A. Kayali, The elevated D-2-hydroxyglutarate level found as a characteristic metabolic change of colon cancer in both in vitro and in vivo models, *Biochem Biophys Res Commun*, 627, 2022, 191–199.
- [25] S.K. Manna, N. Tanaka, K.W. Krausz, M. Haznadar, X. Xue, T. Matsubara, E.D. Bowman, E.R. Fearon, C.C. Harris, Y.M. Shah, F.J. Gonzalez, Biomarkers of coordinate metabolic reprogramming in colorectal tumors in mice and humans, *Gastroenterology*, 146, 2014, 1313–1324.
- [26] E. Subasi, E. Bulut Atalay, D. Erdogan, B. Sen, B. Pakyapan, H.A. Kayali, Synthesis and characterization of thiosemicarbazone-functionalized organoruthenium (II)-arene complexes: Investigation of antitumor characteristics in colorectal cancer cell lines, *Mater Sci Eng C Mater Biol Appl*, 106, 2020, 110152.
- [27] S. Dietmair N.E. Timmins P.P. Gray, L.L. Nielsen, J.O. Krömer, Towards quantitative metabolomics of mammalian cells: development of a metabolite extraction protocol, *Anal Biochem*, 404, 2010, 155–164.

- [28] E.B. Atalay, S. Senturk, H.A. Kayali, Wild-type IDH1 Knockout Leads to G0/G1 Arrest, Impairs Cancer Cell Proliferation, Altering Glycolysis, and the TCA Cycle in Colon Cancer, *Biochem Genet*, 2023, 1–17.
- [29] G.L. Miller, Use of dinitrosalicylic acid reagent for determination of reducing sugar, *Anal Chem*, 31, 1959, 426–428.
- [30] K.S. Yoo, E.J. Lee, B.S. Patil, Underestimation of pyruvic acid concentrations by fructose and cysteine in 2, 4-dinitrophenylhydrazine-mediated onion pungency test, *J Food Sci*, 76, 2011, C1136–C1142.
- [31] H. Ayar-Kayali, L. Tarhan, Vancomycin antibiotic generation and TCA-glyoxalate pathways depending on the glucose concentration in *Amycolatopsis orientalis*, *Enzyme Microb Technol*, 38, 2006, 727–734.
- [32] G.M. Bodner, Metabolism Part II: The tricarboxylic acid (TCA), citric acid, or Krebs cycle, *J Chem Educ*, 63, 1986, 673.
- [33] P.H. Chen, L. Cai, K. Huffman, C. Yang, J. Kim, B. Faubert, L. Boroughs, B. Ko, J. Sudderth, E.A. McMillan, L. Girard, D. Chen, M. Peyton, M.D. Shields, B. Yao, D.S. Shames, H.S. Kim, B. Timmons, I. Sekine, R. Britt, S. Weber, L.A. Byers, J.V. Heymach, J. Chen, M.A. White, J.D. Minna, G. Xiao, R.J. DeBerardinis, Metabolic diversity in human non-small cell lung cancer cells, *Mol Cell*, 76, 2019, 838–851.
- [34] A.N. Lau, Z. Li, L.V. Danai, A.M. Westermarck, A.M. Darnell, R. Ferreira, V. Gocheva, S. Sivanand, E.C. Lien, K.M. Sapp, J.R. Mayers, G. Biffi, C.R. Chin, S.M. Davidson, D.A. Tuveson, T. Jacks, N.J. Matheson, O. Yilmaz, M.G. Vander Heiden, Dissecting cell-type-specific metabolism in pancreatic ductal adenocarcinoma, *Elife*, 9, 2020, e56782.
- [35] R.A. Cairns, I.S. Harris, T.W. Mak, Regulation of cancer cell metabolism, *Nat Rev Cancer*, 11, 2011, 85–95.
- [36] E.D. Montal, R. Dewi, K. Bhalla, L. Ou, B.J. Hwang, A.E. Ropell, C. Gordon, W.J. Liu, R.J. DeBerardinis, J. Sudderth, W. Twaddell, L.G. Boros, K.R. Shroyer, S. Duraisamy, R. Drapkin, R.S. Powers, J.M. Rohde, M.B. Boxer, K.K. Wong, G.D. Girnun, PEPCK coordinates the regulation of central carbon metabolism to promote cancer cell growth, *Mol Cell*, 60, 2015, 571–583.
- [37] H. Krebs, W.A. Johnson, The role of citric acid in intermediate metabolism in animal tissues, *FEBS letters*, 117, 1980, K2-K10.
- [38] J. Eniafe, S. Jiang, The functional roles of TCA cycle metabolites in cancer, *Oncogene*, 40, 2021, 3351–3363.
- [39] K. Dettmer, F.C. Vogl, A.P. Ritter, W. Zhu, N. Nürnberger, M. Kreuzt, P.J. Oefner, W. Gronwald, E. Gottfried, Distinct metabolic differences between various human cancer and primary cells, *Electrophor*, 34, 2013, 2836–2847.
- [40] D.A. Scott, A.D. Richardson, F.V. Filipp, C.A. Knutzen, G.G. Chiang, Z.A. Ronai, A.L. Osterman, J.W. Smith, Comparative metabolic flux profiling of melanoma cell lines beyond the warburg effect, *J Biol Chem*, 286, 2011, 42626–42634.
- [41] G. Czibik, V. Steeples, A. Yavari, H. Ashrafian, Citric acid cycle intermediates in cardioprotection, *Circ Cardiovasc Genet*, 7, 2014, 711–719.
- [42] K. Smolková, A. Dvořák, J. Zelenka, L. Vitek, P. Ježek, Reductive carboxylation and 2-hydroxyglutarate formation by wild-type IDH2 in breast carcinoma cells, *Int J Biochem Cell Biol*, 65, 2015, 125–133.
- [43] P.K. Mukherjee, P. Funchain, M. Retuerto, R.J. Jurevic, N. Fowler, B. Burkey, C. Eng, M.A. Ghannouma, Metabolomic analysis identifies differentially produced oral metabolites, including the oncometabolite 2-hydroxyglutarate, in patients with head and neck squamous cell carcinoma, *BBA Clin*, 7, 2017, 8–15.



Evaluation of photocytotoxic activity of water-soluble Zn(II) phthalocyanine on cancer cells and molecular docking studies

Ugur UZUNER¹ , Selcen CELIK-UZUNER¹ , Hakkı İsmail KAYA^{1,2} , Cagla AKKOL³ , Meryem YILMAZ¹ , Ece Tugba SAKA^{3*} 

¹ Karadeniz Technical University, Department of Molecular Biology and Genetics, Trabzon, 61080, Türkiye

² Karadeniz Technical University, Department of Biotechnology, Trabzon, 61080, Türkiye

³ Karadeniz Technical University, Department of Chemistry, Trabzon, 61080, TÜRKİYE

Abstract

In this work, 2(3), 9(10), 16(17), 23(24)-tetrakis-[N-methyl-(1-benzylpiperidin-4-yl)oxy] phthalocyaninato]zinc(II) iodide was synthesized and its aggregation behavior was investigated in different solvents and at varying concentrations. After the cytotoxic effect of 2(3), 9(10), 16(17), 23(24)-tetrakis-[N-methyl-(1-benzylpiperidin-4-yl)oxy]phthalocyaninato]zinc(II) iodide was tested, the treatment at certain conditions with phthalocyanine resulted in significant cell death (around 30%) in AR42J pancreatic cancer cells and Sol8 normal muscle cells but the same results were not observed in MDA-MD-231 metastatic breast cancer cells. To evaluate mitochondrial membrane potential (MMP), Mitotracker Red staining was performed and the treatment at certain conditions with 2(3), 9(10), 16(17), 23(24)-tetrakis-[N-methyl-(1-benzylpiperidin-4-yl)oxy]phthalocyaninato]zinc(II) iodide resulted in a significant decrease in mitochondrial membrane potential (represented by $\Delta\psi_m$) in MDA-MB-231 cells, but the same situation was not observed in other cells. *In silico* analyses were performed for intracellular target prediction of 2(3), 9(10), 16(17), 23(24)-tetrakis-[N-methyl-(1-benzylpiperidin-4-yl)oxy]phthalocyaninato]zinc(II) iodide and we found that it has inhibitory effects on Sigmar1 protein and Adiponectin receptors 1-2 with the lowest binding energies of (-13.07kcal/mol, -10.93kcal/mol and -9.49 kcal/mol, respectively). Sigmar1 is an integral protein localized in mitochondrial membranes while communication between mitochondria and endoplasmic reticulum and Adiponectin receptors are known to be associated with mitochondrial function. These results suggest that 2(3), 9(10), 16(17), 23(24)-tetrakis-[N-methyl-(1-benzylpiperidin-4-yl)oxy]phthalocyaninato]zinc(II) iodide has a cytotoxic potential on cancer cells and inhibited MMP in breast cancer cells only.

Keywords: Zinc (II) phthalocyanine, aggregation, water soluble, metastatic breast cancer, mitochondrial membrane potential, molecular docking

1. Introduction

Phthalocyanines (Pcs) are applied, such as photosensitizers [1,2], liquid crystals [3,4], sensors [5,6], and catalysts [7–9] in a wide range of areas based on chemistry and nanotechnology. They have also been commonly used as pigments and dyes [10]. Metal-centered phthalocyanine (MPc) complexes are known as photoactive and can be used for photosensitization when the central metal is a diamagnetic metal atom [11,12]. Closed shell and diamagnetic ions, *i.e.*, Zn²⁺, Ga³⁺, and Si⁴⁺, play an important role in Pc complexes with high properties, *i.e.*, high singlet oxygen generation that is crucial for photodynamic therapy (PDT) efficiency of photosensitizers [13–17]. ZnPcs are commonly studied due to a central metal ion having a full-fill shell and d¹⁰ configuration in optical spectra that

are not complicated by additional bands, as in transition-metal Pc complexes. Having intensive red visible region absorption, high triplet yields, and efficient singlet oxygen generation make ZnPcs worthwhile photosensitizers for PDT applications or cancer treatments [17]. Aggregation behavior and solubility of phthalocyanine are significant parameters that should be examined prior to *in vitro* cancer studies. The former is observed due to the 18- π electron system of phthalocyanines and decreases their solubility property in many solvents and seriously affects their spectroscopic, photochemical, photophysical, and electrochemical properties [18,19]. It is precisely at this point that the solubility of phthalocyanines in polar or nonpolar solvents becomes important.

Citation: U. Uzuner, S. Celik-Uzuner, H.İ. Kaya, C. Akkol, M. Yilmaz, E.T. Saka, Evaluation of photocytotoxic activity of water-soluble Zn(II) phthalocyanine on cancer cells and molecular docking studies, Turk J Anal Chem, 6(2), 2024, 115–128.

doi <https://doi.org/10.51435/turkjac.1585651>

Author of correspondence: ece_t_saka@hotmail.com

Received: November 14, 2024 **Tel:** +90 (462) 377 2492

Accepted: December 16, 2024 **Fax:** +90 (462) 325 3196

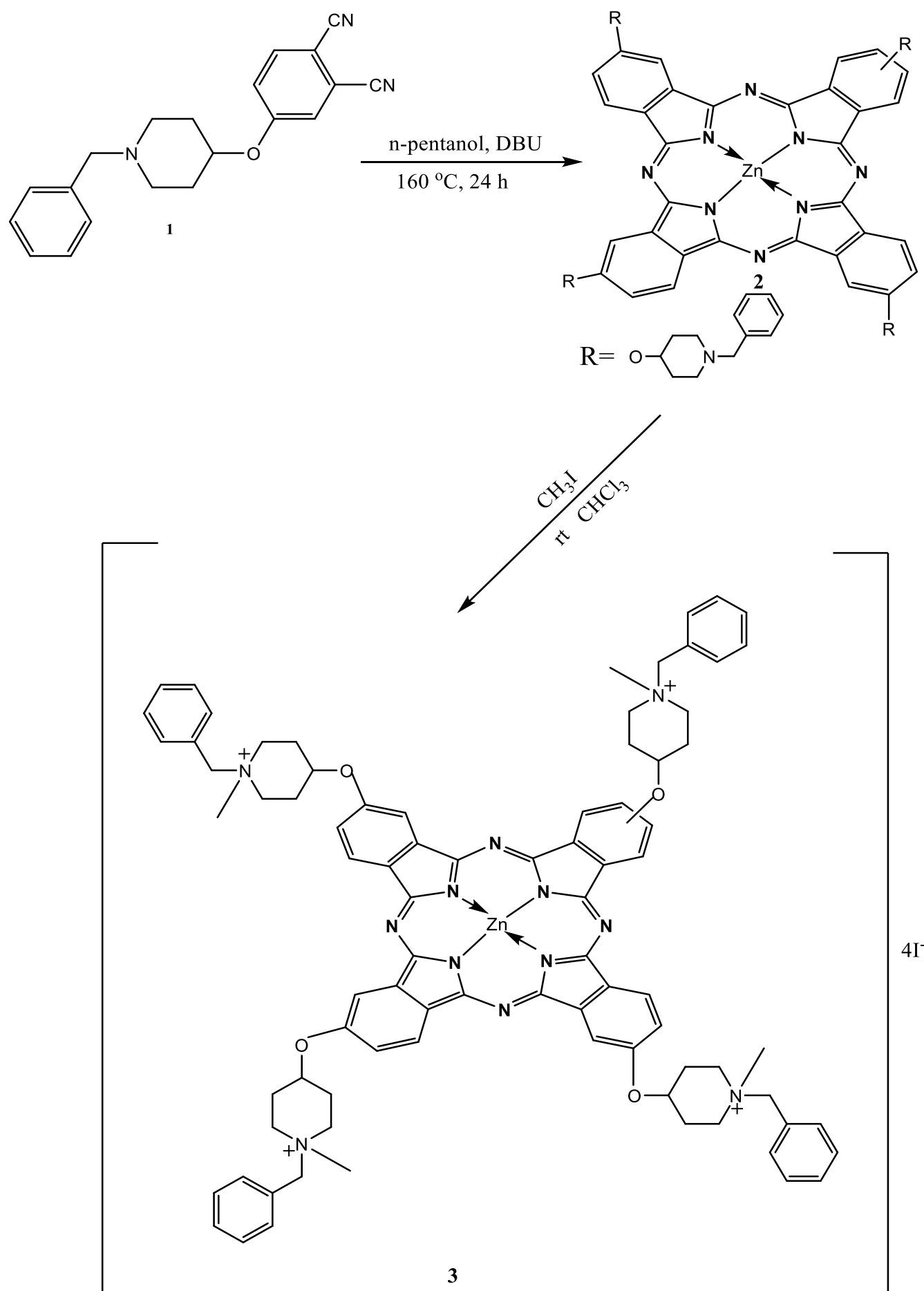


Figure 1. Synthesis of 2(3), 9(10), 16(17), 23(24)-tetrakis-[N-methyl-(1-benzylpiperidin-4-yl)oxy]phthalocyaninato]zinc(II) iodide

Solubility in water has been preferred in biological studies, in particular *in vivo* cancer studies, due to the fact that human blood itself has a hydrophilic system and the chemotherapeutics are applied intravenously [20,21].

Cancer is a common disease with a high Mortality rate around the world after cardiac diseases. Recent molecular technologies appear effective in understanding the complexity of cancer, which is to be targeted specifically for drug development. However, new candidate drugs have been in demand to overcome some limitations of current therapies such as, drug resistance, drug instability, drug insolubility, and harmful drug side effects. Therefore, innovative drug discovery technologies have focused on newly designed and more advantageous drugs. Ineffective cancer therapies can result in cancer cells that gain further molecular changes, such as metastatic characteristics. Metastasis requires aggressive cellular changes that promote increased survival, migration, and energy consumption [22]. PDT has been used to deal with metastable cancers due to the special characteristics of phthalocyanines [23]. In this work, we aimed to synthesize easily quaternizable nitrogen atoms, including 1-benzylpiperidin-4-ol groups and characterized peripherally 2(3), 9(10), 16(17), 23(24)-tetrakis-[N-methyl-(1-benzylpiperidin-4-yl)oxy]phthalocyaninato]zinc(II) iodide to be used as a photosensitizer. Its effects on cytotoxicity and mitochondrial membrane potential were also examined in cancerous and non-cancerous cells. *In silico* target of 2(3), 9(10), 16(17), 23(24)-tetrakis-[N-methyl-(1-benzylpiperidin-4-yl)oxy] phthalocyaninato]zinc(II) iodide within the cells was screened and its inhibition potential on predicted targets was examined by *in silico* molecular docking approach.

2. Experimental

2.1. Materials

4-[(1-Benzylpiperidin-4-yloxy]phthalonitrile (**1**) [24] and 2(3), 9(10), 16(17), 23(24)-tetrakis-[1-benzylpiperidin-4-yl)oxy]phthalocyaninato zinc(II) (**2**) [25] was designed and prepared according to literature. All solvents were dried and purified as described by the reported procedure [26]. 4-Nitrophthalonitrile was purchased from commercial suppliers.

2.2. Methods

2.2.1. Synthesis of 2(3), 9(10), 16(17), 23(24)-tetrakis-[N-methyl-(1-benzylpiperidin-4-yl)oxy]phthalocyaninato]zinc(II) iodide

2(3), 9(10), 16(17), 23(24)-tetrakis-[1-benzylpiperidin-4-yl)oxy]phthalocyaninato zinc(II) (30 mg, 0.020 mmol)

[25] was dissolved in CHCl_3 (3 ml), added iodomethane (3 ml), and stirred at room temperature (RT) for 3 days. The precipitated product was filtered and washed with CHCl_3 and hexane. Yield: 30 mg (72%), m.p. > 250 °C. FT-IR (ATR), ν/cm^{-1} : 3025 (Ar-CH), 2966–2890 (Aliph.-CH), 1605, 1508, 147,1393, 1305, 1242, 1188, 1072, 1059, 1038, 978, 819, 656. UV-Vis (DMF), $\lambda_{\text{max}}(\log\epsilon)$ nm: 679 (4.98), 614 (5.12), 338 (4.28). $^1\text{H-NMR}$. (DMSO), (δ :ppm): 7.78-7.60 (m, 12H, ArH), 7.53-7.38 (m, 20H, ArH), 4.70-4.55(m, 8H, $\text{CH}_2\text{-N}^+$), 4.47-4.28 (m, 4H, CH-O), 3.88-3.63 (m, 16H, $\text{CH}_2\text{-N}^+$), 3.02 (s, 12H, $\text{CH}_3\text{-N}^+$), 1.87-170 (m, 16H, Aliph. CH_2) $^{13}\text{C-NMR}$. (DMSO), (δ :ppm): 170.13 (ArC), 165.63 (ArC), 149.56 (ArC), 148.71 (ArC), 147.25 (ArC), 135.34 (ArC), 132.18 (ArC), 130.27 (ArC), 128.66 (ArC), 127.38 (ArC), 125.78 (ArC), 125.60 (ArC), 122.17 (ArC), 120.89 (ArC), 80.23 (Aliph.CH-O), 61.35 (Aliph. $\text{CH}_2\text{-N}^+$), 60.02 (Aliph. $\text{CH}_2\text{-N}^+$), 51.30 (Aliph. $\text{CH}_2\text{-N}^+$), 50.25 (Aliph. $\text{CH}_3\text{-N}^+$), 33.82 (Aliph. CH_2), 32.05(Aliph. CH_2). Anal. Calcd for $\text{C}_{84}\text{H}_{88}\text{ZnN}_{12}\text{O}_4\text{I}_4$ (1902.6821 g/mol) C, 53.02; H, 4.66; N, 8.83, Found: C, 53.09; H, 4.68; N, 8.81; MALDI-TOF-MS m/z calc. 1902.682; found: 344.81 [M-4I-H₂O]⁺⁴.

2.2.2. Cell culture

Pancreatic cancer cell line (AR42J) (ATCC Cat CRL-1492), metastatic breast cancer cell line (MDA-MB-231) (ATCC Cat HTB-26), and normal myoblast cells (Sol8) (ATCC Cat CRL-2174) were used in this study. AR42J, MDA-MB-231, and Sol8 cells were incubated in RPMI, EMEM, and DMEM media, respectively and each complete media also contained 20% fetal bovine serum and 1% Penicillin-Streptomycin antibiotics. Cells were cultured at 37°C, the normal physiological temperature of the human body, in a humidified environment with 5% CO₂ to maintain the normal rate of blood gas in the human body. After cells reached full confluency (except for Sol8 cells which are recommended to be cultured by a maximum of 80% confluency by the manufacturer as these cells can undergo cellular differentiation at the full confluent stage), cells were seeded into 96-well plates for cytotoxicity and mitochondrial assessments.

2.2.3. 2(3), 9(10), 16(17), 23(24)-Tetrakis-[N-methyl-(1-benzylpiperidin-4-yl)oxy] phthalocyaninato]zinc(II) iodide treatment and MTT cytotoxicity assay

Cells were cultured in 96-well plates as 10.000 cells per well. After they proliferated as desired, media including 2(3), 9(10), 16(17), 23(24)-tetrakis-[N-methyl-(1-benzylpiperidin-4-yl)oxy]phthalocyaninato]zinc(II) iodide at 1.5, 3, 6 and 12 micromolar was added to cells and incubated for 24 or 48 hours. Different concentrations were prepared by serial dilution in the culture media.

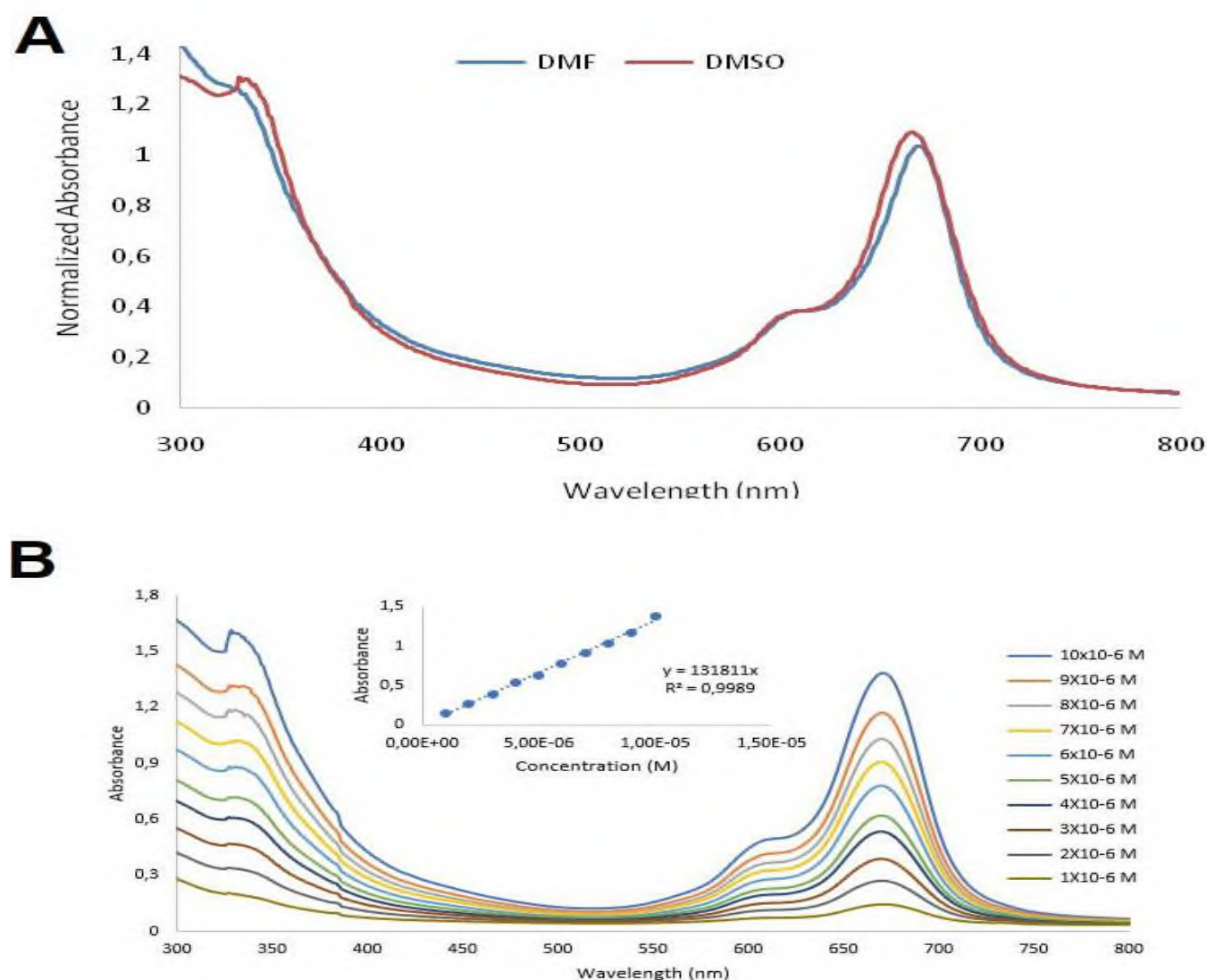


Figure 2. UV-Vis spectrum of 2(3), 9(10), 16(17), 23(24)-tetrakis-[N-methyl-(1-benzyl)piperidin-4-yl]oxyphthalocyaninato]zinc(II) iodide. A- represents two spectra of the red line is the UV-Visible spectrum of phthalocyanine in DMSO and the blue one is also the UV-Visible spectrum of phthalocyanine in DMF. B- shows the concentration effect of aggregation in DMSO with phthalocyanine between 1×10^{-6} - 10×10^{-6} molar concentration.

Some cells were treated in the dark (covered by foil and incubated in a dark room) as a control group. Internal groups of cells for each experimental design were untreated and used as a control. After pre-incubation with water soluble Zn(II) phthalocyanine, cells were exposed to red light at a wavelength of 680 nm. The total irradiation dose was adjusted to 10 j/cm^2 as before [27–30]. Duration of light exposure was calculated by the formula; $J = W \times S$ (J = desired amount of light energy, W = Light power received by the sensor and S = Duration (hour) to be applied depending on desired light energy and light power). After 1 hour of exposure, cells were incubated for a further 24 hours followed by the MTT protocol [31]. For this protocol, media was removed from all the wells, wells were washed once with 1xPBS, then 190 μl fresh media (without phthalocyanine) and 10 μl MTT dye were added to each well and incubated for 2 hours at 37°C . MTT incubation was stopped by 200 μl

solvent addition to each well after media with MTT was removed. Wells were incubated with the solvent overnight in the dark on the shaker. The day after, absorbances were read at 570 nm using a spectrophotometer. Cell viabilities (%) were relatively calculated according to untreated cells which are considered as 100% viable.

2.2.4. Assessment of mitochondrial membrane potential

Cells were incubated and treated as mentioned above. Differentially, after 24h incubation with ZnPc wells were washed with 1xPBS followed by the treatment with media including $4.0 \times 10^{-3} \text{ M}$ MitoTracker Red (ThermoFisher, M7512) for 45 minutes at 37°C [32]. MitoTracker treated wells were washed with 1xPBS three times and fluorescence was read at 579/599 using a microplate reader.

2.2.5. *In silico* target prediction for 2(3), 9(10), 16(17), 23(24)-tetrakis-[N-methyl-(1-benzylpiperidin-4-yl)oxy]phthalocyaninato]zinc(II) iodide

In silico target prediction for 2(3), 9(10), 16(17), 23(24)-tetrakis-[N-methyl-(1-benzylpiperidin-4-yl)oxy]phthalocyaninato]zinc(II) iodide was performed using the Similarity ensemble approach (SEA) [33]. The SEA approach is effective in performing analyses based on set-based chemical similarity between ligands of proteins. It is useful for quickly browsing large composite databases and generating *in silico* predictions from similarity maps by identifying cross-targets.

2.2.6. 3D structure preparation of zinc (II) phthalocyanine and target proteins and molecular docking

To evaluate the ligand-based affinity of phthalocyanine, the SDF file of 2(3), 9(10), 16(17), 23(24)-tetrakis-[N-methyl-(1-benzylpiperidin-4-yl)oxy]phthalocyaninato]zinc(II) iodide was initially created using Open Babel software [34]. Energy minimization was performed by AutoDock MGL Tools and Gasteiger charges were assigned to the compound prior to molecular docking studies [35]. The 3D structures of ADPNR1 (PDB ID: 5LXG), ADPNR2 (PDB ID: 6YX9), and Sigmar1 (PDB ID: 5HK1) were retrieved from the Protein Data Bank (www.rcsb.org). All structures were processed before molecular docking studies. Bound water molecules were initially removed from the 3D protein structures, polar hydrogens were added to each protein and eventually the structures were charged with Kollman charges before saving their pdbqt files. Grid box sizes were adjusted based on the catalytic core of each protein target to surround the amino acid domain involved in the binding active sites. For this, grid center coordinates and box size values for ADPNR1-2(3), 9(10), 16(17), 23(24)-tetrakis-[N-methyl-(1-benzylpiperidin-4-yl)oxy]phthalocyaninat]zinc(II) iodide docking was set as 23, 31 and 2,4 and the box size was 35, 35, 35. On the other hand, the related calculations were set as 12, -21, -22 and the box size was 35, 35, 35 for ADPNR2. However, the catalytic core of Sigmar1 was identified as buried into the target receptor. Therefore, we performed blind docking experiment on Sigmar1 receptor to determine the best binding pose of 2(3), 9(10), 16(17), 23(24)-tetrakis-[N-methyl-(1-benzylpiperidin-4-yl)oxy] phthalocyaninato]zinc(II) iodide. For this goal, the grid center coordinates were set as 14, 38, -36 and the dimensions of the box size value were adjusted as 50, 45, and 47. Molecular docking studies were then performed for ADPNR1 and ADPNR2 proteins using AutoDockZn software [36], whereas, targeting 2(3), 9(10), 16(17), 23(24)-tetrakis-[N-methyl-(1-benzylpiperidin-4-yl)oxy] phthalocyaninato]zinc(II) iodide compound to Sigmar1 receptor was performed using AutoDock4 [37].

2.2.7. Statistics

The fluorescence values of MMP activity were analyzed by the UNIANOVA test of SPSS software. The comparison for cell viability (%) was also performed using the UNIANOVA. The significance is considered if p value is less than 0.05. Significant levels used were $p < 0.05$ (*), $p < 0.01$ (**), $p < 0.001$ (***) and $p < 0.0001$ (****). Experiments were completed as at least three independent repeats and standard errors of the means (+/-s.e.m.) were calculated by the SPSS (Version 13) program.

3. Results and Discussion

4-[(1-Benzylpiperidin-4-yloxy]phthalonitrile 1 and 2(3), 9(10), 16(17), 23(24)-tetrakis-[1-benzylpiperidin-4-yl)oxy]phthalocyaninato zinc(II) were synthesized according to literatures, as mentioned in the material and method section [24-25]. 2(3), 9(10), 16(17), 23(24)-tetrakis-[N-methyl-(1-benzylpiperidin-4-yl)oxy]phthalocyaninato]zinc(II) iodide was synthesized by the reaction of 2(3), 9(10), 16(17), 23(24)-tetrakis-[1-benzylpiperidin-4-yl)oxy] phthalocyaninato zinc(II) with $\text{CH}_3\text{-I}$ in CHCl_3 (Fig. 1). Quaternization of 2(3), 9(10), 16(17), 23(24)-tetrakis-[1-benzylpiperidin-4-yl)oxy]phthalocyaninato zinc(II) with an excess of methyl iodide in chloroform led to water soluble tetra cationic Zn(II) phthalocyanine. After the reaction contents were stirred at room temperature for 72 hours, the dark green crude product was precipitated at the bottom of the reaction vessel. The crude product was filtered and washed three times with chloroform and hexane. When looking at the infrared spectra of 2(3), 9(10), 16(17), 23(24)-tetrakis-[1-benzylpiperidin-4-yl)oxy] phthalocyaninato zinc(II) and its water-soluble derivative, it can be seen that both are similar. Both of them have aromatic, aliphatic carbon resonance peaks and do not have $\text{C}\equiv\text{N}$ sharp resonance peak around 2230 cm^{-1} which is the very identical peak for 4-[(1-benzylpiperidin-4-yloxy]phthalonitrile as the starting molecule. The FT-IR spectra of 2(3), 9(10), 16(17), 23(24)-tetrakis-[N-methyl-(1-benzylpiperidin-4-yl)oxy]phthalocyaninato]zinc(II) iodide has had aromatic carbon resonance peaks at 3025 cm^{-1} and aliphatic carbon resonance peaks at $2966\text{--}2890$.

The $^1\text{H-NMR}$ data of 2(3), 9(10), 16(17), 23(24)-tetrakis-[N-methyl-(1-benzylpiperidin-4-yl)oxy]phthalocyaninato]zinc(II) iodide in DMSO-d_6 showed signals due to the appearance of aromatic protons at 7.78-7.60 and 7.53-7.38 ppm. The CH_3 group of 2(3), 9(10), 16(17), 23(24)-tetrakis-[N-methyl-(1-benzylpiperidin-4-yl)oxy]phthalocyaninato]zinc(II) iodide was indicated as a singlet at 3.02 ppm.

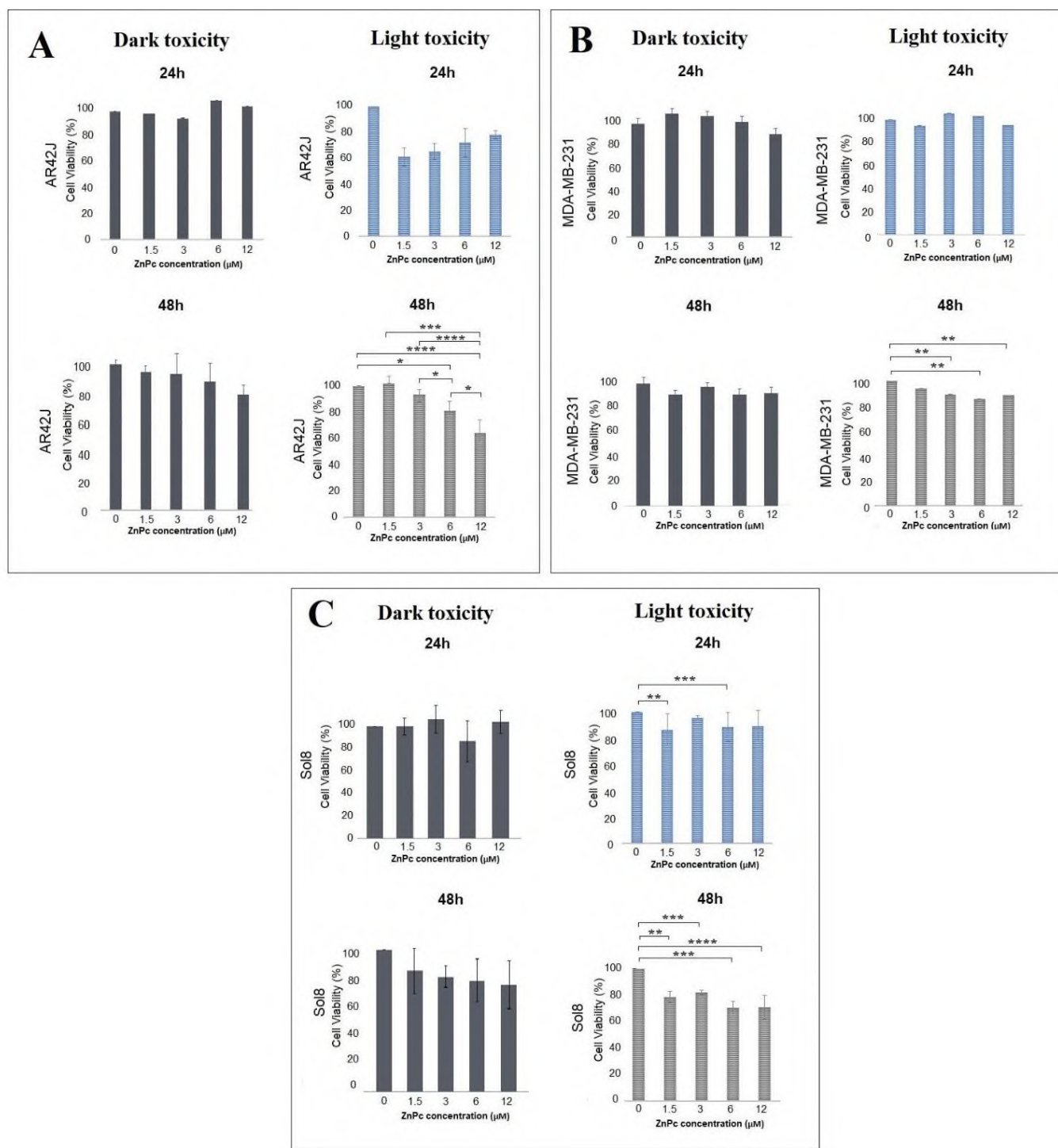


Figure 3. Cell viability 2(3), 9(10), 16(17), 23(24)-tetrakis-[N-methyl-(1-benzylpiperidin-4-yl)oxy]phthalocyaninato]zinc (II) iodide treatment in AR42J, MDA-MB-231 and Sol8 cells. Cell percentages (%) are shown for AR42J (A), MDA-MB-231 (B), and Sol8 (C) cells after phthalocyanine treatments (0, 1.5, 3, 6, and 12 μM) both for 24h (up panels) and 48h (down panels), after light (right panels) and dark (unlightened) exposure (left panels). $p < 0.05$ (*), $p < 0.01$ (**), $p < 0.001$ (***) and $p < 0.0001$ (****)

The aliphatic protons were observed at 4.70–4.55, 4.47–4.28, 3.88–3.63, and 1.87–1.70 ppm. The ^{13}C -NMR spectrum of the quaternary ammonium group containing zinc (II) phthalocyanine was taken in $\text{DMSO-}d_6$ and construed as having 21 carbon atoms in the structure. In the ^{13}C -NMR spectrum, 14 different signals for aromatic carbon atoms between 170.13 and 120.89 ppm and also 7 signals for aliphatic carbon atoms between 80.23 and 32.05 ppm comply with the proposed structure.

The molecular ion peak of 2(3), 9(10), 16(17), 23(24)-tetrakis-[N-methyl-(1-benzylpiperidin-4-yl)oxy]phthalocyaninato]zinc(II) iodide was seen at $m/z=344.81$ $[(M-4I-H_2O)]^{+4}$ (S. Fig. 1). Elemental analysis also supports the proposed structure of Zn(II) phthalocyanine. UV-Vis spectrum of 2(3), 9(10), 16(17), 23(24)-tetrakis-[N-methyl-(1-benzylpiperidin-4-yl)oxy]phthalocyaninato]zinc(II) iodide was measured in water (S. Fig. 2).

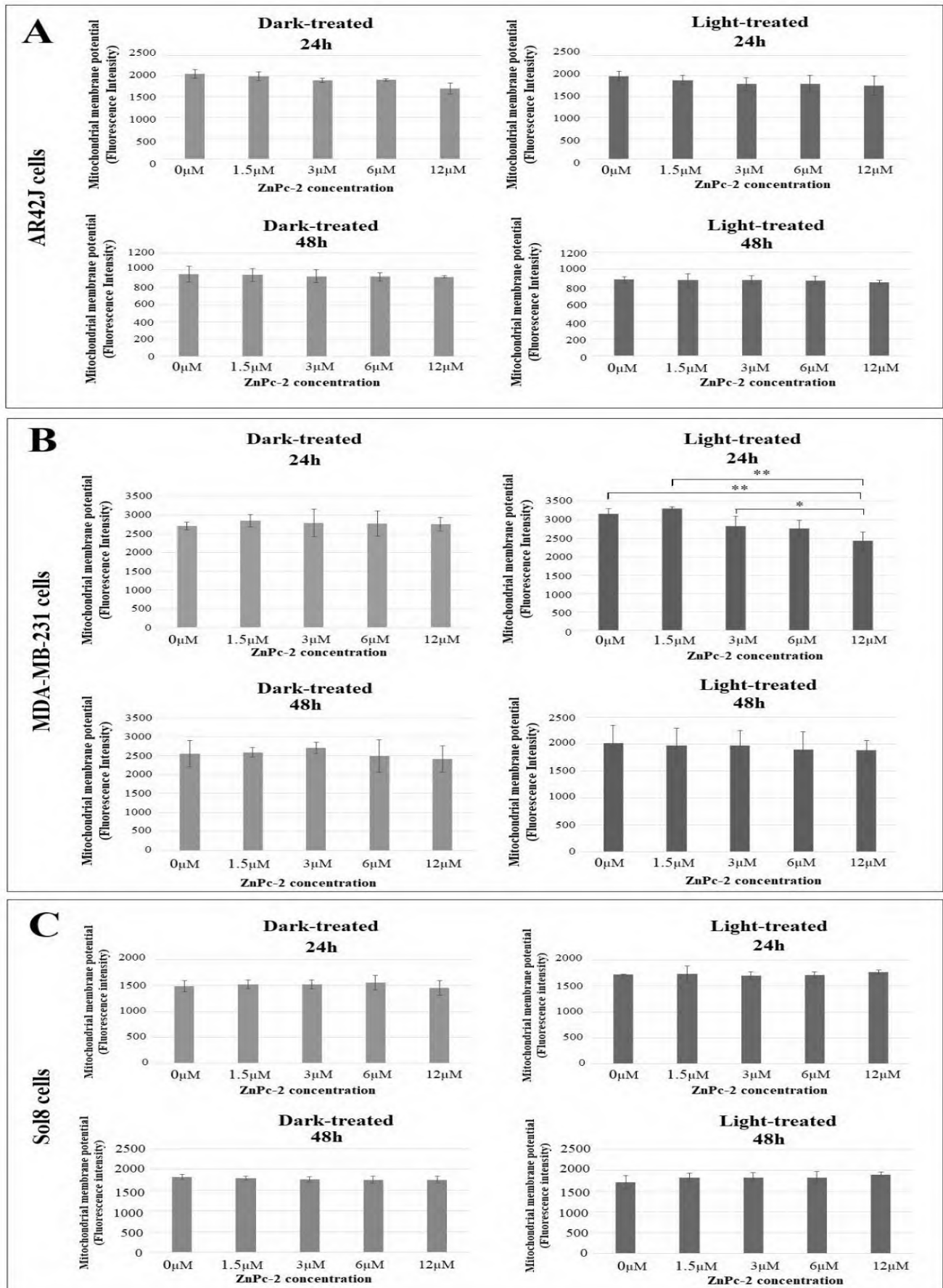


Figure 4. Mitochondrial membrane potential after phthalocyanine treatment. Mitochondrial membrane potential values were calculated in immunostaining photos by Image J software, and these are shown for AR42J (A), MDA-MB-231 (B), and Sol8 (C) cells after 24h (up panels) or 48h (down panels) treatment with different doses of phthalocyanine treatment before light exposure followed by light (right panels) or dark (unlightened) exposure (left panels). $p < 0.05$ (*), $p < 0.01$ (**), $p < 0.001$ (***) and $p < 0.0001$ (****)

Additionally, the aggregation behavior of 2(3), 9(10), 16(17), 23(24)-tetrakis-[N-methyl-(1-benzylpiperidin-4-yl)oxy] phthalocyaninato]zinc(II) iodide was measured in DMSO (Fig. 3A). Dimethyl sulfoxide (DMSO) is a dipolar aprotic solvent ($\mu = 3.96$ D) of moderate dielectric constant ($\epsilon = 45.0$) totally miscible with water, having two sites of coordination of different softness and being consequently a good solvent for cations. The UV-vis absorption spectrum of 2(3), 9(10), 16(17), 23(24)-tetrakis-[N-methyl-(1-benzylpiperidin-4-yl)oxy]phthalocyaninato]zinc(II) iodide in dry DMSO, presented in Fig. 2A, shows a peak at about 679 nm in the Q band region, with a much less intense one at 614 nm, as usually observed in organic media for a monomeric zinc(II) phthalocyanine [38–41]. The maximum absorbance at 338 nm in the Soret region is lower than that of the Q band in the visible region. This spectrum is typical of many metallophthalocyanines: the two Q and Soret bands are $\pi \rightarrow \pi^*$ transitions, $a_{1u} \rightarrow e_g$ for the Q band and $a_{2u} \rightarrow e_g$ for the Soret [42–44]. The spectrum can be totally different in pure water. The Q band maximum is much less intense than the peak in DMSO and this band looks broader because two other absorption bands are apparent as shoulders somewhat below 600 nm and at 680–690 nm. This spectrum is typical of dimeric M(II)phthalocyanines, for example, one of the Cu(II) sulfophthalocyanine [45–46]. L'Her et al. examined the influence of the concentration on the spectrum in water over a large range of concentration, from 6.4×10^{-4} M to 6.4×10^{-7} M, using cells with optical lengths from 0.1 mm to 10 cm. No evolution of the spectra reduced to ϵ was observed, which means that Beer's law is obeyed, and that dilution has no influence on the composition of the solution over this extended concentration range. As a consequence, these aggregates are very stable, even at the lowest concentration, and their dissociation constant cannot be estimated, unlike what has been possible for many phthalocyanines [47]. From the comparison with DMSO and water, it is evident that the zinc phthalocyanine exists as a mixture of the monomer and aggregates [48]. Additionally, solvent type effects were investigated (Fig. 2B) with different concentrations (S. Fig. 2) on the behavior of 2(3), 9(10), 16(17), 23(24)-tetrakis-[N-methyl-(1-benzylpiperidin-4-yl)oxy]phthalocyaninato]zinc(II) iodide.

2(3), 9(10), 16(17), 23(24)-Tetrakis-[N-methyl-(1-benzylpiperidin-4-yl)oxy] phthalocyaninato]zinc(II) iodide was then proceeded for *in vitro* biological analysis. First, its cytotoxic potential in AR42J pancreatic cancer cells, MDA-MB-231 metastatic breast cancer cells, and Sol8 normal muscle cells was evaluated. Dark treated cells (as a control group to light) were also included in the experiment. None of the conditions in the

dark (at 24 or 48 hours) resulted in a significant change in cell viability (Fig. 3A–Fig. 3C, left panels). However cytotoxic effects after light exposure have been shown in AR42J cells and Sol8 at 48h with around 30% reduction (Fig. 3A and Fig. 3C, right panels). Although a reduction was detected, The IC-50 values could not be calculated. Pair-wise comparisons are performed by post-hoc test and the significant levels are shown by asterisks between the compared doses (Fig. 3A–Fig. 3C, right panels). Detailed statistical analyses for cytotoxicity after light are provided in S. Fig. 3 (blue squares indicate significant comparisons). IC50 value for Zn(II) phthalocyanines (ZnPcs) conjugated with thiopyridinium units was determined as 20 μ M in melanoma cells [49]. Octal-bromide zinc phthalocyanine (ZnPcBr8) resulted in the death of almost all (around 100%) Hep-2 (laryngeal carcinoma) cells at 24h [50]. These suggest that the effectiveness of ZnPc molecules may depend on the structure and the type of cancer cells examined. ZnPc was used to be incorporated into extracellular vesicles and this was found to reduce colon cancer growth over 2 weeks [51]. However, phthalocyanines can also be effectively cytotoxic regardless of light induction. A study showed that the two dyads composed of zinc(II) phthalocyanine and tin complexes were more cytotoxic in MCF-7 human breast cancer when it was treated in the dark compared to light with an IC50 between 0.016 and 0.453 μ M [52]. On the other hand, photodynamic therapy with zinc phthalocyanine was shown to enhance the anti-cancer effect of some common chemotherapeutics, *i.e.*, tamoxifen in breast cancer cell lines [53].

However, mitochondrial membrane potential was gradually decreased in MDA-MB-231 cells at 24 h after zinc (II) phthalocyanine treatment ($p < 0.05$) (Fig. 4B) compared to both AR42J (Fig. 5A) and Sol8 cells (Fig. 5C). 48h pretreatment with 2(3), 9(10), 16(17), 23(24)-Tetrakis-[N-methyl-(1-benzylpiperidin-4-yl)oxy]phthalocyaninato]zinc(II) iodide did not induce MMP decrease as much as 24h pretreatment (Fig. 4B). Detailed statistical analyses for mitochondrial membrane potential are provided in S. Fig. 4 (blue squares indicate significant comparisons). Representative staining for mitochondrial membrane potential after 12 μ M water soluble Zn(II) phthalocyanine (after 24h) is shown in Fig. 5D. A, B, and C show $\Delta\psi_m$ values in AR42J, MDA-MB-231, and Sol8 cells, respectively. Fig. 5 shows representative fluorescence imaging of mitochondrial staining. Mitochondrial membrane potential was shown to reduce in different cancer cell lines after ZnPc compounds [54–56].

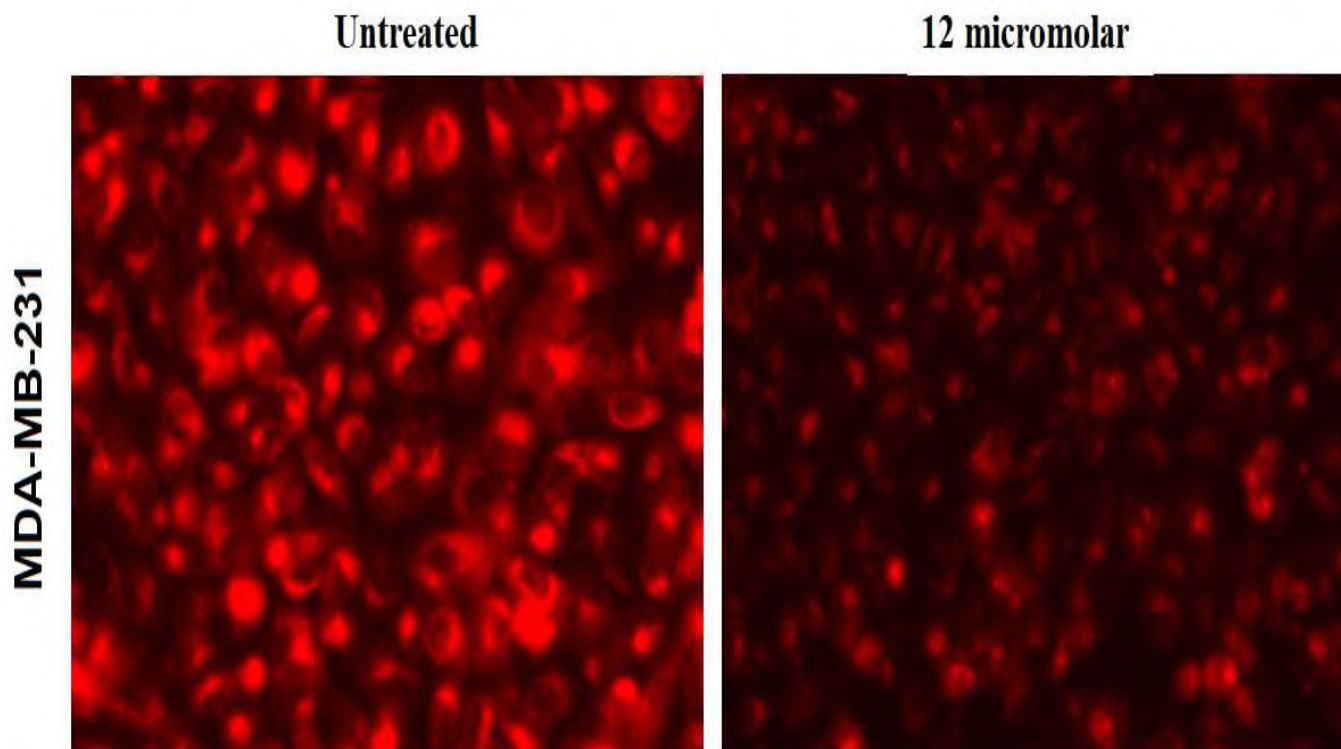


Figure 6. Representative fluorescent labeling of mitochondria by MitoTracker Red. The figure shows the staining in untreated and treated (by 12 micromolar phthalocyanine for 24 hours) followed by irradiation in MDA-MB-231 cells.

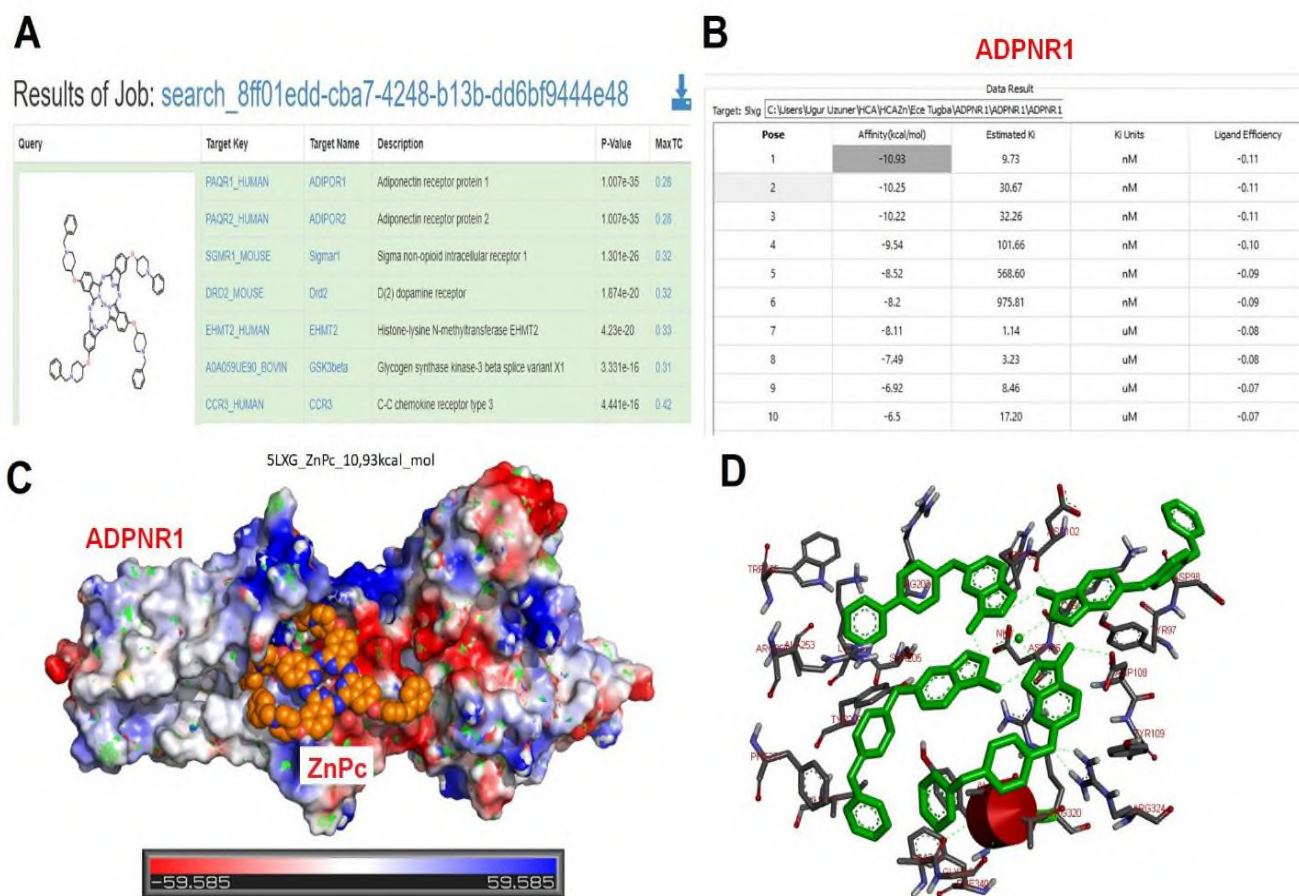


Figure 5. Target prediction of 2(3), 9(10), 16(17), 23(24)-tetrakis-[N-methyl-(1-benzylpiperidin-4-yl)oxy]phthalocyaninato]zinc(II) iodide in the cells and docking with Adiponectin Receptor 1. A shows the top 7 targets for phthalocyanine in the cells with the highest *p* values. The top three targets include 1) Adiponectin receptor 1 (ADPNR1), 2) Adiponectin receptor 2 (ADPNR2), and 3) Sigma non-opioid intracellular receptor 1 (Sigmar1). B shows 10 different poses for the docking of phthalocyanine with ADPNR1 protein by binding affinities, estimated *K_i* values, *K_i* units, and ligand efficiency. C shows the best representative of pose for docking. D shows the predicted 2D interaction map of phthalocyanine with

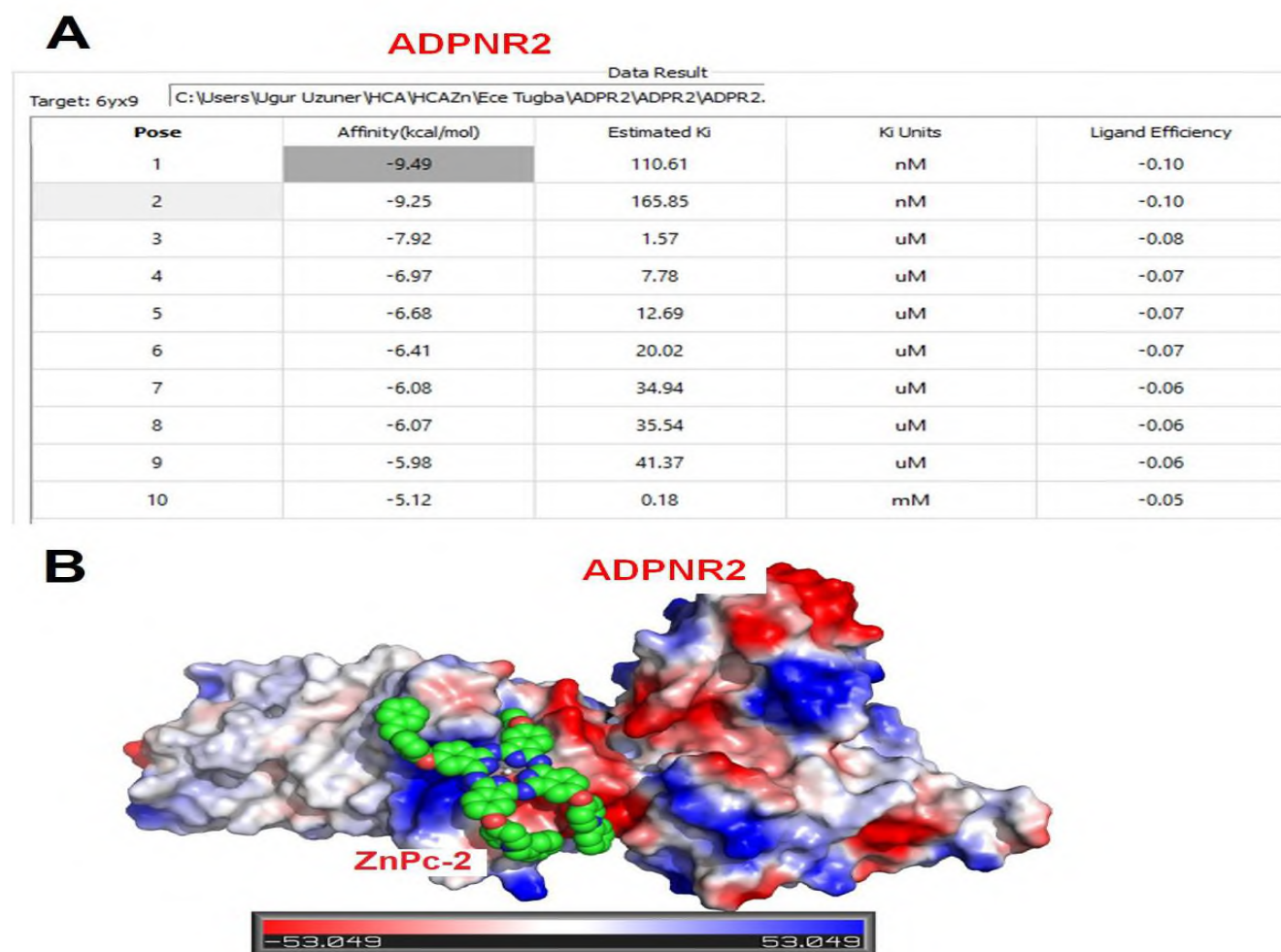


Figure 7. 2(3), 9(10), 16(17), 23(24)-Tetrakis-[N-methyl-(1-benzylpiperidin-4-yl)oxy] phthalocyaninato]zinc(II) iodide docking with Adiponectin Receptor 2 (ADPNR2). A shows 10 different poses for the docking of phthalocyanine with ADPNR2 protein by binding affinities, estimated Ki values, Ki units and ligand efficiency. B shows the best representative of pose for docking.

When potential protein or receptor targets were screened, the top three targets of 2(3), 9(10), 16(17), 23(24)-tetrakis-[N-methyl-(1-benzylpiperidin-4-yl)oxy]phthalocyaninato]zinc(II) iodide were identified as Adiponectin receptor 1 (ADPNR1), Adiponectin receptor 2 (ADPNR2) and sigma non-opioid intracellular receptor 1 (Sigmar1) proteins. *In silico* target prediction analysis were hit for the two intracellular targets for 2(3), 9(10), 16(17), 23(24)-tetrakis-[N-methyl-(1-benzylpiperidin-4-yl)oxy]phthalocyaninato]zinc(II) iodide including ADPNRs and Sigmar1 protein with the highest significance (Fig. 6A). *In silico* docking analyses were then performed for ADPNR1 (Fig. 6B–Fig. 6D). 10 different binding poses for the active domain of target proteins were analyzed (Fig. 6B) and the docking for the highest affinity along with the lowest binding energy (–10.93 kcal/mol) was modeled (Fig 6C and Fig 6D). ADPNR1 and ADPNR2 proteins are secreted from white adipose tissue [57], and mitochondrial function was dysregulated in mice lacking ADPNR1 [58]. ADPNR1 increased mitochondrial function in skeletal muscle cells [57], and it is highly associated with the regulation of glucose and lipid metabolism and with mitochondrial biogenesis [59]. However, the effect of ADPNR1

deficiency on mitochondrial protein composition has been found to be highly tissue-specific [58]. ADPNR2 was also docked with phthalocyanine and the binding affinity of 2(3), 9(10), 16(17), 23(24)-tetrakis-[N-methyl-(1-benzylpiperidin-4-yl)oxy] phthalocyaninato]zinc(II) iodide to ADPNR2 (–9.49 kcal/mol) (Fig. 7A) was found to be less than the binding affinity to ADPNR1 (–10.93 kcal/mol). Both ADPNRs are able to bind metals in particular zinc (from the Uniprot database) which are included in the core structure of synthesized water soluble Zn(II) phthalocyanine. ADPNR1/ADPNR2 were reported to recover non-alcoholic hepatitis and fibrosis by their roles in between ER and mitochondria communication [60].

We then analyzed the third *in silico* target of phthalocyanine, Sigmar1. The best pose for Sigmar1 was detected with the lowest binding energy as –13.07 kcal/mol (Fig. 8A). The docking of this pose was modeled (Fig 8B–Fig 8C). Sigma receptor 1 (Sigmar1) is a chaperone significantly localized in the mitochondrial membrane of cardiomyocytes [61], but Sigmar1 is expressed in a range of tissues so that it is considered as having housekeeping function in each cell type [61,62].

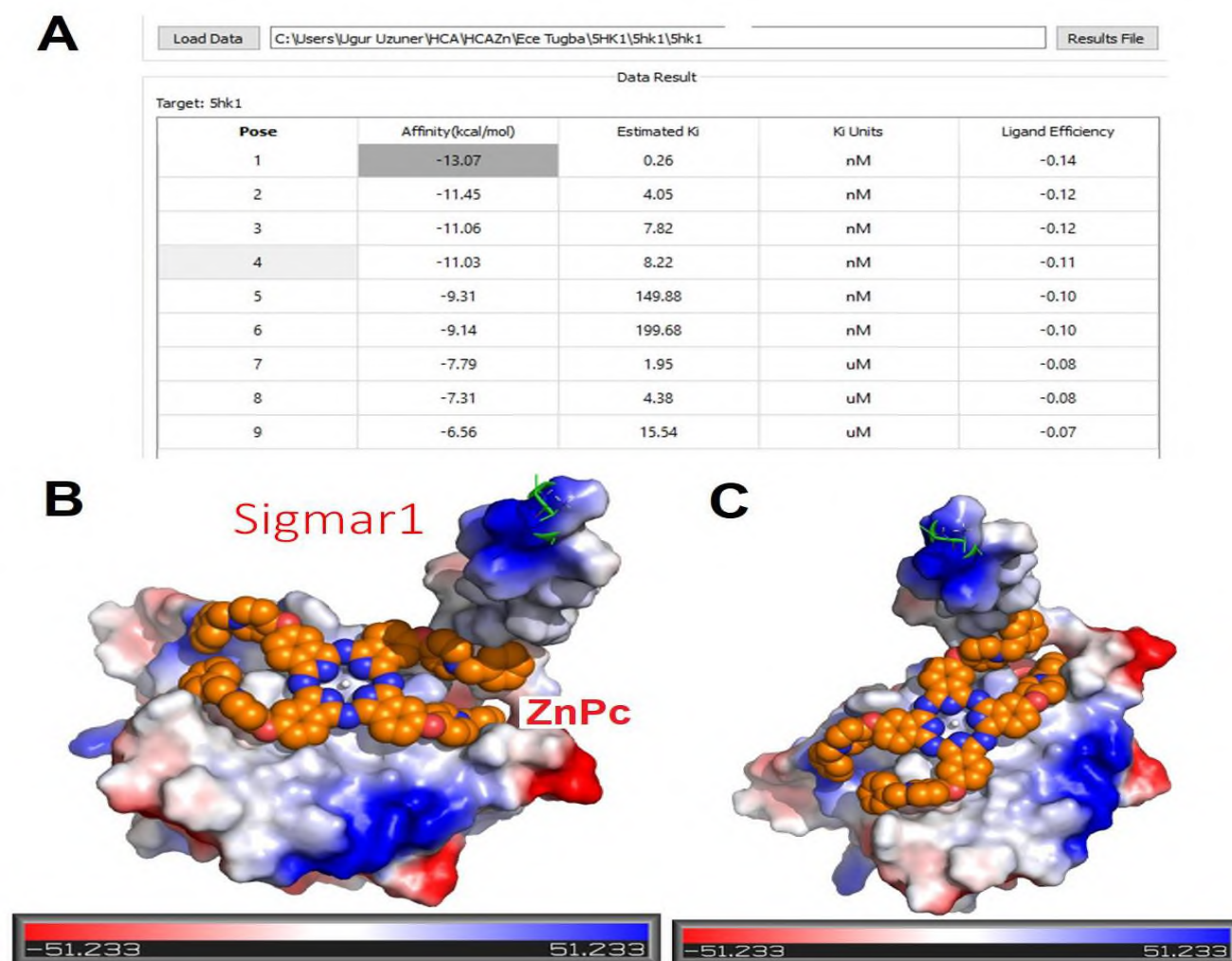


Figure 8. 2(3), 9(10), 16(17), 23(24)-Tetrakis-[N-methyl-(1-benzylpiperidin-4-yl)oxy] phthalocyaninato]zinc(II) iodide docking with Sigmar1 protein. A shows 10 different poses for the docking of phthalocyanine with Sigmar1 protein by binding affinities, estimated Ki values, Ki units, and ligand efficiency. B and C show the best representative of the pose for docking from different angles.

This is also localized in the cell membrane and nuclear membrane [63]. The Sigmar-1 upregulation was found to be associated with enhanced membrane invasiveness [62]. Sigmar1 receptor is required for proper respiration in mitochondria [61] and also has a role in the communication between mitochondria and endoplasmic reticulum [63]. The cells with knock-downed Sigmar1 showed an increase in cell death rate suggesting its association with cell survival [63]. Deficiency in Sigmar1 is associated with a range of diseases such as neurodegenerative diseases, cancer, and cardiovascular diseases [62]. Clinical studies showed that Sigmar1 is abundant in breast cancer patients [64]. Its increase has also been detected in other cancers including liver, colon, prostate, and lung [62], whereas the change in the level of Sigmar1 was not significant in patients with pancreatic cancer compared to healthy controls [63]. Current molecular docking studies show that 2(3), 9(10), 16(17), 23(24)-tetrakis-[N-methyl-(1-benzylpiperidin-4-yl)oxy]phthalocyaninato]zinc(II) iodide exhibits high binding affinity to the intramembrane interaction surface of the Sigmar1 trimeric complex, thereby causing

inactivation of the sigmar1 complex, which is essential for the maintenance of mitochondrial functions.

Both Sigmar1 and ADPNR1 play key roles during the maintenance of mitochondrial function. Mitotracker red dye has been used for confirmation of Sigmar1 localization [60] as well as mitochondrial function mediated by Sigmar1 [63,65]. Sigmar1 and ADPNR genes are located in 9p13.3 and 3q27.3, respectively (from Genecards). The genome of MDA-MB-231 cells is reported as in the triploid range with the absence of chromosomes 8 and 15 by the manufacturer (ATCC), however AR42J cells are in normal diploid range with specific gene expression changes. Therefore, the levels of proteins in the examined cells are expected to be different from each other. The genomic differences between cells may suggest the variation of mitochondrial membrane potential changed by phthalocyanine. However, further investigation is required for revealing the profiles of gene expression levels in detail.

Therefore, an ultimate phthalocyanine molecule might be an effective photosensitizer that naturally

gathers in mitochondria [66]. Targeting mitochondria has been used to enhance the efficacy of photodynamic therapy [67]. Mitochondrial membrane potential ($\Delta\psi_m$) (MMP) is an indicator of mitochondrial function. $\Delta\psi_m$ is associated with the role of mitochondria in apoptosis, and its decrease has been shown to be induced by insufficient substrates for the mitochondria, disruption in respiration, or separation of the inner membrane [68]. However, mitochondrial membrane potential has been suggested not to be an early event in the apoptosis [69]. Mitochondrial activity was found to increase after radiation treatment [70]. Some cytotoxic conditions, such as radiation, may not be associated with an increase in cell death detected by metabolic viability assays including MTT [70]. In this study, results suggest conditions for targeting mitochondrial activity by membrane potential in metastatic breast cancer only which is not correlated with cytotoxicity assessed by MTT assay. We previously showed that a silicon phthalocyanine molecule was highly cytotoxic in AR42J cells after 24h, but not in Sol8 cells, and IC50s were calculated for each cell line [27], however 2(3), 9(10), 16(17), 23(24)-tetrakis-[N-methyl-(1-benzylpiperidin-4-yl)oxy]phthalocyaninato]zinc(II) iodide was not cytotoxic in the same conditions. The critical function of Zn is that it does not quench the ability of phthalocyanine to form ROS upon irradiation. The high doses of phthalocyanine (with prolonged incubation time points) may induce cytotoxicity with calculable IC50 values which represent the effective dose to kill half of the cell population.

4. Conclusion

In this study, 2(3), 9(10), 16(17), 23(24)-tetrakis-[N-methyl-(1-benzylpiperidin-4-yl)oxy]phthalocyaninato]zinc(II) iodide was synthesized and characterized with FT-IR, UV-Vis and mass spectra and elemental analysis. Aggregation is an important factor for phthalocyanine compounds because it prevents the usage of phthalocyanine in many application areas. Aggregation of 2(3), 9(10), 16(17), 23(24)-tetrakis-[N-methyl-(1-benzylpiperidin-4-yl)oxy]phthalocyaninato]zinc(II) iodide was also investigated in different solvents using UV-spectra to examine changes in the Q and B bands. This study indicates that 2(3), 9(10), 16(17), 23(24)-tetrakis-[N-methyl-(1-benzylpiperidin-4-yl)oxy]phthalocyaninato]zinc(II) iodide has an inhibitory effect on mitochondrial, particularly in MDA-MB-231 metastatic breast cancer cells. 2(3), 9(10), 16(17), 23(24)-Tetrakis-[N-methyl-(1-benzylpiperidin-4-yl)oxy]phthalocyaninato]zinc(II) iodide was cytotoxic to all cells at the different conditions experienced. The

possible cellular targets of 2(3), 9(10), 16(17), 23(24)-tetrakis-[N-methyl-(1-benzylpiperidin-4-yl)oxy]phthalocyaninato]zinc(II) iodide were predicted as Sigmar1 and Adiponectin receptors by in silico analysis. These proteins are associated with mitochondrial structure and activity. These results are required to be detailed by more comprehensive molecular studies within the cells.

Acknowledgment

This study was supported by the 2209-A project of TUBITAK (Scientific and Technological Research Council of Turkey) (Project ID: 1919B012106704).

Funding Information:

2209-A project of TUBITAK (Scientific and Technological Research Council of Turkey) (Project ID: 1919B012106704).

Declaration of interests

The authors declare that they have no known competing financial interests or personal relationships that could have appeared to influence the work reported in this paper.

References

- [1] B. Ertem, H. Yalazan, O. Gungor, G. Sarkı, M. Durmus, E.T. Saka, H. Kantekin, Synthesis, structural characterization, and investigation on photophysical and photochemical features of new metallophthalocyanines, *J Lumin*, 204, 2018, 464–471.
- [2] E.T. Saka, K. Tekintas, Light driven photodegradation of 4-nitrophenol with novel Co and Cu phthalocyanine in aqueous media, *J Mol Struct*, 1215, 2020, 128189.
- [3] G. Onsal, Improvement of the dielectric and electro-optic properties of phthalocyanine-and quantum dot-doped nematic liquid crystals under UV illumination, *J Electron Mater*, 51, 2022, 3820–3830.
- [4] Z.J. Comeau, R.R. Cranston, H.R. Lamontagne, C.S. Harris, A.J. Shuhendler, B.H. Lessard, Surface engineering of zinc phthalocyanine organic thin-film transistors results in part-per billion sensitivity towards cannabinoid vapor, *Commun Chem*, 5, 2022, 178–184.
- [5] K. Rytel, K. Kedzierski, B. Barszcz, A. Biadasz, L. Majchrzycki, D. Wrobel, The influence of zinc phthalocyanine on the formation and properties of multiwalled carbon nanotubes thin films on the air–solid and air–water interface, *J Mol Liq*, 350, 2022, 118548.
- [6] V. Ivanova, D. Klyamer, P. Krasnov, E.N. Kaya, I. Kulu, S.T. Kostakoglu, M. Durmus, T. Basova, Hybrid materials based on pyrene-substituted metallo phthalocyanines as sensing layers for ammonia detection: Effect of the number of pyrene substituents, *Sens Actuators B Chem*, 375, 2023, 132843.
- [7] A. Sukhikh, D. Klyamer, D. Bonegardt, P. Popovetsky, P. Krasnov, T. Basova, Tetrafluorosubstituted titanil

- phthalocyanines: Structure of single crystals and phase transition in thin films, *Dyes and Pigments*, 231, 2024, 112391.
- [8] E.T. Saka, N. Kahriman, (E)-4-(4-(3-(2-fluoro-5-(trifluoromethyl)phenyl)acryloyl)phenoxy)Substituted Co(II) and Cu(II) phthalocyanines and their catalytic activities on the oxidation of phenols, *J Organomet Chem*, 895, 2019, 48-58.
- [9] E.T. Saka, Z. Biyiklioglu, H. Kantekin, Microwave-assisted synthesis and characterization of Co(II) phthalocyanine and investigation of its catalytic activity on 4-nitrophenol oxidation, *Turk J Chem*, 38, 2014, 1166.
- [10] H. Yalazan, C. Akkol, E.T. Saka, H. Kantekin, Investigation of photocatalytic properties of cobalt phthalocyanines on benzyl alcohol photooxidation, *Appl Organomet Chem*, 37, 2023, e6975.
- [11] E.T. Saka, H. Yalazan, Z. Biyiklioglu, H. Kantekin, K. Tekintas, Synthesis, aggregation, photocatalytic and electrochemical properties of axially 1-benzylpiperidin-4-oxy units substituted silicon phthalocyanine, *J Mol Struct*, 1199, 2020, 126994.
- [12] E. Ben-Hur, M. Green, A. Prager, R. Kol, I. Rosenthal, Phthalocyanine Photosensitization of Mammalian Cells: Biochemical and Ultrastructural Effects, *Photochem Photobiol*, 4, 1987, 651.
- [13] I.J. MacDonald, T.J. Dougherty, Basic principles of photodynamic therapy, *J Porphyrins Phthalocyanines*, 5, 2001, 105.
- [14] H. Ali, J.E. van Lier, Metal complexes as photo-and radiosensitizers, *Chem Rev*, 99, 1999, 2379.
- [15] R. Bonnett, Photosensitizers of the porphyrin and phthalocyanine series for photodynamic therapy, *Chem Soc Rev*, 24, 1995, 19.
- [16] A.C. Tedesco, J.C.G. Rotta, C.N. Lunardi, Synthesis, Photophysical and Photochemical Aspects of Phthalocyanines for Photodynamic Therapy, *Curr Org Chem*, 7, 2003, 187.
- [17] C. Göl, M. Durmus, Investigation of photophysical, photochemical and bovine serum albumin binding properties of novel water-soluble zwitterionic zinc phthalocyanine complexes, *Synth Met*, 162, 2012, 605.
- [18] A. Günsel, A. Yıldırım, P. Taslimi, Y. Erden, T. Taskın Tok, H. Piskin, A.T. Bilgicli, I. Gulcin, M. N. Yarasir, Cytotoxicity effects and biochemical investigation of novel tetrakis phthalocyanines bearing 2-thiocytosine moieties with molecular docking studies, *Inorg Chem Commun*, 138, 2022, 109263.
- [19] D. D. Dominguez, A.W. Snow, J.S. Shirk, R.G.S. Pong, Role of Structural Factors in the Nonlinear Optical Properties of Phthalocyanines and Related Compounds, *J Porphyrins Phthalocyanines*, 5, 2002, 581.
- [20] N. Masilela, T. Nyokong, The synthesis and photophysical properties of water soluble tetrasulfonated, octacarboxylated and quaternised 2,(3)-tetra-(2 pyridiloxo) Ga phthalocyanines, *Dyes Pigments*, 84, 2010, 242.
- [21] S. Wei, J. Zhou, D. Huang, X. Wang, B. Zhang, J. Shen, Synthesis and Type I/Type II photosensitizing properties of a novel amphiphilic zinc phthalocyanine, *Dyes Pigments*, 71, 2006, 61.
- [22] S. Aggarwal, L. Gabrovsek, L.K. Langeberg, M. Golkowski, S. Ong, F.D. Smith, J.D. Scott, Depletion of dAKAP1–protein kinase A signaling islands from the outer mitochondrial membrane alters breast cancer cell metabolism and motility, *J Biol Chem*, 294(9), 2019, 3152.
- [23] C. Sari, I. Degirmencioglu, F. Celep, Synthesis and characterization of novel Schiff base silicon (IV) phthalocyanine complex for photodynamic therapy of breast cancer cell lines, *Photodiagnosis Photodyn Ther*, 42, 2023, 103504.
- [24] E.T. Saka, Z. Biyiklioglu, Co(II) and Fe(II) phthalocyanines: synthesis, investigation of their catalytic activity towards phenolic compounds and electrochemical behaviour, *Appl Organomet Chem*, 29, 2015, 392.
- [25] G. Dilber, M. Durmus, H. Kantekin, Investigation of the photophysical and photochemical behavior of substituted zinc phthalocyanines and their water-soluble quaternized derivatives, *Turk J Chem*, 41, 2017, 917.
- [26] D.D. Perrin, W.L.F. Armarego, *Purification of Laboratory Chemicals*, 1989, Oxford, Pergamon Press.
- [27] H.İ. Kaya, C. Boguslu, E. Kabak, C. Akkol, E.T. Saka, S.C. Uzuner, The effect of silicon phthalocyanine on cell death and mitochondrial membrane potential in pancreatic cancer cells, *Turk J Anal Chem*, 4(2), 2022, 111.
- [28] J. Schmidt, W. Kuzyniak, J. Berkholtz, G. Steinemann, R. Ogbodu, B. Hoffmann, G. Nouailles, A.G. Gurek, B. Nitzsche, M. Höpfner, Novel zinc- and silicon-phthalocyanines as photosensitizers for photodynamic therapy of cholangiocarcinoma, *Int J Mol Med*, 42(1), 2018, 534.
- [29] A.R. Simioni, F.L. Primo, A.C. Tedesco, Silicon(IV) phthalocyanine-loaded-nanoparticles for application in photodynamic process, *J Laser Appl*, 24(1), 2012, 012004.
- [30] A. Nalçaoğlu, C. Sarı, I. Degirmencioglu, F. Celep Eyuboglu, Novel piperazine-substituted silicon phthalocyanines exert anti-cancer effects against breast cancer cells, *Photodiagnosis Photodyn Ther*, 37, 2022, 102734.
- [31] U. Cakmak, F. Oz-Tuncay, S. Basoglu-Ozdemir, E. Ayazoglu-Demir, I. Demir, A. Colak, S. Celik-Uzuner, S.S. Erdem, N. Yildirim, Synthesis of hydrazine containing piperazine or benzimidazole derivatives and their potential as α -amylase inhibitors by molecular docking, inhibition kinetics and in vitro cytotoxicity activity studies, *Med Chem Res*, 30(10), 2021, 1886.
- [32] S.C. Uzuner, E. Birinci, S. Tetikoğlu, C. Birinci, S. Kolaylı, Distinct Epigenetic Reprogramming, Mitochondrial Patterns, Cellular Morphology, and Cytotoxicity after Bee Venom Treatment, *Recent Pat Anticancer Drug Discov*, 16(3), 2021, 377.
- [33] M.J. Keiser, B.L. Roth, B.N. Armbruster, P. Ernsberger, J.J. Irwin, B.K. Shoichet, Relating protein pharmacology by ligand chemistry, *Nat Biotechnol*, 25(2), 2007, 197–206.
- [34] N.M. O'Boyle, M. Banck, C.A. James, C. Morley, T. Vandermeersch, G.R. Hutchison, Open Babel: An open chemical toolbox, *J Cheminform*, 3(1), 2011, 33.
- [35] J. Eberhardt, D. Santos-Martins, A.F. Tillack, S. Forli, AutoDock Vina 1.2.0: New Docking Methods, Expanded Force Field, and Python Bindings, *J Chem Inf Model*, 61(8), 2001, 3891.
- [36] D. Santos-Martins, S. Forli, M.J. Ramos, A.J. Olson, AutoDock4Zn: An Improved AutoDock Force Field for Small-Molecule Docking to Zinc Metalloproteins, *J Chem Inf Model*, 54(8), 2014, 2371.
- [37] G.M. Morris, R. Huey, W. Lindstrom, M.F. Sanner, R.K. Belew, D.S. Goodsell, A.J. Olson, AutoDock4 and AutoDockTools4: Automated docking with selective receptor flexibility, *J Comput Chem*, 30(16), 2009, 2785.
- [38] M. Durmuş, H. Yaman, C. Göl, V. Ahsen, T. Nyokong, Water-soluble quaternized mercaptopyridine-substituted zinc-phthalocyanines: Synthesis, photophysical, photochemical and bovine serum albumin binding properties, *Dyes Pigments*, 91, 2011, 153.
- [39] V. Çakir, D. Çakir, M. Pişkin, M. Durmuş, Z. Biyiklioglu, New peripherally and non-peripherally tetra-substituted water soluble zinc phthalocyanines: Synthesis, photophysics and photochemistry, *J Organomet Chem*, 783, 2015, 120-129.
- [40] C. Uslan, B.Ş. Sesalan, M. Durmuş, Synthesis of new water-soluble phthalocyanines and investigation of their photochemical, photophysical and biological properties, *J Photochem Photobiol A Chem*, 235, 2012, 56-64.
- [41] E.T. Saka, C. Göl, M. Durmus, H. Kantekin, Z. Biyiklioglu, Photophysical, photochemical and aggregation behavior of novel peripherally tetra-substituted phthalocyanine derivatives, *J Photochem Photobiol A Chem*, 241, 2012, 67-78.
- [42] L. Edwards, M. Gouterman, Porphyrins: XVI. Vapor absorption spectra and redox reactions: Octalkylporphyrins, *J Mol Spectrosc*, 35, 1970, 90-109.

- [43] N. El Khatib, B. Boudjema, M. Maitrot, H. Chermette, L. Porte, Electronic structure of zinc phthalocyanine, *Can J Chem*, 66, 1988, 1087–1095.
- [44] T. Nyokong, Z. Gasyna, M.J. Stillman, Analysis of the Absorption and Magnetic Circular Dichroism Spectra of Zinc Phthalocyanine and the 7-Cation-Radical Species [ZnPc(-1)]⁺, *Inorg Chem*, 26, 1987, 1087–1095.
- [45] K. Bernauer, S. Fallab, *Helv. Phtalocyanine in wässriger Lösung I*, *Helv Chim Acta*, 44, 1961, 1287-1292.
- [46] M.J. Stillman, T. Nyokong, Absorption and Magnetic Circular Dichroism Spectral Properties of Phthalocyanines, Editors: C.C. Leznoff, A.B.P. Lever, 1989, New York, VCH.
- [47] A.W. Snow, Phtalocyanine Aggregation, The Porphyrin Handbook, Editors: K.M. Kadish, K.M. Smith, R. Guilard, Academic Press, 2003, Amsterdam, Academic Press.
- [48] M. L'Her, O. Göktuğ, M. Durmuş, V. Ahsen, A water soluble zinc phthalocyanine: physicochemical, electrochemical studies and electropolymerization, *Electrochim Acta*, 213, 2016, 655-662.
- [49] K.A.D.F. Castro, J.A. Prandini, J.C. Biazotto, J.P.C. Tome, R.S. da Silva, L.M.O. Lourenço, The Surprisingly Positive Effect of Zinc-Phthalocyanines with High Photodynamic Therapy Efficacy of Melanoma Cancer, *Front Chem*, 10, 2022, 82716.
- [50] E.P.O. Silva, E.D. Santos, C.S. Gonçalves, M.A.G. Cardoso, C.P. Soares, M. Beltrame Jr, Zinc phthalocyanine-conjugated with bovine serum albumin mediated photodynamic therapy of human larynx carcinoma, *Laser Phys*, 26, 2016, 105601.
- [51] P. Lara, R.V. Huis in 't Veld, C. Jorquera-Cordero, A.B. Chan, F. Ossendorp, L.J. Cruz, Zinc-Phthalocyanine-Loaded Extracellular Vesicles Increase Efficacy and Selectivity of Photodynamic Therapy in Co-Culture and Preclinical Models of Colon Cancer, *Pharmaceutics*, 13, 2021, 1547.
- [52] I. Toubia, C. Nguyen, S. Diring, M. Pays, E. Mattana, P. Arnoux, C. Frochot, M.G. Bobo, M. Kobeissi, F. Odobel, Study of Cytotoxic and Photodynamic Activities of Dyads Composed of a Zinc Phthalocyanine Appended to an Organotin, *Pharmaceutics*, 14, 2021, 413.
- [53] N. Rajabi, F. Mohammadnejad, M.A. Doustvandi, M.A. Shadbad, M. Amini, H. Tajalli, A. Mokhtarzadeh, E. Baghbani, N. Silvestris, B. Baradaran, Photodynamic therapy with zinc phthalocyanine enhances the anti-cancer effect of tamoxifen in breast cancer cell line: Promising combination treatment against triple-negative breast cancer?, *Photodiagnosis Photodyn Ther*, 41, 2023, 103212.
- [54] Y. Ge, X. Weng, T. Tian, F. Ding, R. Huang, L. Yuan, J. Wu, T. Wang, P. Guo, X. Zhou, A mitochondria-targeted zinc(ii) phthalocyanine for photodynamic therapy, *RSC Adv*, 3, 2013, 12839.
- [55] J. Shao, J. Xue, Y. Dai, H. Liu, N. Chen, L. Jia, J. Huang, Inhibition of human hepatocellular carcinoma HepG2 by phthalocyanine photosensitizer PHOTOCYANINE: ROS production, apoptosis, cell cycle arrest, *Eur J Cancer*, 48, 2012, 2086.
- [56] B.F. Perrin Tamietti, A.H.A. Machado, M. Maftoum Costa, N.S. da Silva, A.C. Tedesco, C. Pacheco Soares, Analysis of Mitochondrial Activity Related to Cell Death after PDT with AIPCS4, *Photomed Laser Surg*, 25, 2007, 2040.
- [57] M. Okada-Iwabu, M. Iwabu, T. Kadowaki, Drug development research for novel adiponectin receptor-targeted antidiabetic drugs contributing to healthy longevity, *Diabetol Int*, 10, 2019, 237.
- [58] M.E. Pepin, C. Koentges, K. Pfeil, J. Gollmer, S. Kersting, S. Wiese, M.M. Hoffmann, K.E. Odening, C. Mühlen, P. von zur Diehl, P. Stachon, D. Wolf, A.R. Wende, C. Bode, A. Zirlik, H. Bugger, *Front Endocrinol*, 10, 2019, 872.
- [59] M. Iwabu, T. Yamauchi, M. Okada-Iwabu, K. Sato, T. Nakagawa, M. Funata, M. Yamaguchi, S. Namiki, R. Nakayama, M. Tabata, H. Ogata, N. Kubota, I. Takamoto, Y.K. Hayashi, N. Yamauchi, H. Waki, M. Fukayama, I. Nishino, K. Tokuyama, T. Kadowaki, Adiponectin and AdipoR1 regulate PGC-1 α and mitochondria by Ca²⁺ and AMPK/SIRT1, *Nature*, 464, 2010, 1313–1319.
- [60] H. Xu, Q. Zhao, N. Song, Z. Yan, R. Lin, S. Wu, L. Jiang, S. Hong, J. Xie, H. Zhou, R. Wang, X. Jiang, AdipoR1/AdipoR2 dual agonist recovers nonalcoholic steatohepatitis and related fibrosis via endoplasmic reticulum-mitochondria axis, *Nat Commun*, 11, 2020, 5807.
- [61] C.S. Abdullah, R. Aishwarya, S. Alam, N.S. Remex, M. Morshed, S. Nitu, S. Miriyala, M. Panchatcharam, B. Hartman, J. King, M. Alfrad Nobel Bhuiyan, J. Traylor, C.G. Kevil, A.W. Orr, S. Md. Bhuiyan, The molecular role of Sigmar1 in regulating mitochondrial function through mitochondrial localization in cardiomyocytes, *Mitochondrion*, 62, 2022, 159-175.
- [62] R. Aishwarya, C.S. Abdullah, M. Morshed, N.S. Remex, Md. S. Bhuiyan, Sigmar1's Molecular, Cellular, and Biological Functions in Regulating Cellular Pathophysiology, *Front Physiol*, 12, 2021, 705575.
- [63] T. Hayashi, T.P. Su, Sigma-1 Receptor Chaperones at the ER-Mitochondrion Interface Regulate Ca²⁺ Signaling and Cell Survival, *Cell*, 131, 2007, 596-610.
- [64] J. Simony-Lafontaine, M. Esslimani, E. Bribes, S. Gourgou, N. Lequeux, R. Lavail, J. Grenier, A. Kramar, P. Casellas, Immunocytochemical assessment of sigma-1 receptor and human sterol isomerase in breast cancer and their relationship with a series of prognostic factors, *Br J Cancer*, 82, 2000, 1958–1966.
- [65] D. Magouliotis, V. Tasiopoulou, K. Dimas, N. Sakellaridis, D. Zacharoulis, Gene expression profile of sigma-1 (s1R) and sigma-2 (s2R) receptors in pancreatic cancer, *HPB*, 20, 2018, S564.
- [66] S.M. Mahalingam, J.D. Ordaz, P.S. Low, Targeting of a Photosensitizer to the Mitochondrion Enhances the Potency of Photodynamic Therapy, *ACS Omega*, 3, 2018, 6066–6074.
- [67] A.P. Thomas, L. Palanikumar, M.T. Jeena, K. Kim, J.H. Ryu, Cancer-mitochondria-targeted photodynamic therapy with supramolecular assembly of HA and a water soluble NIR cyanine dye, *Chem Sci*, 12, 2017, 8351-8356.
- [68] E. Gottlieb, S.M. Armour, M.H. Harris, C.B. Thompson, Mitochondrial membrane potential regulates matrix configuration and cytochrome c release during apoptosis, *Cell Death Differ*, 10, 2003, 709–717.
- [69] J.D. Ly, D.R. Grubb, A. Lawen, The mitochondrial membrane potential ($\Delta\psi_m$) in apoptosis; an update, *Apoptosis*, 8, 2003, 115–128.
- [70] Y. Rai, R. Pathak, N. Kumari, D.K. Sah, S. Pandey, N. Kalra, R. Soni, B.S. Dwarakanath, A.N. Bhatt, Mitochondrial biogenesis and metabolic hyperactivation limits the application of MTT assay in the estimation of radiation induced growth inhibition, *Sci Rep*, 8, 2018, 1531.

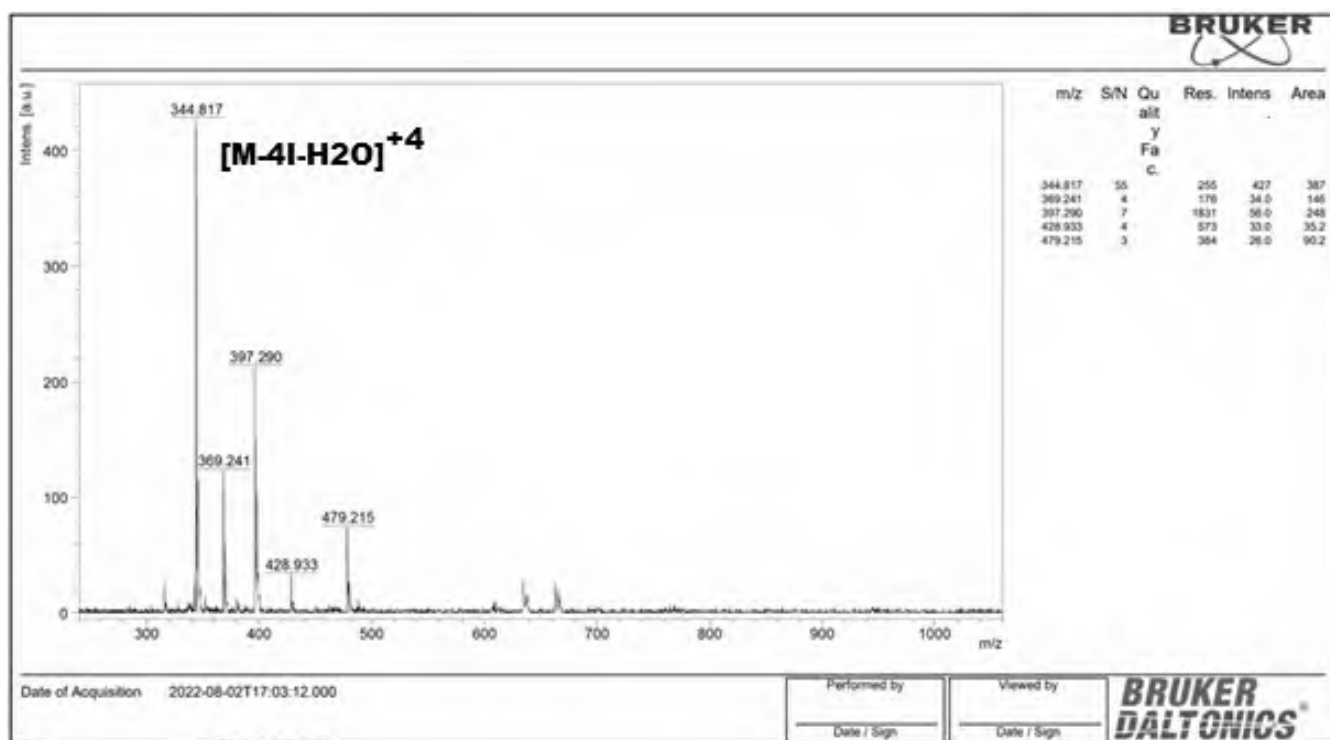
SUPPLEMENTARY INFORMATION

1. Materials

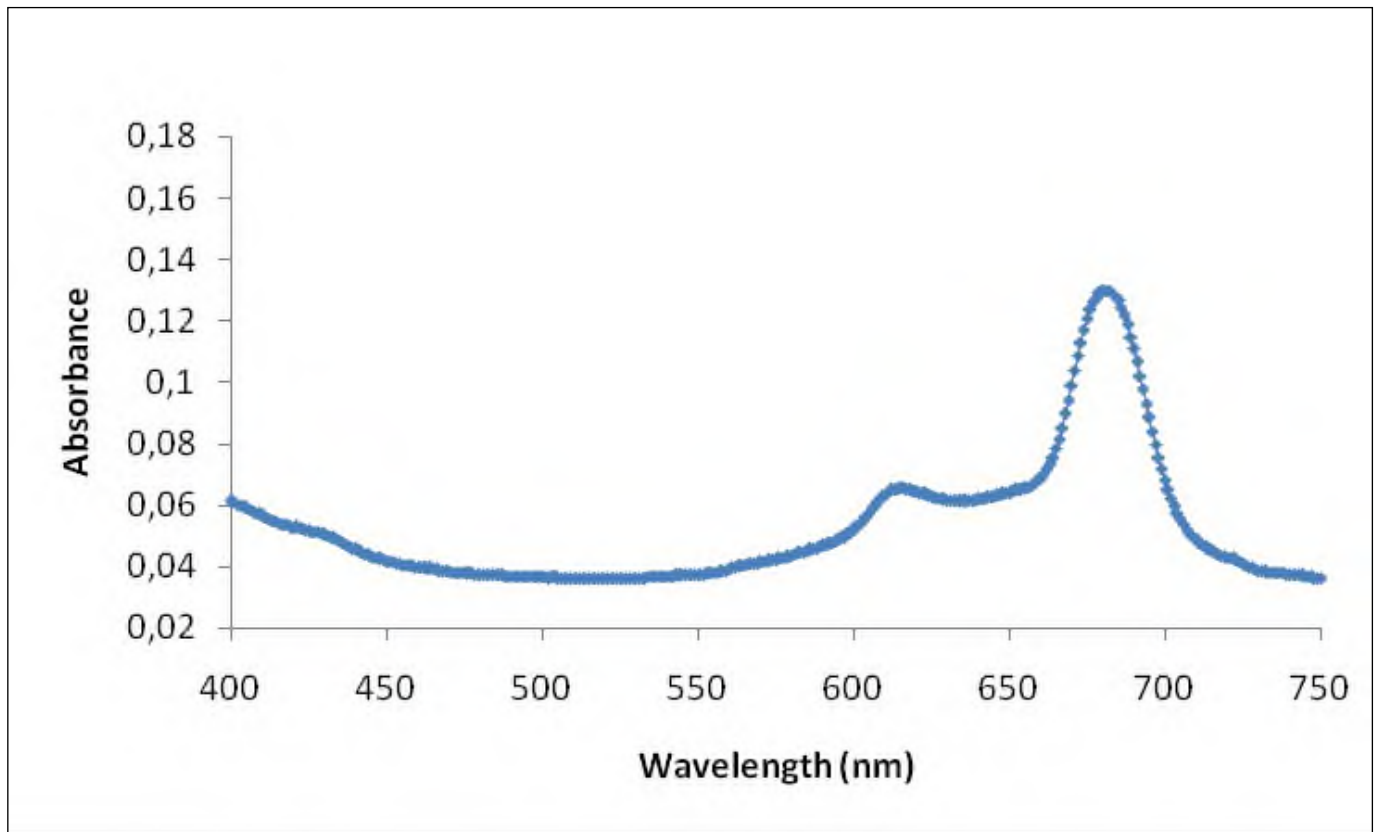
All reactions were carried under a dry nitrogen atmosphere using Standard Schlenk techniques. All chemicals, solvents, and reagents were of reagent grade quality and were used as purchased from commercial sources. All solvents were dried and purified as described by reported procedure [1]. 4-Nitrophthalonitrile [2] were prepared according to the literature procedure. 4-nitrophenol, were purchased from Sigma-Aldrich and used without further purification and chemical treatment.

2. 1.2. Equipment

The IR spectra were recorded on a Perkin Elmer 1600 FT-IR spectrophotometer using KBr pellets. $^1\text{H-NMR}$ and $^{13}\text{C-NMR}$ spectra were recorded on a Varian Mercury 400 MHz spectrometer in CDCl_3 . Chemical shifts were reported (δ) relative to Me_4Si as internal standard. MALDI-MS of complexes were obtained in dihydroxybenzoic acid as MALDI matrix using nitrogen laser accumulating 50 laser shots using Bruker Microflex LT MALDI-TOF mass spectrometer and Micromass Quatro LC/ULTIMA LC-MS/MS spectrometer. Elemental analysis equipment is EUROVECTOR EURO EA3000. Optical spectra in the UV-vis region were recorded with a Perkin Elmer Lambda 25 spectrophotometer.



S. Figure 1. MALDI-TOF spectra of 2(3), 9(10), 16(17), 23(24)-tetrakis-[N-methyl-(1-benzylpiperidin-4-yl)oxy]phthalocyaninato]zinc(II) iodide.



S. Figure 2. UV-Vis spectrum of 2(3), 9(10), 16(17), 23(24)-tetrakis-[N-methyl-(1-benzylpiperidin-4-yl)oxy]phthalocyaninato]zinc(II) iodide in water.

AR42J (Figure 7A statistics)

**24 h incubation
Dose comparisons**

**48 h incubation
Dose comparisons**

Post Hoc Tests

dose

Multiple Comparisons

Dependent Variable: perc
LSD

(I) dose	(J) dose	Mean Difference (I-J)	Sig.	95% Confidence Interval	
				Lower Bound	Upper Bound
,00	1,50	14,1738	,585	-45,9040	74,2516
	3,00	34,6694	,208	-25,4084	94,7472
	6,00	13,5145	,602	-46,5633	73,5923
	12,00	29,3381	,277	-30,7397	89,4158
1,50	,00	-14,1738	,585	-74,2516	45,9040
	3,00	20,4956	,475	-45,3163	86,3075
	6,00	-,6593	,981	-66,4712	65,1526
	12,00	15,1643	,593	-50,6476	80,9762
3,00	,00	-34,6694	,208	-94,7472	25,4084
	1,50	-20,4956	,475	-86,3075	45,3163
	6,00	-21,1549	,461	-86,9668	44,6570
	12,00	-5,3313	,849	-71,1432	60,4806
6,00	,00	-13,5145	,602	-73,5923	46,5633
	1,50	,6593	,981	-65,1526	66,4712
	3,00	21,1549	,461	-44,6570	86,9668
	12,00	15,8236	,578	-49,9883	81,6355
12,00	,00	-29,3381	,277	-89,4158	30,7397
	1,50	-15,1643	,593	-80,9762	50,6476
	3,00	5,3313	,849	-60,4806	71,1432
	6,00	-15,8236	,578	-81,6355	49,9883

Based on observed means.
The error term is Mean Square(Error) = 723,390.

Post Hoc Tests

dose

Multiple Comparisons

Dependent Variable: perc
LSD

(I) dose	(J) dose	Mean Difference (I-J)	Sig.	95% Confidence Interval	
				Lower Bound	Upper Bound
,00	1,50	-7,4313	,151	-19,4332	3,5706
	3,00	1,4629	,770	-9,5390	12,4648
	6,00	14,1327 [*]	,017	3,1308	25,1345
	12,00	32,6810 [*]	,000	21,6791	43,6829
1,50	,00	7,4313	,151	-3,5706	18,4332
	3,00	8,8942	,071	-,9462	18,7346
	6,00	21,5639 [*]	,001	11,7236	31,4043
	12,00	40,1123 [*]	,000	30,2719	49,9527
3,00	,00	-1,4629	,770	-12,4648	9,5390
	1,50	-8,8942	,071	-18,7346	,9462
	6,00	12,6698 [*]	,017	2,8294	22,5101
	12,00	31,2181 [*]	,000	21,3777	41,0585
6,00	,00	-14,1327 [*]	,017	-25,1345	-3,1308
	1,50	-21,5639 [*]	,001	-31,4043	-11,7236
	3,00	-12,6698 [*]	,017	-22,5101	-2,8294
	12,00	16,5483 [*]	,002	8,7080	28,3887
12,00	,00	-32,6810 [*]	,000	-43,6829	-21,6791
	1,50	-40,1123 [*]	,000	-49,9527	-30,2719
	3,00	-31,2181 [*]	,000	-41,0585	-21,3777
	6,00	-16,5483 [*]	,002	-28,3887	-8,7080

Based on observed means.
The error term is Mean Square(Error) = 29,384.

S. Figure 3. Detailed statistical analyses for cytotoxicity

AR42J (Figure 8A statistics)

**24 h incubation
Dose comparisons**

**48 h incubation
Dose comparisons**

Post Hoc Tests

Dose

Multiple Comparisons

Dependent Variable: MMP

LSD

(I) Dose	(J) Dose	Mean Difference (I-J)	Sig.	95% Confidence Interval	
				Lower Bound	Upper Bound
.00	1,50	73,0364	,792	-487,9434	634,0163
	3,00	165,3276	,552	-395,6523	726,3074
	6,00	63,5499	,819	-497,4300	624,5297
	12,00	66,9000	,609	-494,0799	627,8799
1,50	.00	-73,0364	,792	-634,0163	487,9434
	3,00	92,2911	,739	-468,6887	653,2710
	6,00	-9,4866	,973	-570,4664	551,4933
	12,00	-6,1364	,982	-567,1183	554,8434
3,00	.00	-165,3276	,552	-726,3074	395,6523
	1,50	-92,2911	,739	-653,2710	469,6887
	6,00	-101,7777	,714	-662,7576	459,2022
	12,00	-99,4276	,723	-659,4074	462,5523
6,00	.00	-63,5499	,819	-624,5297	497,4300
	1,50	9,4866	,973	-551,4933	570,4664
	3,00	101,7777	,714	-459,2022	662,7576
	12,00	3,3501	,990	-557,6297	564,3300
12,00	.00	-66,9000	,609	-627,8799	494,0799
	1,50	6,1364	,982	-554,8434	567,1163
	3,00	98,4276	,723	-462,5523	659,4074
	6,00	-3,3501	,990	-564,3300	557,6297

Based on observed means.
The error term is Mean Square(Error) = 264079,832.

Post Hoc Tests

Dose

Multiple Comparisons

Dependent Variable: MMP

LSD

(I) Dose	(J) Dose	Mean Difference (I-J)	Sig.	95% Confidence Interval	
				Lower Bound	Upper Bound
.00	1,50	-15,5889	,967	-776,7808	745,6031
	3,00	10,3054	,978	-750,8865	771,4973
	6,00	-75,4469	,841	-836,6388	665,7451
	12,00	-120,3156	,749	-881,5075	640,8763
1,50	.00	15,5889	,967	-745,6031	776,7808
	3,00	25,8943	,945	-735,2976	787,0862
	6,00	-59,8580	,873	-821,0499	701,3339
	12,00	-104,7267	,781	-865,9186	656,4652
3,00	.00	-10,3054	,978	-771,4973	750,8865
	1,50	-25,8943	,945	-787,0862	735,2976
	6,00	-85,7523	,820	-846,9442	675,4396
	12,00	-130,6210	,728	-891,8129	630,5709
6,00	.00	75,4469	,841	-685,7451	836,6388
	1,50	59,8580	,873	-701,3339	821,0499
	3,00	85,7523	,820	-675,4396	846,9442
	12,00	-44,8687	,905	-806,0606	716,3232
12,00	.00	120,3156	,749	-640,8763	881,5075
	1,50	104,7267	,781	-656,4652	865,9186
	3,00	130,6210	,728	-630,5709	891,8129
	6,00	44,8687	,905	-716,3232	806,0606

Based on observed means.
The error term is Mean Square(Error) = 486215,751.


S. Figure 4. Detailed statistical analyses for mitochondrial membrane potential

References

- [1] D.D. Perrin, W.L.F. Armarego, Purification of Laboratory Chemicals (2nd edn), Pergamon Press: Oxford, (1989).
- [2] Y.G. Young, W. Onyebuagu, J Organomet Chem 55 (1990) 2155-2159.



Schiff Base Catalysts for the Oxidation of Benzyl Alcohol to Benzaldehyde

Çağla Akkol^{1*} , Serdar Karaböcek² , Ece Tuğba Saka¹ , Bekir Sıtkı Çevrimli³ 

¹ Karadeniz Technical University, Department of Chemistry, Trabzon, 61080, Türkiye

² Amasya University, Technical Sciences Vocational School, 05100, Amasya, Türkiye

³ Gazi University, Technical Sciences Vocational School, Chemistry and Chemical Technologies Department, 06374, Ankara, Türkiye

Abstract

Catalysts are crucial in promoting sustainability by facilitating chemical transformations under milder conditions, saving energy, and reducing pollution and by-product formation. In this work, we aimed to synthesize and characterize Schiff base complexes of copper, nickel, cobalt in benzyl alcohol oxidation, three asymmetric Schiff bases derived from 2,2'-(propenylenedioxy) di benzaldehyde bis(thiosemicarbazone) After that, catalytic activity of Schiff base complexes (Cu(II), Ni(II) and Co(II)) was investigated on the benzyl alcohol oxidation. Ni(II) complex served as an effective catalyst in converting benzyl alcohol to benzaldehyde with 89% conversion in the presence of *tert*-butyl hydroperoxide (TBHP) oxidant. Moreover, in the catalytic tests performed using *tert*-butyl hydroperoxide (TBHP), hydrogen peroxide (H₂O₂) and *m*-chloroperbenzoic acid (*m*-CPBA) oxidants, the highest product conversion (95% benzaldehyde conversion) was achieved in the presence of *tert*-butyl hydroperoxide (TBHP). In this study, in which the effect of the substrate-catalyst ratio on catalytic activity was investigated, the reaction was completed at the end of 1 hour at 90 °C in DMF solvent using 2.05×10⁻⁶ mol catalyst, 1.02×10⁻³ mol oxidant, and homogeneous catalysis system.

Keywords: Catalysts, Schiff bases, ligands, metal complexes, alcohol oxidation

1. Introduction

Schiff bases are extensively utilized organic materials with a broad range of applications, including catalysis [1], polymer stabilization [2], intermediates in organic synthesis [3], the food industry [4], pigments [5], dyes [6], chemo sensors [7], and more [8]. Moreover, Schiff bases demonstrate useful catalytic biological performance [9]. Metal Schiff base complexes have been thoroughly examined as homogeneous catalysts in diverse oxidation reactions [10].

Today, using economical and environmentally friendly solvents, especially water, is of great importance in terms of green chemistry [11,12]. Improving processes and protocols results in increased sustainability and efficiency [6]. Scientists prioritize green chemistry approaches that employ innovative recyclable, heterogeneous, or phosphine-free catalysts [13,14]. Catalysts are important in promoting sustainability by facilitating chemical transformations under milder conditions, saving energy, and reducing pollution, and by-product formation [15].

The catalytic oxidation of alcohols to aldehydes and ketones is crucial in various industries, including

agrochemicals, fragrances, dyes, pesticides, cosmetics, flame retardants, food flavorings, vitamins, and pharmaceuticals [16–22]. Benzyl alcohol (BA) is a crucial intermediate in the synthesis of various organic compounds, including benzylic alcohols, which are important in medicinal chemistry and as synthetic intermediates [23–25]. It can be converted through oxidation processes into benzaldehyde, which is widely used in medicine, dyes, perfumes, and various other fields [26,27].

Transition metal complexes are widely used as catalysts to promote the oxidation of alcohols [28]. Due to the high abundance, low cost, and low toxicity of the first-row transition metals, we aimed to synthesize and characterize Schiff base complexes of copper, nickel, cobalt in benzyl alcohol oxidation, three asymmetric Schiff bases derived from 2,2'-(propenylenedioxy) di benzaldehyde bis(thiosemicarbazone) After that, catalytic activity of Schiff base complexes (Cu(II), Ni(II) and Co(II)) was investigated on the benzyl alcohol oxidation. Ni(II) complex served as an effective catalyst in converting benzyl alcohol to benzaldehyde with 89% conversion in the presence of TBHP oxidant.

Citation: Ç. Akkol, S. Karaböcek, E.T. Saka, B.S. Çevrimli, Schiff Base Catalysts for the Oxidation of Benzyl Alcohol to Benzaldehyde, Turk J Anal Chem, 6(2), 2024, 129–137.

Author of correspondence: akkolcagla@gmail.com

Received: November 14, 2024 **Tel:** +90 (462) 377 2525

Accepted: December 16, 2024 **Fax:** +90 (462) 325 3196

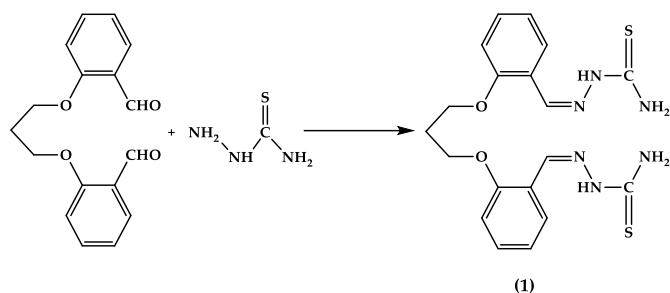


Figure 1. Synthetic reaction of 2,2'-(propenylenedioxy)di benzaldehyde bis(thiosemicarbazone)

In photocatalytic studies where all three complexes were used as catalysts, benzaldehyde was determined as the main product and benzoic acid as the by-product in the light of the data obtained.

2. Experimental

2.1. Materials

The details of the materials, equipment, and photocatalytic procedure used are given in Supplementary Information. 2,2'-[propane-1,3-diylbis(oxy)] di benzaldehyde was prepared according to the literature [29].

2.2. Methods

2.2.1. General Procedure for Synthesis of 2,2'-(propenylenedioxy)di Benzaldehyde Bis(thiosemicarbazone) (1)

2.84 g (10 mmol) dialdehyde and 1.82 g (20 mmol) thiosemicarbazide were dissolved in 25 mL ethanol (EtOH) and boiled under reflux for 10 hours. The mixture was then added to 50 mL of cold water and the precipitated solid was filtered through the glass crucible. The raw solid material obtained was dissolved in ethyl alcohol in hot water, 1 g of activated charcoal was added, boiled for 30 minutes, and filtered, then left to crystallize at room temperature. After this, the white solid precipitated in amorphous form was filtered and dried over P₂O₅ in a vacuum desiccator. Mp: 223 °C. Yield: 75%. IR (KBr disc, cm⁻¹): 3419 (=N-H), 3275-3158 (NH₂), 1597 (C=N), 1245(C-O). ¹H-NMR(DMSO-d₆)/ppm δ: 11.37 (s, 2H, =N-H), 8.47 (s, 2H, N=CH), 7.88-8.07 (d, 4H, NH₂), 6.91-8.1 (m, 8H, Ar-H), 4.24 (t, 4H, -OCH₂), and 2.48 (p, 2H, -CH₂-). Mass (ESI) Calculated: 430.55, Found: 431.44 [M+H]⁺. Elemental analysis (C₁₉H₂₂N₆O₂S₂) (%): Calculated: C, 53.0; H, 5.2; N, 19.5. Found: C, 52.9; H, 5.3; N, 19.6.

2.2.2. General Procedure for Synthesis of Schiff Base Metal Complexes (2-4)

2,2'-(propenylenedioxy) dibenzaldehyde bis(thiosemicarbazone) (1) (2.15 g, 5 mmol) was dissolved in 10 mL dimethyl formamide (DMF) and metal salts (0.85 g, 5mmol) solution dissolved in 20 mL

EtOH was added dropwise. The mixture was boiled under reflux for 5 hours. The reaction was monitored by thin-layer chromatography while the solution was being mixed. It was determined that the reaction ended after 5 hours. At the end of this period, 1 mL of hot water was added dropwise to the hot mixture, and the mixture was allowed to crystallize. Then, the precipitated greenish-brown solid was filtered through the glass crucible, washed with H₂O, EtOH, and Et₂O, respectively, and dried over P₂O₅ in a vacuum desiccator.

2.2.2.1. Cu(II) complex 2

300 °C < Mp Cu(II) complex was obtained in 65% yield. FT-IR (ATR), ν_{\max} (cm⁻¹): 3441, 3337 (-NH), 2937, 2920, 2849 (AlipH), 1660, 1600 (C=N). Elemental analysis (C₁₉H₂₂CuN₆O₂S₂C₁₂) Calculated (%): C, 40.38; H, 3.90; N, 14.90; Cu, 11.25. Found: C, 40.32; H, 3.70; N, 15.15; Cu, 11.0. Mass (ESI Calculated: 492.08, Found: 491.53 [M-H]⁺).

2.2.2.2. Ni(II) complex 3

300 °C < Mp Ni(II) complex was obtained in 60% yield. FT-IR (ATR), ν_{\max} (cm⁻¹): 3160 (=N-H), 3437, 3384, 3312, 3260 (-NH), 3080 (ArH), 2951 (Alip H), 1667, 1588 (C=N), 1046 (C=S). ¹H-NMR (400 MHz, δ , ppm, DMSO): 9.74 (s, CH=N, 2H), 8.09 (s, N-NH, 2H), 8.04 (s, NH=C, 2H), 7.27-7.16 (m, Ar-H, 8H), 4.29 (t, J: 8.02, CH₂-O, 4H), 1.10-1.06 (m, Alip.CH₂, 2H). ¹³C-NMR (400 MHz, δ , ppm, DMSO): 161.11, 158.77, 157.38, 157.01, 149.88, 135.28, 134.28, 126.09, 125.55, 117.50, 116.18, 69.03, 49.11, 35.27, 20.30. Elemental analysis (C₁₉H₂₂Ni-N₆O₂S₂C₁₂). Calculated (%): C, 40.75; H, 3.95; N, 15.0; Ni, 10.50. Found: C, 40.90; H, 4.15; N, 14.65; Ni, 10.75. Mass (ESI): m/z = Calculated: 487.23, Found: 487.15 [M]⁺.

2.2.2.3. Co(II) complex 4

300 °C < Mp The Co(II) complex obtained an 80% yield. FT-IR (ATR), ν_{\max} (cm⁻¹): 3161 (=N-H), 3438, 3385, 3314, 3262 (-NH), 3030 (ArH), 2986, 2952, 2882 (Alip.H), 1666 (C=N), 1043 (C=S). Elemental analysis (C₁₉H₂₂CoN₆O₂S₂C₁₂). Calculated (%): C, 40.72; H, 3.96; N, 15.0; Co, 10.52. Found: C, 40.56; H, 4.0; N, 15.30; Co, 10.8. Mass (ESI): Calculated: 487.46, Found: 487.31 [M]⁺.

3. Results and Discussion

3.1. Synthesis and Characterization

2,2'-(propenylenedioxy) dibenzaldehyde bis(thiosemicarbazone), was synthesized by the reaction of 2,2'-[propane-1,3-diylbis(oxy)] dibenzaldehyde and thiosemicarbazide in ethanol (Fig. 1). Spectroscopic and physical results support the proposed structure. Copper(II), nickel(II), and cobalt(II) complexes (2-4) of 2,2'-(propenylenedioxy)dibenzaldehyde bis(thiosemicarbazone) ligand were prepared (Fig. 2).

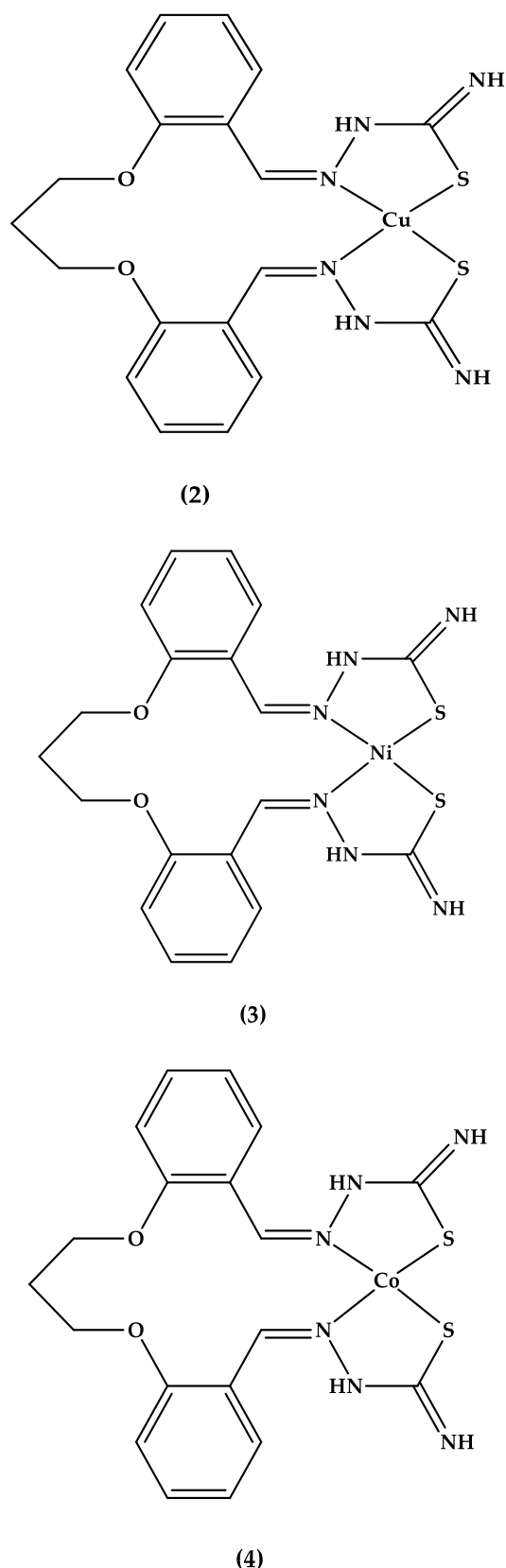


Figure 2. The structure of Cu(II), Ni(II) and Co(II) complexes (2-4)

The N₆S₂ donor set in the proposed structure of the ligand is available. This donor atom group is suitable for forming complexes with metal ions in a one-to-one ratio. Mononuclear Cu(II), Ni(II), and Co(II) complexes of the present ligand were prepared, and the structures were elucidated by spectroscopic methods.

In the IR spectrum of (1), the doublet $\nu(-\text{NH}_2)$ at 3419-3274 cm^{-1} , the $\nu(-\text{NH})$ group at 3157 cm^{-1} , the $\nu(\text{C}=\text{N})$ group observed at 1597 cm^{-1} and the vibration band observed at 1043 cm^{-1} confirms the existence of the $\nu(\text{C}=\text{S})$ group (S. Fig. 1). The shift in the frequencies of the characteristic vibration bands of $\nu(\text{N}-\text{H})$, $\nu(-\text{NH}_2)$, $\nu(\text{C}=\text{N})$, $\nu(\text{C}=\text{S})$ in the IR spectra to lower or higher frequencies of 5-60 cm^{-1} indicates the formation of complexes [30]

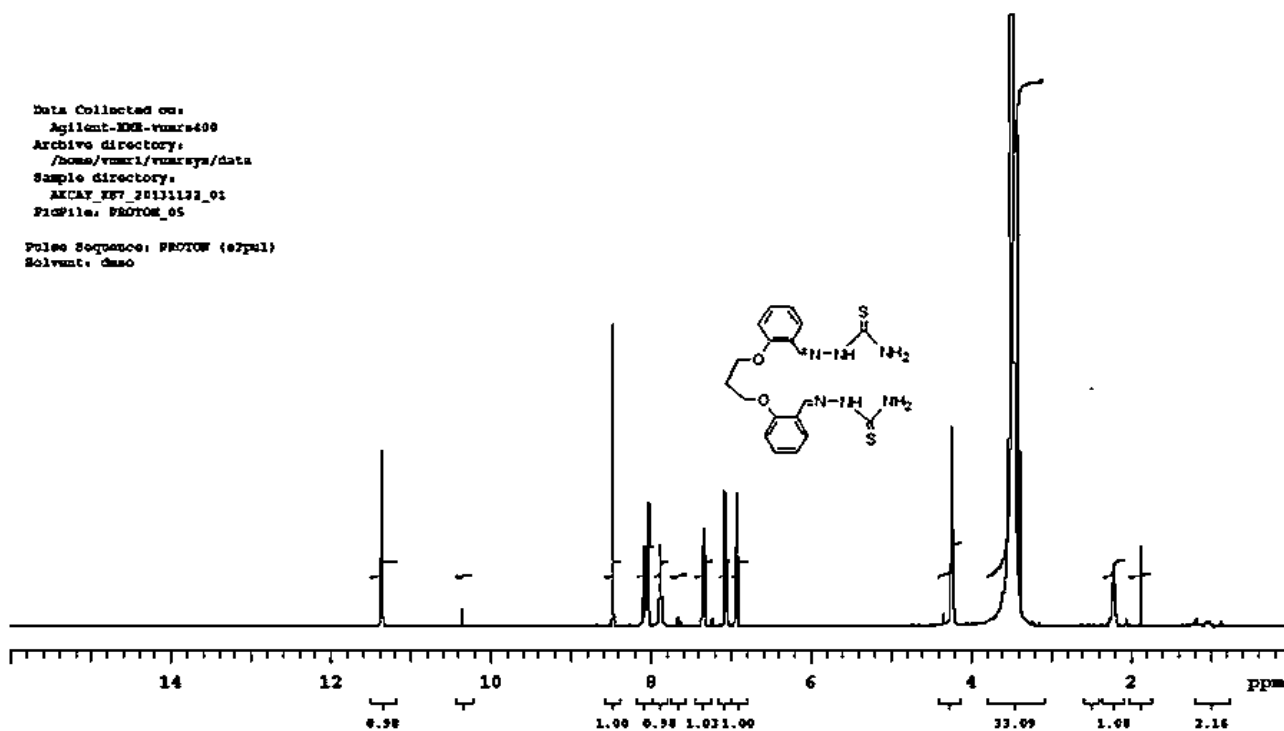
In the $^1\text{H-NMR}$ spectrum of (1), there are multiple CH₂-1 protons observed at 2.48 (2H) ppm, triplet OCH₂-2 protons observed at 4.24 (4H) ppm, multiplet aromatic ring protons observed at 6.91-8.1(8H) ppm and 7.88-8.07 (4H) ppm. It was interpreted that the doublet broad singlets observed belonged to $-\text{NH}_2$ the singlet observed at 8.5 (2H) ppm belonged to $-\text{NH}$ protons, and the singlet observed at 11.37 ppm belonged to HC=N protons (Fig. 3). Additionally, the signals at 7.88 and 11.37 ppm could not be observed because it was replaced by deuterium after the addition of D₂O. This confirms the existence of $-\text{NH}$ protons that can replace deuterium. When the integral values of the signals in the $^1\text{H-NMR}$ spectra are examined, the expected proton distributions are observed. The signal at 2.48 ppm corresponds to 2H, the signal at 4.24 ppm corresponds to 4H, the signal at 6.91-8.1 ppm corresponds to 8H, the signal at 7.88-8.07 ppm corresponds to 4H, and the signal at 11.37 ppm corresponds to 2H.

10 signals from 10 carbon atoms with different chemical environments were observed in the $^{13}\text{C-NMR}$ spectrum, which is an expected situation for the structure. These results confirm the structure and the $^{13}\text{C-NMR}$ resonance values are 27.1 C-1, 39.2 C-2, 138.8 C-3, 126.4 C-4, 122.7 C-5, 121.1 C-6, 112.9 C-7, 131.8 C-8, It shows the presence of C-9, C-9, and 178.1 C-10 carbons (Fig. 4) In the mass spectra of (1) 431.44 [M+H]⁺ was seen and elemental analysis results confirm the structure (S. Fig. 2).

Metal complexes (2-4) were characterized by IR, UV-Vis, mass, and elemental analysis. The IR spectrum of metal complexes (2-4) were not different from each other and aromatic vibration bands at 3000-3100 cm^{-1} , aliphatic vibration bands at 2950-2850 cm^{-1} , $=\text{N}-\text{H}$ around at 3160 $-\text{NH}_2$ at 3400-3200 cm^{-1} , C=N at 1580-1600 cm^{-1} , C=S around at 1100-1050 cm^{-1} (S. Fig. 3–S. Fig. 5).

Table 1. Physical data of ligand and metal complexes

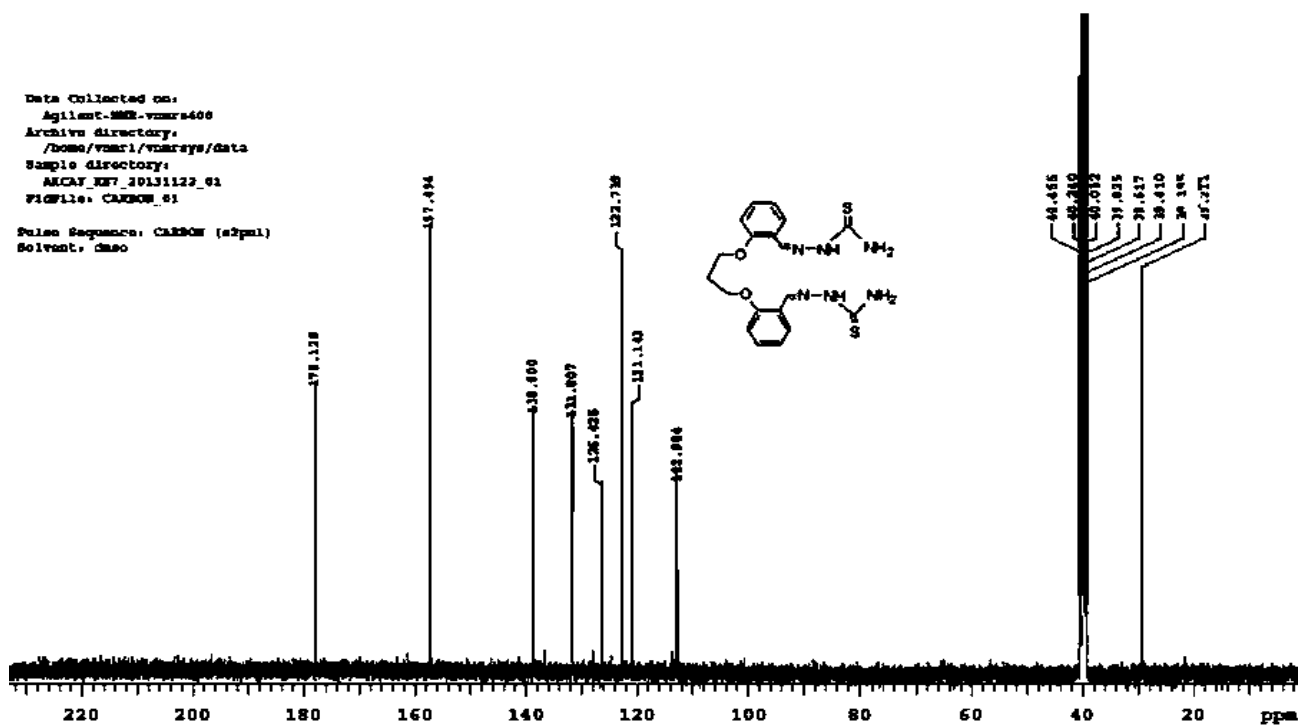
Compound	Empirical formula	Color	Yield	MS(m/z)	μ^{eff}
(1)	C ₁₉ H ₂₂ N ₆ O ₂ S ₂	white	75	430	-
(2)	C ₁₉ H ₂₂ CuN ₆ O ₂ S ₂ Cl ₂	green-brown	70	492	1.76
(3)	C ₁₉ H ₂₂ NiN ₆ O ₂ S ₂ Cl ₂	matt red	61	488	2.80
(4)	C ₁₉ H ₂₂ CoN ₆ O ₂ S ₂ Cl ₂	brown	80	487	4.34



It is widely known that $^1\text{H-NMR}$ and $^{13}\text{C-NMR}$ spectra of paramagnetic metal-centered complexes could not be taken, $^1\text{H-NMR}$ and $^{13}\text{C-NMR}$ of Cu(II) and Co(II) metal complexes (2 and 4) were not taken [31–33]. Mass spectra of metal complexes signals were m/z : 491.53 $[\text{M-H}]^+$ for Cu(II) complex (2), m/z : 487.15 $[\text{M}]^+$ for Ni(II) complex (3), and m/z : 487.31 $[\text{M}]^+$ for Co(II) complex (4) (S. Fig. 6–S. Fig. 8).

Magnetic moment measurements were made for all complexes at room temperature. The obtained values are given in Table 1. While the magnetic moment for the

mononuclear Cu(II) complex (2) was theoretically 1.73 BM, the finding of 1.76 BM as a result of the measurements showed that this complex created a normal magnetic moment. This value belonged to the Cu(II) ion belonging to the unpaired single-spin d^9 system and the structure was interpreted as a square plane. The value of 2.80 B.M. found for the Ni(II) complex (3) confirms the existence of the d^8 system and the presence of two unpaired spins. This result was interpreted as the formation of Ni(II) complex. The solid-state magnetic moment value of 4.34 B.M. found for the



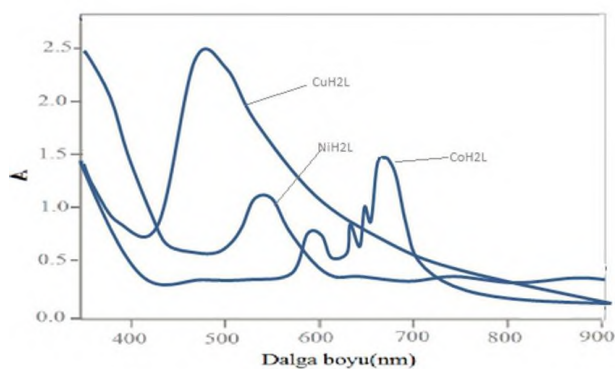


Figure 5. UV-Vis spectrum of Cu(II), Ni(II), and Co(II) complexes (2-4)

Co(II) complex (4) corresponds to three unpaired electrons, in which case it was interpreted that the Co(II) complex (4) has a tetrahedral structure [34–36]

UV-Vis spectra of ligands and complexes were taken in DMF (Fig. 5). Absorption bands are given in Table 4. The absorbances observed at 280–300 nm of the UV-Vis spectra of the ligand (1) and its Cu(II), Ni(II), and Co(II) complexes (2-4) were interpreted as $\pi-\pi^*$ transitions, and the absorbances observed at 320–360 nm were interpreted as $n-\pi^*$ transitions. The 480 nm d-d transition observed in the UV-Vis spectrum of Cu(II) complex was interpreted as the environment of the Cu(II) ion having a square plane geometry [37]. Only a single broad peak was observed in the electronic transition spectrum of Ni(II) complex, which was interpreted as a geometry between a distorted square plane and tetrahedral around the metal atom [38]. Transitions at 675, 660, 645, and 600 nm were observed in the UV-Vis spectrum of Co(II) complex, and among these bands, the transition at 675 nm is allowed and corresponds to the $^4A_2(F) \rightarrow ^4T_1(P)$ transition. The other bands at 660, 645, and 600 nm correspond to the prohibited transitions $^4A_2(F) \rightarrow ^2E(G)$, $^4A_2(F) \rightarrow ^2T_1(G)$, and $^4A_2(F) \rightarrow ^2T_2(G)$, respectively. These values observed for the Co(II) complex were interpreted as tetrahedral geometry [39]. The proposed structures of Cu(II) and Ni(II) Co(II) Schiff base complexes appear to be consistent with spectroscopic studies.

3.2. Catalytic Studies

In catalytic studies, a stock solution of 25 mg of catalyst in 100 ml of DMF was prepared and stored in the refrigerator. The purpose of choosing a homogeneous catalytic reaction system in this study is that the catalyst can provide higher selectivity and higher product conversion since all reactants are in the same phase. For the catalysis system that took place under homogeneous conditions, oxidants (H_2O_2 , TBHP, and *m*-CPBA), substrate (benzyl alcohol), and solvent (DMF) were used at 90 °C. As a result of the tests carried out without a catalyst or oxidant, no more than 2% product conversion was detected. The results obtained from all catalytic tests can be seen in Table 2.

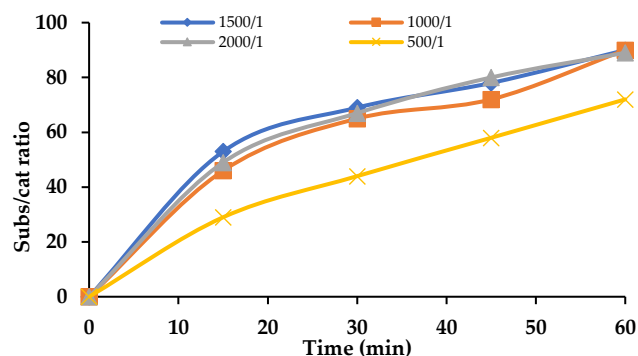


Figure 6. Substrate catalyst ratio in the oxidation of benzyl alcohol with (3)

To investigate the effect of the substrate catalyst ratio on the catalytic activity, the relationship between 1.05×10^{-3} mol, 2.05×10^{-3} mol, 3.08×10^{-3} mol, 4.10×10^{-3} mol benzyl alcohol amounts and 2.05×10^{-6} mol Ni(II) complex was investigated (Fig. 6). As the amount of benzyl alcohol increases from 1.05×10^{-3} moles to 2.05×10^{-3} moles, the activity of the nickel catalyst increases, meaning the total product conversion increases from 72% to 89%. When 3.08×10^{-3} mol and 4.10×10^{-3} mol benzyl alcohol were used with nickel Schiff base complexes as catalysts, the total product conversion was determined as 90%. Unfortunately, no significant increase in product selectivity was determined despite the high product conversion (Fig. 7).

After the substrate/catalyst ratio was determined as 1000/1, catalytic studies using this ratio were also repeated using cobalt(II) and copper(II) Schiff base complexes. In the catalytic study where Cu(II) Schiff base complex was used as a catalyst, 60% product conversion was determined with 600 as the turnover number, and Co(II) Schiff base complex was used as a catalyst, 65% product conversion was determined with 650 as turnover number (Fig. 8a and Fig. 8b).

Table 2. All catalytic results with (2, 3, and 4) in the oxidation of benzyl alcohol to aldehyde

Subs./cat. R.	Oxidant	Catalyst	Sol.	Conv. (%)	Benz. Sel. (%)	TON
500/1	TBHP	3	DMF	72	65	360
1000/1	TBHP	3	DMF	89	95	890
1500/1	TBHP	3	DMF	90	78	1350
2000/1	TBHP	3	DMF	90	70	1820
1000/1	H_2O_2	3	DMF	66	57	660
1000/1	<i>m</i> -CPBA	3	DMF	45	35	450
1000/1	TBHP	2	DMF	60	60	600
1000/1	TBHP	4	DMF	65	59	650
Without cat.	TBHP	3	DMF	< 2	—	—
1000/1	without ox.	3	DMF	< 2	—	—

Subs./cat. R.: Substrate/Catalyzer Ratio, Sol.: Solvent, Conv.: Conversion, Benz. Sel.: Benzaldehyde Selectivity,

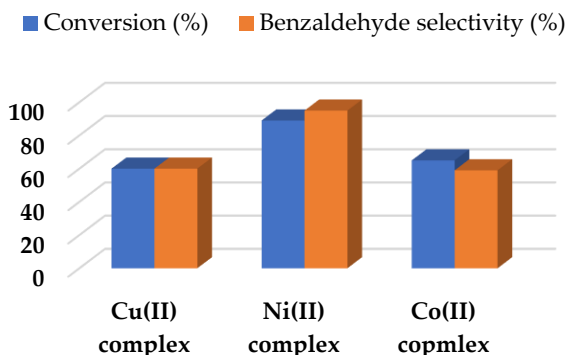


Figure 7. Conversion (%) and benzaldehyde selectivity (%) of (3)

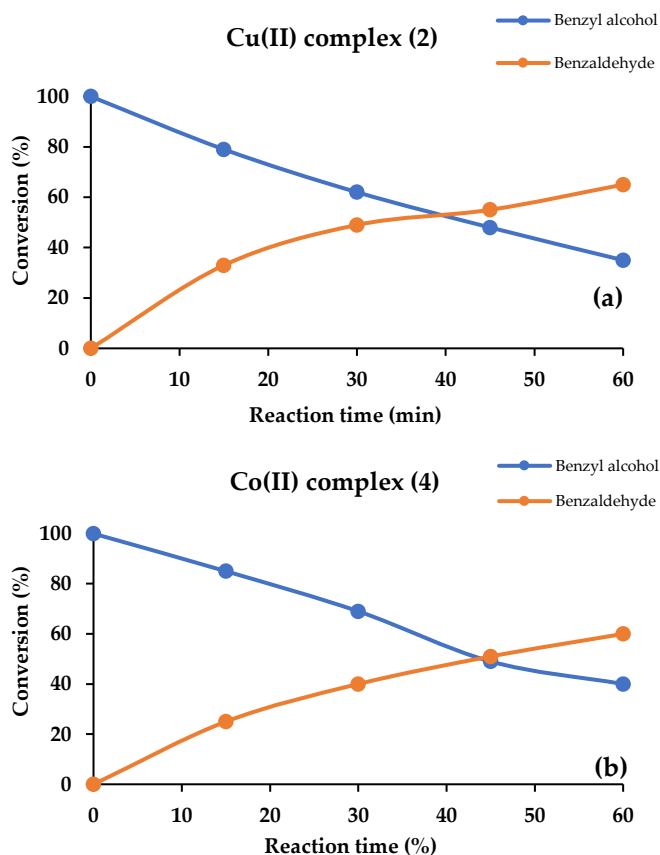


Figure 8. Benzaldehyde conversion with (2) (a) and (4) (b)

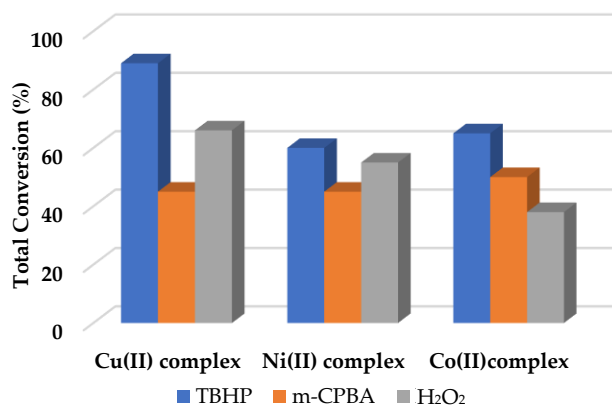


Figure 9. Oxidant type effect on benzyl alcohol oxidation with (2–4)

Table 3. All works using Schiff base complexes as catalysts in the oxidation reaction of benzyl alcohol in the last decade

Catalyst	SM	Ox.	Sol.	RT	RT (°C)	C/S	Ref.
Cu(II)SB ^a	MWCN	TBHP	1,4-dioxane	30 min	80	93/nr	[44]
*Cu(II)SB ^b	—	O ₂	water	24 h	70	>99/>99	[45]
Co(II)SB ^c	GO	H ₂ O ₂	free	40 min	25	95/70	[46]
Cu/NiSB ^d	MONP	H ₂ O ₂	DMSO	2 h	70	94/98	[47]
*Cu(II)SB ^e	—	O ₂	MeCN	1 h	25	99/nr	[48]
Co(II)SB ^f	—	H ₂ O ₂	water	80 min	82	85/100	[49]
Mo(VI)SB ^g	—	TBHP	free	2 h	25	92/98	[50]
**V(V)SB ^h	—	H ₂ O ₂	MeCN	1 h	80	21.5/85	[51]
Cu(II)SB ⁱ	Fe ₃ O ₄ @SiO ₂	TBHP	MeCN	2 h	nr	95/63	[52]
Ni(II)SB	—	TBHP	DMF	1 h	90	89/95	This work

SM: Supporting Material, Ox.: Oxidant, Sol.: Solvent, RT: Reaction Time RT: Reaction Temperature, C/S: Conversion/ Selectivity, Ref.: Reference

^aThese works were carried out in a basic aqueous solution in the presence of TEMPO [(2,2,6,6-tetramethylpiperidin-1-yl)oxyl] radical.

^{**}This work was carried out in the presence of co-catalyst HNO₃ with assisted light and ultrasound.

Cu(II)SB^a: commercially available, Cu(II)SB^b: Copper(II)-(2,2,6,6-tetramethylpiperidine-1-oxyl) complex, Co(II)SB^c: Different Schiff base complexes were prepared by immobilizing three aldehydes (4-Hydroxybenzaldehyde, 2-hydroxybenzaldehyde, and 2-Pyridinecarboxaldehyde), Cu/NiSB^d: Cu and Ni Schiff-base complexes, namely ahpvCu, ahpnCu, and ahpnNi, incorporating imine ligands derived from the condensation of 2-amino-3-hydroxypyridine, with either 3-methoxysalicylaldehyde (ahpv) or 4-nitrobenzaldehyde (ahpn), Cu(II)SB^e: Bearing the *N*-(*X*)-1-(furan-2-yl)methanimine ligands, Co(II)SB^f: synthesized with 1-(4-dimethylaminobenzyl-idenethiosemicarbazide (ABTSC) and 1-(2-pyridinylcarboxyl-idenethiosemicarbazide (TCTS), Mo(VI)SB^g: ioxidobis[2-((E)-p-tolyliminomethyl]phenolato)molybdenum(VI) complex, V(V)SB^h: Oxidovanadium (V) complex, Co(II)SBⁱ: Complex name was not identified, commercially taken.

Three different oxidants (TBHP, H₂O₂ and *m*-CPBA) were used to investigate the effect of the oxidant type on the catalytic system. Catalytic tests using Ni(II) Schiff base complex showed that the best oxidant source was TBHP with 95% benzaldehyde selectivity. The lowest product conversion for the same catalytic system was obtained at 45% when *m*-CPBA was used (Fig. 9). It is widely known that the peroxidative oxidation process proceeds via radical species [40–42]. Kani and co-workers investigated the reaction mechanism of catalytic oxidation of different organic compounds using TBHP and Mn(II) complexes in aqueous acetonitrile reaction medium using various radical scavengers [43]. In the first step, the oxidant (TBHP) coordinates to metal center (i) via the non-bonding electrons. Due to the bond dissociation energies of the peroxy and the O–H bonds in the TBHP, *tert*-butoxyl and hydroxyl radicals can be formed on the metal ions in the structure(ii). The *tert*-butoxy radical can leave the scaffold and further interact with another TBHP to form a *tert*-butyl hydroperoxyl radical ((CH₃)₃COO•) and *tert*-butanol ((CH₃)₃COH) by a rapid follow-up reaction. The cycle continues as the hydroxyl radicals become a hydroxyl ion by abduction of an electron from metal ion to form metal-(OH) (iii).

Table 4. Electronic transitions of ligand and metal complexes, (λ_{max} in nm)

Compound	π–π*	n–π*	d-d bant
(1)	280	320	—
(2)	290	321	480
(3)	298	356	540
(4)	292	363	675, 660, 645, 600

The oxidized structure (iii) reacts with another TBHP molecule to form water and a manganese hydroperoxo species (iv). At this stage, possibly due to the rigid coordination geometry of (iv), the metal-O bond is cleaved, leaving the *tert*-butyl peroxy radicals and oxidation state of metal is reduced via electron transfer to recover initiate center (i). Thus, a new catalytic cycle can begin [43].

When we look at the oxidation studies of benzyl alcohol carried out in the last 10 years, we see that the majority of them were carried out using copper, cobalt, vanadium, iron, zinc Schiff bases and their modified forms with various support materials (TiO₂, CeO₂, MCM-41, multi-walled carbon nanotube, rGO, etc.) [44–52]. All works are summarized in Table 3. In these studies, the use of support material extended the durability and life of the catalyst and made it more active and product-selective. In our study, high product conversion and product selectivity were achieved without the need for any support material with Nickel Schiff base, which is rarely used in literature.

4. Conclusion

2,2'-(propenylenedioxy)dibenzaldehyde bis(thiosemicarbazone) (1) and Cu(II), Ni(II), and Co(II) complexes (2-4) were characterized with different spectroscopic methods. Then, their photocatalytic performances were investigated on the oxidation of benzyl alcohol by changing oxidant type, substrate/catalyst ratio. In the catalytic study where Cu(II) Schiff base complex was used as a catalyst, 60% product conversion was determined with 600 as the turnover number, and Co(II) Schiff base complex was used as a catalyst, 65% product conversion was determined with 650 as turnover number. In this study, where homogeneous catalytic reaction system was used, catalysts and their selectivities were investigated on benzyl alcohol oxidation reaction and the results were quite satisfactory. However, the presence of all reactants together with the catalyst limited the recovery and reusability studies of the catalysts. Among the Schiff base complexes, the Ni(II) complex (3) was determined as the most active catalyst with an 890 TON value in the DMF solution. Ni(II) Schiff base complexes, of which there are limited studies in the literature, show not only high conversion but also high product selectivity in this study, revealing the potential of these complexes in catalytic applications.

Declaration of interests

The authors declare that they have no known competing financial interests or personal relationships that could

have appeared to influence the work reported in this paper.

References

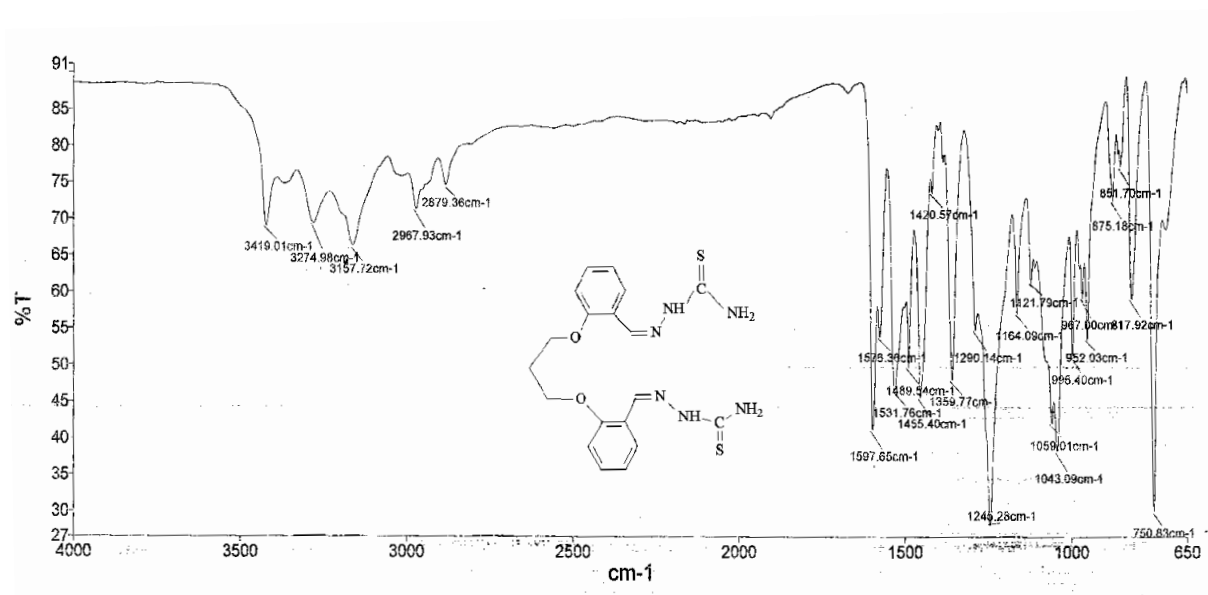
- [1] H.W. Ou, K.H. Lo, W.T. Du, W.Y. Lu, W.J. Chuang, B.H. Huang, H.Y. Chen, C.C. Lin, Synthesis of Sodium Complexes Supported with NNO-Tridentate Schiff Base Ligands and Their Applications in the Ring-Opening Polymerization of L-Lactide, *Inorg Chem*, 2016, 55, 1423–1432.
- [2] P. Gijsman, *Applied Plastics Engineering Handbook (Second Edition)*, 18 – Polymer Stabilization, Editors: Myer Kutz, 2017, Plastics Design Library, William Andrew Publishing.
- [3] B.J. Vasanthi, L. Ravikumar, Synthesis and characterization of new poly(azomethine ester)s having phenylthiourea units, *Eur Polym J*, 2007, 43, 4325–4331.
- [4] M.J. O'Donnell, The Enantioselective Synthesis of α -Amino Acids by Phase-Transfer Catalysis with Achiral Schiff Base Esters, *Am Chem Soc*, 2004, 37, 506–517.
- [5] R.C. Silva, F.S.M. Canisares, A.M.G. Mutti, A.M. Pires, S.A.M. Lima, Small Schiff base molecules derived from salicylaldehyde as colorimetric and fluorescent neutral-to-basic pH sensors, *Dyes Pigments*, 2023, 213, 111191.
- [6] J.J. Kaylor, T. Xu, N.T. Ingram, A. Tsan, H. Hakobyan, G.L. Fain, G.H. Travis, Blue light regenerates functional visual pigments in mammals through a retinyl-phospholipid intermediate, *Nat Commun*, 2017, 8, 16.
- [7] O.A.G. Wahba, A.M. Hassan, A.M. Naser, A.M. Hanafi, Preparation and Spectroscopic studies of some copper and nickel Schiff base complexes and their applications as coloring pigments in the protective paints industry, *Egypt J Chem*, 2017, 60, 25–40.
- [8] N. Mohan, S.S. Sreejith, P.M.S. Begum, M.R. Prathapachandra Kurup, Dual responsive sales-type Schiff bases for the effective detection of L-arginine via a static the quenching mechanism, *New J Chem*, 2018, 15.
- [9] D. Kılınc, Ö. Şahin, Performance of Zn-Schiff Base complex catalyst in NaBH₄ hydrolysis reaction, *Int J Hydrogen Energy*, 2020, 45, 34783–34792.
- [10] V. Mahdavi, M. Mardani, Mn(Salen)Cl complexes immobilized on SBA-15 functionalized with amine as an efficient, selective, and recyclable catalyst for benzyl alcohol oxidation by TBHP: the effects of Mn loading and reaction conditions, *Res Intermed*, 2015, 41, 8907–8927.
- [11] S. Dayan, M. Tercan, F.A. Özdemir, G. Aykutoğlu, N. Özdemir, Z. Şerbetçi, M. Dinçer, O. Dayan, Catalytic and biological activities of homoleptic palladium(II) complexes bearing 2-aminobenzothiazole moiety, *Polyhedron*, 2021, 199, 115106.
- [12] M.I. Ofem, H. Louis, J.A. Agwupuye, U.S. Ameuru, G.C. Apebende, G.E. O, O. Terkumbur, M. Joseph, A. Neksumi, A. Ayi, Synthesis, spectral characterization, and theoretical investigation of the photovoltaic properties of (E)-6-(4-(dimethylamino)phenyl)diazonyl)-2-octyl-benzoisoquinoline-1, 3-dione, *BMC Chem*, 2022, 16, 109.
- [13] N. Turan, K. Buldurun, E. Bursal, G. Mahmoudi, Pd(II)-Schiff base complexes: Synthesis, characterization, Suzuki–Miyaura and Mizoroki–Heck cross-coupling reactions, enzyme inhibition and antioxidant activities, *J Organomet Chem*, 2022, 970–971, 122370.
- [14] S. Hkiriya, S. Touil, A. Samarat, D. Sémeril, Palladium-catalyzed Suzuki–Miyaura cross-coupling with α -amino phosphonates based on 1,3,4-oxadiazole as ligands, *C R Chim*, 2022, 25, 53–65.
- [15] P. Sarmah, B.K. Das, P. Phukan, Novel dicopper(II)-tetra carboxylates as catalysts for selective oxidation of benzyl alcohols with aqueous TBHP, *Catal Commun*, 2010, 11, 932–935.
- [16] E.T. Saka, K. Tekintas, Light-driven photodegradation of 4-nitrophenol with novel Co and Cu phthalocyanine in aqueous media, *J Mol Struct*, 2020, 1215, 128189.

- [17] E.T. Saka, I. Acar, Z. Bıyıklıoğlu, H. Kantekin, I. Kani, Synthesis and characterization of peripheral and non-peripheral substituted Co(II) phthalocyanines and their catalytic activity in styrene oxidation, *Synth Met*, 2013, 169, 12.
- [18] S. Gokce, E.T. Saka, Z. Bıyıklıoğlu, H. Kantekin, Synthesis, characterization of metal-free, metal phthalocyanines and catalytic activity of cobalt phthalocyanine in cyclohexene oxidation, *Synth Met*, 2013, 176, 108.
- [19] G.L. Song, L. Feng, J. Xu, H.J. Zhu, Liquid-phase oxidation of toluene to benzaldehyde with molecular oxygen catalyzed by copper nanoparticles supported on graphene, *Res Chem Intermed*, 2018, 44, 4989.
- [20] S. Abednatanzi, A. Abbasi, M. Masteri-Farahani, Immobilization of catalytically active polyoxotungstate into ionic liquid-modified MIL-100(Fe): A recyclable catalyst for selective oxidation of benzyl alcohol, *Cat Com*, 2017, 96, 6.
- [21] A. Hamza, D. Srinivas, Selective Oxidation of Benzyl Alcohol Over Copper Phthalocyanine Immobilized on MCM-41, *Catal Lett*, 2009, 128, 434.
- [22] L.Y. Wang, D. Pan, M. Zhou, Q. Liang, Z.Y. Li, Effect of phthalocyanines supported carbon nanotube for the catalytic oxidation of benzyl alcohol, *Solid State Sci*, 2021, 113, 106546.
- [23] E. Bisz, P. Podchorodecka, H. Li, W. Ochedzan-Siodłak, J. An, M. Szostak, Sequential Iron-Catalyzed C(sp²)-C(sp³) Cross-Coupling of Chlorobenzamides/Chemoselective Amide Reduction and Reductive Deuteration to Benzylic Alcohols, *Molecules*, 2023, 28, 223.
- [24] C. Meng, K. Yang, X. Fu, R. Yuan, Photocatalytic Oxidation of Benzyl Alcohol by Homogeneous CuCl₂/Solvent: A Model System to Explore the Role of Molecular Oxygen, *ACS Catal*, 2015, 5, 6, 3760–3766.
- [25] F.-F. Pan, P. Guo, X. Huang, X.-Z. Shu, Synthesis of Dibenzyls by Nickel-Catalyzed Homocoupling of Benzyl Alcohols, *Synthesis*, 2021, 53(17), 3094–3100.
- [26] Z. Hao, T. Gao, X. Zhou, Z. Ma, Z. Han, G.L. Lu, Nickel(II) complexes bearing 8-hydroxyquinoline-imine ligands: Synthesis and catalysis in the hydrosilylation of aldehydes and ketones, *J Mol Struct*, 2023, 1294, 136539.
- [27] N. Karaböcek, A. Küçükdumlu, P. Ekmekcioğlu, S. Karaböcek, Synthesis and Structural Studies of 2,2'-(2E,5E)-hexane-2,5-diylidenedi-nitrilo]-dibenzene-thiol and 2-Hydroxybenzaldehyde (2E,5E)-hexane-2,5-diylidenedihydrazone ligands and their Mononuclear Cu(II) and Ni(II) Complexes, *J Macromol Sci A*, 2009, 46, 1007–1014.
- [28] N. Karaböcek, A. Küçükdumlu, S. Karaböcek, Synthesis and Structural Studies of (2E,3E)-3-[(6-[(1E,2E)-2-(Hydroxyimino)-1-Methylpropylidene]Amino)Pyridin-2-yl) İmino]Butan-2-One Oxime, Ligand And Its Mono-, Di- And Trinuclear Copper(II) Complexes, *Transit Met Chem*, 2006, 31, 938–942.
- [29] K. Golcuk, A. Altun, M. Kumru, Spectroscopic and thermal studies of Mn(II), Co(II) and Ni(II) bromide *m*-methylaniline complexes, *J Mol Struct*, 2003, 657, 385–393.
- [30] F.A. Cotton, G. Wilkinson, C.A. Murillo, M. Bochmann, *Advanced inorganic chemistry*. 6th Edition, 1999, Wiley, New York.
- [31] J.R. Allan, Structural and Thermal Studies of The Chloro Complexes of Cobalt, Nickel and Copper with 2,6-Diaminopyridine and Assessment of their Suitability as Antistatic Additives for Polyethylene, *Thermochim Acta*, 1992, 208, 125–131.
- [32] K. Golcuk, A. Altun, M. Kumru, Spectroscopic and thermal studies of Mn(II), Co(II) and Ni(II) bromide *m*-methylaniline complexes, *J Mol Struct*, 2003, 657, 385–393.
- [33] Z. Grabaric, N. Koprivanac, S. Papic, D. Parac-Osterman, H. Matanic, Synthesis, Application Biodegradation of a Chromium Azomethine Dye, *Dyes Pigment*, 1993, 23, 255–265.
- [34] J.R. Allan, D.H. Brown, R.H. Nuttall, D.W.A. Sharp, The thermal decomposition of metal complexes—III: The decomposition of some pyridine and substituted-pyridine complexes of cobalt(II) halides, *J Inorg Nucl Chem*, 1964, 26, 1895–1902.
- [35] E.T. El-Asmy, B. Jeragh, M. Ali, Spectral, thermal, molecular modeling and biological studies on mono- and binuclear complexes derived from oxalo bis(2,3-butanedionehydrazone), *Chem Cent J*, 2015.
- [36] S. Amer, N. El-Wakiel, H. El-Ghamry, Synthesis, spectral, antitumor and antimicrobial studies on Cu(II) complexes of purine and triazole Schiff base derivatives, *J Mol Struct*, 2013, 1049, 326–335.
- [37] T. Bardakçı, T. Altun, A. Kurtulus, K. Golcuk, M. Kumru, Synthesis, structural, spectral (FT-IR, FT-Ra, and UV-Vis), thermal, and density functional studies on *p*-methyl aniline complexes of Mn(II), Co(II), and Ni(II) bromides, *J Mol Struct*, 2015, 1100, 475–485.
- [38] A. Studer, D.P. Curran, Catalysis of Radical Reactions: A Radical Chemistry Perspective, *Angew Chem Int Ed Engl*, 2016, 55, 58–102.
- [39] G. Martemucci, C. Costagliola, M. Mariano, L. D'andrea, P. Napolitano, A.G. D'Alessandro, Free radical properties, source and targets, antioxidant consumption and health, *Oxygen*, 2022, 2, 48–78.
- [40] X. Wen, Y. Ma, J. Chen, B. Wang, A synthetically useful catalytic system for aliphatic C-H oxidation with a nonheme cobalt complex and *m*-CPBA, *Org Biomol Chem*, 2024, 22, 5729–5733.
- [41] M. Balamurugan, E. Suresh, M. Palaniandavar, μ -Oxo-bridged diiron(III) complexes of tripodal 4N ligands as catalysts for alkane hydroxylation reaction using *m*-CPBA as an oxidant: substrate vs. self hydroxylation, *RSC Adv*, 2021, 11, 21514–21526.
- [42] T. Nagataki, S. Itoh, Catalytic Alkane Hydroxylation Reaction with Nickel(II) Complexes Supported by Di- and Triphenol Ligands, *Chem Lett*, 2007, 36, 748.
- [43] I. Kani, I. Taskinlar, Z. Uzel, I. Avan, Catalytic oxidation of thymol and carvacrol with Mn(II)-benzoylbenzoate-bipyridine complex, *Polyhedron*, 2024, 249, 116772.
- [44] A.R. Pourali, M. Cheraghi-Parvin, M. Omid-Ghallemohamadi, Synthesis of Cu(II) Schiff base complex supported on multi-wall carbon nanotube for the oxidation of benzyl alcohols, *Inorg Chem Commun*, 2023, 155, 111099.
- [45] W. Czepa, M.A. Fik, S. Witomska, M. Kubicki, G. Consiglio, P. Pawluc, V. Patroniak, Simple Schiff-Base Cu(II) Complexes as Efficient Catalysts for Benzyl Alcohol Oxidation, *ChemistrySelect*, 2018, 3(32), 9504–9509.
- [46] M.A. Sharif, G.R. Najafi, M.T. Nakhjiri, Co-Schiff base complexes functionalized on graphene as efficient heterogeneous nanocatalysts for alcohols oxidation, *Inorg Nano-Met Chem*, 2023, Early Access.
- [47] S. AlSaeedi, L.H. Abdel-Rahman, A.M. Abu-Dief, S.M. Abdel-Fatah, T.M. Alotaibi, A.M. Alsalmeh, A. Nafady, Catalytic Oxidation of Benzyl Alcohol Using Nanosized Cu/Ni Schiff-Base Complexes and Their Metal Oxide Nanoparticles, *Catalysts*, 2018, 8(10), 452.
- [48] E. Lagerspets, K. Lagerblom, E. Heliövaara, O.M. Hiltunen, K. Moslova, M. Nieger, T. Repo, Schiff base Cu(I) catalyst for aerobic oxidation of primary alcohols, *Mol Catal*, 2019, 468, 75–79.
- [49] M. Tayebani, B. Shafaat, M. Irvani, Hydrogen peroxide oxidation of primary alcohols by thiosemicarbazide Schiff base metal complexes, *Iran J Chem*, 2015, 5(3), 213–221.
- [50] M. Hatefi-Ardakani, S. Saeednia, Z. Pakdin-Parizi, M. Rafeezadeh, Efficient and selective oxidation of alcohols with *tert*-BuOOH catalyzed by a dioxomolybdenum(VI) Schiff base complex under organic solvent-free conditions, *Res Chem Intermed*, 2016, 42(10), 7223–7230.
- [51] M. Sutradhar, M.G. Martins, D.H.B.G.O.R. Simoes, R.M.N. Serodio, H.M. Lapa, E.C.B.A. Alegria, M.F.C.G. da Silva, A.J.L. Pombeiro, Ultrasound and photo-assisted oxidation of toluene and benzyl alcohol with oxidovanadium(V) complexes, *Appl Catal A Gen*, 2022, 638, 118623.

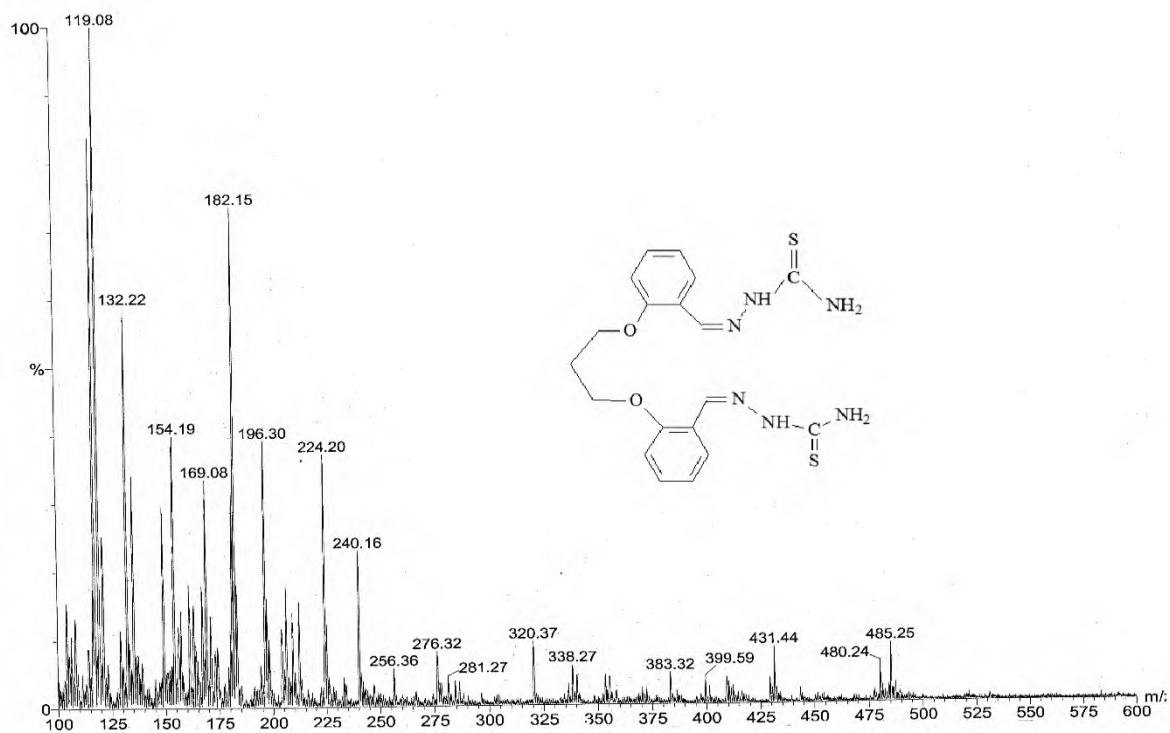
- [52] M. Sarkheil, M. Lashanizadegan, Copper(II) Schiff Base Complex Immobilized on Superparamagnetic Fe₃O₄@SiO₂ as a Magnetically Separable Nanocatalyst for Oxidation of Alkenes and Alcohols, *Appl Organomet Chem*, 2017, 31(10), e3726.

SUPPLEMENTARY INFORMATION

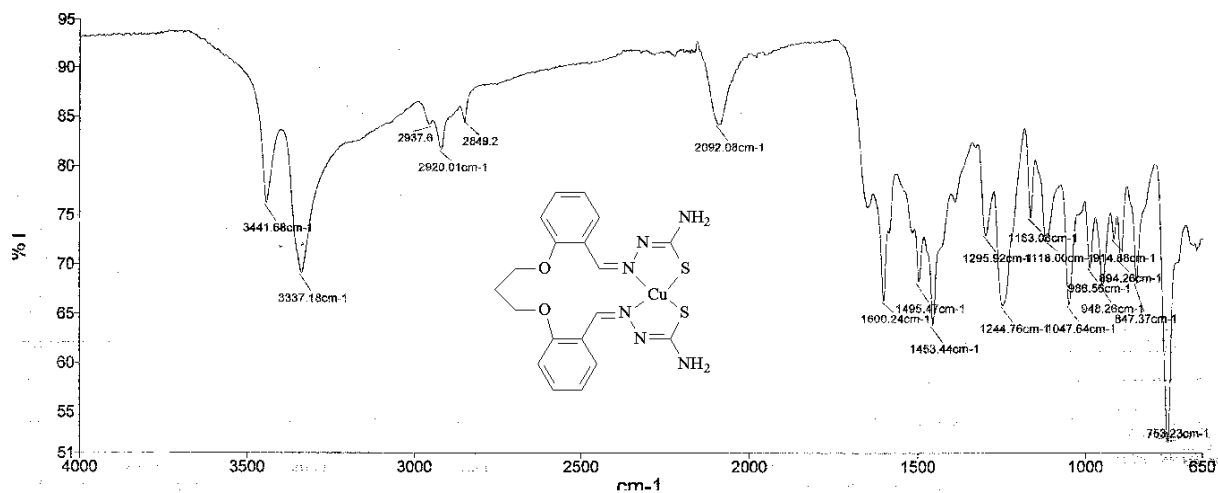
Schiff Base Catalysts for the Oxidation of Benzyl Alcohol to Benzaldehyde



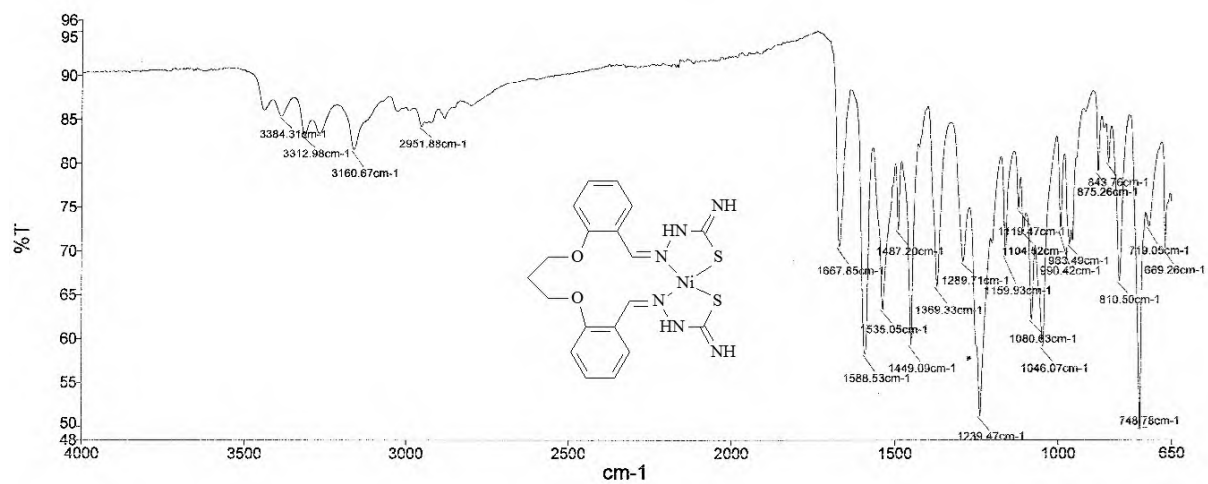
Supplementary Figure 1. IR spectrum of (1)



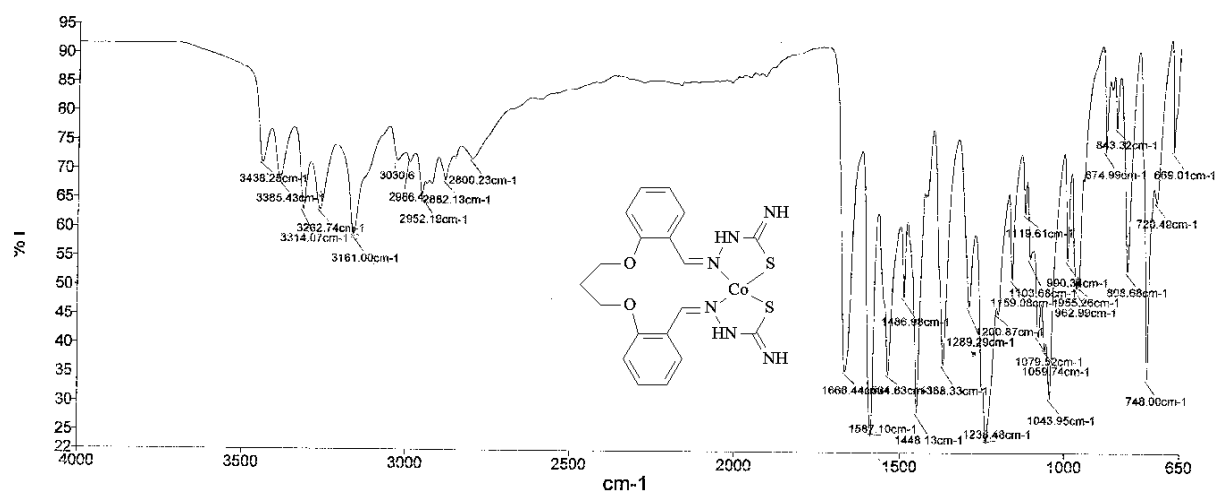
Supplementary Figure 2. Mass spectra of (1)



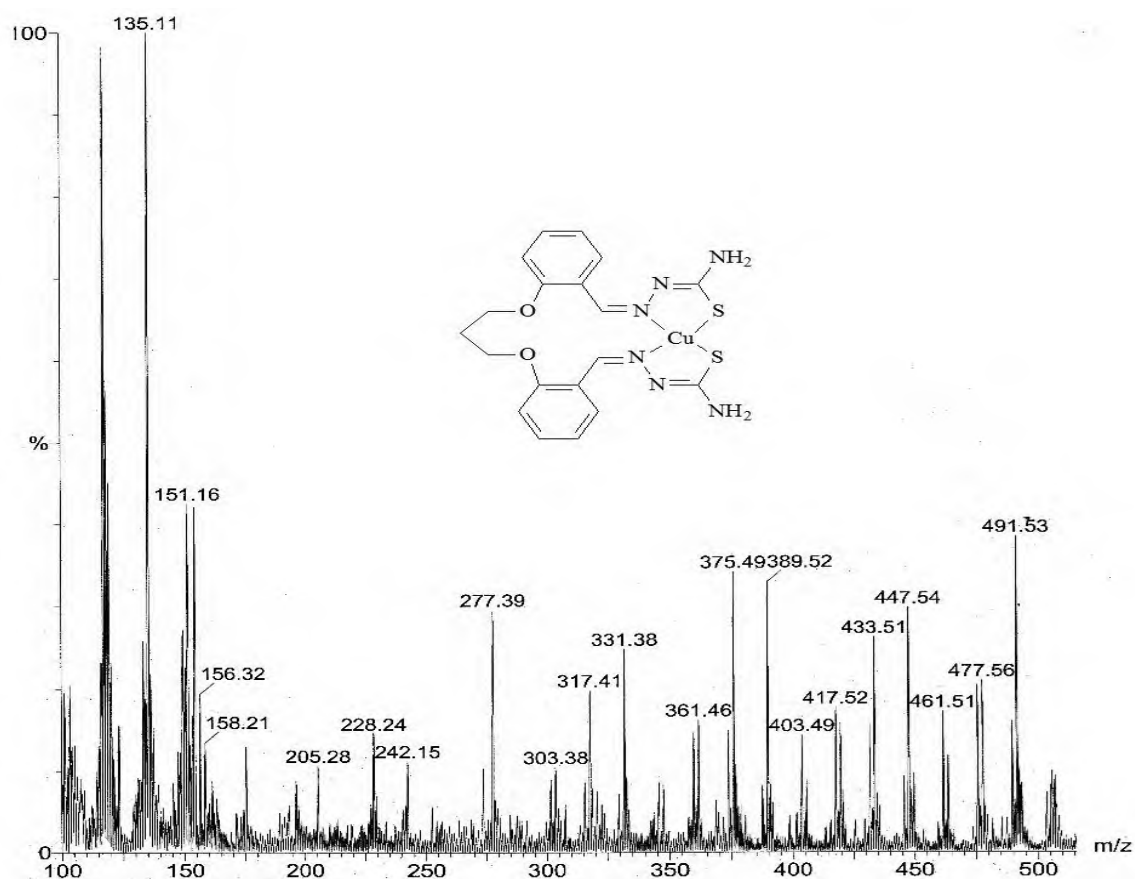
Supplementary Figure 3. IR spectrum of (2)



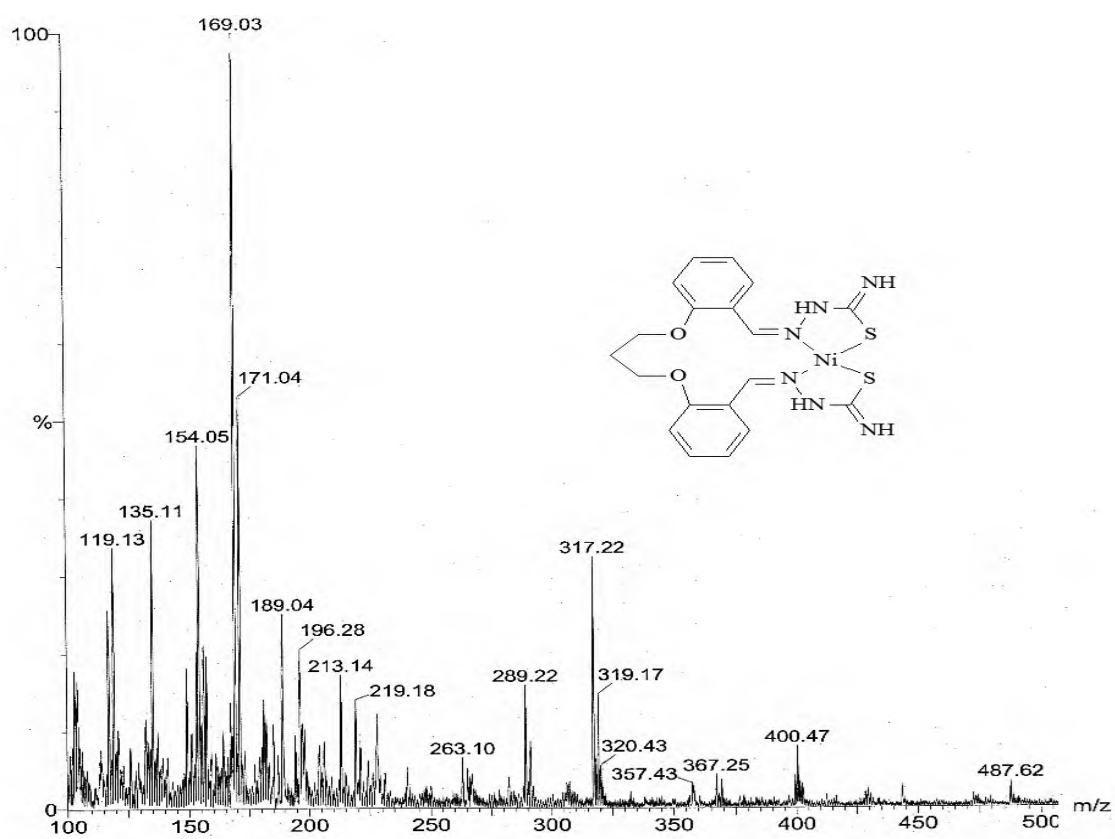
Supplementary Figure 4. IR spectrum of (3)



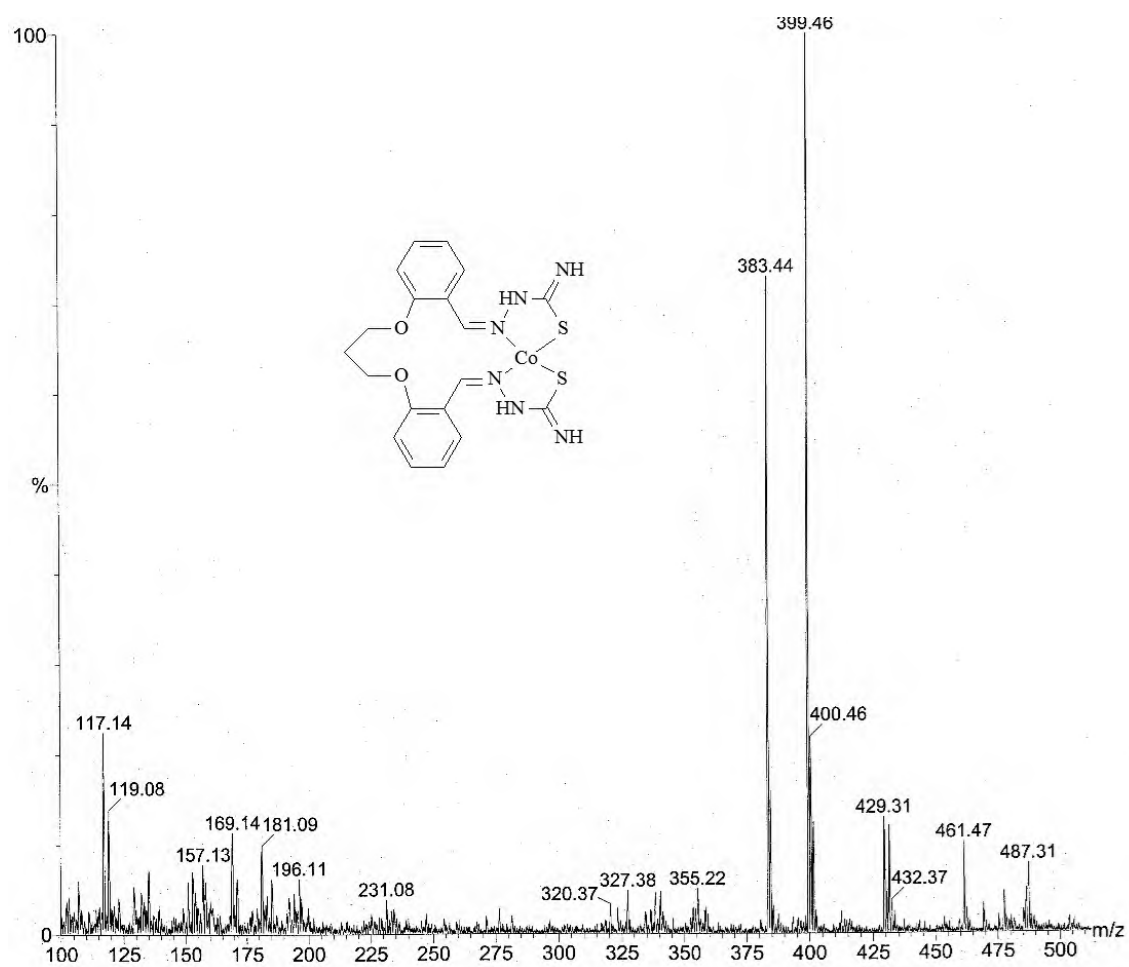
Supplementary Figure 5. IR spectrum of (4)



Supplementary Figure 6. Mass spectra of (2)



Supplementary Figure 7. Mass spectra of (3)



Supplementary Figure 8. Mass spectra of (4)

